12-2021

Hobby Grade Lithium-Ion Batteries for Spacecraft Applications: Establishing an Automated Electrical Characteristics Testing Procedure For Flight Acceptance of non-Space-Grade Small Secondary Batteries

Braidon Hughes
University of Arkansas, Fayetteville

Hobby Grade Lithium-Ion Batteries for Spacecraft Applications: Establishing an Automated Electrical Characteristics Testing Procedure For Flight Acceptance of non-Space-Grade Small Secondary Batteries

A thesis submitted in partial fulfillment.
of the requirements for the degree of
Master of Science in Mechanical Engineering

by

Braidon Hughes
University of Arkansas
Bachelor of Science in Mechanical Engineering, 2015

December 2021
University of Arkansas

This thesis is approved for recommendation to the Graduate Council.

_____
Po-Hao Adam Huang, Ph.D.
Thesis Director:

_____
Rick Couvillion, Ph.D.
Committee Member

_____
Xiangbo Meng, Ph.D.
Committee Member

Abstract

Li-ion batteries are widely used due to the large amount of rechargeable energy they pack into a small, light package. This higher energy density makes Li-ion batteries ideal for small satellite applications, specifically CubeSats. CubeSats have grown in popularity in higher level education due to the National Aeronautics and Space Administration's implementation of the Cube Satellite Launch Initiative, making it easier and cheaper to conduct small, low orbit missions. Because these CubeSats are occupying the same space as a crewed spacecraft, it is imperative that they are safe. There are numerous reports of Li-ion batteries creating fires that result in injury or death.

The goal of this work is to establish testing setups and procedures that will give an accurate profile of the electrochemical properties of lithium-ion batteries. Ten of the tested batteries will be used as the secondary power supply on ARKSAT-1, a CubeSat mission being conducted at the University of Arkansas. These batteries will be monitored for level of self-discharge, thermal stability, capacity retention, vibration resistance, charge-discharge cycling behavior, and tolerance low atmosphere. The electrochemical properties of the batteries must meet various criteria to show that they will be stable and safe to use in a CubeSat.

During all testing, thermistors in a simple voltage divider circuit were used to monitor the battery temperatures. The initial prep of the batteries required removing manufacturer stickers and additional circuitry. The barren batteries were inspected for physical deformations and their volume and mass recorded. Next the batteries were placed under a constant load of 50 mA for 30 seconds to record their closed-circuit voltage. Then they were discharged to 3.6V and left to rest for 14-days. A circuit was built and automated with LabView to record the open circuit voltage of the batteries every hour for the 14-days period. Next a charge-discharge cycling test was

conducted, which was used to measure the capacitance of the tested batteries. The batteries need to be checked for mechanical resistance to shock and low-pressure environments, but these tests are outside of the scope of this thesis. The physical dimension and capacitance measurements are to be reconducted after the shock and vacuum testing to verify that no physical damage or capacity fading have occurred.

These tests were created with the intent to be easily adapted to any commercial off the shelf battery, specifically non-space-grade batteries, to allow for more flexibility in the battery choices as electrical supplies on future ARKSAT missions. It was found that the cells tested for this thesis were able to meet the testing requirements as set forth by NanoRacks, a private company whose purpose is to provide other organizations with necessary services to conduct research projects in space. NanoRacks reviews the testing procedures created for this thesis and gives initial approval of the CubeSat missions so that they can be launched from the International Space Station.

Acknowledgements

I want to thank Dr. Huang for providing the workspace and project to make this thesis possible. I absolutely would not have been able to finish without your help and guidance. Thank you for pushing me when I wanted to quit.

I also would like to thank all of my committee members Dr. Huang, Dr. Couvillion, and Dr. Meng for being great teachers. As I transition into the career of academia, I hope that I can inspire and guide others as they have inspired and guided me.

Thank you to the University of Arkansas, specifically the Mechanical Engineering department which has always provided in any way they can. The faculty and staff at all levels and experience have been invaluable in my success.

Table of Contents

List of Figures

List of Tables

1 Introduction

In this thesis, the testing and verification of lithium-ion batteries' (LIBs) acceptance for use as the secondary electrical power supply (EPS) onboard a small, low earth orbit (LEO) satellite is presented. LIBs have become an enormous part of modern life; as technology advances rapidly and requires more power to operate, portable power supplies must be adapted to keep up. The advancement of technology creates demand for a portable power supply that can operate at higher voltage and higher charge/discharge rates, while maintaining capacity and safety over a long cycle life. This can be challenging, because there are many trade-offs when it comes to battery properties, one of the most important being safety. There are numerous accounts of LIBs' safety being compromised to achieve higher performance. Batteries come in various chemistries, with each chemistry having their own pros and cons. Due to the differences in chemistries and how they preform, the application of the battery will determine the chemistry required for optimal results. Some of the more prominent and most used chemistries will be presented and discussed later.

The chemistry used in the tested LIBs is a lithium cobalt pouch (LiPo) cathode battery, this is not to be confused with lithium polymer batteries, whose cathode comprises of cobalt polymers. A focus is given to the testing requirements needed to prove flight acceptability of the LiPo batteries in a 1U cube satellite (CubeSat). The tested batteries can be seen in Fig 1.1, and the specifications for these batteries are given in Table 1.1 These specific batteries and chemistries were chosen because they were commercially available and fell in-line with the requirements of the ARKSAT missions, as will be discussed later.

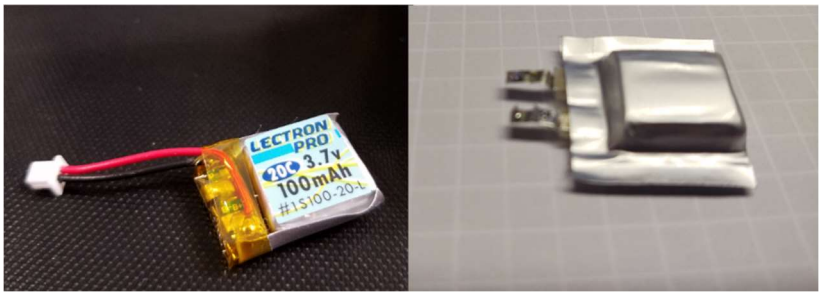

Fig. 1.1: Tested LiPo cells for use on CubeSat. The left shows the battery as received from the manufacturer. The right shows the battery after it has been prepared for testing.

Table 1.1: Tested Battery Specifications

Capacity	100 mWh
Operating Voltage	3.2-4.2 V
Ideal Discharge Rate	1 C
Electrolyte	"Gel"

The LiPo LIBs tested for flight acceptance are comprised of one cell, so the terms "cell" and "battery" are used interchangeably throughout this thesis. In general, large batteries are comprised of multiple cells. The MSDS gives the combinations of "hazardous ingredients" listed in table 2.1 for the tested cells. It should be noted that the concentrations specified in table 2.1 are approximate value provided by the manufacturer, due to variations in manufacturing and so that the exact makeup cannot be mimicked by competition. The concentrations of $LiCoO_2$ and Ni mean the tested LiPo cells are just an LCO cathode doped with Ni for a little additional capacity without sacrificing safety.

Table 1.2:Provided MSDS information about tested LiPo battery compositions

Material	Concentration
Carbon	10-25%
$LiCoO_2$	20-40%
$LiPF_6$	1-4%
Organic Carbonates (EC/EMC/DEC)	8-18%
Polyvinylidene Fluoride (PVDF)	1-5%
PP+PE	4-6%
Copper	15-30%
Aluminum	10-20%
Nickel	0.5-1%

The tested batteries will be used as the secondary EPS on the ARKSAT-1 CubeSat, which will be launched from the International Space Station (ISS) via National Aeronautics and Space Administration's (NASA) Educational Launch of Nanosatellites (ELaNa) mission program. The testing setups for ARKSAT-1's batteries will be used for future CubeSat missions to streamline future flight acceptance of any commercial off the shelf (COTS) portable power supplies.

The testing of these batteries included before & after mass/volume comparisons, capacity, cycling, working & resting voltages, vibrational, and vacuum testing. It should be noted that the vibrational and vacuum testing are outside the scope of this thesis. The extensive testing is required because LIBs have a significant amount of energy contained in a small package. If a failure occurs within the battery, this energy can be released in a short amount of time causing large amount of heat and gas generation, as well as expulsion of flammable or toxic material. This can obviously be a health concern for any portable electronic being used by an individual, but this risk raises exponentially if those batteries are in an occupied spacecraft. There are already examples of LIB failures starting fires in cargo planes or electric vehicles that ended with the loss of life. This is why it is imperative to create an accurate testing setup to verify the

electrochemical properties of a cell. There are numerous indicators that will foreshadow a battery failure, the tests presented in this thesis are designed to look for these indicators.

1.1 What is a battery?

It is likely that anyone reading this paper has some concept of what a battery is. For this thesis, the term battery refers to either a single (or group) of portable electrochemical cell(s). These cells may be designed to only be used once (referred to as primary cells), or they may be designed to be used and recharged many times (referred to as secondary cells). During discharge, an electrochemical cell is technically a galvanic cell, a cell that harnesses a spontaneous chemical reaction to produce electricity [1]. During charge, an electrochemical cell is referred to as an electrolytic cell, it reverses the spontaneous reaction by applying electricity [1]. It should be apparent that primary cells will only ever operate as galvanic cells since their reaction cannot easily be reversed.

1.1.1 Parts of a battery

Though there are several differences between primary and secondary batteries, their general functionality is the same. The active parts of a battery are the electrodes, and electrolyte. The electrodes are referred to as anode and cathode, where the anode is the “negative” side of the battery, and the cathode is the “positive” side, see Fig. 1.2.

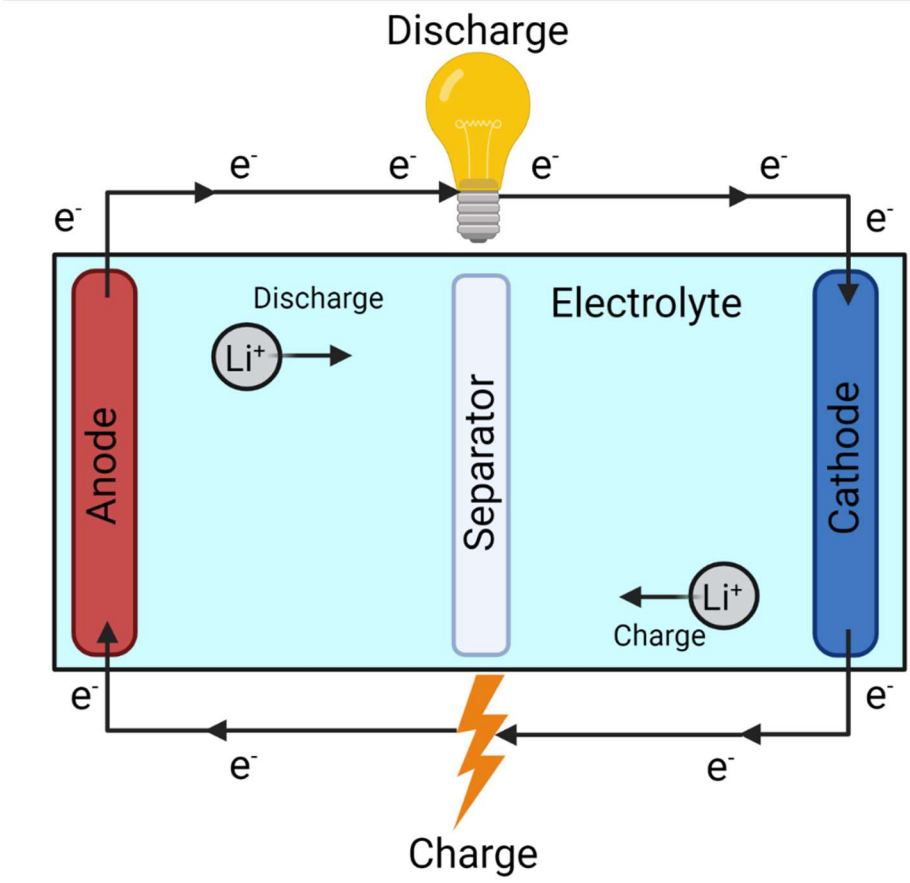

Fig. 1.2: Parts of a battery, showing electron and Li^+ motion during charge & discharge

It should be noted that the "anode is negative" and "cathode is positive" naming conventions in this paper will be consistent as just presented, but technically these name assignments are based on the reactions that occur during discharge only. In the discharging redox reaction, the anode is the reducer (gives electrons and is therefore oxidized), and the cathode is the oxidizer (gains electrons and is therefore reduced) [2]. During charging the chemical process is reversed, and so too are the technical anode/cathode nomenclatures [3].

All parts of the battery are contained within a metal casing, most commonly made of steel, aluminum alloys, and aluminum-laminate polyethylene film [4]. The tested LIBs are referred to as "pouch cells" because their casing is a thin, lightweight, and flexible. Connected to each electrode are current collectors, which extend outside the battery's casing. The collector

leads connect to an external circuit which allow electrons to flow, powering the circuit. Current collectors come in both positive (such as aluminum foil) and negative (such as copper foil) terminals, as the current collector needs to be chemically inert when in contact with their respective electrodes [5]. The connection between the collector and electrode can be damaged if they are allowed to react with one another, lowering the effectiveness of the battery.

The electrodes are typically either submerged in an aqueous electrolyte or set into a gel-like electrolyte. The electrolyte is an ionically conductive, but electronically insulating, connector between the two electrodes [6]. Within the electrolyte there is a porous separator, which prevents physical contact between the two electrodes. Physical contact between two electrodes would form an internal short circuit within the cell, providing electrons an unimpeded path to the lower voltage electrode resulting in an unusable battery. The term "wet" is used to describe aqueous electrolytic solutions, whereas "dry" electrolytes have a fairly high viscosity, just low enough to ensure good contact with the electrodes and separator. In recent years, there has been an increased interest in the development of a solid electrolyte to overcome some of the limitations of liquid electrolytes, such as being flammable and causing parasitic reactions.

1.2 History of Batteries

To fully understand how the battery was developed as it is known today, one needs to look at a brief history. Leyden jars are typically recognized as the first electric storage device, developed in 1745 by Ewald Jürgen von Kleist and Pieter van Musschenbroek [7]. Leyden jars are the first capacitors; they use thin metal foil (the electrical conductors) on the interior and exterior of a glass jar (a dielectric). But the term "battery" was not used in reference to electrical cells until 1748, when Benjamin Franklin used the term to describe a series of group Leyden Jars as an "electrical-battery" [8]. Franklin was simply borrowing the term from "artillery battery",

which is used to describe a group of artillery guns that are connected, and applied the term to describe a group of Leyden jars that were connected together.

In 1800, Alessandro Volta created the “Volta pile”, which is attributed as the world’s first galvanic cell comprised of multiple sets of a zinc disk (anode), copper disk (cathode), and salt water-soaked cloth (electrolyte). The “Daniell cell”, created in 1836 by John Frederic Daniell, used the same zinc and copper electrodes as the Volta pile, but replaced the one saltwater electrolyte with a salt bridge connecting zinc sulfate electrolyte and a copper (II) sulfate electrolyte, which the anode and cathode was submerged in, respectively [9]. In 1859 the first lead-acid battery was created by Gaston Plante, revolutionary as the first secondary battery [10].

The “wet” Leclanché primary cell was developed in 1866, early in primary battery history, as a reserve power supply comprising of a zinc anode, an ammoniac solution as the electrolyte, and magnesium dioxide cathode [11]. The “dry” version of the cell, developed by Carl Gassner in 1888, is still used today with zinc and carbon electrodes and a gel electrolyte, commonly used in flashlights and other portable electronics [12]. In 1899 Waldemor Junger created the nickel-cadmium battery, the first alkaline battery, utilizing a nickel oxide cathode, cadmium anode, and a potassium hydroxide electrolyte [13]. Quite a while later, by 1970 nickel-hydrogen (Ni-H) hybrid batteries were used in commercial communications satellites, comprising of a typical nickel oxide cathode but a hydrogen-oxygen fuel cell negative electrode [12]. A fuel cells operate similarly to a battery except in place of the electrodes a replenishable fuel supply is used (hydrogen-oxygen for Ni-H cells). The used of the Ni-H battery eventually led to the nickel metal hydride (NiMH) battery in 1989.

The first “lithium ion” (Li^+) battery was made public in 1991 by the Sony corporation, revolutionizing modern technology, providing enough voltage from a single cell to operate a

mobile phone [14]. This revolutionized portable technology as we know it today, with LIBs dominating the market. Looking towards the future, fuel cells, flow cells, and super capacitors have been gaining research interest due to their ability to act as portable power supplies, but investigations into their operations are outside of the scope of this thesis.

1.3 How They Work

As LIB are electrochemical cells, they operate based on chemical reactions. There are a few methods that typical batteries operate under: alloying, conversion, and intercalation. While all three will be explored more in-depth later, the emphasis within this thesis is on intercalation electrodes, not only because they are the most common, the tested batteries rely on an intercalation electrode. Li has a single valence electron that it will readily give away, creating a positively charged Li^+, hence the name Li-ion battery. When a LIB is in use the Li^+ is able to travel through the electrolyte, but because the electrolyte is not electronically conductive, it acts as a barrier for the freed valence electrons which are forced to use an external path [15].

The electrodes within a cell are made up of two dissimilar materials, specifically materials that have a significant difference in electrochemical potential. The electrochemical potential differential between the electrodes is more commonly known as voltage, which is the driving force for electron motion. Whenever an external circuit is connected to a charged battery, electrons will flow from the anode, through the circuit, and back into the cathode spontaneously, because the electrons are trying to reach the lower energy state [16]. As the electrons reach the cathode and it is reduced, a negative charge builds, attracting the positively charged Li^+ in an attempt to maintain charge neutrality within the electrode.

When charging a secondary battery, the reaction is reversed, Li^+ leaves the cathode and travel through the electrolyte to the interstitial sites at the anode [17]. When the charging or

discharging circuit is disconnected, the electrons become trapped in an electrode and the respective Li^+ atoms stay with them due to attempted charge neutrality. For a cell, the simplified charge/discharge equation is shown in Eq. 1.1, where left to right is the reaction during charge and right to left is the reverse reaction during discharge. It should be noted that there are multiple types of chemical reactions that batteries operate on, and Eq. 1.1 only applies to intercalation reactions [18].

$$LiMO_2 \leftrightarrow Li_xC + Li_{1-x}MO_2 \quad (1.1)$$

Where M is one or a combination of transition metals (TMs), such as, but not limited to, Co, Ni, Mn or Fe. Not that the reverse reaction (right to left) is only true for secondary batteries.

1.3.1 Primary vs. Secondary batteries

As previously mentioned, primary batteries are designed to be used once; while secondary batteries are designed to be charged/discharged multiple times. Since the chemical reaction within primary cells only occurs once, it makes sense that these types of chemistries would be phased out as secondary batteries grow in prominence. But it is unlikely that one-time use cells will ever be rendered completely obsolete. Primary batteries tend to have higher energy densities and stereotypically long shelf life cause them to still be common in low drain applications (watch/calculator) [19]. Their long shelf life also makes some primary batteries useful as an emergency reserve power source, such as when used in a flashlight or a sump pump.

Secondary batteries have become increasingly common over the years as the popularity of portable electronics has increased. It should be of no surprise that high energy drain technologies that are used daily, such as the smart phone, encourage the use of secondary batteries. There are consumer benefits to being able to use a battery multiple times, in lieu of relying on a reaction that only occurs once before the battery must be disposed of. Benefits

include not having to purchase batteries as often, or in as large of quantities. This reduces battery waste, which can be dangerous or toxic, and saves the consumer money. Another, albeit less obvious, benefit of using a secondary battery is not having to maintain access to the device to replace the battery after one discharge. This is incredibly useful for things such as satellite applications, where it would be insanely time consuming and expensive to conduct a space launch just to replace a few primary batteries. As long as there is a reliable source of renewable energy onboard, a secondary battery can be used many times without the need for human interference.

1.3.2 The Lithium Ion

The tested LiPo batteries fall under the quite common "lithium-ion" label. The lithium-ion of the "Li-ion battery" is the working cation within the cell, the ion that moves back and forth between the electrodes during use. It is a very promising element for electrochemical storage due to its small atomic radius (0.76 Å) and relatively high diffusion coefficients within popular cathodes, allowing for high energy density batteries as well as the ability to meet high-power demands [20], [21]. Lithium also has the largest, negative, electrochemical potential of the alkali metals (-3.01 V) [22], [23]. This low electrochemical potential increases the selection of anode materials, because lithium will only be able to intercalate with a material that has a higher electrochemical potential.

But lithium is not the only ion that can be used as the working ion within a battery, and others are being investigated. In theory, other ions should work similarly to lithium, but their differences in electrochemical properties and atomic radius play significant factors in how they interact with the various electrode chemistries. Li only has one valence electron, but by using an ion that has multiple valence electrons available, it should be possible to get the same amount of

energy with fewer working ions. The idea is to increase the energy density of the cell, since the energy is increased as the weight is decreased. Besides an increase in energy density, other ions are also being investigated because there is some concern of the long-term sustainability of the lithium supply chain [24]. It is a very reactive metal that is impossible to find in a natural state, it must be extracted from a compound that already has lithium atoms in it. Sodium ion (1.02 Å) batteries have been studied extensively as a potential replacement for Li^+ as the working ion within the cell [21], [25]. As early as 2017, there have been aluminum-ion (0.99 Å) batteries on the market, which are especially attractive due to their three available valence electrons [21], [26]. Other potential ions include potassium (1.38Å), magnesium (0.72 Å), calcium (0.99 Å), and zinc (0.74 Å) [21]. Since many electrode chemistries use an intercalation reaction, the larger radius of some of the proposed alternate ions will pose a problem if the spacing they travel via within the electrodes is too small.

1.4 Goals and Objectives of Present Thesis Work

The overarching goal of this thesis work is to take measurements to create a clear picture of the electrical characteristics and reliability of the tested batteries, as dictated by NanoRacks FAT-C requirements (summarized below) [109]. These are explained in more detail later.

Summary of NanoRacks Requirements:

1. Measurement of Physical Properties

   Summary: The length, width, height, and mass of the batteries is recorded

   Purpose: Verify physical properties do not change after other tests are conducted

   Fail Criteria: See other tests fail criteria

2. 14 Day – OCV

   Summary: Cells are left for 14 days in a discharged state

Purpose: To verify there is no self-discharge occurring within the cells

Fail Criteria: A drop of more than 2 mV in open circuit voltage

3. Charge-Discharge Test

   Summary: Cells are cycled through charge and discharge stages

   Purpose: To see if any abnormalities in the curves occur

   Fail Criteria: If abnormal behavior is experienced, as determined by NanoRacks

4. Vibrational Spectrum

   Summary: Cells are subjected to a range of vibrational frequencies

   Purpose: To verify no electrical or physical property changes occur

   Fail Criteria: Greater than 0.1% change in OCV or 5% change in capacity

5. Vacuum Test

   Summary: Cells are placed in a vacuum for 6 hours

   Purpose: To verify the cells can withstand low pressure environments

   Fail Criteria: Leaks, deformation, or than greater 0.1% change in mass

Note that the vibrational spectrum test and vacuum chamber test are outside the scope of this thesis. The goals set forth to verify the NanoRacks' criteria are listed below:

Goal: Automate measurement of open circuit voltage (OCV) for up to 12 LiPo batteries over a 14-day period.

Objectives:

- Use a circuit that will keep the batteries disconnected when not being measured.
- Develop a LabView program that will send signals to control relays open/close state while reading & recording analog in voltages on a regular, 1 hour, basis for the full 14-day period

- Create MATLAB code to plot data collected by LabView and verify the OCV drop is less than 2mV for the duration of the test

Goal: Automate circuit for 6 LiPo batteries for charge-discharge cycling and capacity calculation

Objectives:

- Circuit will follow the cycling as laid out in section 3.5
- Develop LabView program to monitor OCV voltages of 6 LiPo batteries and their respective charge/discharge currents, depending on what part of the cycle each individual battery is in.
- Use LabVIEW to adjust charge/discharge current to insure a constant rate of C/2 (± 5%)
- Use MATLAB to calculate the capacity of each battery from data saved by LabView

-Needs to take measurements at precise time intervals to ensure accurate capacity calculations and record these measured values to a ".txt" file format.

Goal: Automate temperature measurements using a thermistor in a voltage divider circuit

Objectives:

- Verify thermistor B-values to ensure accurate temperature measurements.

-Incorporate voltage measurements and recording into the other circuits' LabView codes

-Calculate temperature measurements based on calculated thermistor resistances

-Find a method to hold the thermistors in physical contact with the batteries that are being tested.

1.4.1 Powering Small Craft in Space

Per NASA, there are three main sources of power for a spacecraft: solar, batteries, and radioisotopes [27]. Generally, CubeSats rely on the first two, solar for power generation, and a secondary battery that can maintain operations when the photovoltaic cells are unable to meet the

power demands of the craft [28]. Due to the 2003 Mars Exploration Rovers' (MER) outstanding success (expected to operate for 90-sol, opportunity ~5000 sol), lithium-ion batteries have become the preferred energy storage choice for NASA [29]. Pouch cells have become attractive for space applications because a lighter casing will increase the specific energy of the cell [30]. The casing on pouch cells is lighter than the typical steel casing, for the same amount of energy because with spaceflight, every gram matters.

1.4.2 CubeSat Launch Initiative

The research presented later was done in part to develop a process of verifying COTS lithium-ion batteries for flight acceptance as an EPS for the CubeSat ARKSAT-1. The intent to use the setup on future CubeSat mission conducted by the University of Arkansas.

The CubeSat Launch Initiative (CSLI) was established by NASA in 2010 with the goal of proving that it is possible to integrate secondary payloads on a rocket launch vehicle, hopefully providing CubeSat developers a financially feasible way to access space [31]. The ELaNa project, which is heavily intertwined with the CSLI, focuses on attracting (and keeping) students in the science, technology, engineering, and mathematic (STEM) fields by involving them with all aspects of a CubeSat development [32]. Launching a CubeSat through the ELaNa program allows a free ride to space via a rocket launch that is already planned to carry a large and expensive primary program payload, lowering the cost barrier for more amateur programs to access space [33].

The term CubeSat describes a very specific type of satellite. CubeSats launched via the ELaNa, with the express purpose of addressing non-critical missions for NASA in exchange for their ride share service. NASA is not the only space agency that will launch CubeSats, but most are commercial companies that will charge for their service. The cube designation comes from

the unit size of 10 cm cubed, referred to as 1U. These dimensions are crucial if intending to be launched from the ISS as the launch method has been standardized around these values, there is little room for deviation. The cube shape was chosen because it allows for multi-directional solar panels while having sufficient surface area for power generation [34]. CubeSats are not limited to a 1U size though, 2U and 3U are common and up to 6U have been created. 2U and 3U CubeSats are usually stacked, creating up to a 10cm x 10cm x 30cm rectangular box. At the larger sizes, the CubeSats are widened to 2U. For example, a 6U CubeSat would be 10cm x 20 cm x 30 cm.

There is extensive testing that must occur before a CubeSat is accepted for launch. If one of the batteries fails catastrophically in transit or on the ISS, it may cause loss of life in the occupied vehicle. Vibrational shock is of one of the largest concerns as the batteries will experience extreme vibrations during initial launch of the rocket to the ISS. As will be discussed later, mechanical failures such as from vibrations, can easily lead to internal short circuits or thermal failures.

1.4.3 The ARKSAT Missions

The ARKSAT missions (ARKSAT-1 and ARKSAT-2) do have an educational impact, and therefore fall within the umbrella of the ELaNa program. Both satellites will be tested in LEO circular orbit, launching from the ISS at a nominal altitude of 400 km. The ARKSAT-1 and ARKSAT-2 missions are expected to last approximately 6 and 9 months, respectively.

The primary goal of ARKSAT-1 is to demonstrate that a 10,000 lumens LED, as seen in Fig. 1.3, can be tracked from the ground. The secondary goal is to test the feasibility of a novel small satellite deorbiting system. The secondary EPS will be charged by the primary EPS, which

is powered by the solar cells. Ten of the tested batteries will be connected in series as the secondary EPS whose sole purpose is to power the LED at a nominal 36V [34.1].

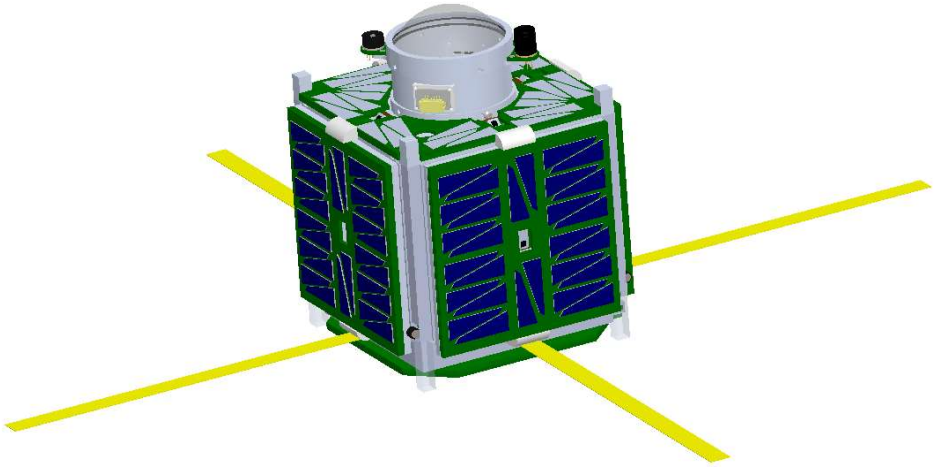

Fig. 1.3: Rendering of ARKSAT-1. The LED can be seen on the top face. Fig. taken from [35]

Since ARKSAT-1 will be launched from the ISS, large amounts of testing are required to prove that the payload batteries do not pose a safety risk to the crew members of either the launch vehicle or those in the ISS. There are two ways to prove that the EPS are safe, one is to use power supplies that have already been extensively tested, used, and approved by NASA, such as the primary EPS on ARKSAT-1 from Clydespace. The other is to extensively test the batteries to prove they are safe for flight acceptance. Since the hope is to continue a CubeSat program at the University of Arkansas, it was ideal to create testing procedures that could be used on future EPS. This will allow for more versatility in battery choices on future missions, as opposed to the more limited "pre-approved" options. Being able to more readily tailor the battery to the application will be a huge help for future CubeSat developments. This requires a reliable and acceptable testing setup for various electrochemical properties.

Assuming a successful first mission, ARKSAT-2, as seen in Fig. 1.4, is intended to exhibit chasing and tracking capabilities, as well as implement an altitude control system. These

two satellites are intended to be the initial steps in establishing a pair of CubeSats that can be used to take high quality measurements of an atmosphere, or other material, that is between them.

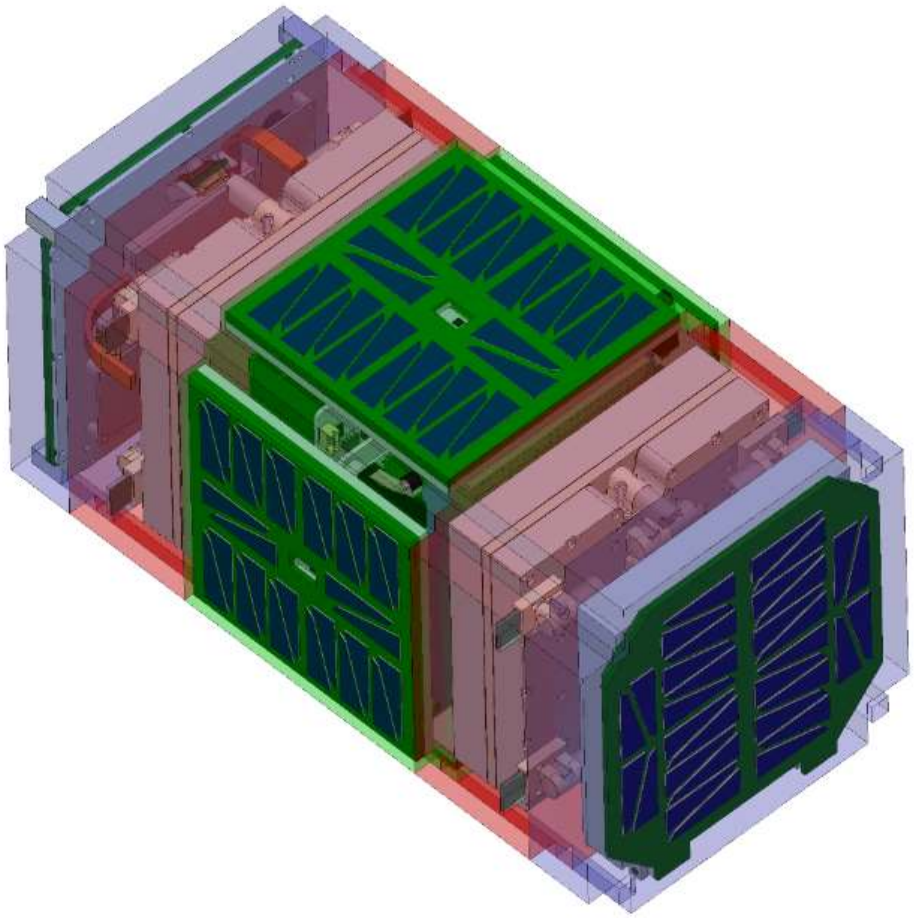

Fig. 1.4: Rendering of ARKSAT 2. Fig. taken from [35]

2 Review of Literature

There is extensive literature about current battery technology, so a very limited scope had to be chosen for the purposes of this thesis. The available information is ever increasing, filtering results from the beginning of 2020 to mid-June 2021 searching for "Li-ion battery" on Engineering Village gives >4,500 publications. The information presented here was chosen to be as condensed and relevant as possible to the research presented later.

2.1 Battery Properties

When choosing a battery chemistry for a specific application, there are several properties to consider: capacity, voltage, C-rates, temperature, lifetime, and physical requirements. They are all heavily interconnected, and often one cannot be improved without sacrificing the efficiency of another. Research has mostly been focusing on increasing electrode capacity, voltage windows, and cyclability. The focus on these properties is fueled by the global push towards adoption of electric vehicles, high power demand devices that will be charged and discharged often.

2.1.1 Capacity

The capacity of a battery is a measure of usable electrical charge stored that is available upon discharge, measured in ampere-hours (Ah), or watt-hours (Wh), related by Eq. 2.1 [23].

$$Wh = Ah * V_{ave} \tag{2.1}$$

The amount of energy within the electrode is important for increasing how long the cell can be used before it must be recharged. The capacity within a cell is often referred to by state-of-charge (SOC); or sometimes in the opposite state-of-discharge (SOD), though the former seems to be the most commonly used. The SOC is the percent of the total capacity that is still

available within the cell, i.e., SOC = 100 % at full charge and SOC = 0% at full discharge. The capacity of a battery can simply be calculated by Eq.2.2:

$$C = I * t \tag{2.2}$$

Where C is capacitance in ampere-hours, I is current in amperes, and t is time in hours of the charge/discharge length. For this research, a constant current is used making this an easy equation. For a variable current, the capacitance can be found by integrating under the current vs. time function.

There is a distinction made between charge and discharge capacity, though charge capacity is rarely discussed. More energy is needed to charge a battery than the amount of energy delivered during discharge because extra energy is required to move electrons from the lower energy state (cathode) to the higher energy state (anode) when compared to the energy released during the spontaneous reaction that occurs during discharge [36].

As with voltage, the capacity of the cell is determined by the chemical makeup of the electrodes. Unlike voltage though, the capacity of the cell can be increased by increasing the amount of active electrode material within the cell. It makes sense that more active material will allow for more electricity generating reactions to occur, if there is more material then there are more electrons that can be shuttled between the electrodes. In an ideal cell, the total capacity of each electrode would be the same, as the battery's capacity is limited to the smaller capacity of the two electrodes [37]. If the anode has a higher capacity than the cathode, then at the end of charge there will be empty spaces remaining in the anode that Li could occupy. There would not be any more Li for the cathode to provide though, essentially making a part of the anode useless. Since different materials have different energy densities, the electrodes are likely to exist in different proportions within the battery.

The amount of energy stored in a battery is important, but the application may be more concerned with the energy densities of the cell instead of just flat capacity. This is either represented by specific energy or volumetric energy, the energy per mass or energy per volume, respectively. For instance, if the batteries are being used for electrical grid energy storage, then capacity may be the main concern since the weight and volume will not matter as much for a stationary power source after it has been installed. For an electric car however, the specific energy will be more of a concern as the weight of the vehicle is a principal factor. Whereas a cell phone manufacturer, may put more worth on the volumetric energy to save space within the phone. Both aspects are crucial to CubeSat batteries as there is both limited space and weight for the small satellite.

2.1.2 Voltage

The cell's voltage is tied directly to the chemical makeup of the electrodes. This voltage is usually the voltage difference in the electrodes' electrical potentials, which drives the movement of electrons when the electrodes are connected. There are two types of voltages used to describe a battery, open circuit voltage (OCV) and closed-circuit voltage (CCV). The OCV of a cell is the electrochemical voltage between the two electrodes and is the advertised voltage of the battery. The operational voltage range of a battery is limited by the electrochemical potentials of the anode and cathode, μ_A & μ_C respectively. Per [38], the operating voltage (V) can be expressed as shown in Eq.2.3:

$$V = \frac{\mu_A - \mu_C}{-n} - I_I R \tag{2.3}$$

Where n is the number of electrons involved in the reaction, F is Faraday's constant, I_I is the cell's internal current, and R is the cell's internal resistance [38]. From Eq. 2.3, it should be easy to see that increasing the difference in the electrochemical potential between the two

electrodes will give a larger voltage window for the battery to operate in. With the push towards electric vehicles, there has been a focus within the field to increase the working voltage of a cell as it would allow for more power to be obtained from battery packs. This is easily seen with Ohm's Law, Eq. 2.4:

$$P = IV \tag{2.4}$$

Where P is power in Joules, I is current in Amperes, and V is voltage.

The voltage of a cell must be monitored closely as overcharging results in various gas evolutions, such as CO_2, CO, H_2, CH_4, C_2H_6, and C_2H_4, as well as heat generation [39]. Heat generation and these very flammable gases (sans the CO_2) are a dangerous combination, potentially causing an explosion. If the voltage of the cell is allowed to get too low, the electrodes can undergo irreversible phase changes leading to reduced capacity.

Thermodynamic stability within the cell is important as it prevents undesired side reactions between the electrodes and electrolyte. For thermodynamic stability within the cell, the electrochemical energy level of the anode must be less than the energy level of the lowest unoccupied molecular orbital (LUMO) and cathode must have a greater energy than the highest occupied molecular orbital (HOMO) of the electrolyte [40]. If the electrodes do not fall within this range, the anode will reduce and the cathode will oxidize, to form a passivation layer [2]. This chemically inert solid electrolyte interphase (SEI) will be discussed more in depth with the electrolyte.

The OCV of a cell will rise after charge/discharge if given time to rest afterwards, this is attributed to the lithium concentration being uneven within the electrode upon initial charge/discharge [41]. The OCV of a "resting cell", a cell not in use, can change over time, either through self-discharge, or it may slowly rise if the cell has been recently charged or

discharged. The self-discharge of a cell can indicate a fault within the cell. Ideally there would be no self-discharge but that is not the case as the electrolyte is not a perfect electronic insulator.

2.1.3 Charge/Discharge Rates

The charge/discharge rate of the battery is application dependent; but usually referred to in "C-rates". The C-rate is a measurement of either charge or discharge rates, which is simply the speed at which the energy in the battery is used (or restored, in the case of charging). While the units for current are typically amperes, battery charge/discharge rates are scaled to their own maximum capacitance and are given in units of "C", hence the name. The C-rate is the ratio of current and time that will tell how quickly the cell will use its capacity. A discharge rate of 1C will drain the cell in 1 hour, so the 100 mAh LiPo tested cells discharge at 1C (100mA) for an hour, C/2 (50 mA) for 2 hours, and 20 C (2 A) for 3 minutes.

The maximum C-rate that a battery can achieve is dependent upon the maximum internal current that the battery's chemistries will allow [42]. The internal current limitation is dependent upon the internal resistances of the battery. As degradation occurs, the battery's internal resistances will increase, limiting the max C-rate of the battery. At high C-rates, the internal resistances within the cell will cause heat generation which will damage the cell. With insertion electrodes, a quicker insertion from a higher C-rate can cause mechanical failure via minor volume expansions and contractions, which can damage collector connections or by forming cracks in the necessary SEI layer, the significance of which will be addressed in section 2.3.2. There is a benefit to using a lower C-rate as they cause less damage to the cell. The tested batteries claim they can safely discharge at 20C, but it is assumed the cell will be severely damaged afterwards.

2.1.4 Operating temperature

The operating temperature is the temperature range that the cell was designed to work within. Since batteries operate off chemical reactions, it should be easy to see why the temperature can affect the efficiency of these reactions. The ideal temperature range for LIBs is 25-40 °C for optimized performance and life [43]. This will vary depending on the electrode and electrolytes used, but it a good rule of thumb.

If operating at too cold of a temperature, there is less of a safety risk, but it will cause the reactions within the battery to slow. There is even potential for the electrolyte to completely freeze, stopping ion transportation. That is why it can be difficult to start your car in the winter. If operating at too high of a temperature will result in phase changes and the associated capacity fading within the electrodes as the best case. The worst case is that the battery will enter thermal runaway and explode.

Thermal runaway is a self-fueling cycle that occurs when the internal heat generation of the battery is at a higher rate than the heat dissipated. As the cell heats up, more exothermic parasitic reactions occur. This self-fueling heat generation is often accompanied by flammable gas generation. As the cell heats up the existing gas expands as more gas is created, eventually either igniting the built-up gasses, or the pressure causes the cell's casing to rupture. The release in pressure, also referred to as venting, sprays hot electrolyte outside the cell. In the case of ignition, it can expand to other neighboring cells in a battery pack causing previously undamaged cells to also enter thermal runaway.

2.1.5 Lifetime

There are two distinct types of lifetime measurements for a battery. In a primary battery, one is only concerned with its shelf life; how long the battery can remain unused and still

provide energy when needed. In a secondary battery, one is concerned not only with shelf life, but with the cycle life of the battery; how many times the battery be charged & discharged while maintaining its capacity.

When discussing the lifetime of a battery, the shelf life of a battery, is how long the battery can be stored at room temperature while maintaining most of its capacity. As time goes on, side reactions between electrodes and electrolytes will cause the battery capacity to fade. Also, self-discharge, for some chemistries, can be incredibly small, which is useful for reserve power situations. If this capacity fade is too large though, the battery is useless when needed.

Usually though, one will be referring to the cyclability of a battery when discussing the battery's lifetime. It should be noted that it is not expected that a secondary battery loses no capacity when cycling, it is more a matter of how many cycles the cell can undergo and still be useable. A high cyclability means that a battery can go through many charges & discharges with no, or minimal, loss in performance. Most secondary cells will undergo capacity fading upon first charge of the cell, but that is necessary and considered during the design process. Cycle lifetime is important for high drain devices that get used often, such as cell phones, laptops, or electric vehicles. Or as used in a space craft, which needs to conserve on weight as much as possible. Secondary cells as EPS that can be charged via solar cells many times over the crafts life are preferable to primary batteries.

2.1.6 Physical Properties

The physical properties of the cell such as weight, shape, and size are properties that can be altered fairly easily to be adapted to the application, especially the latter two. A change in the physical properties is a good sign that the cell is undergoing some form of degradation.

Another quality that would fall under the physical property umbrella is safety. While a battery casing and electrodes can be adapted to a specific application, the safety cannot be compromised. Of all the properties listed above, safety is the most important one to maintain. A battery should not be implemented if it poses a significant risk to a user's health.

2.2 Electrodes

There are several different methods of electrode behavior that can be used to access the electrochemical energy stored within the cell. Electrodes can operate via either alloying, conversion reaction, or intercalation [44]. Alloying consists of pairing a lithium atom with another metal to form an alloy [44]. Conversion electrodes rely on pairing a lithium atom with another element from the electrode's structure to form a new compound. This conversion allows for more lithium ions to react per metal atom (when compared to intercalation electrodes) giving those impressive capacities [45]. The distinction between alloy and conversion is that after the alloy reaction, the entirety of the electrode is a lithium alloy. In the conversion method, the electrodes undergo a complete transformation as the lithium bonds with one element of the existing molecule, leaving a lone element. With this transformation of materials, it should be noted that a change in structure may severely alter the volume of the electrode, which can pose many problems within a cell. Volume expansion and contraction can create disconnects within the cell, either between electrode-collector, and electrode-separator. While alloy and conversion methods have attractive qualities, there are drawbacks that must be overcome.

An intercalation (or "insertion") compound acts as the host structure, with room for guest atoms to be inserted and extracted with no rearrangement of the host structure because these materials have space between the host atoms to allow transport of the working ions [46]. These host structures usually take the form of a layered structure, such as graphite shown in Fig. 2.2,

where the host structure forms slabs and the guest atoms travel between those slabs. The other from of host structure is referred to as the framework structure, but it is more specifically known as spinel or olivine, such as $Li_4Ti_5O_{12}$ in Fig. 2.1, where the guest travels between interstitial sites within the host's structure [46]. While these terms are used interchangeably within this paper, it should be noted that generally "intercalation" is used for electrodes with a layered structure, while "insertion" is used more for materials that have a framework structure relying on interstitial sites [47].

2.2.1 Anode

The three most common anodes used in commercial batteries are lithium, $Li_4Ti_5O_{12}$ (LTO), or carbon. The ideal anode for a lithium ion-based battery is uncharged lithium metal, because of its high theoretical capacity and low electrochemical potential [48].

A pure lithium anode has an impressive theoretical capacity of 3,860 mAh/g [49]. This does not fall into one of the "alloy, conversion, or intercalation" categories, as the process of Li^+ attaching to the Li anode is called "plating" [48]. A pure Li anode is not commonly used though, due to the common issues that arise such as, depletion and decomposition of the electrolyte, thick SEI layers (which removes Li from the electrochemical reactions within the cell), dendrite formation and the large volumetric expanse [50]. On top of that, Li metal anodes have been shown to be unstable with any organic solvents within electrolytes, as significant side reactions between the two causing a passivation film, often called solid electrolyte interface (SEI) [51]. This dendrite can pierce the separator and cause an internal short circuit.

LTO is a conversion electrode with a spinel framework, as seen in Fig. 2.1, whose chemical reaction is shown here:

$Li_4\ Ti_5O_{12} + 3Li + 3e^- \rightarrow Li_7Ti_5O_{12}$ [52]

Unfortunately, LTO also has a high redox potential (1.55 V vs Li^+/Li), which is less ideal for the anode, but it does undergo minimal volume change with lithium insertion [54]. Because of the high redox potential vs. lithium metal, LTO has a lower operating voltage, and subsequently a lower energy, than compared to other anodes such as graphite. LTO does not have particularly good conductivity or Li^+ diffusion coefficient (less than 10^{-13} cm^2 s^{-1}) [55]. While LTO has some benefits over graphite, such as being more thermally and cyclically stable [53]. LTO's theoretical capacity is 170 mAh/g, which is much lower than lithium and about half that of graphite [6].

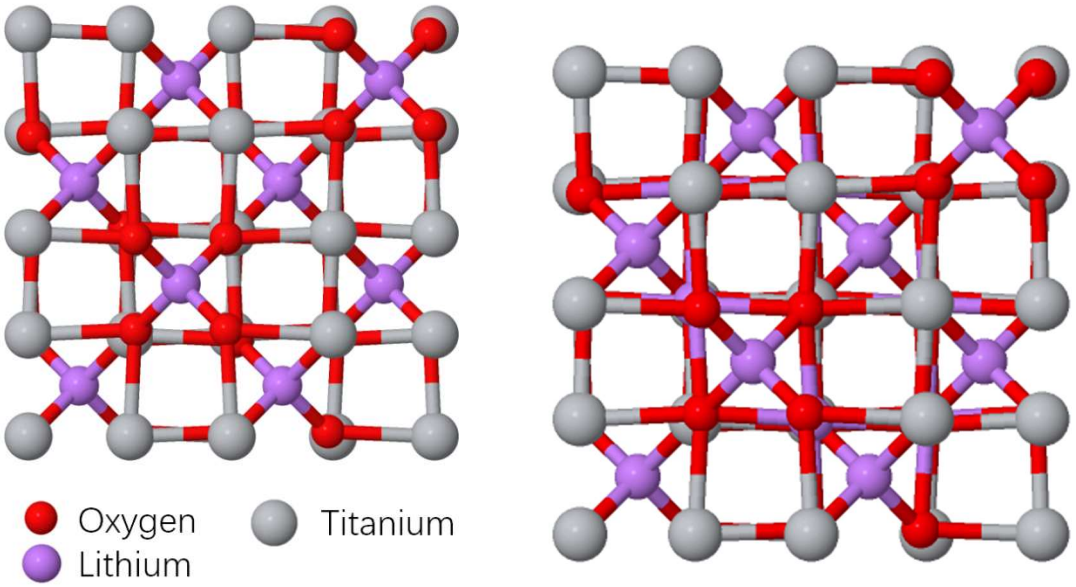

Fig. 2.1: Delithiated and lithiated LTO. **Left**: $Li_4Ti_5O_{12}$ **Right**: $Li_7Ti_5O_{12}$. See Fig. H.1 in Appendix F for isometric comparisons.

Carbon materials are separated into two groups, graphitizable and non-graphitizable, with the former being preferential for use as the anodes due to its high crystallinity [56]. The high power of modern commercial LIBs is achievable due to graphite's low electrochemical potential (0.25 and 0.01 V) with respect to the Li^+/Li redox [57]. Unfortunately, graphite is limited to lower charge rates because at high rates of charge, the volume change from the insertion of

lithium atoms damages the host structure [57]. Graphite's theoretical capacity is ~372 mAh g^{-1} [58]. Due to the repulsion between neighboring lithium atoms within the hexagonal structure of LiC_6 is stronger than the binding energy of Li to C, which does not allow for neighboring sites to be lithiated [59]. As one can see in Fig. 2.2, there are several empty interstitial sites that are free, but only 1 in 6 is usable, severely limiting graphite's capacity.

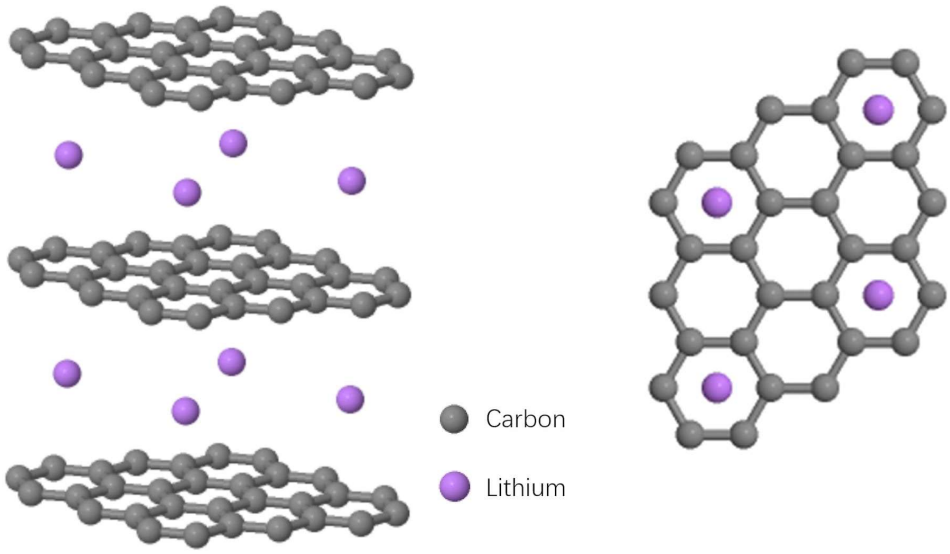

Fig. 2.2: Fully lithiated C_6 electrode. **Left**: Lithium is located in between the graphite slabs. **Right**: Top-down view showing vacant sites. Downloaded 6/23/21 "Graphite" by Nick Greeves is licensed under CC BY-NC-SA 2.0 UK.

There are many other anodes, this is not an exhaustive list. Currently, graphite is the most commonly used anode due to its abundance, incredible mechanical properties, voltage (when compared to Li^+/Li), and stability.

2.2.2 Transition Metal Oxide Cathodes

There are four main cathodes used in lithium-ion batteries: layered $LiCoO_2$ (LCO) & $LiNiO_2$ (LNO), spinel $LiMn_2O_4$ (LMO), and olivine $LiFePO_4$ (LFP) [60]. All four of these cathodes are intercalations materials. Within the cathode, the lithium ions are "intercalated", or inserted, into the interstitial sites of the host material while their respective valence electrons

enter an opening within the d-orbitals of the TM atoms [36]. It is common for transition metal (TM) oxides to be used as cathode material in secondary LIBs. TMs make promising electrodes due to their variable oxidation states, which easily allows for charge compensation as the lithium-ion is shuttled back and forth between anode & cathode [61].

The use of transition metal oxides as a cathode came to fruition because they met all of the "ideal" criteria for an electrode material [62]. Per Whittingham (2004), there are several requirements for a material to be successfully used as an intercalation cathode: [63]

1. Contains an oxidizable ion
2. Capable of reversible reactions with lithium (or another working ion)
3. Have a high capacity, at least one lithium atom per TM atom
4. Operate at voltages greater than 4V
5. High lithium intercalation/deintercalation
6. Be a good electronic conductor at all contact points of the electrolyte.
7. Immune to phase changes and degradation during normal operations
8. Low cost
9. Environmentally benign

Cathode material property advancement is a big focus within battery research since the rate and specific capacity tend to already be better in anodes than cathodes [64].

A limiting factor for most insertion electrodes' life is the volume change that occurs during charge/discharge, as this volume change creates cracks and contact losses between the electrode and the electrolyte/charge collector [65]. Because metal oxides have relatively low conductivity, the electrodes are created thin and flat to increase the surface area to volume ratio; increasing transfer rates and decrease impedances [66].

2.2.2.1 LiCoO2

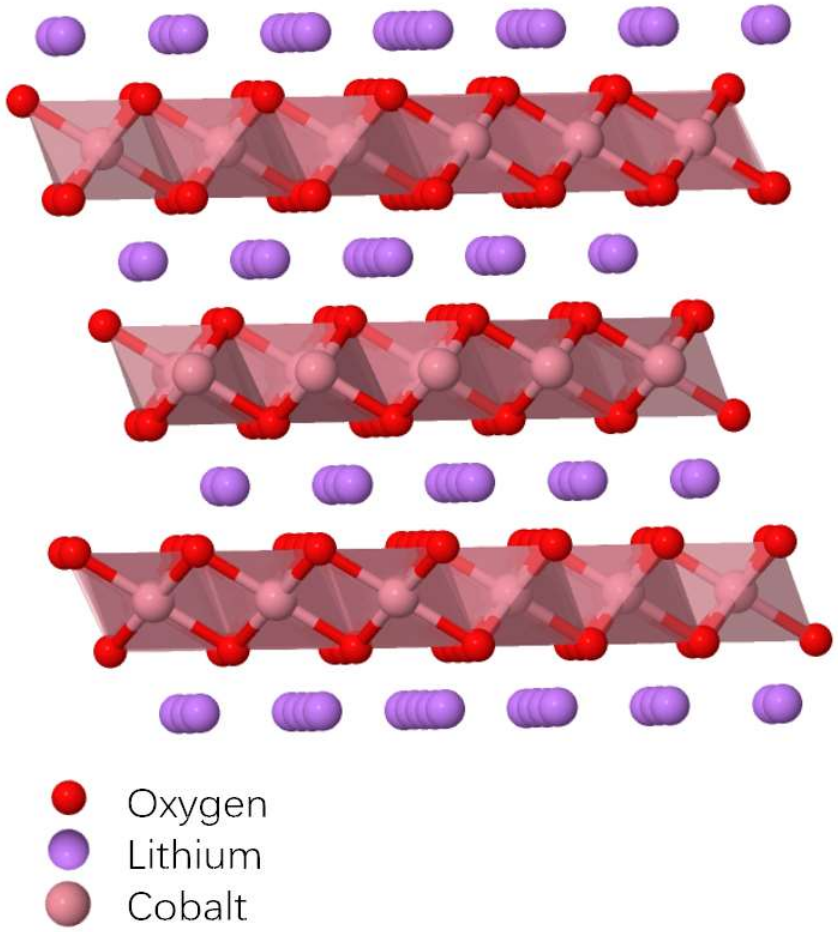

Fig. 2.3: LCO layered structure, showing intercalated Li atoms. Downloaded 6/23/21 "LCO" by Nick Greeves is licensed under CC BY-NC-SA 2.0 UK.

The most commonly used cathode in secondary LIBs is LCO, with a capacity of ~140 mAh g^{-1} [67]. This is only half of LCO's theoretical capacity (280 mAh g^{-1}) because as Li is removed from the layered lattice, the structure transforms from a hexagonal to monoclinic phase [68]. Ideally, LCO has a layered framework (space group R3-m) with the octahedral 3a and 3b sites of the cubic close-packed oxygen array being occupied by Co and Li, respectively [69]. If care is not taken in preparation though, the less ideal spinel like structure will form at low temperatures [70]. The CoO_6 arrangement, in an octahedral array, is attributed as the reason the cathode allows for ease of electron transfer [71]. During charging of LCO, the oxidation of Co^{3+}

to Co^{4+} is attributed to the decrease in lithium's ability to diffuse near the end of charge due to the stronger electrostatic interaction between Li and Co^{4+} [72]. LCO has a higher Li^{+} atom conductivity when compared to other TM oxides, but it is incredibly dependent on current lithium concentrations within the cathode. The Li^{+} conductivity varies in order of magnitude from ~10^{-11} – 10^{-7} cm^2/s, at 300 K in the typically 0%-50% delithiated state [40]. The higher conductivity is attributed to the greater slab spacing, the oxygen layers strong polarization towards the Co layers, and the ease in synthesis of ordered, stochiometric LCO [73]. The size of the lithium slab opening (referred to as the c-lattice) has a significant impact on lithium's ability to migrate within the layer (especially when compared to the effects of a- or b-lattice distances) due to the electrostatic repulsion between Li^{+} and Co^{3+} getting reduced [72].

In recent years there has been a push to move away from cobalt. Not only is it toxic and expensive, but the supply chain is questionable. A substantial portion of the world's Co supply comes from the Copperbelt of the Democratic Republic of the Congo, where it is estimated that 28% of the miners are under the age of 18 [74].

2.2.2.2 LiNiO2

Stochiometric LNO is in space group R3-m, as LCO see Fig. 2.3, with nickel located at octahedral 3a sites instead of Co, with lithium still occupying 3b sites [75]. Unfortunately, stochiometric LNO is not synthesizable due to its unstable structure.

It is important to have stochiometric LNO as it has been shown that as the Ni/Li ratio increases, the number of nickel atoms in the lithium layer increases [76]. The drift of trivalent nickel ions is attributed to the comparable size of lithium atoms to nickel atoms (0.62 Å and 0.70 Å at Ni^{+4} and Ni^{+3}, respectively), and the instability of the trivalent nickel ions [77]. This can

obviously hamper the capacity of the cell as the Ni atoms occupy sites that Li atoms could occupy, and increase the internal resistance by blocking pathways for Lithium diffusion.

2.2.2.3 $LiMn_2O_4$

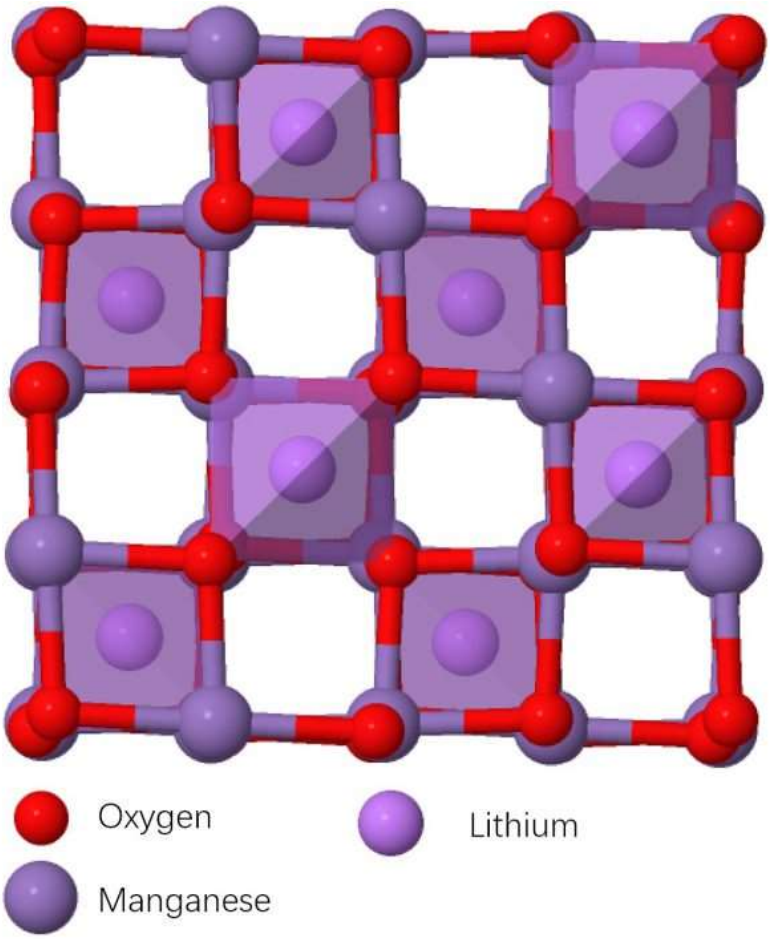

Fig 2.4: LMO's framework structure. Downloaded 6/23/21 "LMO" by Nick Greeves is licensed under CC BY-NC-SA 2.0 UK

Upon first charge the monoclinic crystal structure phase shifts into a hexagonal crystal structure upon oxidation of Mn^{3+} to Mn^{4+} and after several cycles, once 25% of the Mn ions have taken over lithium intercalation cites, it degrades again to a cubic spinel [78]. The spinel framework of $LiMn_2O_4$ allows for 3D interstitial locations for the lithium guest to quickly travel through the host structure [79]. On capacity fading mechanism that affects the actual cathode is the believed degradation to a less symmetric and more disordered phase close to the surface of

the electrode, is suspected to reduce the capacity by ~1/3 upon first cycling [80]. The main capacity fading mechanism of $LiMn_2O_4$/graphite cell is believed to be the Mn ion dissolution into the electrolyte and subsequent deposition onto the anode [81].

2.2.2.4 $LiFePO_4$

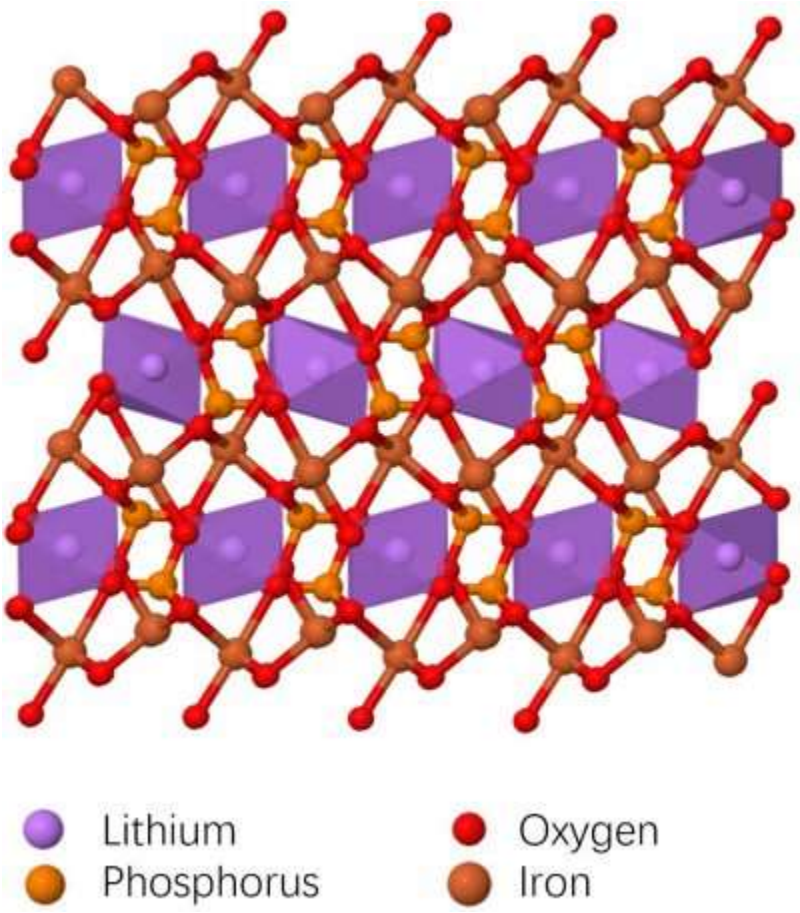

Fig. 2.5: LFP's spinel framework. Downloaded 6/23/21 "LFP" by Nick Greeves is licensed under CC BY-NC-SA 2.0 UK

$LiFePO_4$ is a cathode material with an ordered-olivine structure, giving it a theoretical specific capacity of 170 $mAhg^{-1}$ at a V = 3.45 V (vs. Li^+/Li) [82]. Generally, olivine structures are characterized as having lower voltages (compared to layered oxides) and their relatively long, flat voltage plateaus during charge and discharge make it difficult to measure the SOC of the battery [83].

2.2.3 Mixed Transition Metal Cathodes

Using a combination of TM metals is fairly common. One of the most common uses a combination of nickel, manganese, and cobalt, referred to as NMC. There are many versions of NMC, with the distinction being made between the ratios of each TM. For example, NMC333 is $1/3^{rd}$ nickel, $1/3^{rd}$ manganese, and $1/3^{rd}$ cobalt but NMC532 is 50% Ni, 30% Mn, and 20% Cobalt. The ratios of the various TMs within NMC vastly affect the properties. As nickel content increases, the cathode can obtain higher capacities but at the cost of thermal stability. Due to nickel ions reduction from Ni^{4+} to Ni^{2+} it is very unstable, whereas Mn is the much more stable, and Co is somewhere in between. The manufacturer of the tested batteries is just following this idea to try an create a more energy dense battery.

2.3 Electrolyte

The term aqueous electrolyte simply mean that it is a water-based solvent. Within aqueous electrolytes, the H^+ ions carry the Li^+ between electrodes [2]. The most common electrolyte is mostly comprised of non-aqueous solvents, salts, and a few other additives [84]. Commercialized batteries in the 1990s used $LiPF_6$ (a lithium salt) in carbonate solvents within the electrolyte, which is still common today as this electrolyte plays well with graphene [85]. Another benefit of $LiPF_6$ is that it creates an SEI layer of AlF_3 on the aluminum current collectors, preventing the collector from corrosion via the electrolyte [86].

Electrolytes consisting of molten salts, that are liquid at room temperate, either must be used with an anode of Li or an additive must be used to use the typical carbon anode [87]. The lower voltage for electrochemical stability of organic carbonate-based electrolytes is around 0.8 V *vs.* Li^+/Li [88].

2.3.1 Separator

The electrolyte and separator go hand in hand, one cannot discuss the electrolyte of a battery without discussing the separator. The separator is a porous material that is saturated in the electrolyte, which provides electrical insulation between electrodes, while still allowing transport of lithium ions [89]. It is particularly important that the separator allows for constant wetting of the electrode surface so that the electrochemical reactions can occur uninterrupted [90]. The separator must have three requirements, per [91]:

1. Chemically & thermally stable
2. Some shutdown function based on temperature (i.e., melting)
3. Compatibility with the electrolyte (specifically wettability and permeability)

2.3.2 SEI Layer

A pacification layer that forms at the solid electrolyte interphase is both required to achieve higher operating voltages but is a major cause of failure within the cell. $LiPF_6$ is an acidic species which will dissolve transition metal cations and create deposits of metallic clusters on the anode that weaken its SEI layer [92]. Proper SEI development is imperative for a functional high voltage cell, which is why these batteries are put through conditioning cycles after production [93]. Since the SEI is a passivation layer, or an electrochemically inert layer, which ideally prevents future parasitic reactions from occurring [94]. It should be obvious that a chemical reaction that reductions in the amount of active material in either the electrode or electrolyte will cause a decrease in the overall capacity of the cell, or general functionality.
Per [95], the ideal properties for an SEI layer are:

- High electrical resistance while maintaining both high cation selectivity and permeability
- Thickness close to a few nanometers

- High material strength
- Resistant to stresses caused by volume changes
- Insoluble in the electrolyte
- Stability over a wide range of operating temperatures and voltage windows

The listed ideal properties make sense because the failure mechanisms of the SEI are thermal, chemical, and mechanical [96]. Solvents and salts within the electrolyte may continually decompose (and thus, re-dissolve), or negatively react with, the SEI causing decreased columbic efficiency and inferior cycle performance [96]. It has been shown that regardless of anode type (intercalation, conversion, and alloying), unconstrained SEI growth factors into the irreversible capacity loss within the battery [97]. If the anode has a chemical potential less than 1.3 eV (below that of the electrochemical potential of lithium) a chemically inert layer forms between the anode and electrolyte, preventing reduction of the electrolyte by the anode [98]. The continued SEI growth occurs during discharge within layered cathodes due to anionic redox [99].

2.4 Importance of Testing

Battery testing is incredibly important, especially when people's lives are at risk. Earlier, the types of failure methods have been discussed, but the ramification of these failures needs to be made clear. There are three main types of failure when considering lithium-ion batteries: thermal (thermal runaway, fires, explosions), electrical (internal & external short circuits, over charging & over discharging), or mechanical (electrolyte leakage, separator tear, internal disconnects) [100].

The casing of the battery is its main resistance to mechanical failures such as deformation, piercing, or vibrations. If the casing gets bent or punctured there is a high likelihood of the separator getting torn or flammable electrolyte leaking out [101]. Since the

separator is supposed to prevent the electrodes from touching, a tear can lead to an internal short circuit.

A short circuit can occur internally or externally, either way, a short circuit is obviously a bad thing as the electrons are allowed to flow unimpeded from anode to cathode. Since the ion diffusion rate within the battery is smaller than the electron transfer rate, the ions are met with a large resistance as they quickly try to move between electrodes to balance the charge. During either type of short, a high current occurs which causes rapid Ohmic heat generation [102]. Similarly, if the charge or discharge rate of the battery is too high heat will also be generated, as this will simulate a short which can cause a thermal failure within the cell with heat and gas generation.

There is a hierarchy of failure methods. While each failure mode may occur on its own, there is a clear relationship where the mechanical failures may lead to internal shorts, which may lead to thermal runaway. It is of some significance that they follow the same trend for safety. If only mechanical failure occurs, worst case some electrolyte gets spilt. If electrical failure occurs, the cell becomes unusable. Generally, if thermal failure occurs, there will be some degradation of the cells' capacity. But if thermal failure propagates into thermal runaway, there will certainly be a fire, assuming a flammable electrolyte and oxygen generation is present. On the latter, this increase in gas and heat can easily cause an explosion.

2.4.1 Examples of industry failures

There are many examples of batteries used in commercially available portable electronics posing serious health concerns. In early January 2013, there were two separate incidents with the lithium-ion battery packs that caused all Boeing 787 Dreamliners to be grounded until the issues could be resolved. The first occurred on the 7th of January, in Boston, where a battery fire

occurred in a parked Dreamliner's auxiliary power unit [103]. Just 9 days later, on the 16th of January, a battery failure caused a 787 from All Nippon Airway to make an emergency landing (landing at Takamatsu Airport in Kagawa, Japan) only 36 minutes into its flight [103], [104]. While no official cause of failure was found, it is suspected that one of the cells of the battery pack developed an internal short circuit, causing heat generation to the point of thermal runaway and spreading to the adjacent cells [104].

The requirements for the battery safety required that the batteries installed on the 787 should have a probability off less than 1 failure in 10,000,000 flight hours [105]. In actuality, the lithium batteries installed on the Dreamliners experienced 2 failures in ~50,000 flight hours [103]. There are numerous other examples of LIBs causing fires on passenger and cargo planes alike. From January 23^{rd,} 2006-May 31, 2021, the FAA has cataloged over 316 lithium-ion battery events "with smoke, fire, extreme heat or explosion" [106].

In 1988, Moli Energy had to recall its first battery called the Molicel, a MoS_2 cathode with a pure Li anode, due to numerous fire incidents that occurred in cell phones [5]. As discussed previously, using a pure lithium anode leads to dendrite formation. This short-circuit inducing mechanism can easily start thermal run away from the heat generated. Model S In 2016, the Samsung Galaxy Note 7 was recalled due to battery fires and explosions. The cause is believed to be internal short circuiting due to poor battery design as they made the separator too small, allowing a short circuit to occur, followed by thermal runaway [107]. The positive and negative electrodes were allowed to contact within the phone, ultimately resulting in thermal runaway. Similarly, to what happened on All Nippon Airway's 787, in 2018 a large grid storage system caught fire in Lingyan, South Korea [108]. Once one cell failed thermally, its heat dissipated to the surrounding cells, causing a snowball effect.

These failures should never have occurred in the first place, people were harmed because adequate testing was not done prior to implementation. If any of these failures occurred, especially ones with fire, occurred on the ISS or other manned spacecraft, there would be dire consequences for the crew. Oxygen is already limited for them, and a fire will quickly consume whatever oxygen it can interact with.

3 Measurements and Tests

3.1 Battery Basic Documentations

The batteries used in this experiment were COTS lithium polymer pouch batteries. Being COTS, they came with a built-in over-charge/discharge protection circuit pre-attached to the current collectors, see Fig. 3.1. This circuit causes an incredibly small amount of current flow, even while the cell is at rest. While small, the constant current was enough to cause the batteries to fail the 14-day OCV, which is discussed later.

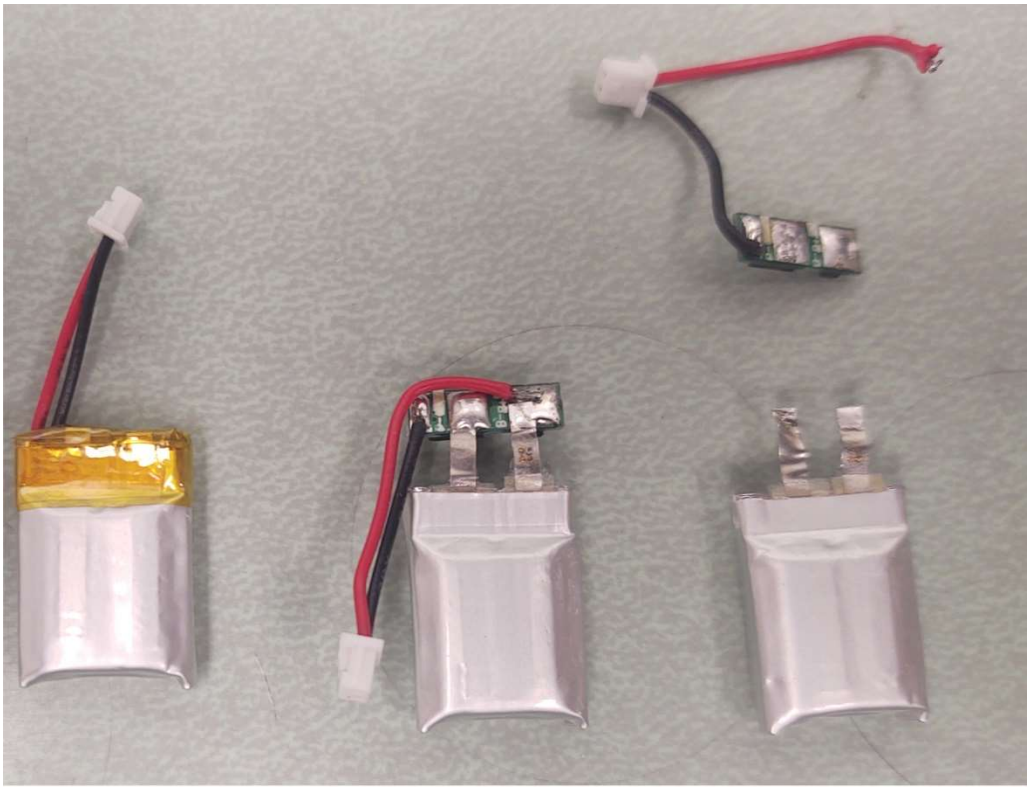

Fig. 3.1: LiPo batteries being prepped for testing. **Left**: COTS battery with manufacturer's stickers removed. **Middle**: Unraveled with safety chip still attached. **Right**: Battery disconnected from safety chip.

To circumvent the small current, the protection chip was removed by desoldering the connectors to the battery collectors. A heat of 375 °C was used to melt the solder, while a desoldering pump was used to remove the liquid solder. During this preparation, it was important

to minimize heat exposure to the current collectors, as they are thermally conductive and attached directly to the temperature sensitive electrodes.

3.2 Temperature Measurements

Throughout the rest of the testing outlined in this section, the temperature of each battery was measured. This was done by using negative temperature coefficient thermistors in a simple voltage divider arrangement, see Fig. 3.2 for 14-day OCV and vacuum chamber testing, see Fig. 3.3 for Charge-discharge and B-value verification. As thermistor X, TR_x in Fig. 3.2, changes temperature, it's resistance will change proportionally based on Eq. 3.1, altering the value of V_{Out}.

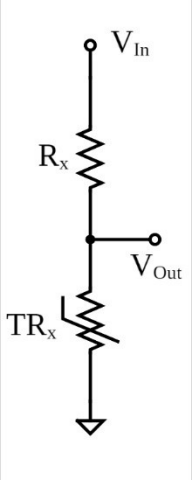

Fig. 3.2: Simple voltage divider use for 14-day OCV testing. Circuit drawings created on https://www.circuit-diagram.org/, altered and finalized with BioRender.com.

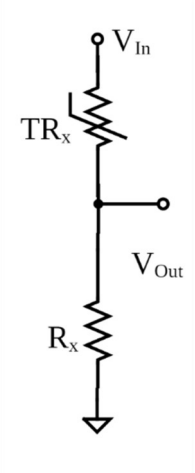

Figure 3.3 Simple voltage divider used for charge-discharge circuit and B-value verification. Circuit drawings created on https://www.circuit-diagram.org/, altered and finalized with BioRender.com.

$$TR_x = TR_{x,0} * e^{\beta\left(\frac{1}{T}-\frac{1}{T_0}\right)} \quad (3.1)$$

Where, TR_x and $TR_{x,0}$ are the resistance of the thermistors at absolute temperatures T and T_0, respectively. R_x is the resistance of the resistor at position X.

By measuring V_{In}, V_{Out}, and R_x and using those values with Eq. 3.2 it is possible to calculate the resistance of TR_x, and thus calculate the temperature of the thermistor.

$$TR_x = \frac{R_x}{\left(\frac{V_{in}}{V_{out}}-1\right)} \quad (3.2)$$

Once TR_x is known, it can be plugged into Eq. B.1 in Appendix B. This equation is just a rearranged version of Eq. 3.1, solving for T instead of TR_x. The B-value is a constant unique to the thermistor. This value is given by the manufacturer but it will need to be verified for each thermistor using a climate control chamber and Eq. B.2 in Appendix B. As with Eq. B.1 this is just a rearranged form of Eq. 3.1. For each thermistor, $TR_{x,0}$ and T_0 will be taken from the climate control chamber B-value measurements.

The full thermistor schematics can be found in Fig. A.1-A.3 in Appendix A. Each thermistor circuit shown is used for a different test. The thermistor circuit uses a voltage

regulator to output a steady 5 V, which is verified at the point V_{in} with the DAQ, which will also measure V_{Out}. With known values for R_x, V_{in}, and V_{out} one can calculate the thermistors resistance. Then with the known B- values, reference resistances and temperatures, the battery temperature can be monitored easily. Depending on the test, the thermistor circuit was used to monitor temperature continuously throughout the entire test, or just periodically in the case of the 14-day OCV.

The calculation for the B-constant value require the resistance of the thermistor at two temperatures, as can be seen in equation 3.1. The temperature points for these B-value calculations were chosen at 253.15K and 333.15K, as these would cover the extreme cases that these batteries would experience. This verification ensures that the battery temperatures were recorded accurately during the battery testing. Measuring the temperature of the batteries is imperative because the characteristics of the battery are so heavily dependent on the temperature. An elevated temperature can be an indicator that undesirable side reactions are occurring between the cathode and the electrolyte. A thermometer was used to verify the temperature of the climate chamber

3.3 Visual and Physical Properties

After the protection circuitry was removed, an inspection for physical deformities was conducted. All stickers were gently removed, to avoid damaging the cell's pouch casing. Any adhesive left by the stickers were removed by wiping the area using isopropyl alcohol (IPA) on a paper towel. Once the exterior was clean, any noticeable scrapes, dents, bulges, or scratches were recorded. Any exterior marking is an indication that the battery was damaged after being manufactured, and it should be noted in case future problems arise.

Each battery was then serialized with a label maker, using the naming convention α#, where α is a letter denoting which test batch the cell was in, and # being the number within that batch. The non-flight batteries had 10 in each batch, but the flight batteries were grouped by the dozen. Care was taken to ensure that the current collectors always faced to the left when applying the serial number. This ensured that the negative and positive leads were in the same location when the serial number was facing up see Fig. D.8 in Appendix D. This made it easier to attach the color-coded alligator clips, as seen in Fig. D.8 to the correct electrode. The battery stand was designed to prevent external shorts and be able to hold the thermistors in place.

The dimensions of the batteries were then measured as shown in Fig. 3.3 with 0.1 mm accuracy, and their mass measured, within 0.1 g accuracy. Dimension definitions are defined by the orientation of the serial number on the cell. The length is defined as the horizontal distance with the serial straight up, width is the vertical distance with the serial standing up, and the height is the smallest dimension as shown in Fig.3.3. These measurements were conducted again after all of the experimentation outlined in this section. Any significant change in the change of volume or mass may be an indication that undesirable reactions are occurring, and thus the battery pose a danger of failing.

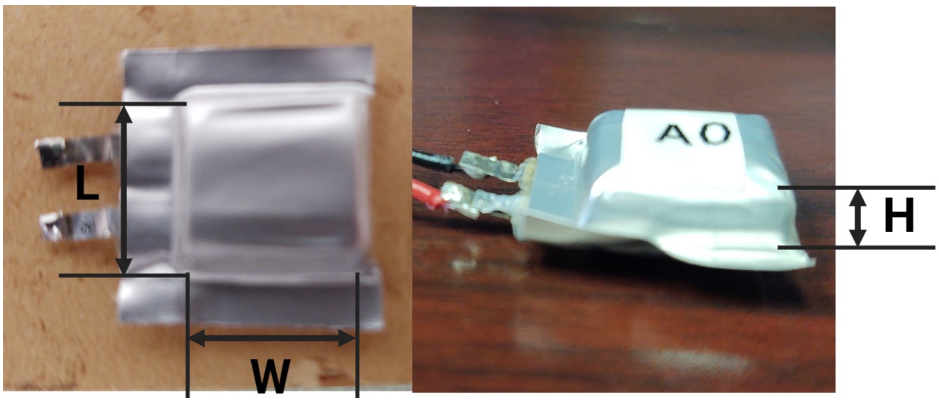

Fig. 3.4: Battery dimensions as defined by the FAT-C requirements. Figure created with BioRender.com

3.4 14-Day Open Circuit Voltage

The 14-day open current voltage testing is to measure the degradation of the battery in storage conditions. After the charge-discharge circuit, see Fig. 3.5, was verified to be operating as intended, a copy of the working LabView code was altered so that it only conducted a single discharge cycle. This single discharge cycle was used to discharge the flight batteries to a voltage of 3.6 V at a rate of C/2, or 50 mA for the batteries in this thesis. After reaching the discharged state, the LiPo batteries were left at room temperature for 14 days.

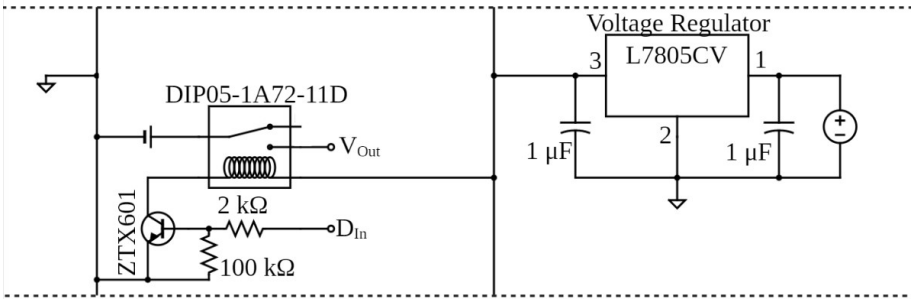

Fig. 3.5: An enlarged view of the circuit showing only the voltage regulator (right) and a single battery measurement. Circuit as provided by Dr. Huang, circuit drawings created on https://www.circuit-diagram.org/, altered and finalized with BioRender.com.

Note that Fig. 3.5 is only part of the circuit, the battery & relay combination are repeated a total of 11 times to allow for 12 batteries to be tested at a time. A full schematic showing all 12 battery connections can be found in Appendix A, Fig A.4. The actual setup can be seen in Appendix D, Fig. D.2.

Referring back to Fig. 3.5, 8 volts is provided to the L7805CV voltage regulator, which outputs 5 V at node 3. The capacitors connecting either side to ground are bypass capacitors which help ensure a more constant, “clean”, DC voltage. Every hour, the computer will put “D_{in}” to the high state (~5V), which causes the transistor to allow current flow, closing the normally open DIP05-1A72-11D relay. Once the relay is closed, the open circuit reference single ended (RSE) voltage of each battery was able to be recorded, 500 readings at a sampling rate of 1 kHz.

The RSE compares the measured voltage to ground, so the cell's negative collector was attached to the same ground as the DAQ to ensure accurate readings.

The number of readings was chosen so that an average could be taken for each measurement to account for any settling time the DAQ would need. The relays ensure the battery was completely disconnected between measurements to prevent any capacity draining other than the self-discharge that is being monitored. The rejection criteria for this test was a drop of more than 2 mV in the OCV from the first voltage measurement.

3.5 Charge-Discharge Cycling

The charge-discharge cycling is used to verify the stability of the cells over multiple cycles. A cell with a changing capacity can indicate an unstable chemistry or design. To test the cell's ability to hold charge after cycling, a circuit was created to charge and discharge the battery under a constant current of C/2 (50 mA). The batteries being tested followed the following testing cycle:

- Charge 1
- 10-minute rest (Rest 1)
- Discharge 1
- 10-minute rest (Rest 2)
- Charge 2
- 10-minute rest (Rest 3)
- Discharge 2
- 10-minute rest (Rest 4)
- Charge 3

In this charge-discharge circuit, see Fig. 3.4, there are two voltage regulators, one provides a positive 12 V, MC7812CT, while the other provides a negative 12 V, MC7912CT. These ±12V are used as the power supplies for the OpAmp1 and OpAmp2, both OPA547T. It should be noted that Fig. 3.4 only shows the setup for one battery. The full schematic can be seen in Fig. A.5 of Appendix A.

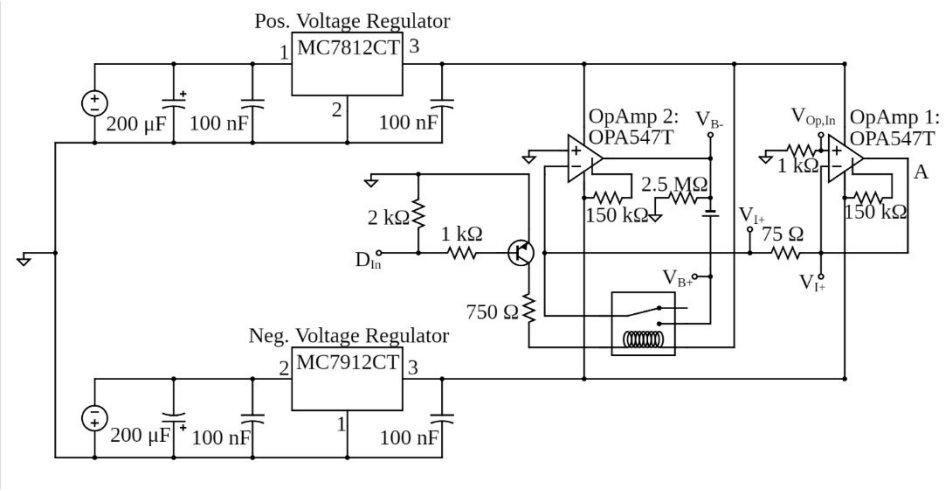

Fig. 3.6: Simplified schematic of charge-discharge circuit, showing the setup for measurement of one battery only. Circuit as provided by Dr. Huang, circuit drawings created on https://www.circuit-diagram.org/, altered and finalized with BioRender.com.

Similar to the circuit presented before, this one uses multiple capacitors to provide a "clean" DC current. There are also two OpAmps in what is called a voltage follower setup. OpAmp 1 acts as the initial voltage follower, where the voltage supplied from the DAQ at $V_{op,in}$ is also the output note of OpAmp1, see "A" in Fig. 3.5., controlling the current that is forced through the battery when the digital signal in, D_{in}, is set to the on state. The value of V_{op} is determined by the measured resistance of the 75Ω resistor, R, and the ideal charge or discharge current I, 50 mA and -50 mA, respectively. Using these values with Ohm's law, Eq. 3.3, gives the required voltage to V_{op} to ensure a constant current of 50 mA.

$$V_{Op,in} = IR \tag{3.3}$$

With OpAmp 2 acting as another voltage follower to stabilize the current & voltage out of OpAmp 1. At multiple points within the circuit the voltage is measured to verify current flow (V_{I+} & V_{I-}), battery voltage (V_{B+} & V_{B-}), and that $V_{Op,In}$ is providing the expected value.

Once the battery hits the set cutoff voltage, D_{in} and V_{op} are set to 0 V to ensure no current flows during the rest period. The 2.5 MΩ resistor on the negative end of the battery is simply to prevent a floating ground. This test was intended to be performed immediately after the 14-day OCV test, as outlined in section 3.4, so usually the batteries started in the discharged state. The charge-discharge test was setup to only handle 6 batteries but the previous 14- day OCV was able to measure 12, the remaining 6 were charged back to ~3.75 V. This is the ideal voltage to prevent degradation of the battery while it is resting.

As with the 14 Day OCV, the batteries were discharged to a voltage of 3.6 V during the discharge cycles. They were charged to full capacity, 4.2 V, during the charge cycles. During the test, the cell voltage, charge & discharge current, and relay signals was constantly measured at a sampling rate of 1220.703125 Hz. This sampling rate was chosen specifically to align with the DAQs' on-board analog clocks to ensure that the time between measurements was precise and constant. The ~1.2kHz sampling rate was chosen because it was compatible with all DAQ's used in this test. More information can be found in Appendix G.

All measured voltages were plotted into graphs; one with all cycles shown, and each of the charge/discharge cycles plotted separately. The data was used to calculate capacity by averaging the measured current, theoretically it should be fairly constant, and multiplying it by the length of time that a cycle took.

3.6 Vibrational Shock Testing

Vibrational testing to look for internal shorts and capacity fade will make sure the batteries are physically capable of making the trip. The vibration test uses a random vibration testing spectrum, as opposed to a more commonplace sinusoidal sweep, along each of the three axes of the battery. The vibrational spectrum is followed for one minute per axis. Before the vibration test is conducted, and after each axis of vibration, the OCV of the flight cells is measured.

After this test was performed, the charge/discharge cycle test, as outlined in section 3.5, is performed again so that the capacity of the cell could be re-measured. The criteria for flight acceptance is a less than a 0.1% change in the OCV and less than a 5% change in capacity after the vibration test. This testing and its setup are outside of the author's research but it is required for the batteries to be used in flight acceptance. As mentioned earlier, the actual conducting of this test is outside of the scope of this thesis.

3.7 Vacuum Chamber Testing

As with the vibration testing, this was just to make sure that the batteries will not rupture in the vacuum of space. As outlined in section 3.3, the dimensions of each cell are measured as well as the mass of each cell. All the cells were then charged, and their OCV measured. The fully charged batteries are placed into the vacuum chamber, which is then evacuated at approximately 8 psi/minute. The vacuum of 8 to 10 psi is held for 6 hours for flight acceptance leak test for LiPo batteries. In addition, the pouch cell designs should be leak tested with the pressure restraints on the wide faces of the cells.

The chamber is then re-pressurized to ambient pressure at a rate of 9 psi/minute. The batteries are then inspected for any leaks, deformations, or bulges. The dimension and mass of each cell are then remeasured. The pass/fail criteria for a change in the dimensions are not

specified, but a change of 0.1% or greater in mass is not acceptable. As stated in the charge/discharge section, the charge/discharge cycle is repeated once again to measure the capacity of the cell to ensure there has not been a change in the capacity. As mentioned previously, the actual conducting of this test was outside the scope of this thesis.

4 Results & Discussion

The overall goal of the experimentation conducted for this thesis was to create a setup that could be used for flight acceptance testing of any COTS batteries. The tested LiPo batteries were separated into “Non-flight” and “Flight” batteries. Batches A and B are non-flight batteries and were used for setup testing and verification only. Most of these are not operational anymore due to various external short circuits, over discharging, over charging, or discharging too quickly.

Flight batteries were batches C, D, and E. Batches C-E are the only ones discussed in this section as they show that the testing setups are functioning. Based on manufacturer provided information, see table 2.1, the tested batteries are primarily LCO/Graphite cells. As presented earlier, the typical capacity for LCO is ~140 mAh g^{-1} . This will be used for comparison later.

4.1 Temperature Measurements

Thermistors were simply number 1-24, since each thermistor circuit was setup to be assigned to a specific test and did not change between batches. Numbers 1-12 were used on the 14-Day OCV, 13-18 were used in the charge-discharge testing, and 19-24 will be used in the vacuum chamber test. The verification on the thermistor B-values is presented in this section. The measured Rx resistances, and voltages are given in tables F.1-F.4 in appendix F. Those values were used to calculate the resistance of each thermistor at both 253K and 333K, as shown in table 4.1.

Table 4.1: Calculated thermistor resistances at 253K and 333K.

Thermistor Number	Calculated Thermistor Resistance [253K] (Ω)	Calculated Thermistor Resistance [333K] (Ω)
1	80,373	3,306
2	82,686	2,856
3	64,938	2,714
4	94,958	2,643
5	94,457	2,650
6	95,550	2,627
7	75,448	2,601
8	95,912	2,598
9	94,414	2,603
10	93,256	2,626
11	92,884	2,602
12	92,364	2,647
13	93,767	2,635
14	93,801	2,597
15	93,217	2,601
16	94,020	2,626
17	93,219	2,613
18	93,035	2,606
19	59,767	2,724
20	90,993	2,632
21	89,667	2,597
22	91,047	2,606
23	95,549	2,688
24	57,165	2,620

These were used with Eq. 3.2, presented before, to calculate out the resistance of each thermistor at 253.15 K and 333.15 K. The calculated resistance of the thermistors was used with Eq. B.2 to calculate the actual B-values for each thermistor. The results of the thermistor resistances and their corresponding B-values are presented in Table 4.2.

Table 4.2: Calculated B-values of thermistors.

Thermistor #	Calculated Thermistor B-Value
1	4,477.771
2	4,538.704
3	4,103.136
4	4,784.742
5	4,768.033
6	4,810.995
7	3,316.673
8	3,757.398
9	3,755.948
10	3,684.519
11	3,713.996
12	3,700.831
13	3,749.803
14	3,763.694
15	3,757.944
16	3,756.793
17	3,750.067
18	3,744.848
19	2,871.129
20	3,662.856
21	3,640.536
22	3,653.679
23	3,754.164
24	2,826.461

Temperature measurements taken throughout the experimentation are discussed with their respective tests.

4.2 Electrochemical Characteristics (14-Day)

There was initial struggle with too much self-discharge, but it became clear that the pre-attached safety circuitry was the cause. Once these issues had been addressed by removing the attached safety chip the 14-day OCV was conducted on the remaining batches as intended. The

top, green horizontal lines in the figures represent the first measured OCV, and the bottom, red horizontal line shows the 2 mV drop limit. As long as the graph stays above the bottom line, the batteries meet this flight acceptance criteria.

In Appendices E.2 & E.3, it can be seen that all but E1 easily meet the listed 14-day criteria. On all of the graphs, all the batteries follow the same trend: fairly quick voltage recover, followed by a slow drop in voltage. This voltage recovery is attributed to inconsistent electron concentrations across the electrode that form during charge or discharge. As times goes on, these concentrations even out. From these results, it can be seen that there is little self-discharge of the cell, indicating electrochemical stability.

Another interesting trend occurs when the thermistor temperatures are plotted alongside the 14-day results. One can see the voltage increasing and decreasing with significant spikes in temperatures. This can be most readily seen in Fig. E.46 & E.47 (Appendix E.3)

Since these temperature fluctuations occur at roughly the same point in time for each battery (during their respective tests), it indicates that the ambient temperature within the lab was fluctuating. If the temperature variation was due to faults within the cell, it is unlikely that they would all change in temperature and voltage at the same time and by roughly the same amount. A fault would also cause problems in future experiments.

4.3 Charge-Discharge Cycling

Figures I.1 –I.58 in Appendix I show the voltage vs time plots for each battery as well as their respective temperatures. There are 6 plots per battery, one showing the entirety of the charge-discharge testing cycles, and the rest show the individual charge or discharge cycle for an enlarged view.

There are periodic oscillations of the voltage measurements. Initially, the vibrational responses were suspected as being caused by environmental affects or from the high sampling rates used for the DAQs. The environmental cause seems the most likely, as the increased amplitude occur at roughly the same time on each graph. Unfortunately, there was not enough time to conduct the experiment again in a sealed environment to see if the oscillations still occurred.

From the charge-discharge tests, capacity was calculated for each battery during each cycle. Those results are given in Tables 4.3-4.5 for the average charge, discharge, and calculated specific energy of each battery. The capacity of the cell was taken as the average over the two discharge cycles, as that is the capacity that can be utilized. The specific energy was calculated by dividing the average discharge capacity by the mass as given in Tables F.5-F.7 in Appendix F. The average charge capacities are given to see if theory holds up. The charge capacity should be greater than the discharge capacity due to columbic inefficiencies. The capacity values will be recalculated after the vibrational test is conducted.

Table 4.3: Measured capacities of Batch C

Serial Number	Average Discharge Capacity (mAh)	Average Charge Capacity (mAh)	Specific Energy (mAh g^{-1})
C2	72.4	72.4	34.5
C3	70.0	69.8	33.3
C4	72.6	72.6	34.6
C5	68.8	68.6	32.8
C6	71.5	71.4	34.0
C7	72.6	72.5	34.5
C8	71.1	71.0	33.8
C9	71.2	71.1	33.9
C11	74.4	74.5	35.4
C12	70.7	70.7	33.6

Table 4.4: Measured capacities of Batch D

Serial Number	Average Discharge Capacity (mAh)	Average Charge Capacity (mAh)	Specific Energy (mAh g^{-1})
D1	72.4	72.7	34.5
D2	75.2	75.5	35.8
D3	72.6	72.8	34.6
D4	73.9	74.1	35.2
D5	25.3	36.6	12.0
D6	73.5	73.7	35.0
D7	73.9	73.8	35.2
D8	68.3	73.0	32.5
D9	69.9	71.8	33.3
D10	69.8	72.1	33.2
D11	70.3	70.7	33.5
D12	69.3	72.2	33

Table 4.5: Measured capacities of Batch E

Serial Number	Average Discharge Capacity (mAh)	Average Charge Capacity (mAh)	Specific Energy (mAh g^{-1})
E1	74.0	74.2	35.2
E2	72.1	72.3	34.3
E3	74.0	74.1	35.2
E4	67.4	67.6	33.7
E5	71.5	71.7	34.0
E6	73.2	73.4	34.9
E7	72.8	73.0	34.6
E8	75.1	75.3	35.7
E9	73.3	73.4	34.9
E10	68.3	68.2	32.5
E11	71.7	71.9	34.1
E12	70.5	70.2	33.4

The astute reader will notice that C1, C10 are missing from Table 4.3. This is due to errors in initial testing that caused them to be short circuited, resulting in them being unusable.

5 Conclusions

In the author's opinion, the testing procedures created for this thesis demonstrated they meet the explicit criteria as set forth by NanoRacks. These testing procedures were developed with the intent on being flexible enough to allow for future testing of other hobby grade batteries so that they may be used in space applications. Ultimately it is up to the discretion of NanoRacks to determine if these specific were met.

The physical properties of the batteries were measured before the testing began (see Appendix F, Tables F.1, F.3, & F.5). For the thermistors to be used, their B-values were measured using a climate-controlled chamber. This allowed for accurate temperature readings during the other testing.

While this step cannot easily be automated, it was done methodically to ensure consistency in measurements. The 14-day OCV testing was successfully automated to read the open circuit voltage of 12 batteries every hour over the course of 14 days. The voltages from the thermistor circuit were also successfully automated so that battery temperatures could be measured at the same time interval.

The most difficult goal to address was the charge-discharge cycle, but it was successfully created. The created cycle forces a chosen constant charge current or discharge current, as required, through 6 batteries, and will stop the current when the battery voltage reaches the set cutoff voltage. This cycle also records each battery's voltage and current so that its capacity can be measured. Being able to dictate the C-rates and cutoff voltages for both charge and discharge allows this setup to be adapted to other batteries with ease. As with the 14-day OCV, the thermistor voltages also record at a set rate so that the temperature of each battery can be

measured throughout the testing. Given the current results of the tests performed, these procedures will continue to be valid for future space missions.

Bibliography

[1] Holze, R. (2014, June). Anodes–materials for negative electrodes in electrochemical energy technology. In *AIP Conference Proceedings* (Vol. 1597, No. 1, pp. 44-65). American Institute of Physics. https://doi.org/10.1063/1.4878479

[2] Goodenough, J. B., & Kim, Y. (2011). Challenges for rechargeable batteries. *Journal of Power Sources*, *196*(16), 6688-6694.

[3] Wallis, L., & Wills, R. G. A. (2014, June). Anodes-Technology review. In *AIP Conference Proceedings* (Vol. 1597, No. 1, pp. 146-154). American Institute of Physics. https://doi.org/10.1063/1.4878485

[4] Liu, B., Jia, Y., Yuan, C., Wang, L., Gao, X., Yin, S., & Xu, J. (2020). Safety issues and mechanisms of lithium-ion battery cell upon mechanical abusive loading: A review. *Energy Storage Materials*, *24*, 85-112.

[5] Winter, M., Barnett, B., & Xu, K. (2018). Before Li ion batteries. *Chemical reviews*, *118*(23), 11433-11456.

[6] Scrosati, Bruno Abraham, K. M. Schalkwijk, Walter Van Hassoun, Jusef. (2013). *Lithium Batteries - Advanced Technologies and Applications.* John Wiley & Sons. Retrieved from https://app.knovel.com/hotlink/toc/id:kpLBATA003/lithium-batteries-advanced/lithium-batteries-advanced. Accessed on 5/20/21.

[7] Schechner, S. (2015). The Art of Making Leyden Jars and Batteries According to Benjamin Franklin. *eRittenhouse*, *26*.

[8] Franklin, B. (1751) Experimental and observations on electricity, made at Philadelphia in America

[9] Krepelková, M. (2017). Evolution of batteries: From experiments to everyday usage. In *21th International Student Conference on Electrical Engineering*.

[10] Warner, John. (2015). *Handbook of Lithium-Ion Battery Pack Design - Chemistry, Components, Types and Terminology.* (pp. 13) Elsevier. Retrieved from https://app.knovel.com/hotlink/toc/id:kpHLIBPDC3/handbook-lithium-ion/handbook-lithium-ion. Accessed on Knovel on 6/8/21

[11] Attewell, A. Review of Reserve Battery Technology. Proceedings of the 4th battery seminar and exhibition, London, 29 January 1985: Maintenance free batteries for standby power.

[12] Cleveland, Cutler J. Morris, Christopher. (2009). *Dictionary of Energy (Expanded Edition).* (pp.292) Elsevier. Retrieved from https://app.knovel.com/hotlink/toc/id:kpDEEE0001/dictionary-energy-xpanded/dictionary-energy-expanded accessed 6/8/21

[13] Boddula, Rajender Inamuddin Pothu, Ramyakrishna Asiri, Abdullah M.. (2020). (pp. 21) *Rechargeable Batteries - History, Progress, and Applications.* John Wiley & Sons. Retrieved from https://app.knovel.com/hotlink/toc/id:kpRBHPA003/rechargeable-batteries/rechargeable-batteries accessed 6/8/21

[14] Yoshino, A. (2012). The birth of the lithium-ion battery. *Angewandte Chemie International Edition*, *51*(24), 5798-5800.

[15] Goodenough, J. B. (2018). How we made the Li-ion rechargeable battery. *Nature Electronics*, *1*(3), 204–204. https://doi.org/10.1038/s41928-018-0048-6

[16] Meng, X. (2021). Atomic and molecular layer deposition in pursuing better batteries Atomic and molecular layer deposition in pursuing better batteries. *Journal of Materials Research*, 1-24.

[17] Lavagna, L., Meligrana, G., Gerbaldi, C., Tagliaferro, A., & Bartoli, M. (2020). Graphene and Lithium-Based Battery Electrodes: A Review of Recent Literature. *Energies*, *13*(18), 4867. https://doi.org/10.3390/en13184867

[18] McKissock, B., Loyselle, P., & Vogel, E. (2009) Guidelines on lithium-ion battery use in space applications. NASA

[19] Taylor, H. (1986). High Power Consumer Replaceable Lithium Manganese Dioxide Batteries. *IEEE Transactions on Consumer Electronics*, (3), 694-699.

[20] Li, M., Lu, J., Chen, Z., & Amine, K. (2018). 30 years of lithium-ion batteries. *Advanced Materials*, *30*(33), 1800561.

[21] Qian, J., Wu, C., Cao, Y., Ma, Z., Huang, Y., Ai, X., & Yang, H. (2018). Prussian blue cathode materials for sodium-ion batteries and other ion batteries. *Advanced Energy Materials*, *8*(17), 1702619.

[22] Lewis, G. N., & Keyes, F. G. (1913). THE POTENTIAL OF THE LITHIUM ELECTRODE. *Journal of the American Chemical Society*, *35*(4), 340-344.

[23] Fuller, Thomas F. Harb, John N.. (2018). *Electrochemical Engineering.* John Wiley & Sons. Retrieved from https://app.knovel.com/hotlink/toc/id:kpEE000023/electrochemical-engineering/electrochemical-engineering. Accessed on 5/20/21.

[24] Alessia, A., Alessandro, B., Maria, V. G., Carlos, V. A., & Francesca, B. (2021). Challenges for sustainable lithium supply: a critical review. *Journal of Cleaner Production*, 126954.

[25] Han, M. H., Gonzalo, E., Singh, G., & Rojo, T. (2015). A comprehensive review of sodium layered oxides: powerful cathodes for Na-ion batteries. *Energy & Environmental Science*, *8*(1), 81-102.

[26] Fard, L. S., Peighambardoust, N. S., Jang, H. W., Dehghan, A., Saligheh, N. N. K., Iranpour, M., & Rajabi, M. I. (2020). The rechargeable aluminum-ion battery with different composite cathodes: A review. *Journal of Composites and Compounds*, *2*(4), 138-146.

[27] https://spaceplace.nasa.gov/what-powers-a-spacecraft/en/ last updated October 24, 2019; accessed 5/13/21.

[28] Knap, V., Vestergaard, L. K., & Stroe, D. I. (2020). A review of battery technology in cubesats and small satellite solutions. *Energies*, *13*(16), 4097.

[29] Chin, K. B., Brandon, E. J., Bugga, R. V., Smart, M. C., Jones, S. C., Krause, F. C., ... & Bolotin, G. G. (2018). Energy storage technologies for small satellite applications. *Proceedings of the IEEE*, *106*(3), 419-428.

[30] Uno, M., Ogawa, K., Takeda, Y., Sone, Y., Tanaka, K., Mita, M., & Saito, H. (2011). Development and on-orbit operation of lithium-ion pouch battery for small scientific satellite "REIMEI". *Journal of Power Sources*, *196*(20), 8755-8763.

[31] Crusan, J., & Galica, C. (2019). NASA's CubeSat Launch Initiative: Enabling broad access to space. *Acta Astronautica*, *157*, 51-60.

[32] https://www.nasa.gov/content/about-elana last updated on Aug 3, 2017; accessed 5/13/21.

[33] Torgerson, D., Nervold, A., Straub, J., Berk, J., Marsh, R., & Kerlin, S. (2013). Interplanetary hitchhiking to support small spacecraft missions beyond earth orbit. *Proc. Int. Astronaut. Congr. IAC*, *5*.

[34] Saeed, N., Elzanaty, A., Almorad, H., Dahrouj, H., Al-Naffouri, T. Y., & Alouini, M. S. (2020). Cubesat communications: Recent advances and future challenges. *IEEE Communications Surveys & Tutorials*, *22*(3), 1839-1862.

[35] Sands, C., Roddy, M., Hodges, H., & Huang, P. A. (2020). ARKSAT-1, 1U CubeSatellite Developed at the University of Arkansas. In *Proceedings, 34th Small Satellite Conference, SSC20-WKV-01*.

[36] Liu, C., Neale, Z. G., & Cao, G. (2016). Understanding electrochemical potentials of cathode materials in rechargeable batteries. *Materials Today*, *19*(2), 109-123.

[37] Zhang, S., Zhao, K., Zhu, T., & Li, J. (2017). Electrochemomechanical degradation of high-capacity battery electrode materials. *Progress in Materials Science*, *89*, 479-521.

[38] Goodenough, J. B. (1994). Design considerations. *Solid State Ionics*, *69*(3-4), 184-198.

[39] Ohsaki, T., Kishi, T., Kuboki, T., Takami, N., Shimura, N., Sato, Y., ... & Satoh, A. (2005). Overcharge reaction of lithium-ion batteries. *Journal of Power Sources*, *146*(1-2), 97-100.

[40] Van der Venz, A., & Ceder, G. (2000). Lithium Diffusion in Layered Li x CoO 2. *Electrochemical and Solid-State Letters*, *3*, 7.

[41] Ueda, A., & Ohzuku, T. (1994). Solid-State Redox Reactions of LiNi1/2Co1/2 O 2 (R 3̄m) for 4 Volt Secondary Lithium Cells. *Journal of the Electrochemical Society*, *141*(8), 2010.

[42] Chen, W., Liu, Y., Shi, F., An, Q., Dai, C., & Fu, X. (2019, June). Efficiency factors and optimization of Lithium-Ion Battery. In *2019 14th IEEE Conference on Industrial Electronics and Applications (ICIEA)* (pp. 644-649). IEEE.

[43] Ye, Y., Saw, L. H., Shi, Y., & Tay, A. A. (2015). Numerical analyses on optimizing a heat pipe thermal management system for lithium-ion batteries during fast charging. *Applied Thermal Engineering*, *86*, 281-291.

[44] Pradeep, N., Sivasenthil, E., Janarthanan, B., & Sharmila, S. (2019, November). A Review of Anode Material for Lithium Ion Batteries. In *Journal of Physics: Conference Series* (Vol. 1362, No. 1, p. 012026). IOP Publishing.

[45] Pistoia, Gianfranco. (2014). *Lithium-Ion Batteries - Advances and Applications.* (pp. 64,66). Elsevier. Retrieved from https://app.knovel.com/hotlink/toc/id:kpLIBAA003/lithium-ion-batteries/lithium-ion-batteries accessed 6/8

[46] Goodenough, J. B., Manthiram, A., & Wnetrzewski, B. (1993). Electrodes for lithium batteries. *Journal of power sources*, *43*(1-3), 269-275.

[47] Lavagna, L., Meligrana, G., Gerbaldi, C., Tagliaferro, A., & Bartoli, M. (2020). Graphene and lithium-based battery electrodes: a review of recent literature. *Energies*, *13*(18), 4867.

[48] Lang, J., Qi, L., Luo, Y., & Wu, H. (2017). High performance lithium metal anode: progress and prospects. *Energy Storage Materials*, *7*, 115-129.

[49] Lin, D., Liu, Y., & Cui, Y. (2017). Reviving the lithium metal anode for high-energy batteries. *Nature nanotechnology*, *12*(3), 194-206.

[50] Liu, J., Bao, Z., Cui, Y., Dufek, E. J., Goodenough, J. B., Khalifah, P., ... & Zhang, J. G. (2019). Pathways for practical high-energy long-cycling lithium metal batteries. *Nature Energy*, *4*(3), 180-186.

[51] Qian, J., Henderson, W. A., Xu, W., Bhattacharya, P., Engelhard, M., Borodin, O., & Zhang, J. G. (2015). High rate and stable cycling of lithium metal anode. *Nature communications*, *6*(1), 1-9.

[52] Kang, E., Jung, Y. S., Kim, G. H., Chun, J., Wiesner, U., Dillon, A. C., ... & Lee, J. (2011). Highly improved rate capability for a lithium-ion battery nano-Li4Ti5O12 negative electrode via carbon-coated mesoporous uniform pores with a simple self-assembly method. *Advanced Functional Materials*, *21*(22), 4349-4357.

[53] Belharouak, I., Koenig Jr, G. M., & Amine, K. (2011). Electrochemistry and safety of Li4Ti5O12 and graphite anodes paired with LiMn2O4 for hybrid electric vehicle Li-ion battery applications. *Journal of Power Sources*, *196*(23), 10344-10350.

[54] Zhao, B., Ran, R., Liu, M., & Shao, Z. (2015). A comprehensive review of Li4Ti5O12-based electrodes for lithium-ion batteries: the latest advancements and future perspectives. *Materials Science and Engineering: R: Reports*, *98*, 1-71.

[55] Tojo, T., Kawashiri, S., Tsuda, T., Kadowaki, M., Inada, R., & Sakurai, Y. (2019). Electrochemical performance of single Li4Ti5O12 particle for lithium ion battery anode. *Journal of Electroanalytical Chemistry*, *836*, 24-29.

[56] Ozawa, K. (1994). Lithium-ion rechargeable batteries with LiCoO2 and carbon electrodes: the LiCoO2/C system. *Solid State Ionics*, *69*(3-4), 212-221.

[57] Zaghib, K., Mauger, A., Groult, H., Goodenough, J. B., & Julien, C. M. (2013). Advanced electrodes for high power Li-ion batteries. *Materials*, *6*(3), 1028-1049.

[58] Goriparti, S., Miele, E., De Angelis, F., Di Fabrizio, E., Zaccaria, R. P., & Capiglia, C. (2014). Review on recent progress of nanostructured anode materials for Li-ion batteries. *Journal of power sources*, *257*, 421-443.

[59] Zheng, T., Liu, Y., Fuller, E. W., Tseng, S., Von Sacken, U., & Dahn, J. R. (1995). Lithium insertion in high capacity carbonaceous materials. *Journal of the Electrochemical Society*, *142*(8), 2581.

[60] Meng, X. (2020). Atomic layer deposition of solid-state electrolytes for next-generation lithium-ion batteries and beyond: Opportunities and challenges. *Energy Storage Materials*, *30*, 296-328.

[61] Akhilash, M., Salini, P. S., John, B., & Mercy, T. D. (2021). A journey through layered cathode materials for lithium ion cells-From lithium cobalt oxide to lithium-rich transition metal oxides. *Journal of Alloys and Compounds*, 159239.

[62] Tarascon, J. M. (2016). The Li-Ion Battery: 25 Years of Exciting and Enriching Experiences. *Interface Magazine*, *25*(3), 79–83. https://doi.org/10.1149/2.f08163if

[63] Whittingham, M. S. (2004). Lithium batteries and cathode materials. *Chemical reviews*, *104*(10), 4271-4302.

[64] Rajagopalan, R., Zhang, Z., Tang, Y., Jia, C., Ji, X., & Wang, H. (2020). Understanding crystal structures, ion diffusion mechanisms and sodium storage behaviors of NASICON materials. *Energy Storage Materials*.

[65] Cherkouk, C., & Nestler, T. (2014, June). Cathodes-technological review. In *AIP Conference Proceedings* (Vol. 1597, No. 1, pp. 134-145). American Institute of Physics.

[66] Tian, Z., Yu, H., Zhang, Z., & Xu, X. (2018). Performance improvements of cobalt oxide cathodes for rechargeable Lithium batteries. *ChemBioEng Reviews*, *5*(2), 111-118.

[67] Deng, T., Fan, X., Cao, L., Chen, J., Hou, S., Ji, X., ... & Wang, C. (2019). Designing in-situ-formed interphases enables highly reversible cobalt-free LiNiO2 cathode for Li-ion and Li-metal batteries. *Joule*, *3*(10), 2550-2564.

[68] Daniel, C., Mohanty, D., Li, J., Wood, D.L. (2014). Cathode materials review. In AIP Conference Proceedings (Vol. 1597, No. 1, pp. 26-43). American Institute of Physics.

[69] Ohzuku, T., & Ueda, A. (1994). Solid-state redox reactions of LiCoO2 (R3m) for 4 volt secondary lithium cells. *Journal of The Electrochemical Society*, *141*(11), 2972.

[70] Antolini, E. (2004). LiCoO2: formation, structure, lithium and oxygen nonstoichiometry, electrochemical behaviour and transport properties. *Solid state ionics*, *170*(3-4), 159-171.

[71] Kim, T., Song, W., Son, D. Y., Ono, L. K., & Qi, Y. (2019). Lithium-ion batteries: outlook on present, future, and hybridized technologies. *Journal of materials chemistry A*, *7*(7), 2942-2964.

[72] Kang, K., & Ceder, G. (2006). Factors that affect Li mobility in layered lithium transition metal oxides. *Physical Review B*, *74*(9), 094105.

[73] Mizushima, K., Jones, P. C., Wiseman, P. J., & Goodenough, J. B. (1981). LixCoO2 ($0< x\leqslant 1$): A new cathode material for batteries of high energy density. *Solid State Ionics*, *3*, 171-174.

[74] Tsurukawa, N., Prakash, S., & Manhart, A. (2011). Social impacts of artisanal cobalt mining in Katanga, Democratic Republic of Congo. *Öko-Institut eV, Freiburg*.

[75] Ohzuku, T., Ueda, A., & Nagayama, M. (1993). Electrochemistry and structural chemistry of LiNiO2 (R3m) for 4 volt secondary lithium cells. *Journal of the Electrochemical Society*, *140*(7), 1862.

[76] Dahn, J. R., von Sacken, U., & Michal, C. A. (1990). Structure and electrochemistry of Li1±yNiO2 and a new Li2NiO2 phase with the Ni (OH) 2 structure. *Solid State Ionics*, *44*(1-2), 87-97.

[77] Rougier, A., Gravereau, P., & Delmas, C. (1996). Optimization of the composition of the Li1− z Ni1+ z O 2 electrode materials: structural, magnetic, and electrochemical studies. *Journal of The Electrochemical Society*, *143*(4), 1168.

[78] Armstrong, A. R., Dupre, N., Paterson, A. J., Grey, C. P., & Bruce, P. G. (2004). Combined neutron diffraction, NMR, and electrochemical investigation of the layered-to-spinel transformation in LiMnO2. *Chemistry of materials*, *16*(16), 3106-3118.

[79] Thackeray, M. M. (2021). Exploiting the Spinel Structure for Li-ion Battery Applications: A Tribute to John B. Goodenough. *Advanced Energy Materials*, *11*(2), 2001117.

[80] Aurbach, D., Levi, M. D., Gamulski, K., Markovsky, B., Salitra, G., Levi, E., ... & Oesten, R. (1999). Capacity fading of LixMn2O4 spinel electrodes studied by XRD and electroanalytical techniques. *Journal of Power Sources*, *81*, 472-479.

[81] Zhan, C., Wu, T., Lu, J., & Amine, K. (2018). Dissolution, migration, and deposition of transition metal ions in Li-ion batteries exemplified by Mn-based cathodes–a critical review. *Energy & Environmental Science*, *11*(2), 243-257.

[82] Yuan, L. X., Wang, Z. H., Zhang, W. X., Hu, X. L., Chen, J. T., Huang, Y. H., & Goodenough, J. B. (2011). Development and challenges of LiFePO 4 cathode material for lithium-ion batteries. *Energy & Environmental Science*, *4*(2), 269-284.

[83] Chikkannanavar, S. B., Bernardi, D. M., & Liu, L. (2014). A review of blended cathode materials for use in Li-ion batteries. *Journal of Power Sources*, *248*, 91-100.

[84] Balbuena, P. B. (2014, June). Electrolyte materials-Issues and challenges. In *AIP Conference Proceedings* (Vol. 1597, No. 1, pp. 82-97). American Institute of Physics.

[85] Reddy, M.V., Mauger, A., Julien, C., Paolella, A., Zaghib, K. (2020) Brief History of Early Lithium-Battery Development. *Materials*, *13(8),* 1884. https://doi.org/10.3390/ma13081884

[86] Mauger, A., & Julien, C. M. (2017). Critical review on lithium-ion batteries: are they safe? Sustainable?. *Ionics*, *23*(8), 1933-1947.

[87] Mauger, A., Julien, C. M., Goodenough, J. B., & Zaghib, K. (2019). Tribute to Michel Armand: from rocking chair–Li-ion to solid-state lithium batteries. *Journal of The Electrochemical Society*, *167*(7), 070507.

[88] Asenbauer, J., Eisenmann, T., Kuenzel, M., Kazzazi, A., Chen, Z., & Bresser, D. (2020). The success story of graphite as a lithium-ion anode material–fundamentals, remaining challenges, and recent developments including silicon (oxide) composites. *Sustainable Energy & Fuels*, *4*(11), 5387-5416.

[89] Francis, C. F., Kyratzis, I. L., & Best, A. S. (2020). Lithium-Ion battery separators for ionic-liquid electrolytes: a review. *Advanced Materials*, *32*(18), 1904205.

[90] Niu, C., Lee, H., Chen, S., Li, Q., Du, J., Xu, W., ... & Liu, J. (2019). High-energy lithium metal pouch cells with limited anode swelling and long stable cycles. *Nature Energy*, *4*(7), 551-559.

[91] Wang, Q., Mao, B., Stoliarov, S. I., & Sun, J. (2019). A review of lithium ion battery failure mechanisms and fire prevention strategies. *Progress in Energy and Combustion Science*, *73*, 95-131.

[92] Etacheri, V., Marom, R., Elazari, R., Salitra, G., & Aurbach, D. (2011). Challenges in the development of advanced Li-ion batteries: a review. *Energy & Environmental Science*, *4*(9), 3243-3262.

[93] Willert, Andreas, and Reinhard R. Baumann. "Development History and Current Achievements of Printed Primary Batteries." In *NIP & Digital Fabrication Conference*, vol. 2017, no. 1, pp. 106-110. Society for Imaging Science and Technology, 2017.

[94] An, S. J., Li, J., Daniel, C., Mohanty, D., Nagpure, S., & Wood III, D. L. (2016). The state of understanding of the lithium-ion-battery graphite solid electrolyte interphase (SEI) and its relationship to formation cycling. *Carbon*, *105*, 52-76.

[95] Peled, E., Menkin, S. (2017) Review – SEI: Past, Present and Future. *Journal of The Electrochemical Society*, *164(7)*, A1703-A1719.

[96] Ding, J. F., Xu, R., Yan, C., Li, B. Q., Yuan, H., & Huang, J. Q. (2020). A review on the failure and regulation of solid electrolyte interphase in lithium batteries. *Journal of Energy Chemistry*, *59*(1), 306-319.

[97] Li, X., Sun, X., Hu, X., Fan, F., Cai, S., Zheng, C., & Stucky, G. D. (2020). Review on comprehending and enhancing the initial Coulombic efficiency of anode materials in lithium-ion/sodium-ion batteries. *Nano Energy*, 105143.

[98] Braga, M. H., Grundish, N. S., Murchison, A. J., & Goodenough, J. B. (2017). Alternative strategy for a safe rechargeable battery. *Energy & Environmental Science*, *10*(1), 331-336.

[99] Wang, H., Li, X., Li, F., Liu, X., Yang, S., & Ma, J. (2020). Formation and modification of cathode electrolyte interphase: A mini review. *Electrochemistry Communications*, 106870.

[100] Hu, X., Zhang, K., Liu, K., Lin, X., Dey, S., & Onori, S. (2020). Advanced fault diagnosis for lithium-ion battery systems: a review of fault mechanisms, fault features, and diagnosis procedures. *IEEE Industrial Electronics Magazine*, *14*(3), 65-91.

[101] Feng, X., Ouyang, M., Liu, X., Lu, L., Xia, Y., & He, X. (2018). Thermal runaway mechanism of lithium ion battery for electric vehicles: A review. *Energy Storage Materials*, *10*, 246-267.

[102] Abaza, A., Ferrari, S., Wong, H. K., Lyness, C., Moore, A., Weaving, J., ... & Bhagat, R. (2018). Experimental study of internal and external short circuits of commercial automotive pouch lithium-ion cells. *Journal of Energy Storage*, *16*, 211-217.

[103] Williard, N., He, W., Hendricks, C., & Pecht, M. (2013). Lessons learned from the 787 dreamliner issue on lithium-ion battery reliability. *Energies*, *6*(9), 4682-4695.

[104] Goto, N. (2014). Aircraft serious incident investigation report: all Nippon airways Co. *Ltd. JA804A*.

[105] National Transportation Safety Board Washington, D.C. Docket No. SA-536 Exhibit No. 17-A Airworthiness Excerpts from Boeing Battery Specification Control Drawing.

[106] Lithium Battery Incident Chart – Federal Aviation Administration. Last Updated May 31, 2021. Accessed 6/9/21. https://www.faa.gov/hazmat/resources/lithium_batteries/media/Battery_incident_chart.pdf

[107] Yun, J. J., Jeon, J., Park, K., & Zhao, X. (2018). Benefits and costs of closed innovation strategy: Analysis of Samsung's Galaxy Note 7 Explosion and withdrawal scandal. *Journal of open innovation: Technology, market, and complexity*, *4*(3), 20.

[108] Li Shouding, Li Yan, Tian Jie, Zhao Yuming, Yang Min, Luo Jun, Cao Yuancheng, Cheng Shijie. Analysis on the fire safety status of lithium-ion battery power storage system. Storage Science and Technology [J], 2020, 9 (5): 1505-1516 Doi: 10.19799 / j.cnki.2095-4239.2020.0111

[109] Flight Acceptance Test Requirements for Lithium-ion Cells and Battery Packs. NanoRacks. Doc No: NR-SRD-139. Revision: C

Appendix

A. Full Circuit Diagrams

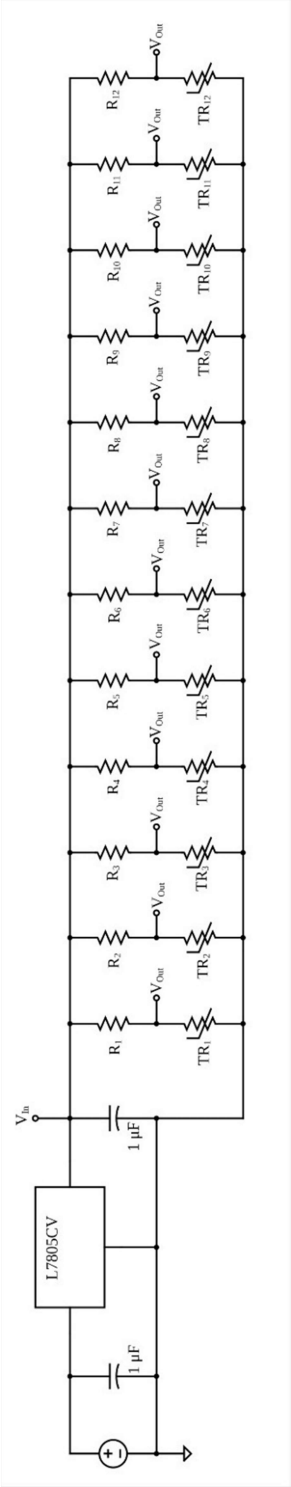

Fig. A.1: Full schematic for 14-day OCV thermistor circuit

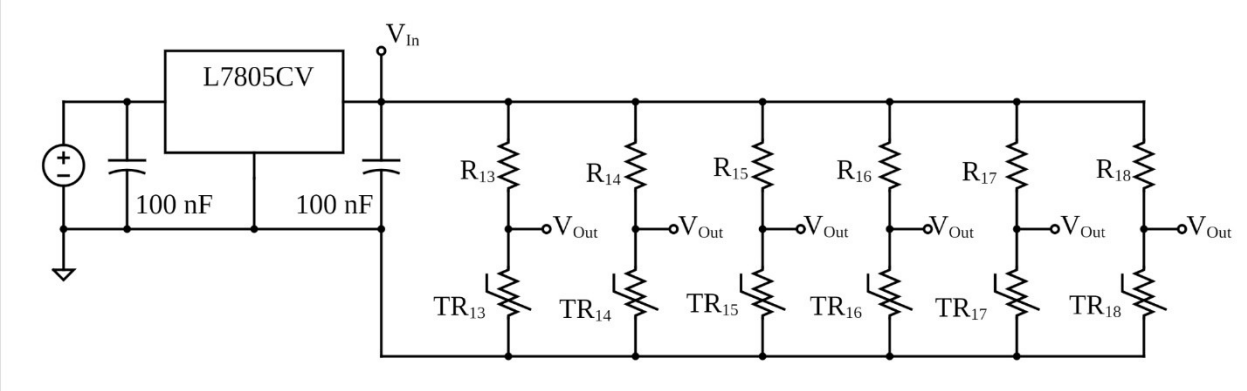

Fig. A.2: Full schematic for charge-discharge thermistor circuit

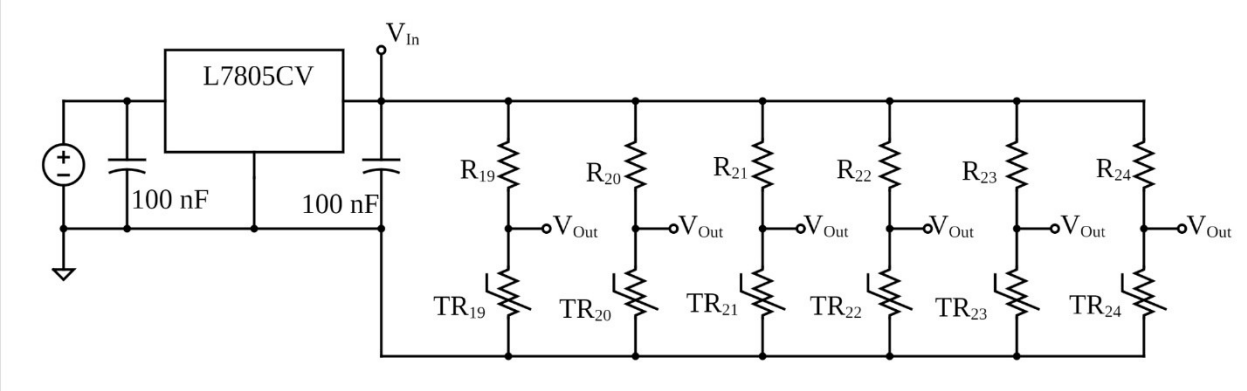

Fig. A.3: Full schematic for vacuum chamber test

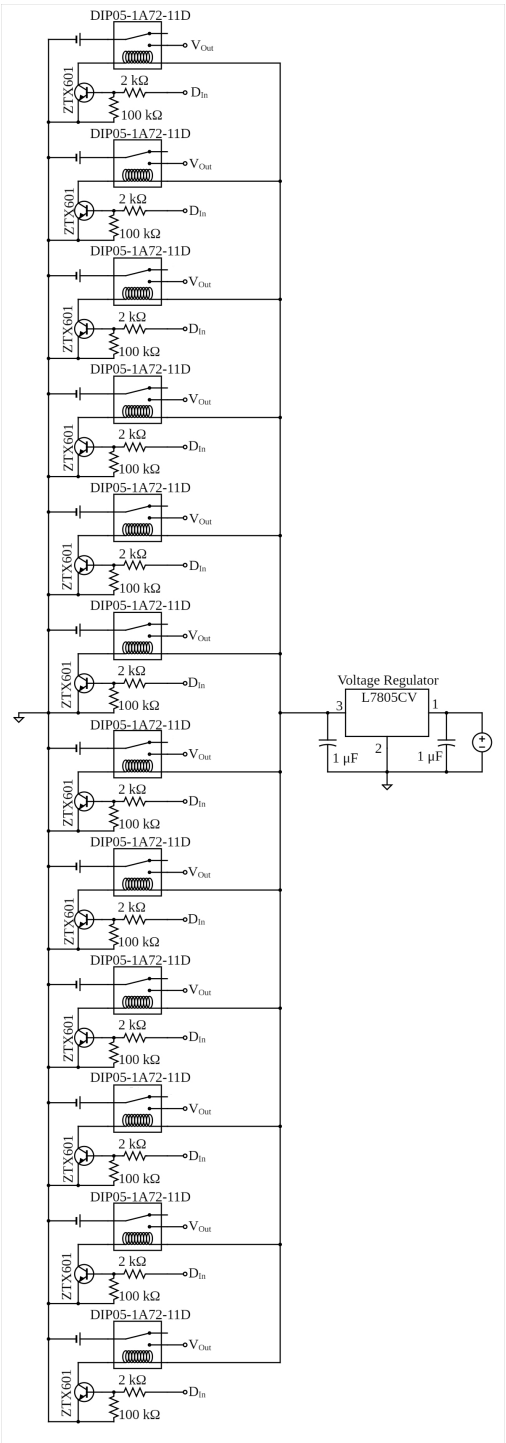

Fig. A.4:Full schematic of 14-Day OCV. Circuit as provided by Dr. Huang, circuit drawings created on https://www.circuit-diagram.org/, altered and finalized with BioRender.com.

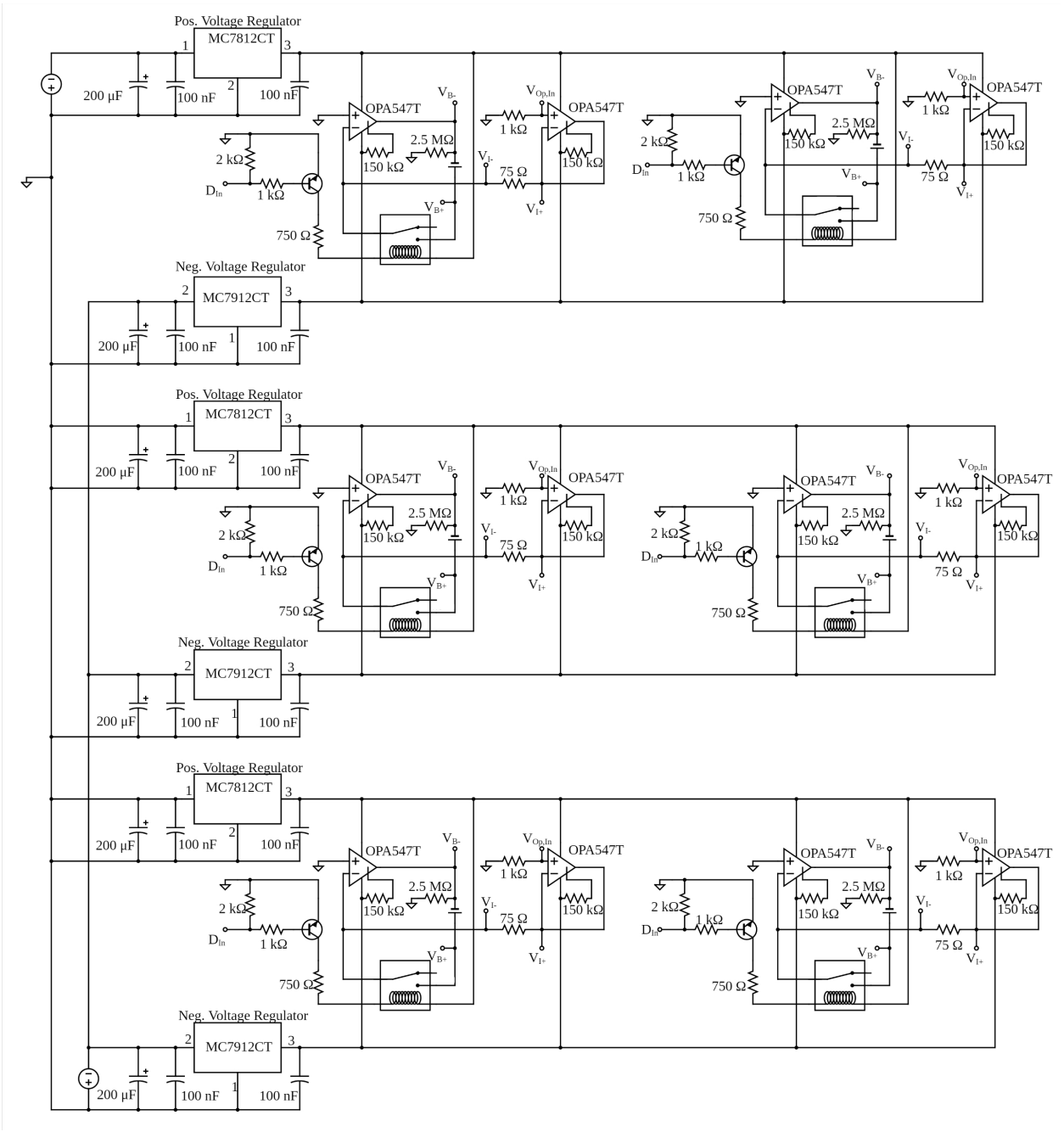

Fig. A.5: The schematic of the full charge-discharge circuit. Circuit as provided by Dr. Huang, circuit drawings created on https://www.circuit-diagram.org/, altered and finalized with BioRender.com.

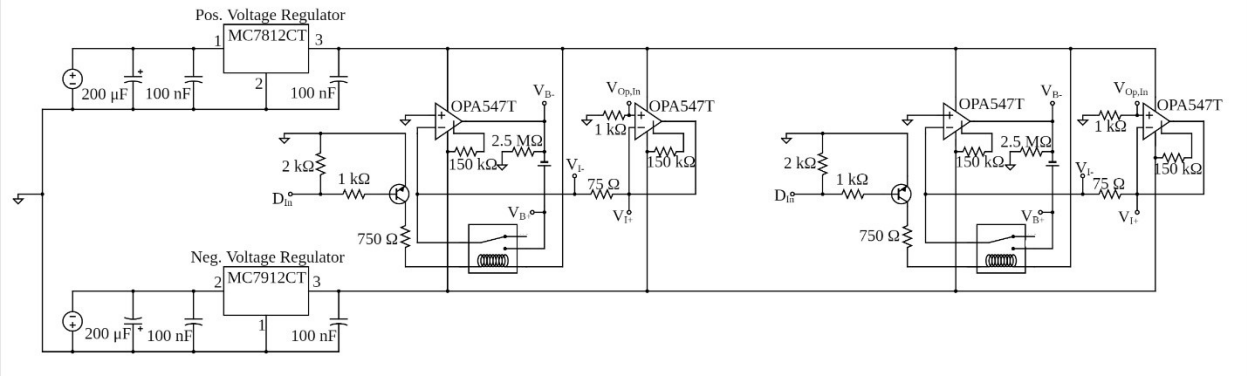

Fig. A.6: Simplified schematic showing one board. This is repeated three times in the full circuit, sans power sources. Circuit as provided by Dr. Huang, circuit drawings created on https://www.circuit-diagram.org/, altered and finalized with BioRender.com.

B. Circuit Prep Calculations

Table B.1: Charge-Discharge circuit watt resistor calculations.

Resistor Location	Measured Current (A)	Measured Voltage (V)	Calculated Resistance (Ω)	Measured Resistances (Ω)
Board 1	0.07910	5.823	73.62	74.7
Board 2	0.07891	5.829	73.87	73.4
Board 3	0.07907	5.826	73.68	73.0
Board 4	0.07903	5.827	73.73	73.6
Board 5	0.07913	5.816	73.50	73.3
Board 6	0.05933	4.377	73.77	73.5

The reason that the current and voltage were both measured and then that was used to calculate resistance instead of just measuring resistance was to eliminate any contact resistances. The calculated resistance values are used for V_{OP} calculations, the measured resistances are just to show that there is a difference between the calculated and measured.

Table B.2: Charge-Discharge circuit input voltage for ideal charge or discharge current.

Resistor Location	Calculated Resistance (Ω)	Charge Current (A)	Charge $V_{Op,in}$ (V)	Discharge Current (A)	Discharge $V_{Op,in}$ (V)
Board 1	73.62	0.050	3.681	-0.050	-3.681
Board 2	73.87		3.694		-3.694
Board 3	73.68		3.684		-3.684
Board 4	73.73		3.686		-3.686
Board 5	73.50		3.675		-3.675
Board 6	73.77		3.689		-3.689

Note: The LabView code automatically does this calculation based on the resistance input by the user. The values it calculates are just "initial" values because it monitors the current and adjusts $V_{Op,In}$ to correct for any deviation of ±5% from ideal 50 mA charge and -50 mA discharge.

$$T = \left[\frac{\ln\left(\frac{TR_x}{TR_{x,0}}\right)}{\beta} + \frac{1}{T_0}\right]^{-1} \quad \text{(B.1)}$$

$$\beta_x = \frac{\ln\left(\frac{TR_x}{TR_{x,0}}\right)}{\left(\frac{1}{T} - \frac{1}{T_0}\right)} \quad \text{(B.2)}$$

C. Equipment & Software

Computer #1

Model #: Dell Optiplex 990

Serial: G5BFHQ1

Room #: Office

Owner: Dr. Adam Huang

Software Name	Purchased By
Matlab 2019a	MEEG
Microsoft Office 2016	ENGR
LabView 2018	MEEG

Computer #2

Model #: Dell Optiplex 990

Serial: 89QVZQ1

Room #: 3915

Owner: Dr. Adam Huang

Software Name	Purchased By
LabView 2018	MEEG

Computer #3

Model #: Dell Optiplex 990

Serial: G5DGHQ1

Room #: 3915

Owner: Dr. Adam Huang

Software Name	Purchased By
LabView 2018	MEEG
Office 2016	ENGR

D. Actual Testing Setup

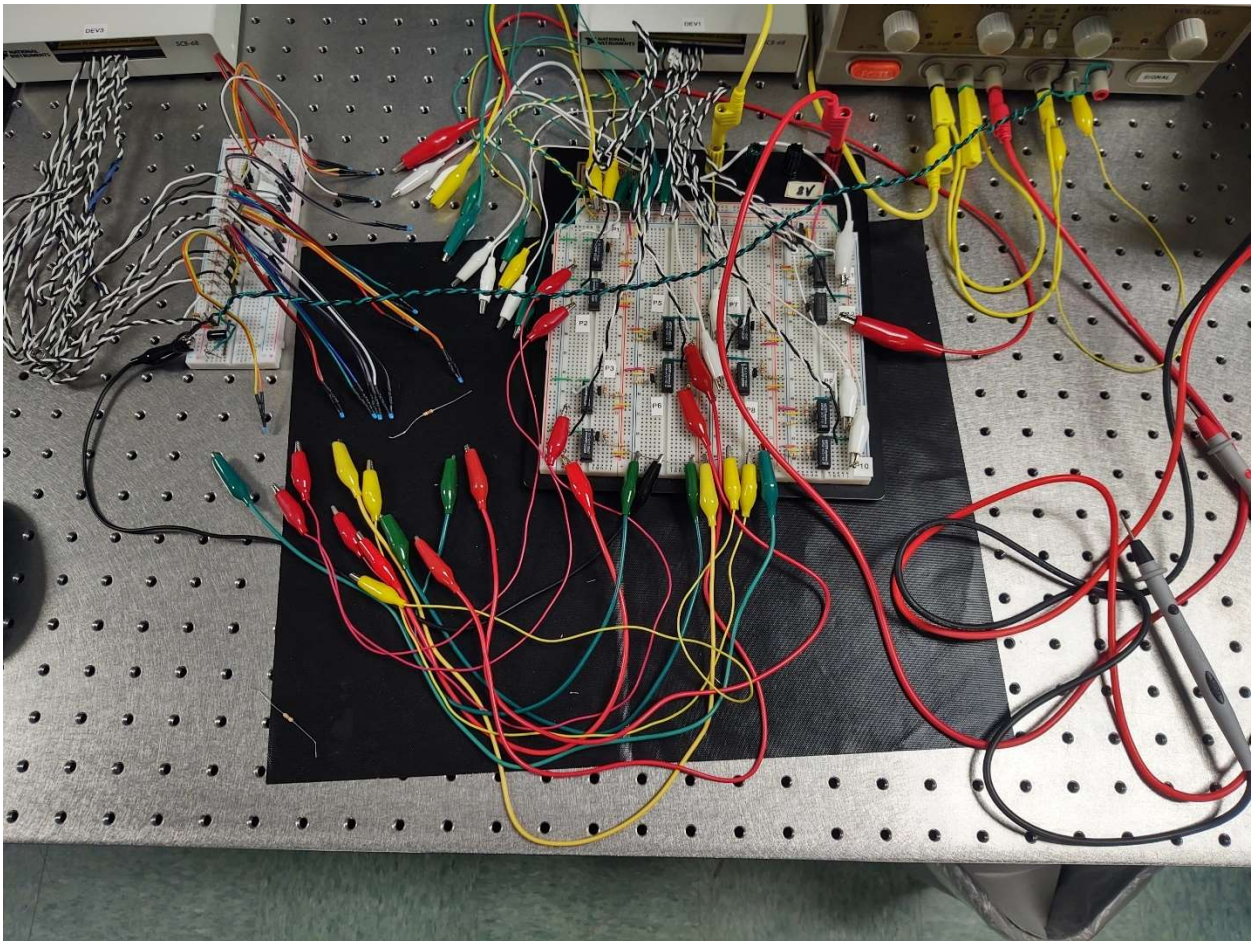

Fig. D.1: Full 14-day OCV setup.

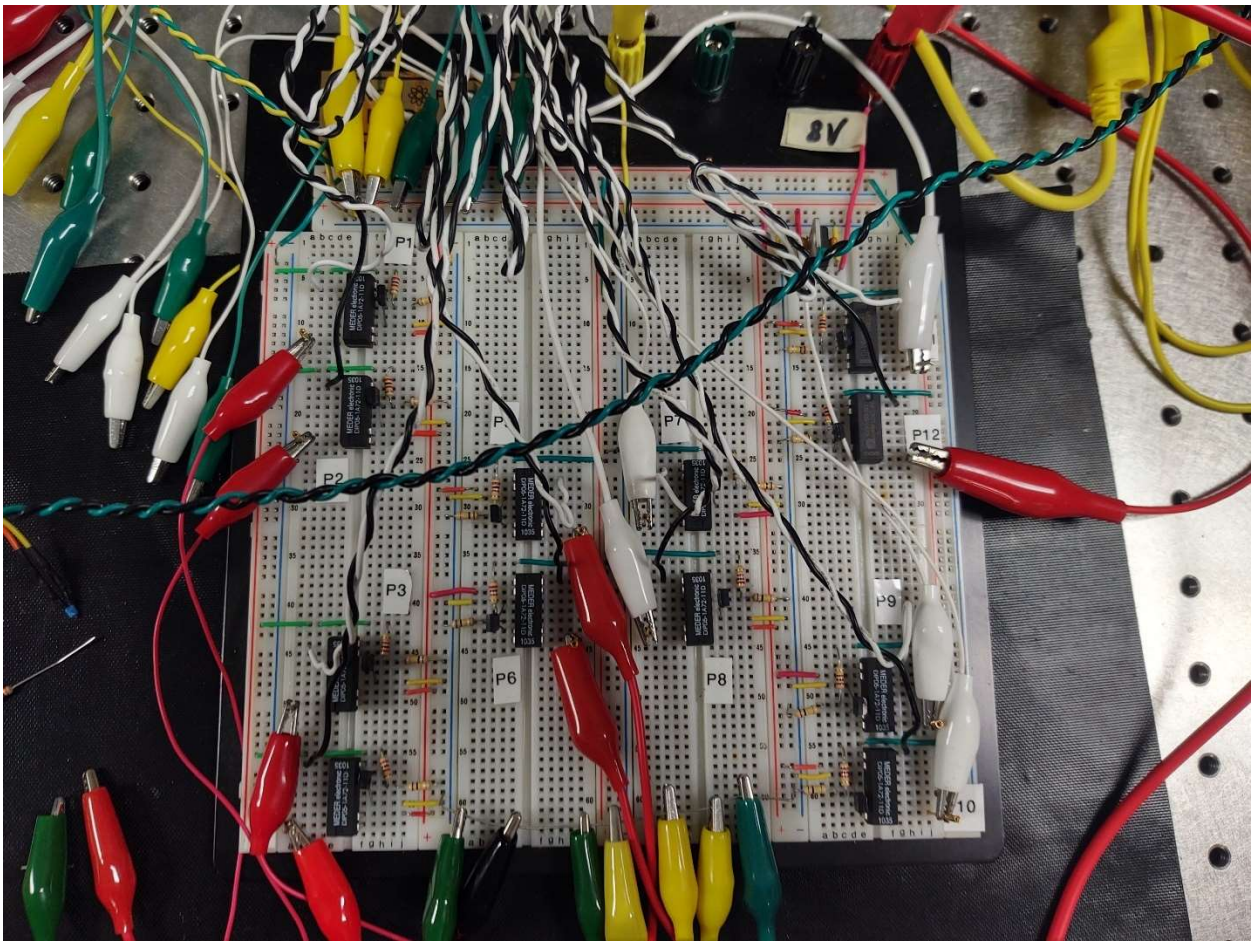

Fig. D.2: 14-day OCV – Main Circuit Only

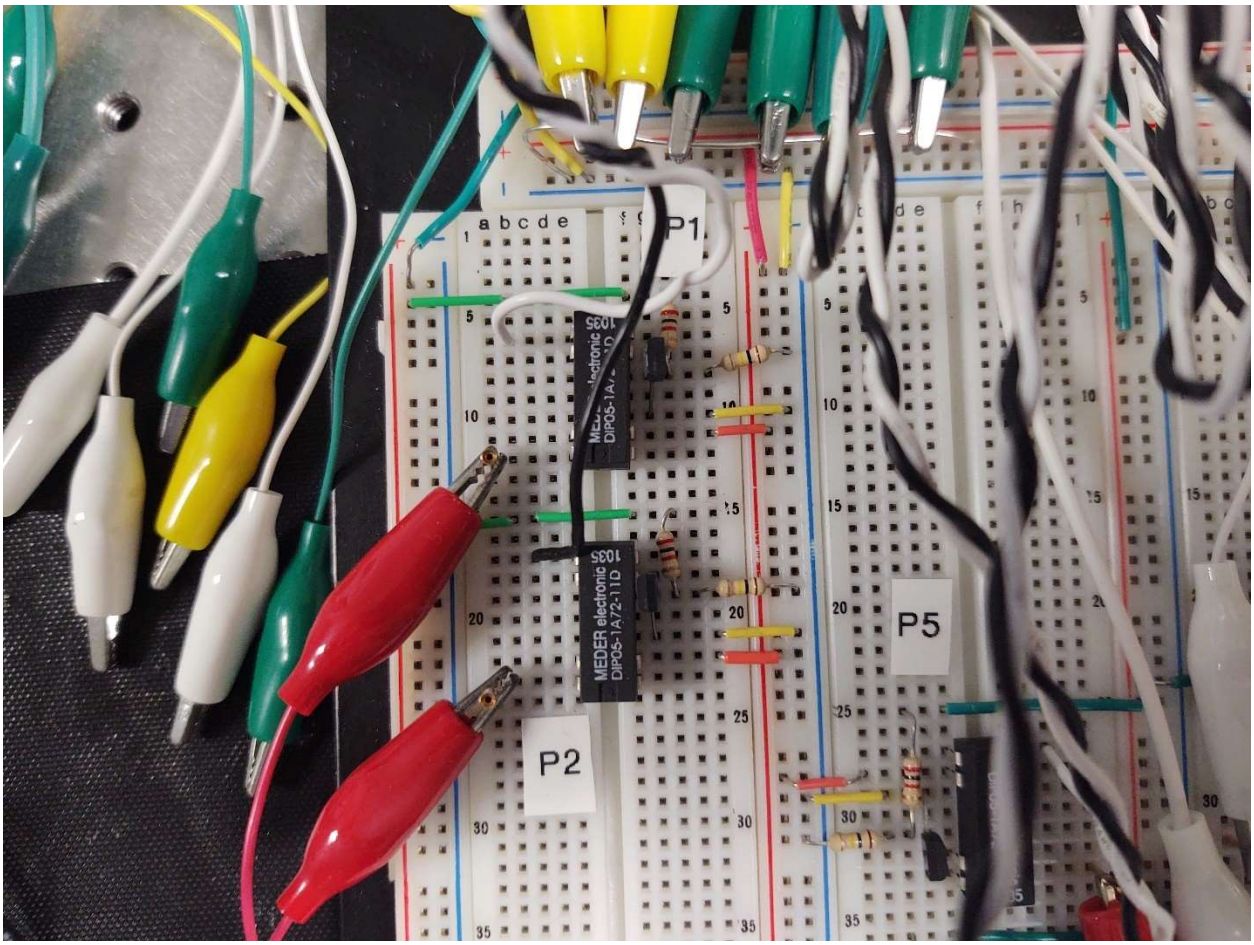

Fig. D.3: 14-day OCV - circuit closeup showing connections for (2) batteries, Position 1 and Position 2 (P1 and P2, respectively)

Fig. D.4: Thermistor circuit, thermistors 1-12, for 14-day OCV test

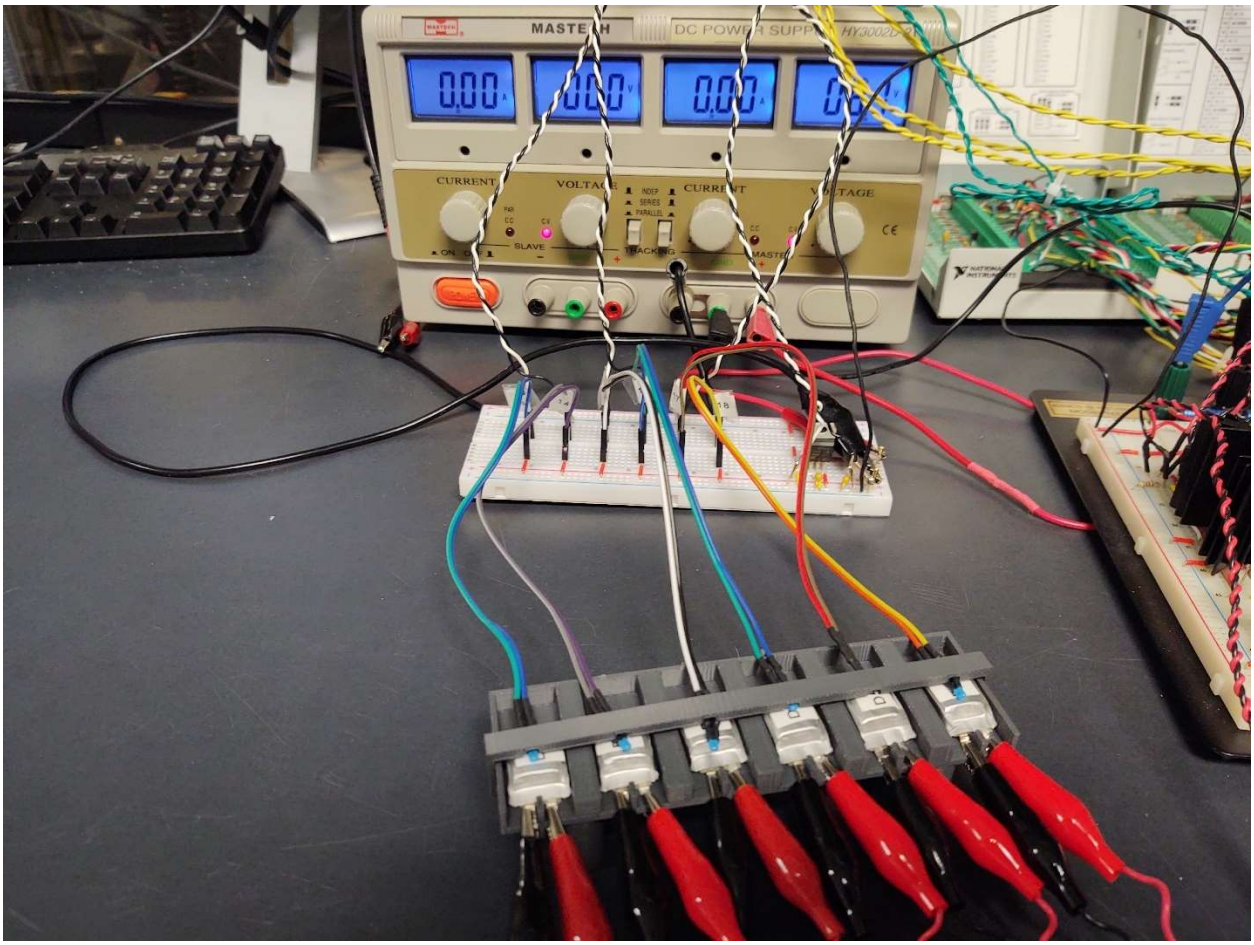

Fig. D.5: Thermistor circuit for charge-discharge test

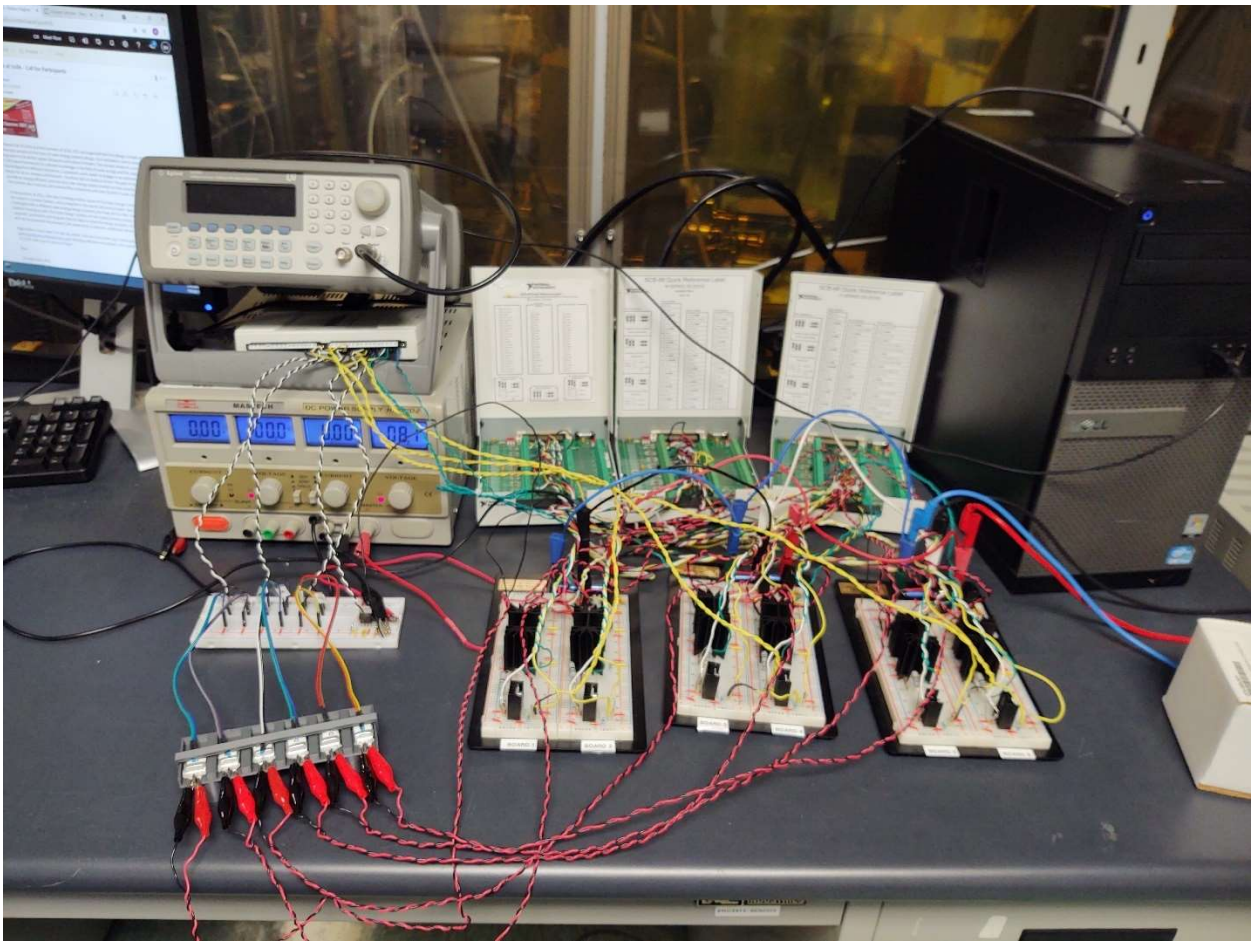

Fig. D.6: Full Charge-Discharge setup

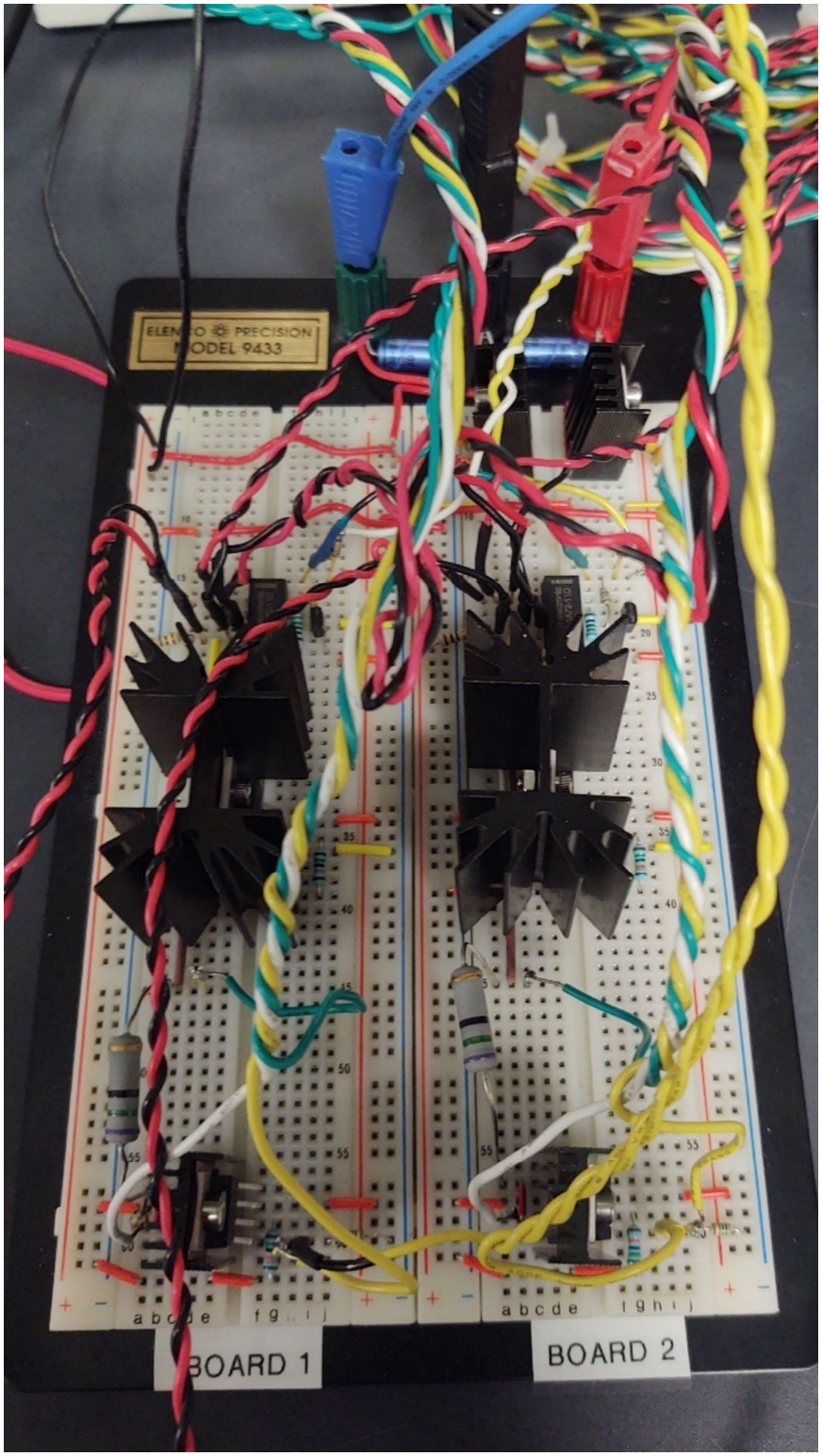

Fig. D.7: Charge-Discharge circuit close up. Only 2 of 6 boards are shown here

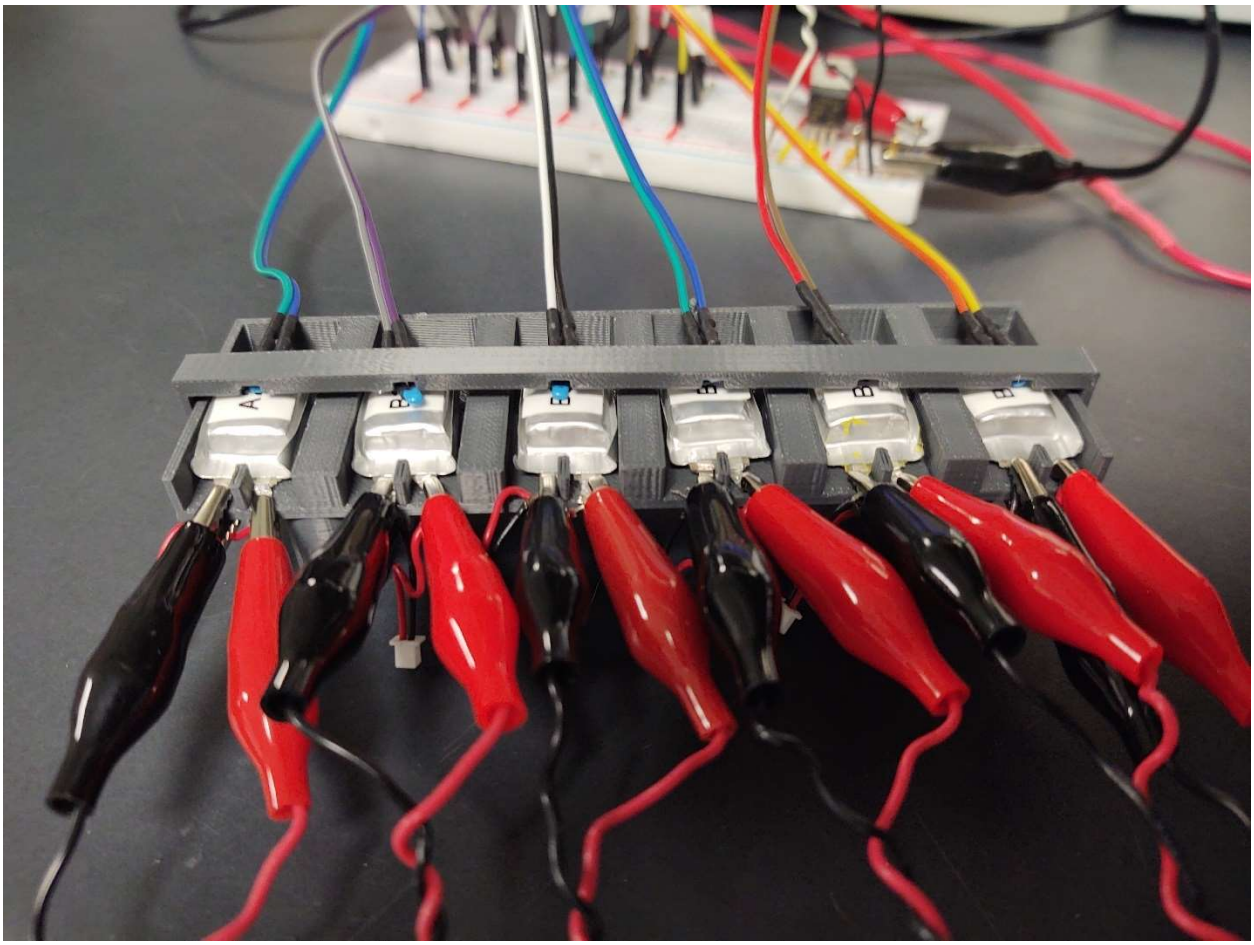

Fig. D.8: Closeup of battery stand, connections, and thermistor restraints.

E. 14-Day OCV Results

E.1 Batch C Plots

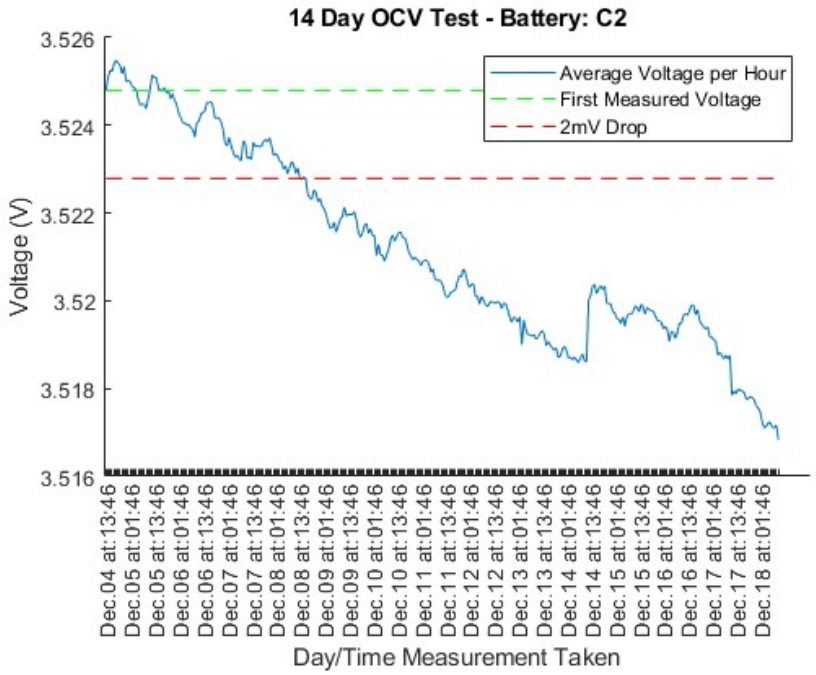

Fig. E.1: 14-day OCV C2 – Failed

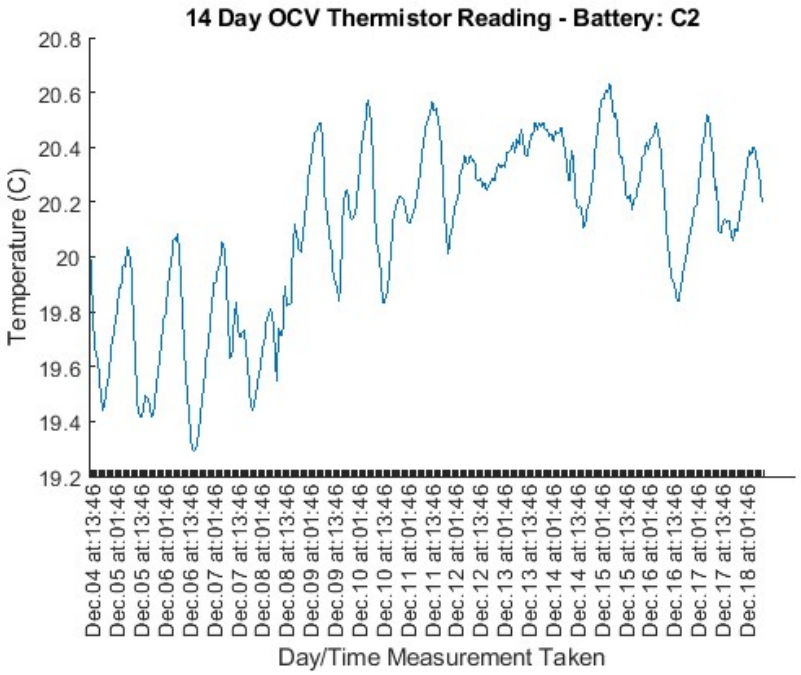

Fig. E.2:14-day OCV Temperature Readings – C2

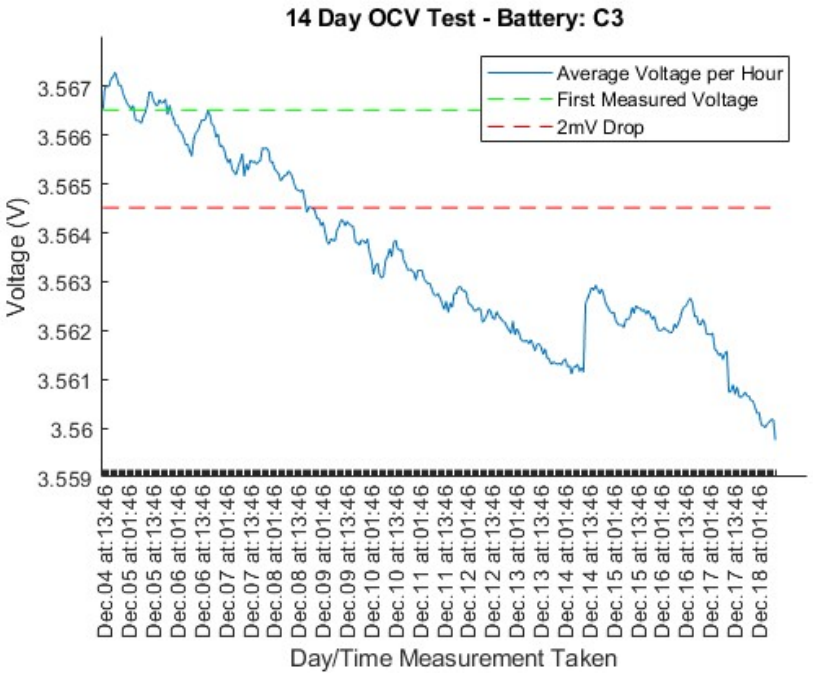

Fig. E.3: 14-day OCV C3 – Failed

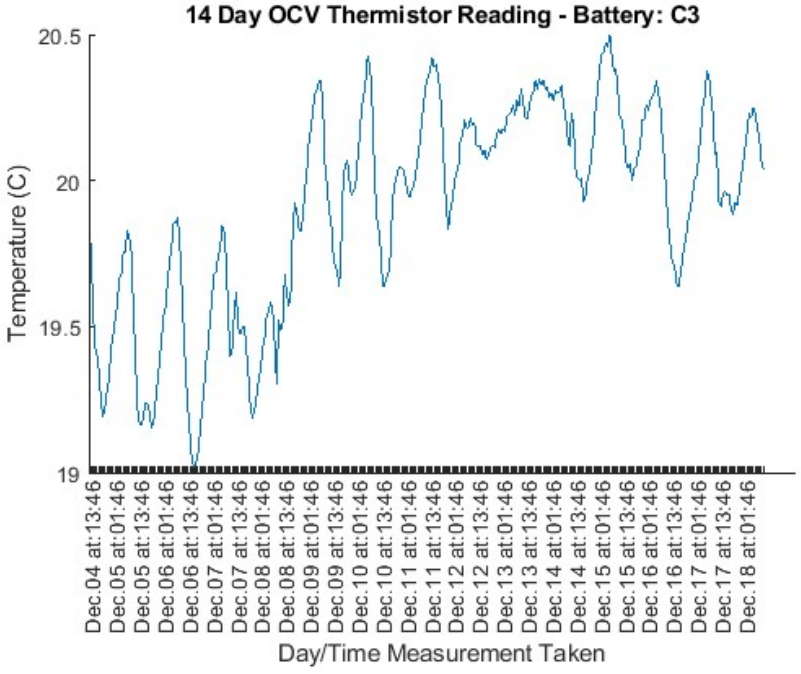

Fig. E.4:14-day OCV Temperature Readings – C3

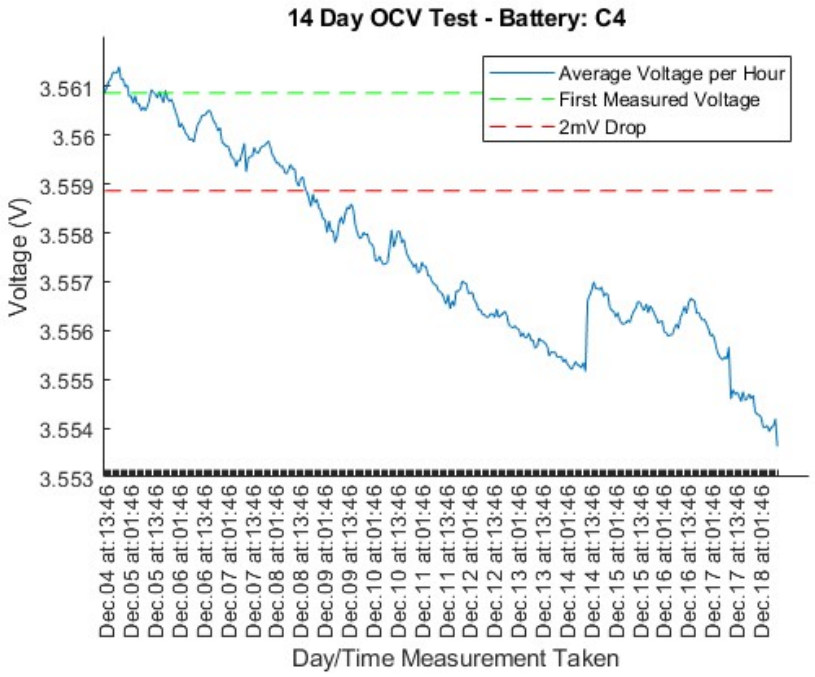

Fig. E.5: 14-day OCV C4 - Failed

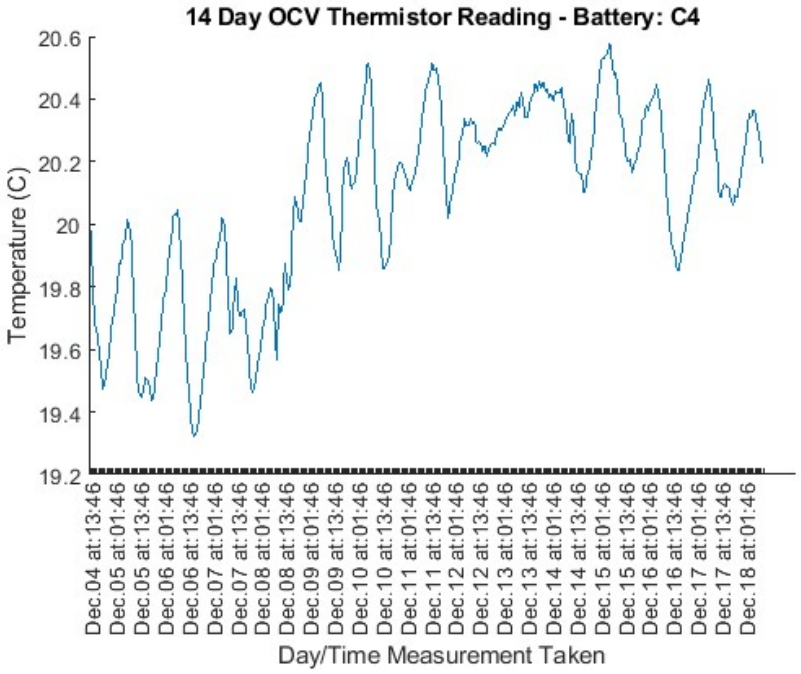

Fig. E.6:14-day OCV Temperature Readings – C4

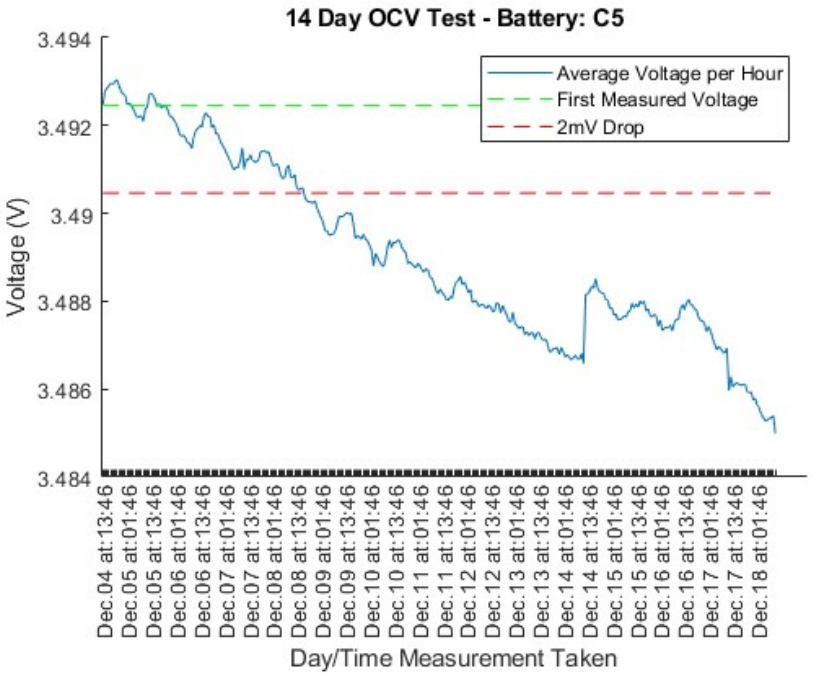

Fig. E.7: 14-day OCV C5 – Failed

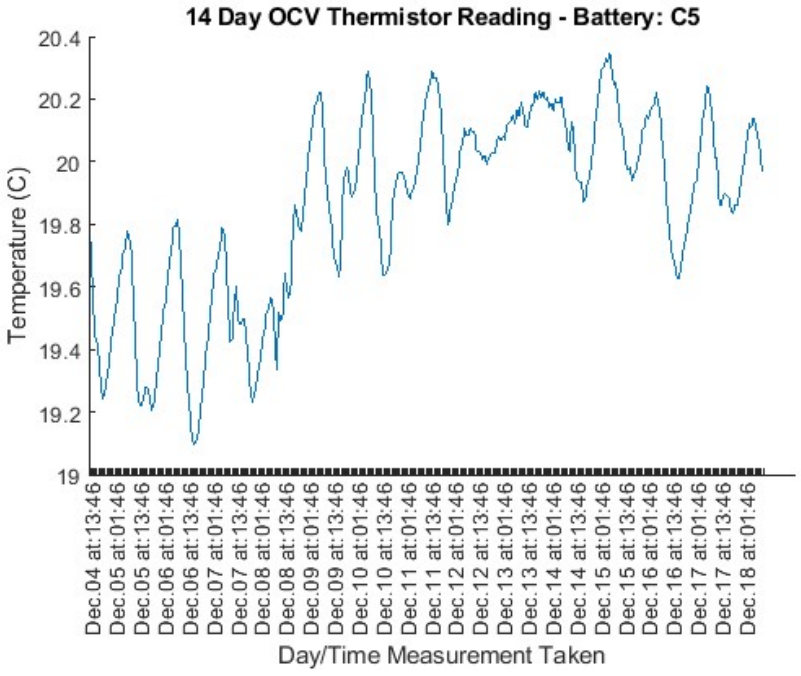

Fig. E.8:14-day OCV Temperature Readings – C5

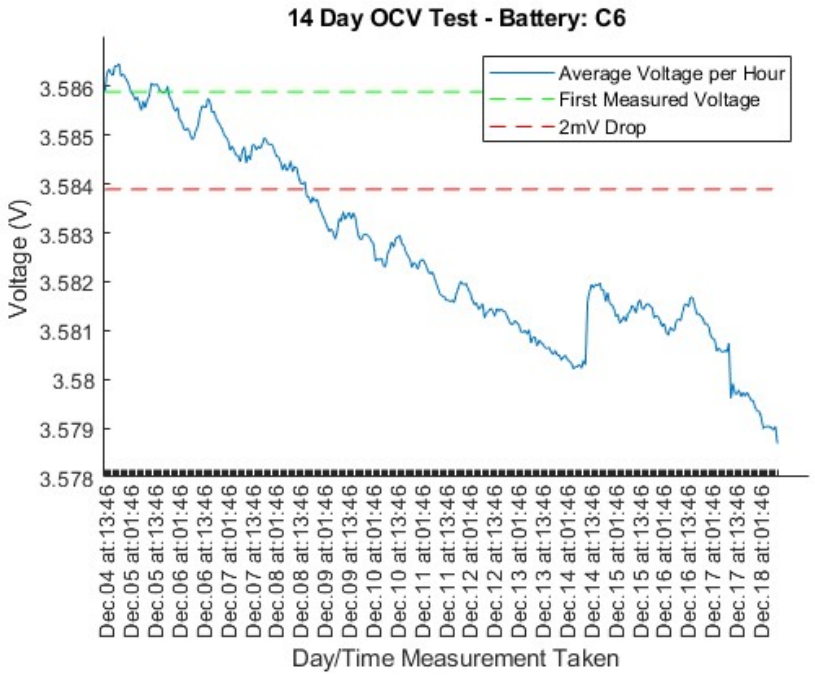

Fig. E.9: 14-day OCV C6 – Failed

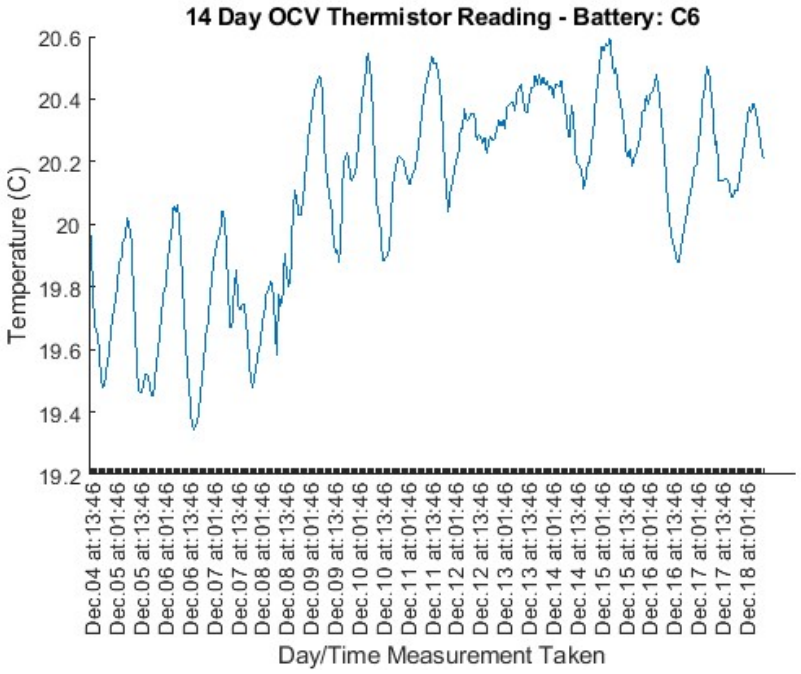

Fig. E.10:14-day OCV Temperature Readings – C6

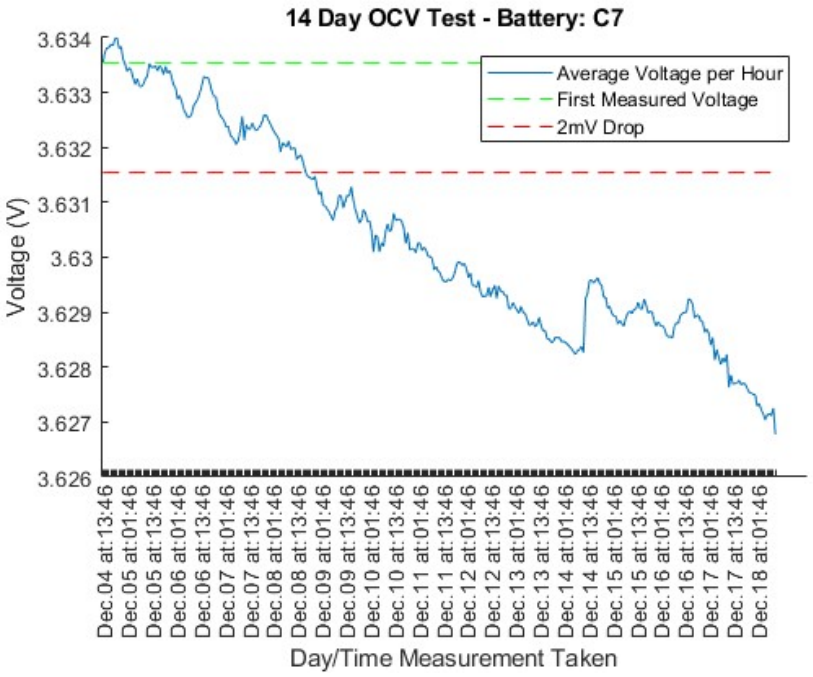

Fig. E.11: 14-day OCV C7 – Failed

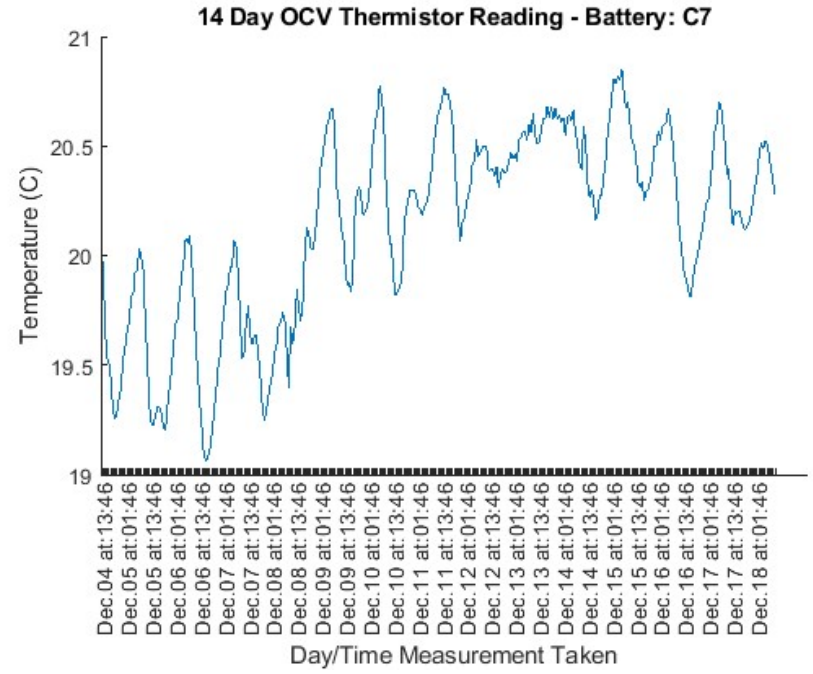

Fig. E.12:14-day OCV Temperature Readings – C7

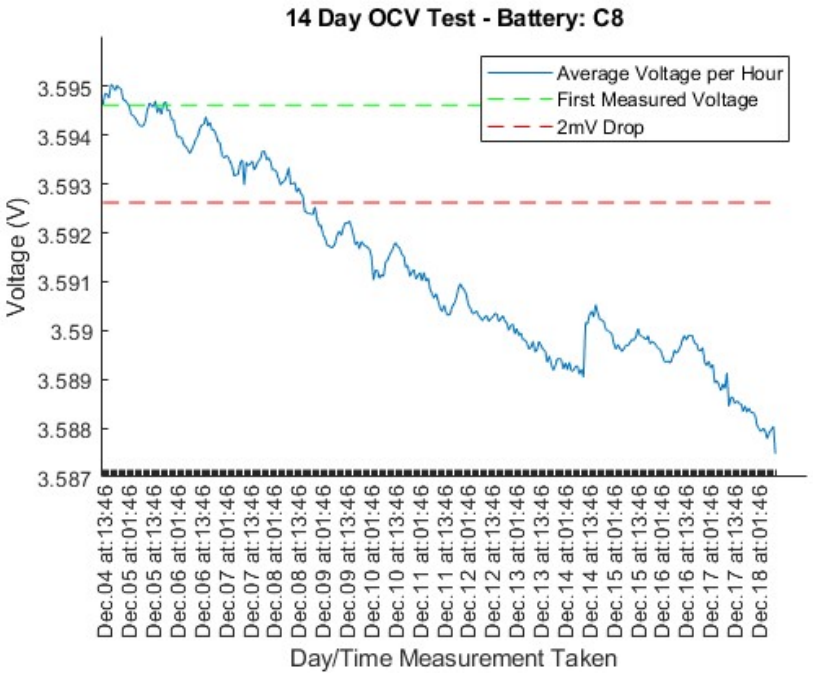

Fig. E.13: 14-day OCV C8 – Failed

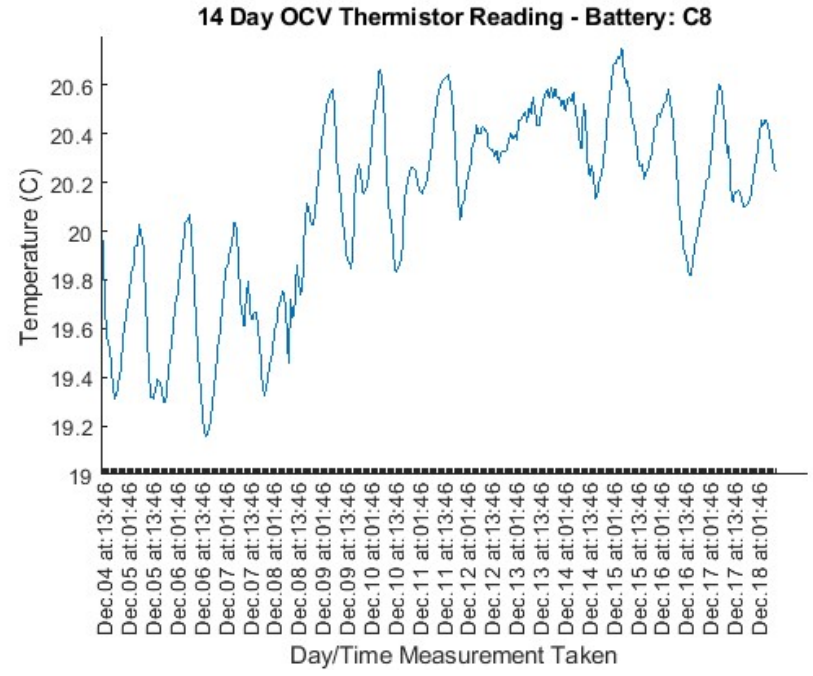

Fig. E.14:14-day OCV Temperature Readings - Battery C8

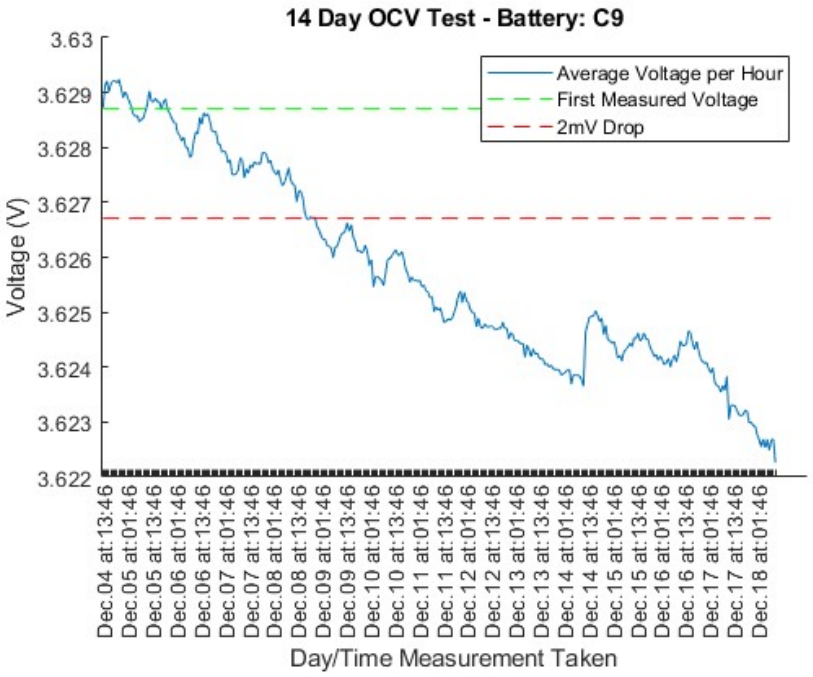

Fig. E.15: 14-day OCV C9 – Failed

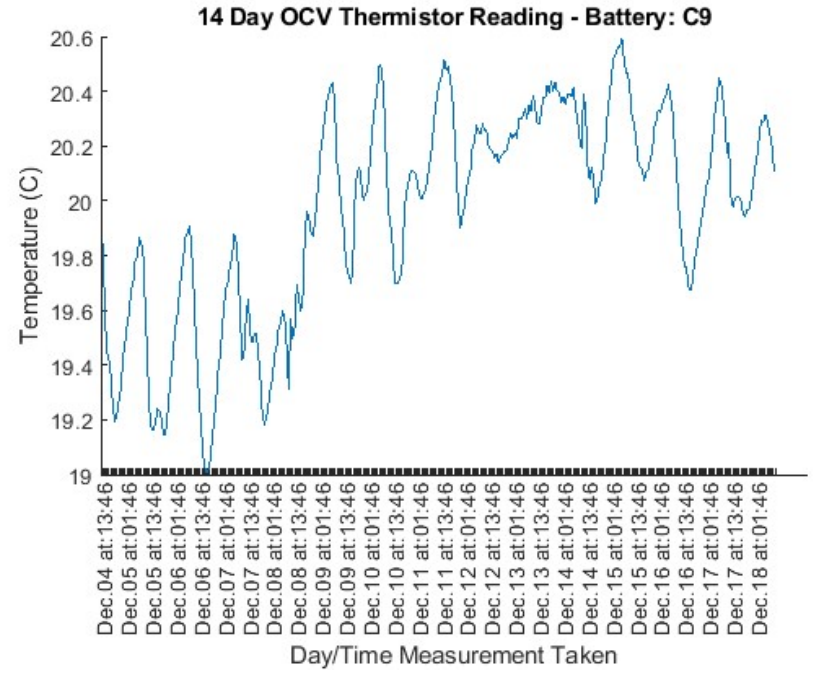

Fig. E.16:14-day OCV Temperature Readings - Battery C9

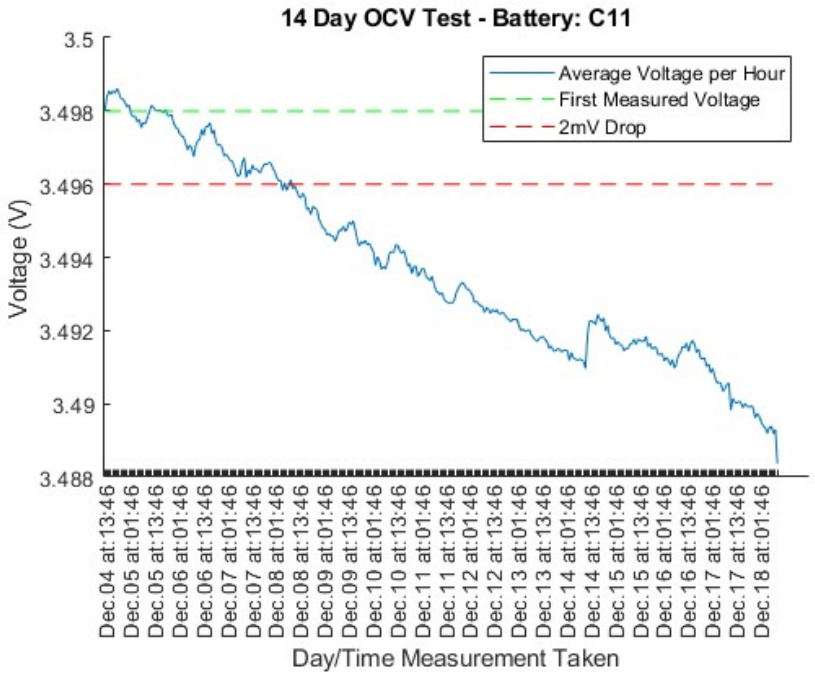

Fig. E.17: 14-day OCV C11 - Failed

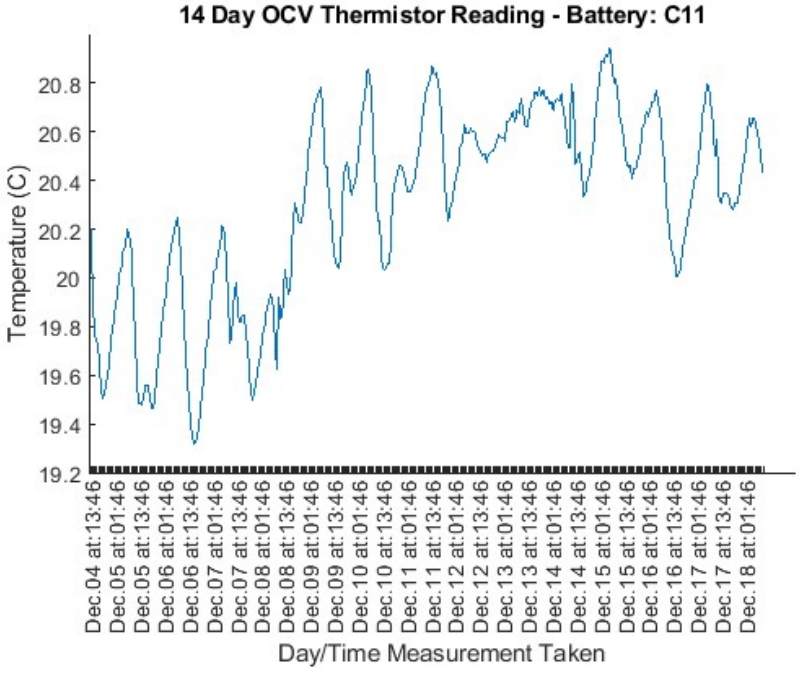

Fig. E.18:14-day OCV Temperature Readings – C11

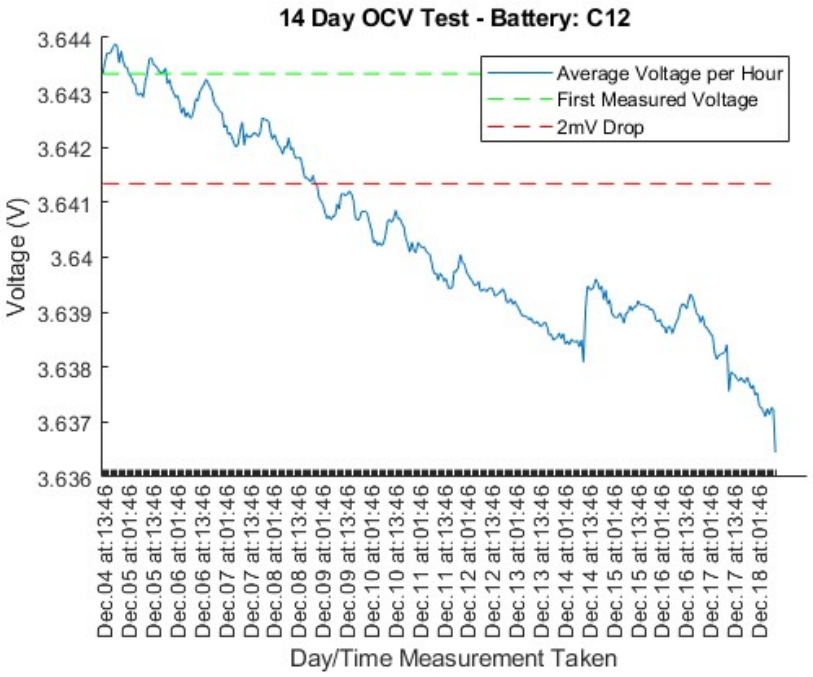

Fig. E.19: 14-day OCV C12 – Failed

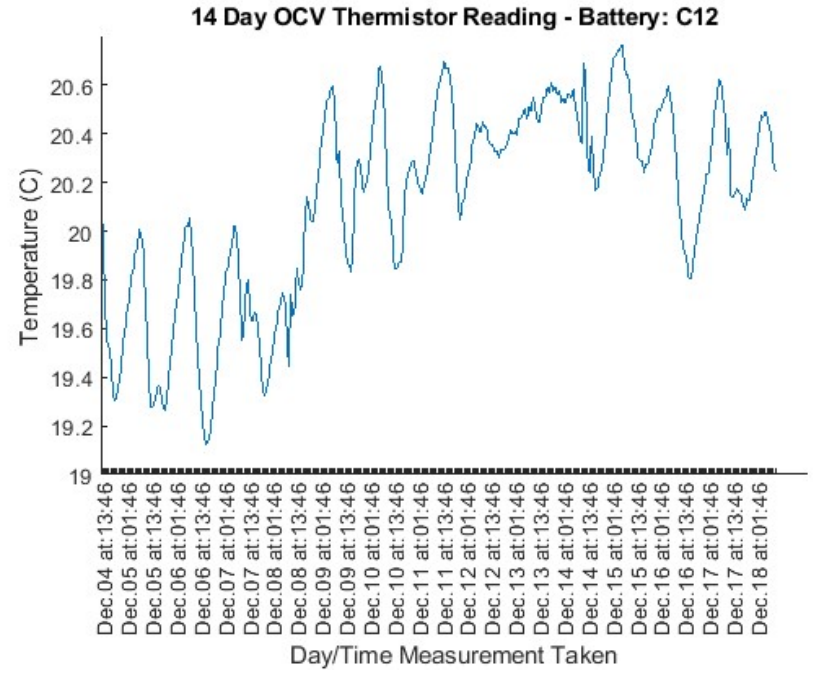

Fig. E.20:14-day OCV Temperature Readings – C12

E.2 Batch D Plots

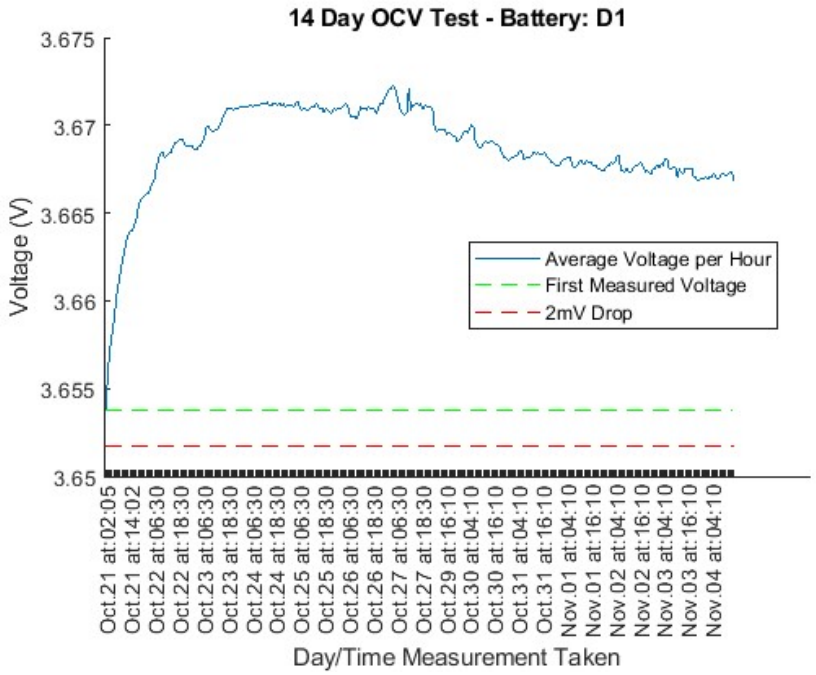

Fig. E.21:14-day OCV D1 – Passed

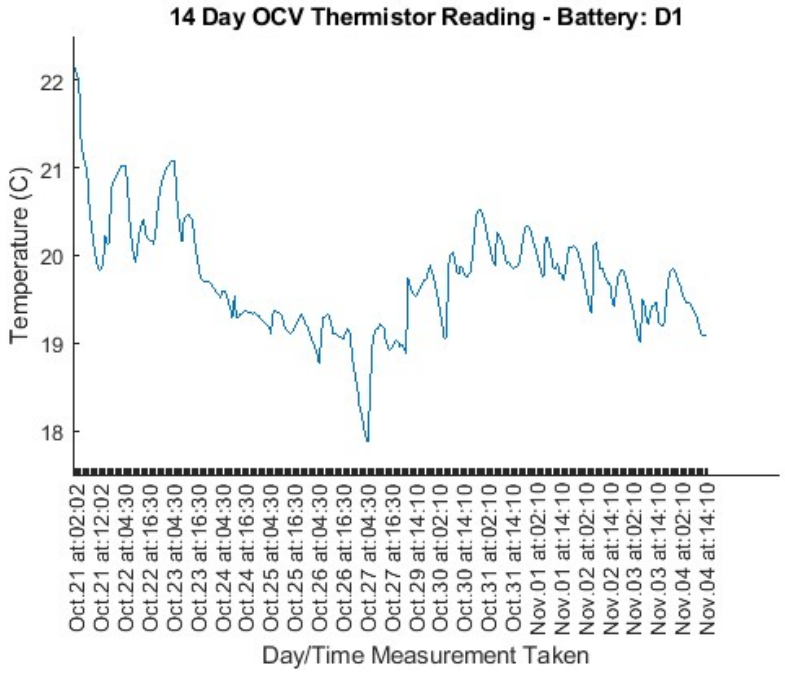

Fig. E.22:14-day OCV Temperature Readings – D1

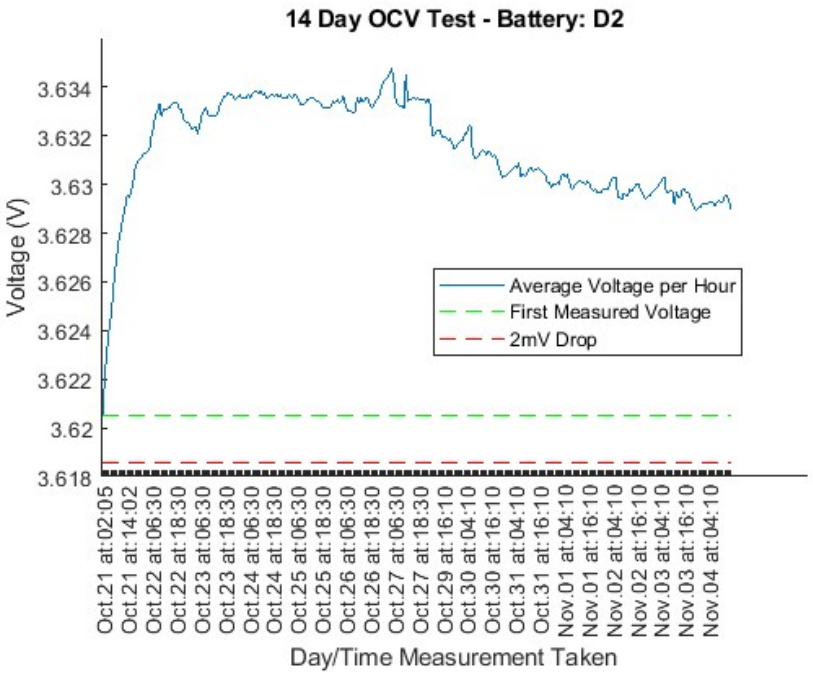

Fig. E.23:14-day OCV D2 – Passed

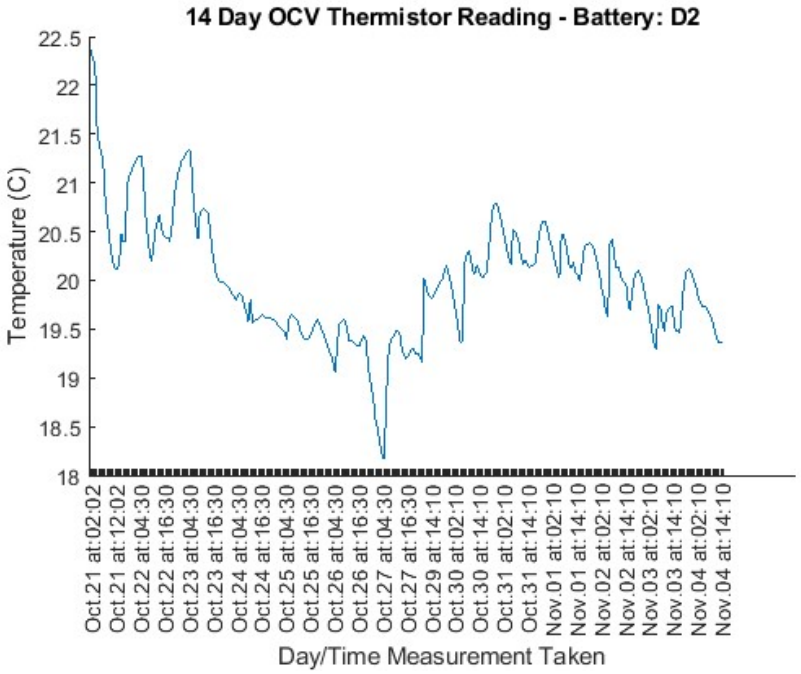

Fig. E.24:14-day OCV Temperature Readings – D2

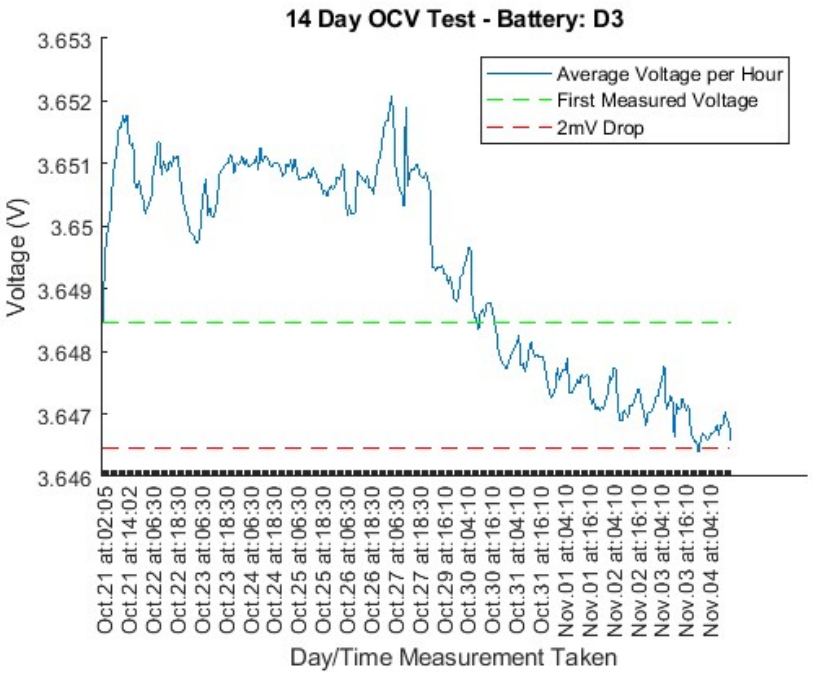

Fig. E.25:14-day OCV D3 – Passed

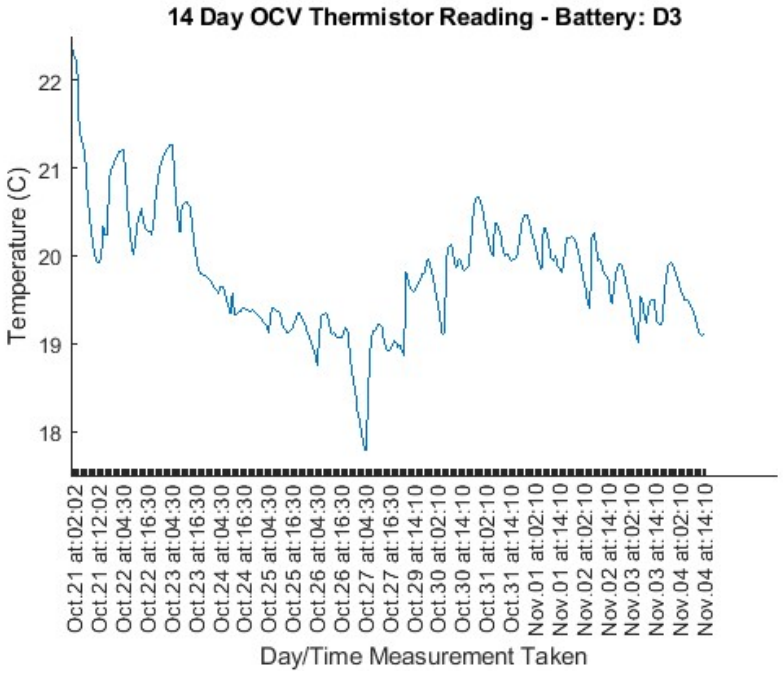

Fig. E.26:14-day OCV Temperature Readings – D3

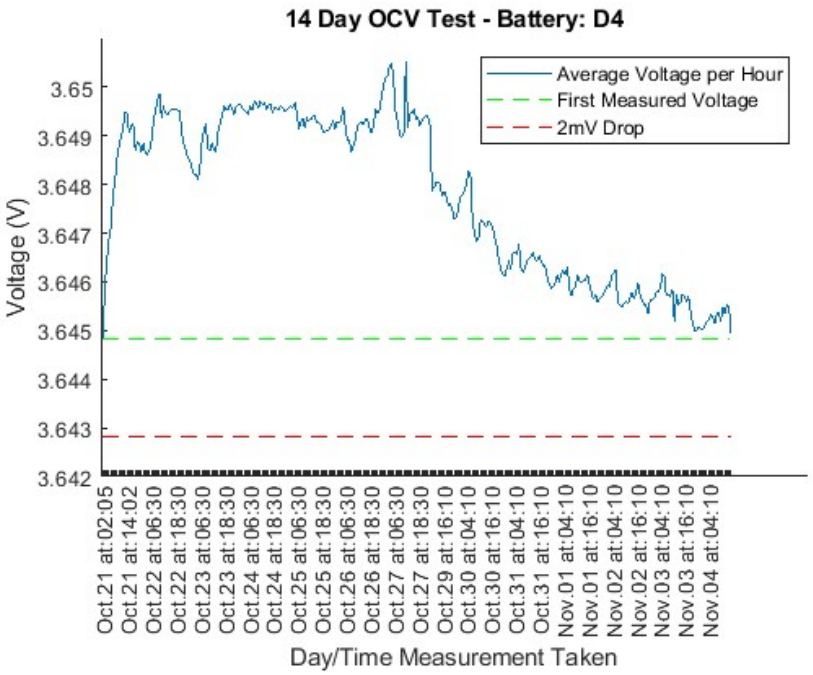

Fig. E.27:14-day OCV D4 - Passed

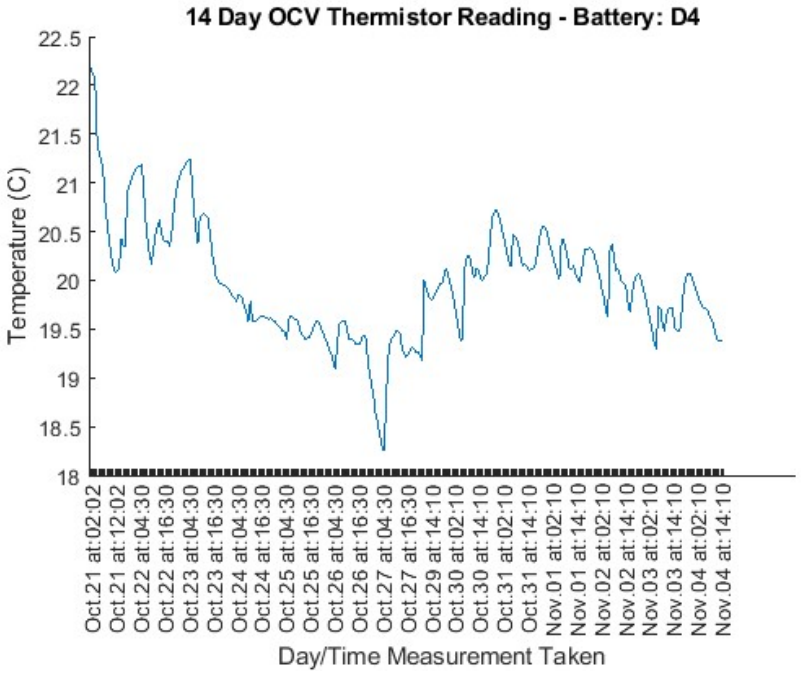

Fig. E.28:14-day OCV Temperature Readings – D4

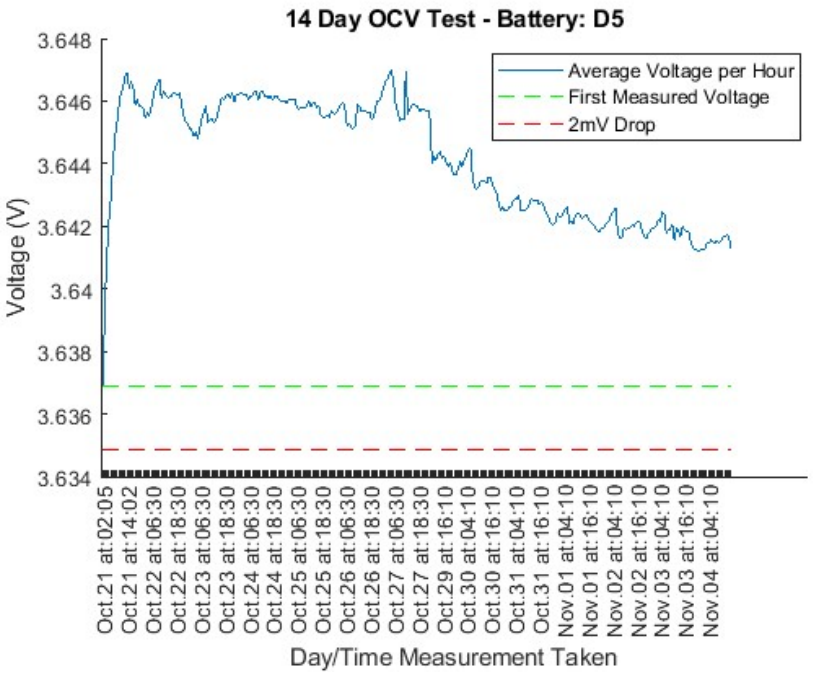

Fig. E.29:14-day OCV D5 - Passed

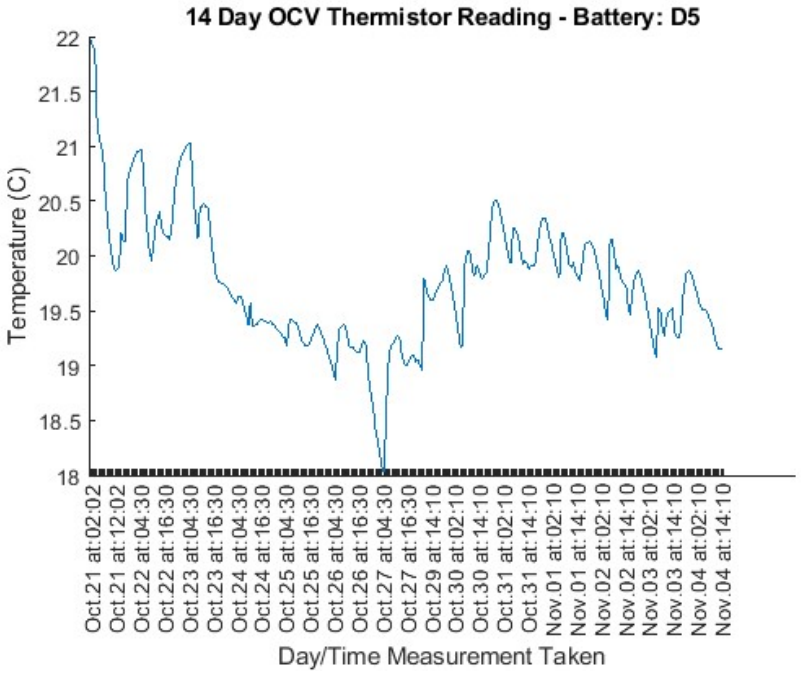

Fig. E.30:14-day OCV Temperature Readings – D5

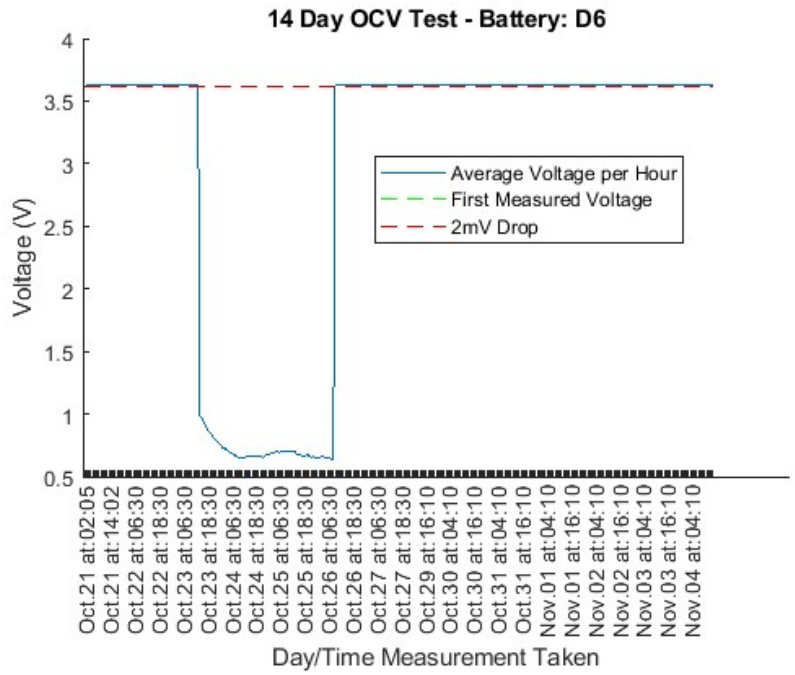

Fig. E.31:14-day OCV D6 - Passed

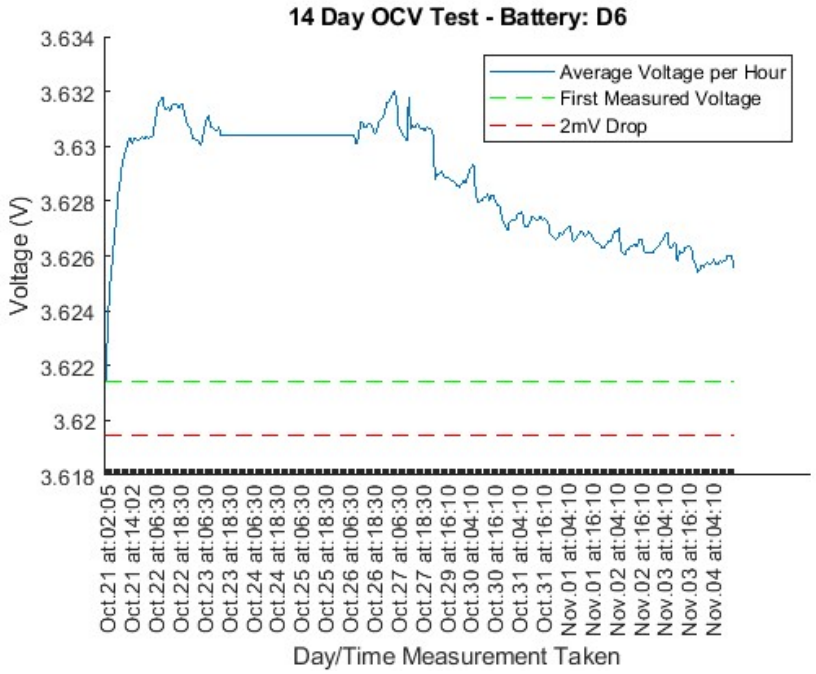

Fig. E.32: 14-day OCV D6 "Fixed" – Passed

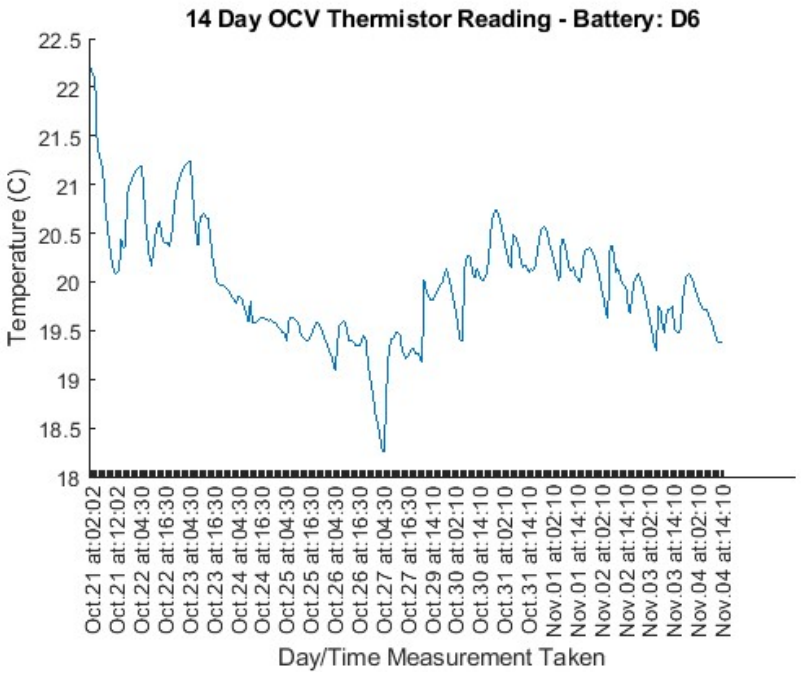

Fig. E.33:14-day OCV Temperature Readings – D6

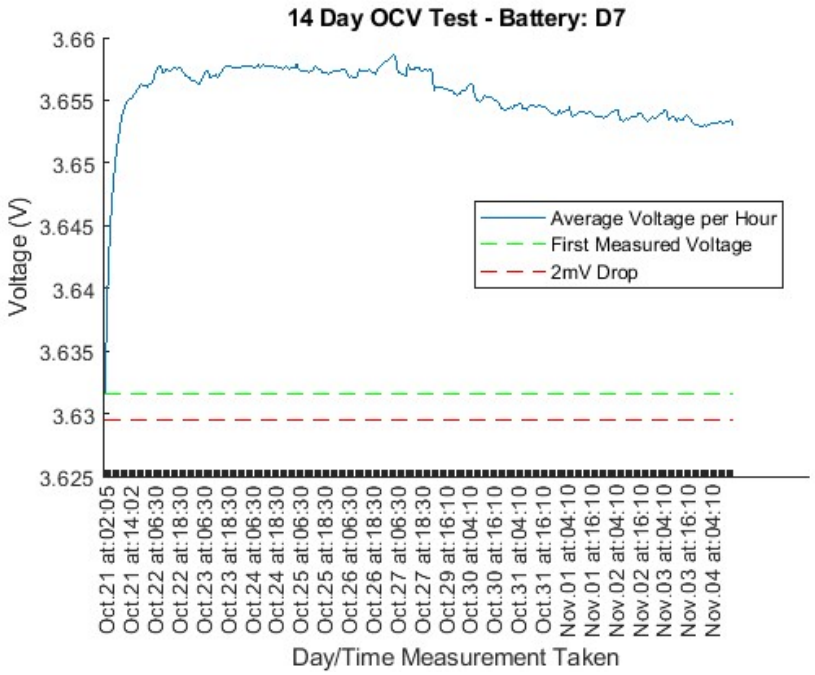

Fig. E.34: 14-day OCV D7 – Passed

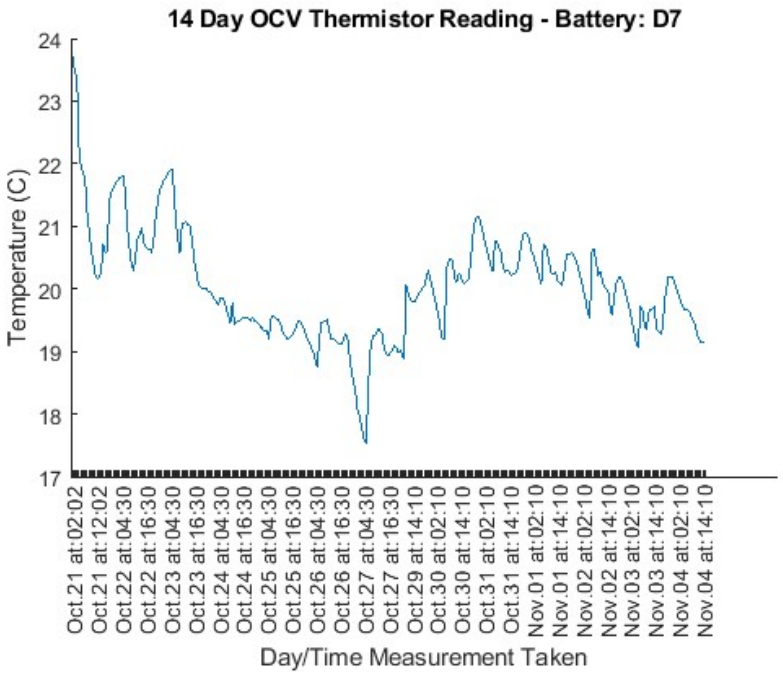

Fig. E.35:14-day OCV Temperature Readings – D7

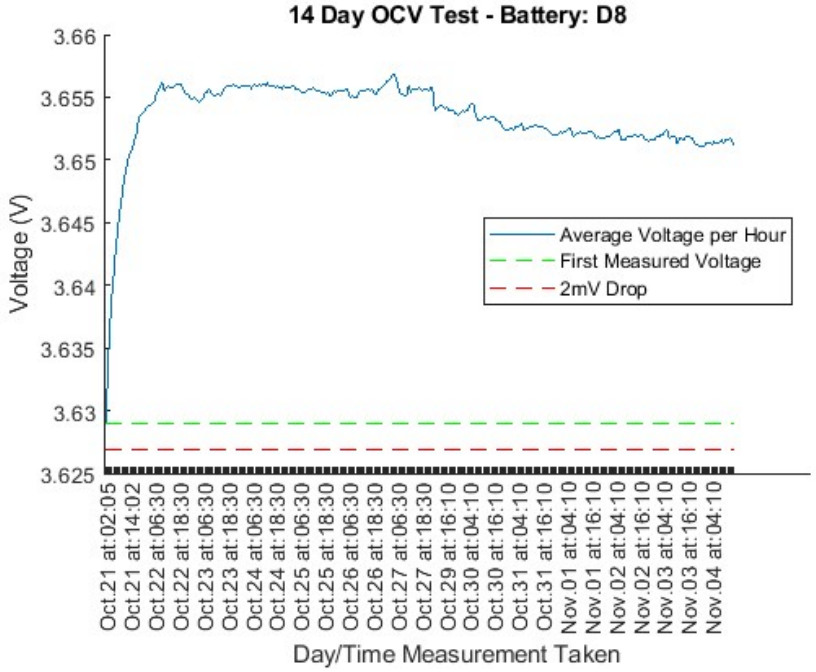

Fig. E.36: 14-day OCV D8 – Passed

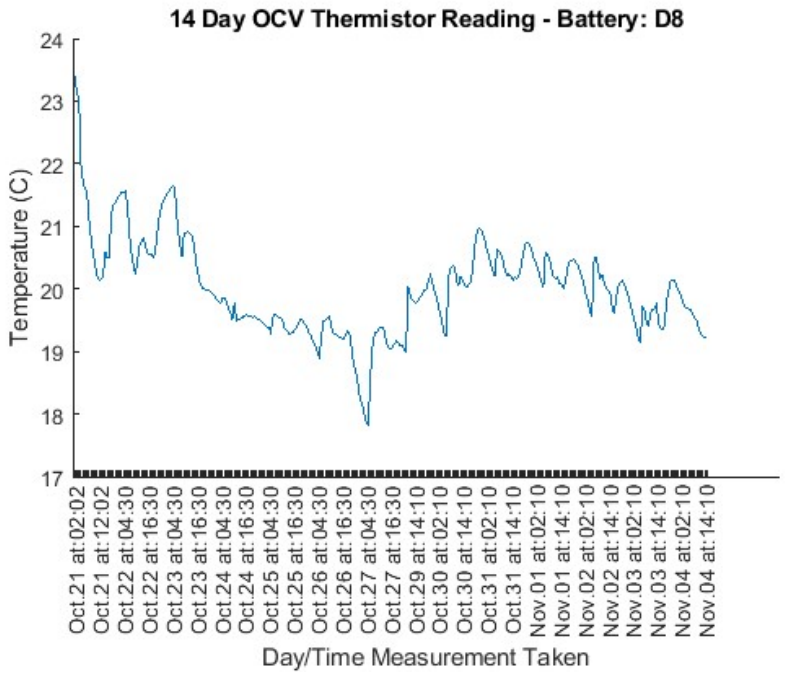

Fig. E.37:14-day OCV Temperature Readings – D8

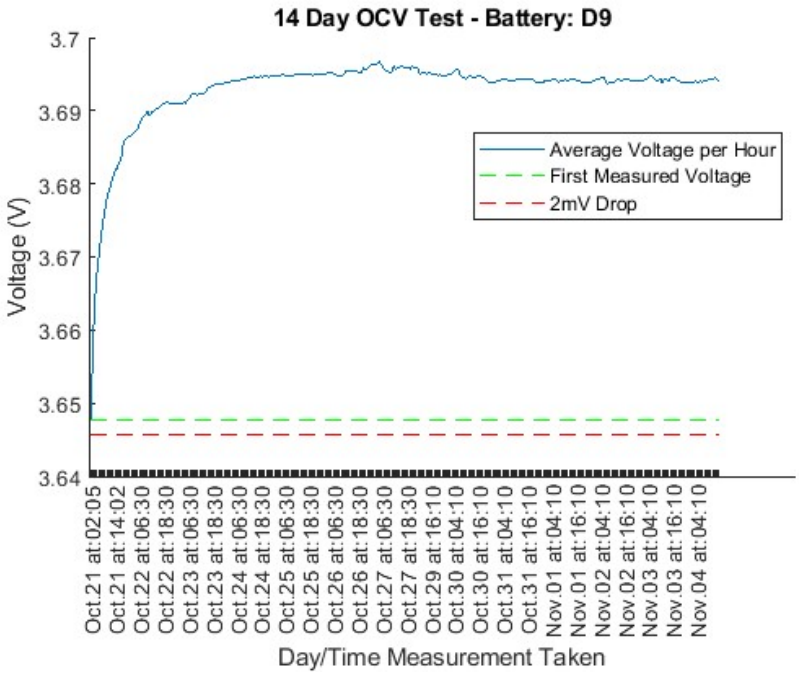

Fig. E.38: 14-day OCV D9 – Passed

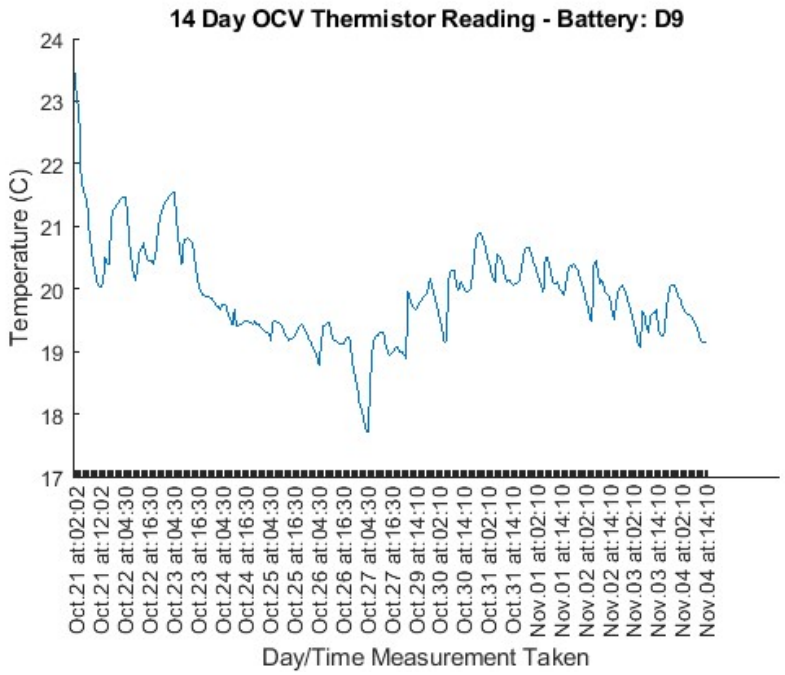

Fig. E.39:14-day OCV Temperature Readings – D9

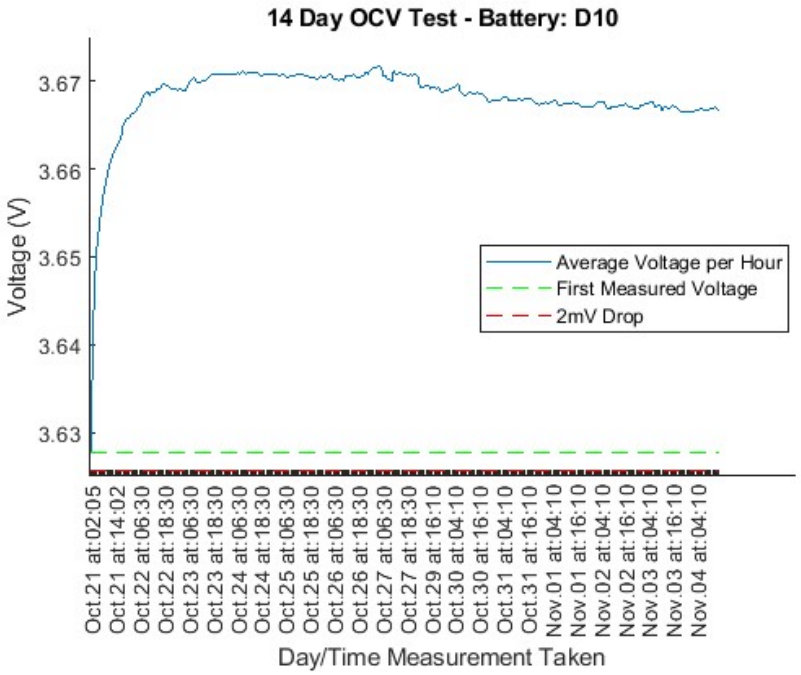

Fig. E.40: 14-day OCV D10 – Passed

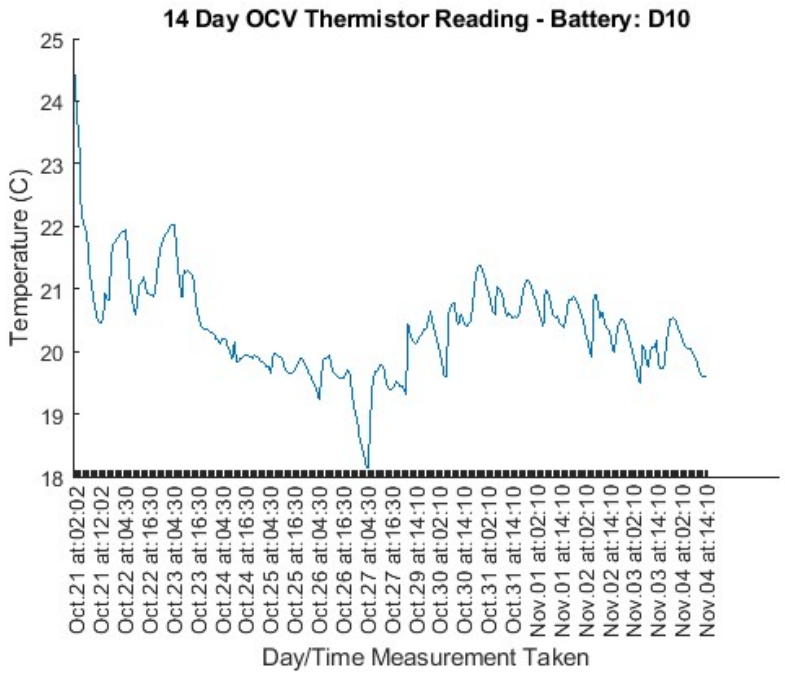

Fig. E.41:14-day OCV Temperature Readings – D10

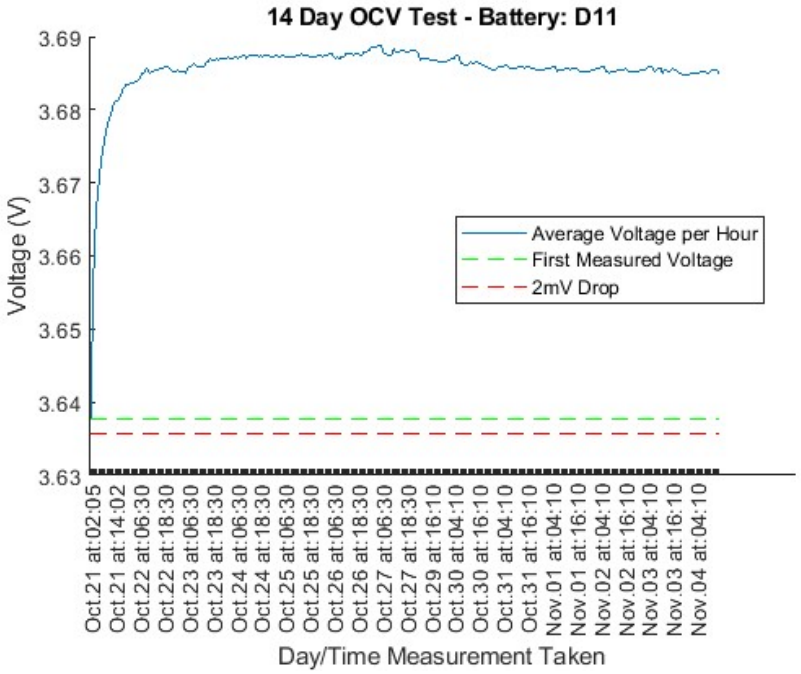

Fig. E.42: 14-day OCV D11 – Passed

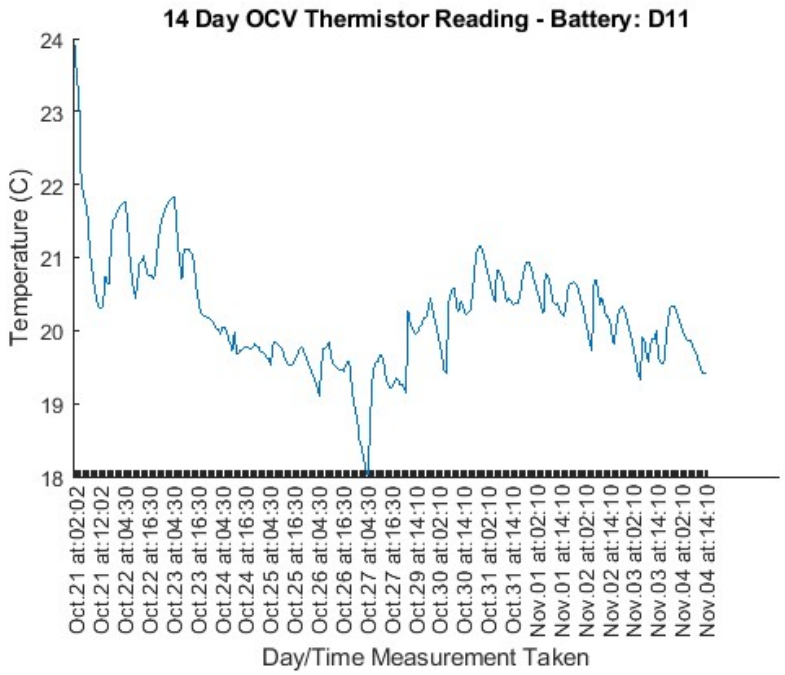

Fig. E.43:14-day OCV Temperature Readings – D11

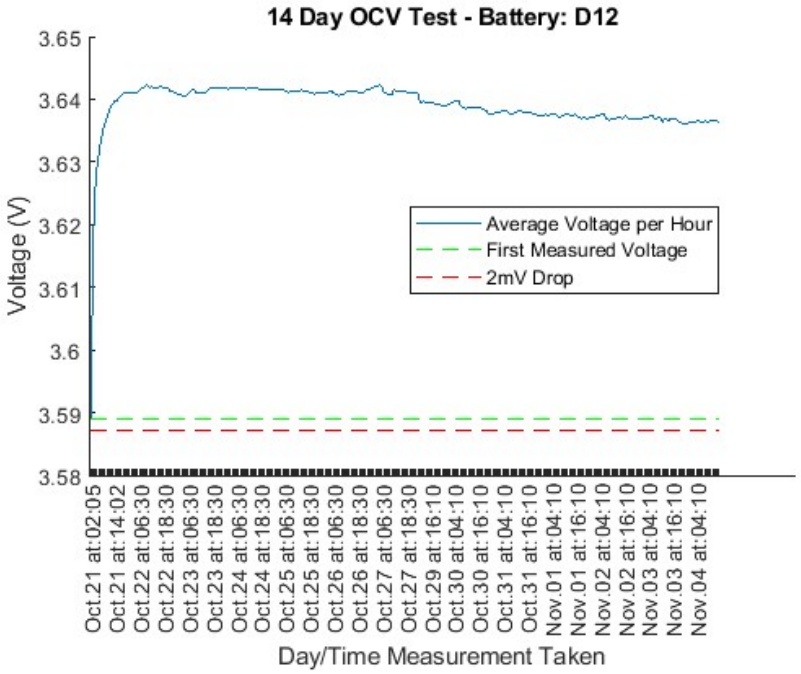

Fig. E.44: 14-day OCV D12 – Passed

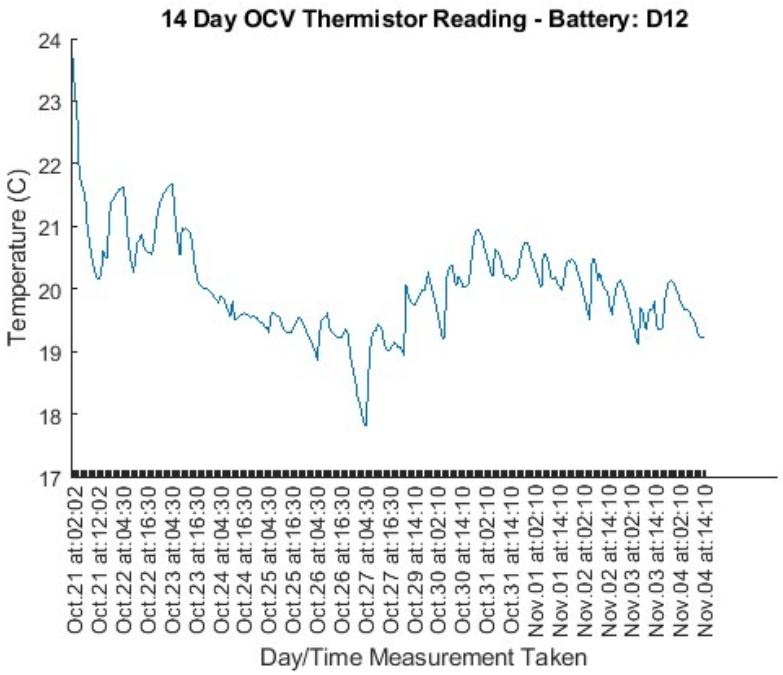

Fig E.45:14-day OCV Temperature Readings – D12

E.3 Batch E Plots

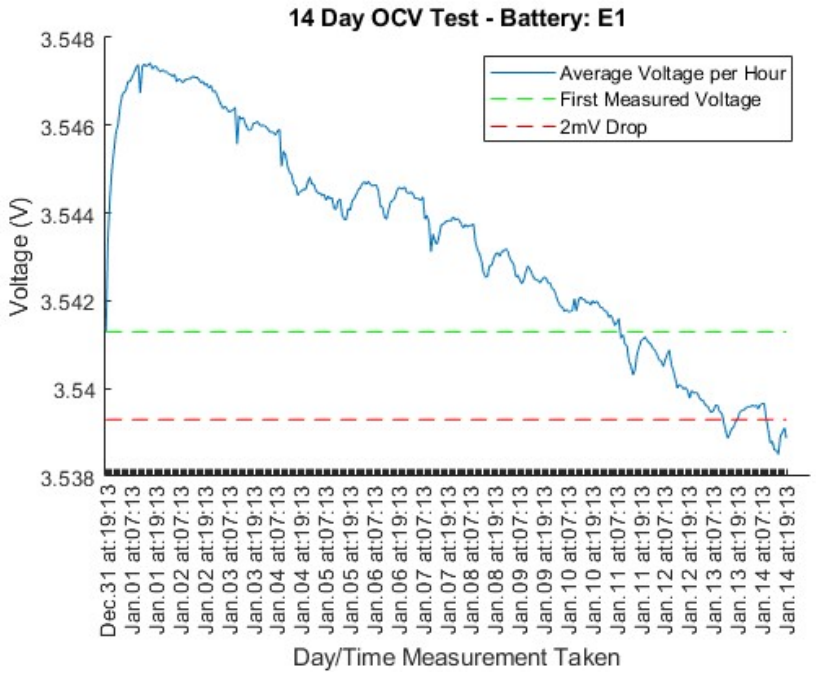

Fig. E.46: 14-day OCV E1 – Failed

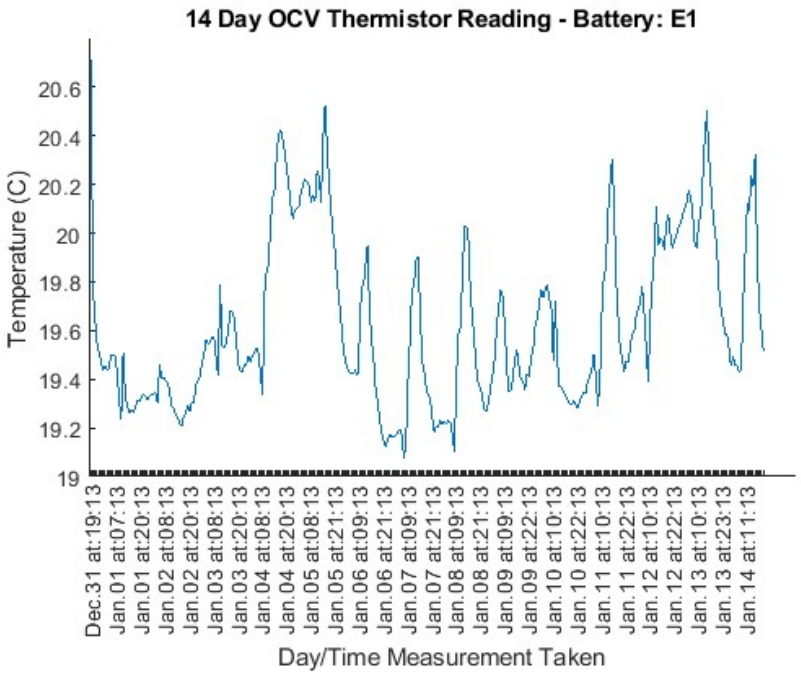

Fig. E.47:14-day OCV Temperature Readings – E1

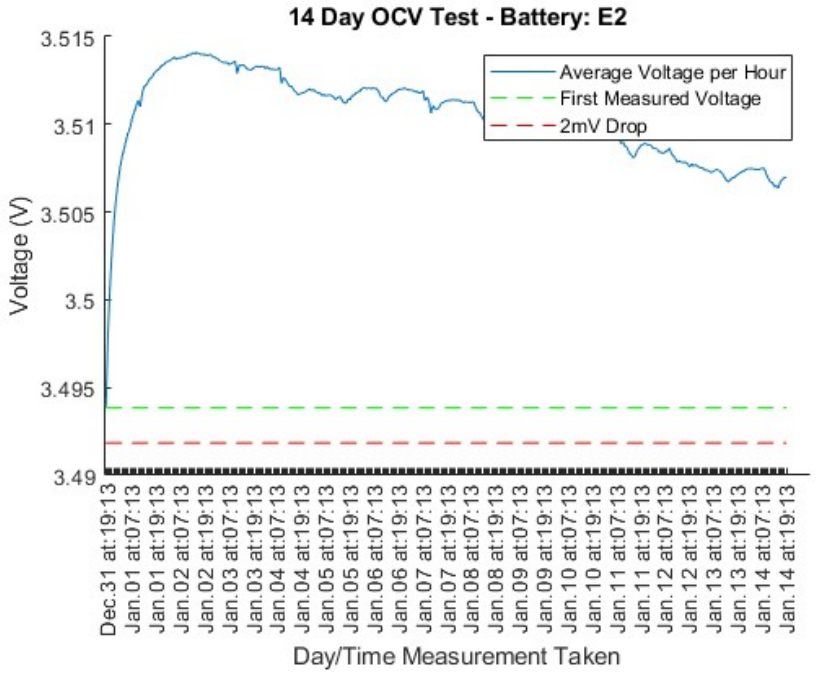

Fig. E.48: 14-day OCV E2 – Passed

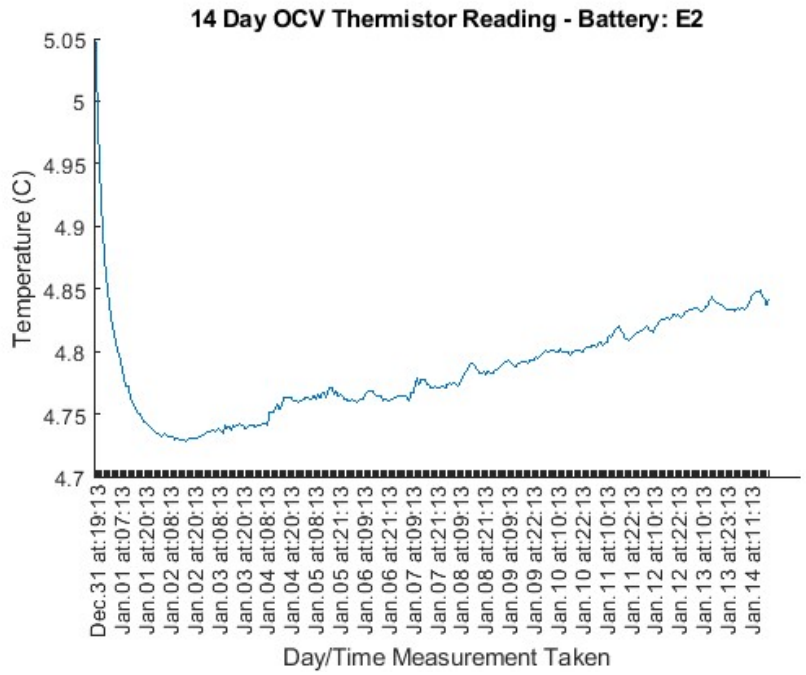

Fig. E.49:14-day OCV Temperature Readings – E2

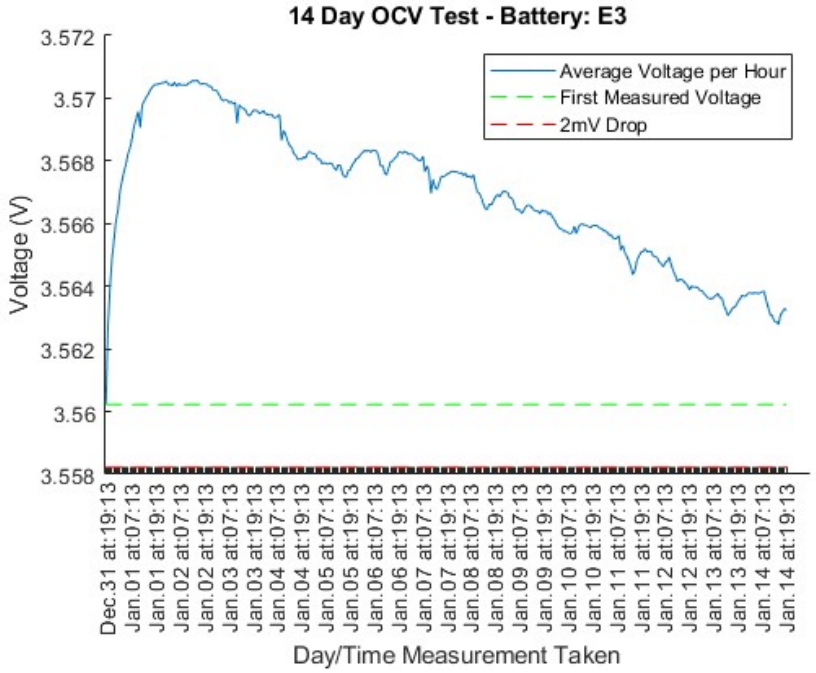

Fig. E.50: 14-day OCV E3 – Passed

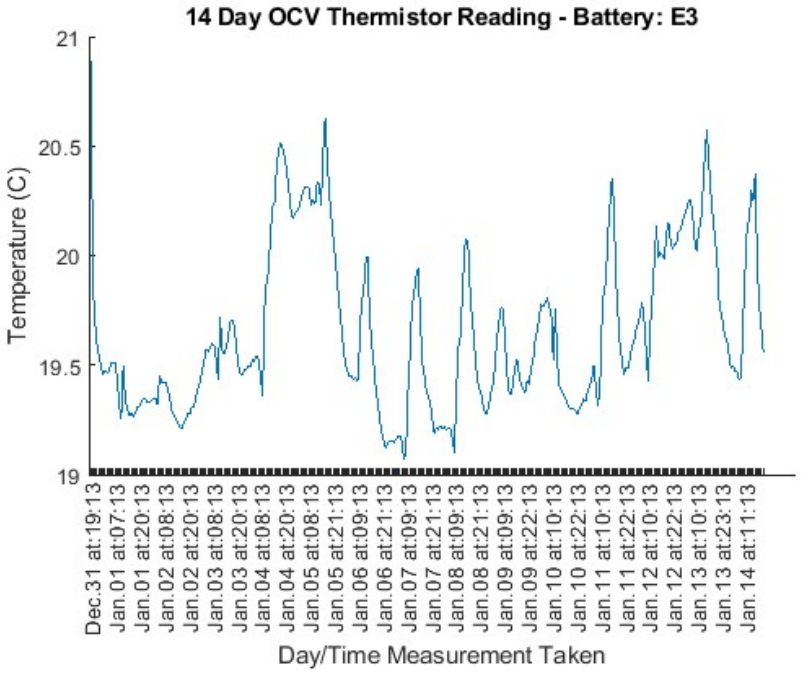

Fig. E.51:14-day OCV Temperature Readings – E3

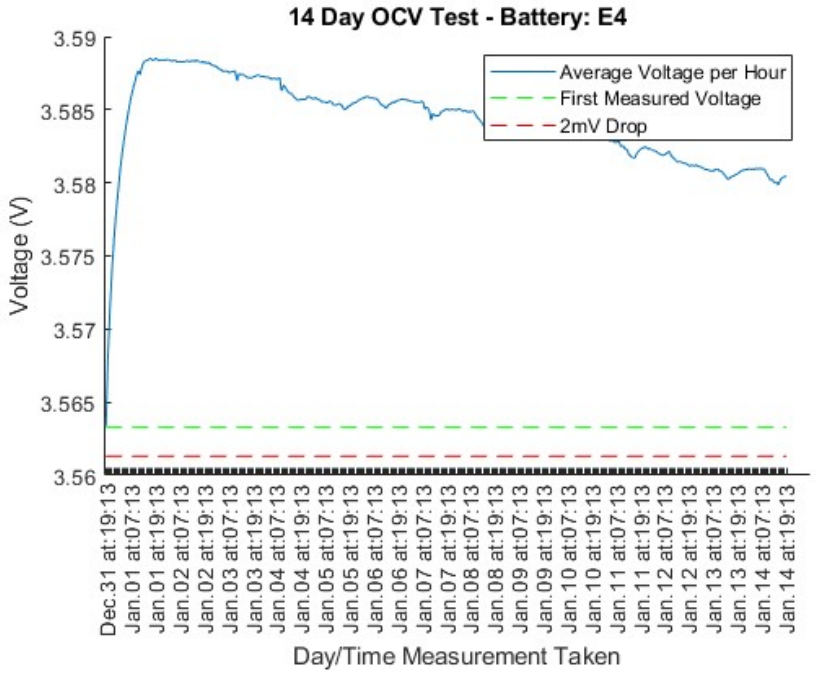

Fig. E.52: 14-day OCV E4 – Passed

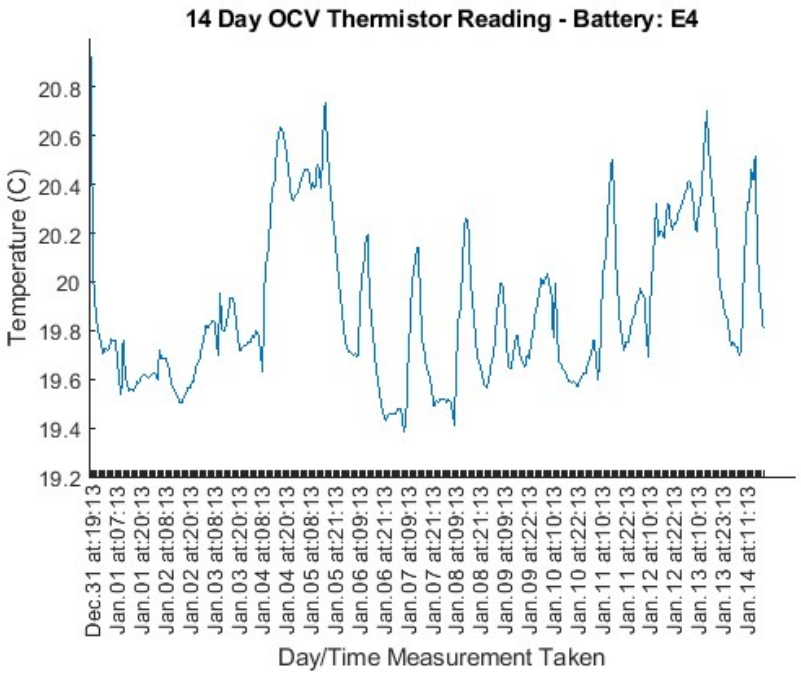

Fig. E.53:14-day OCV Temperature Readings – E4

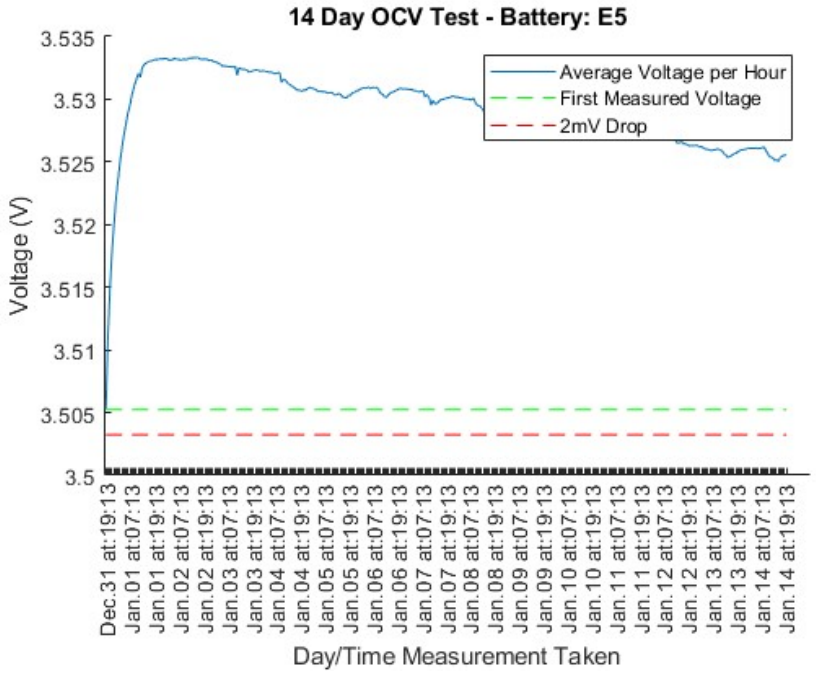

Fig. E.54: 14-day OCV E5 – Passed

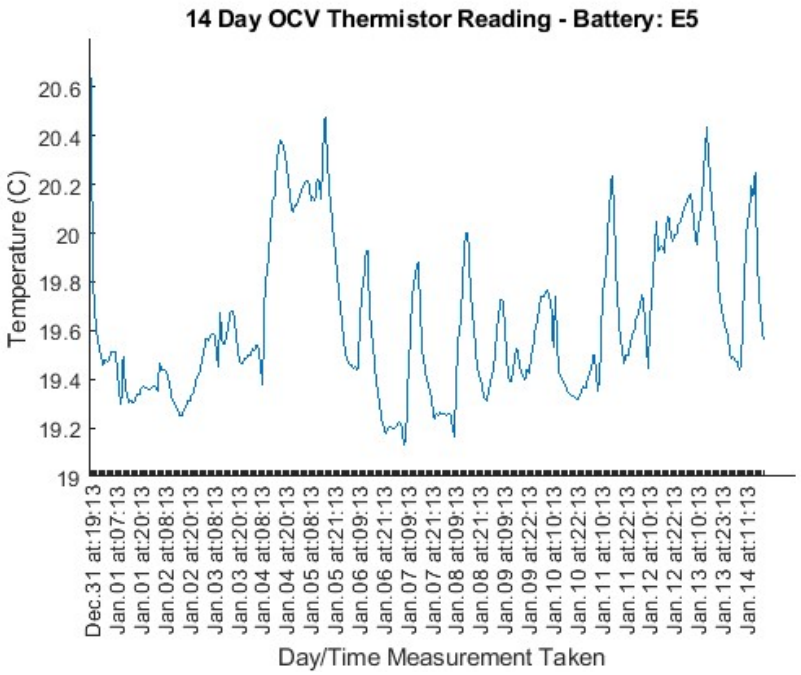

Fig. E.55:14-day OCV Temperature Readings – E5

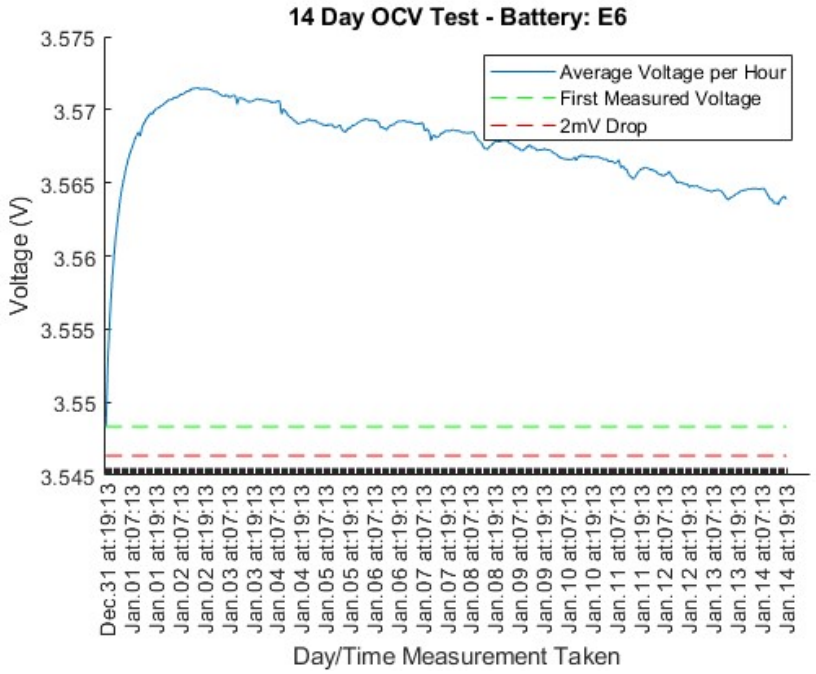

Fig. E.56: 14-day OCV E6 – Passed

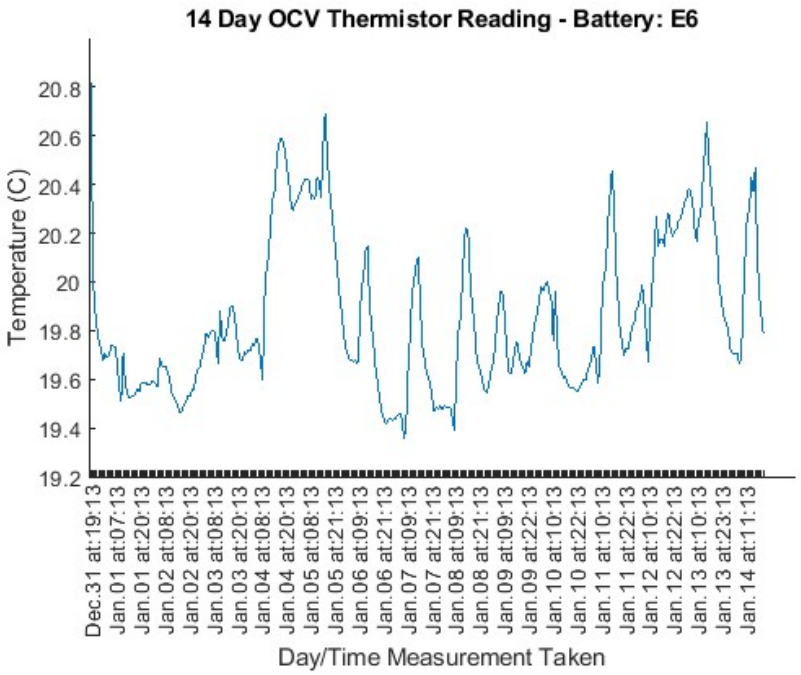

Fig. E.57:14-day OCV Temperature Readings – E6

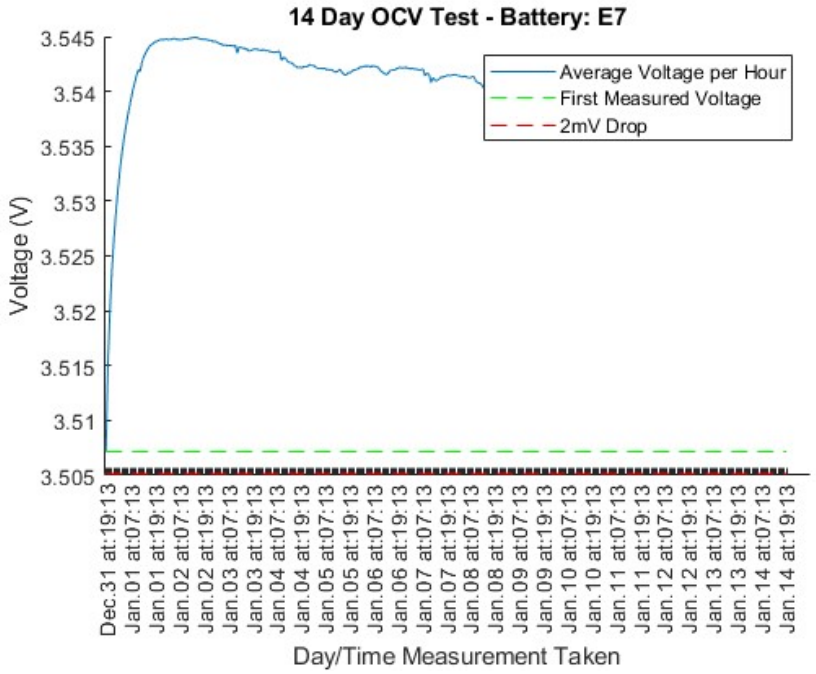

Fig. E.58: 14-day OCV E7 – Passed

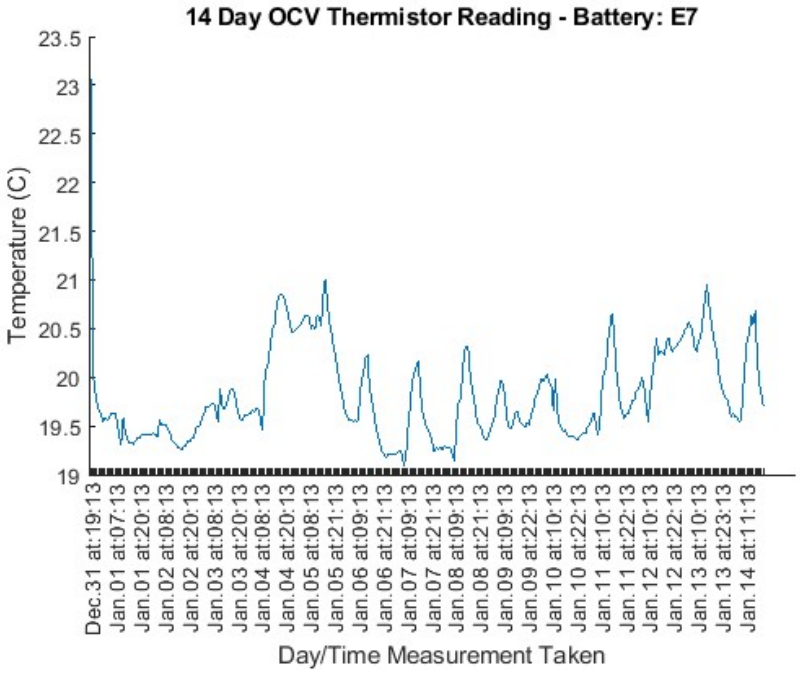

Fig. E.59:14-day OCV Temperature Readings – E7

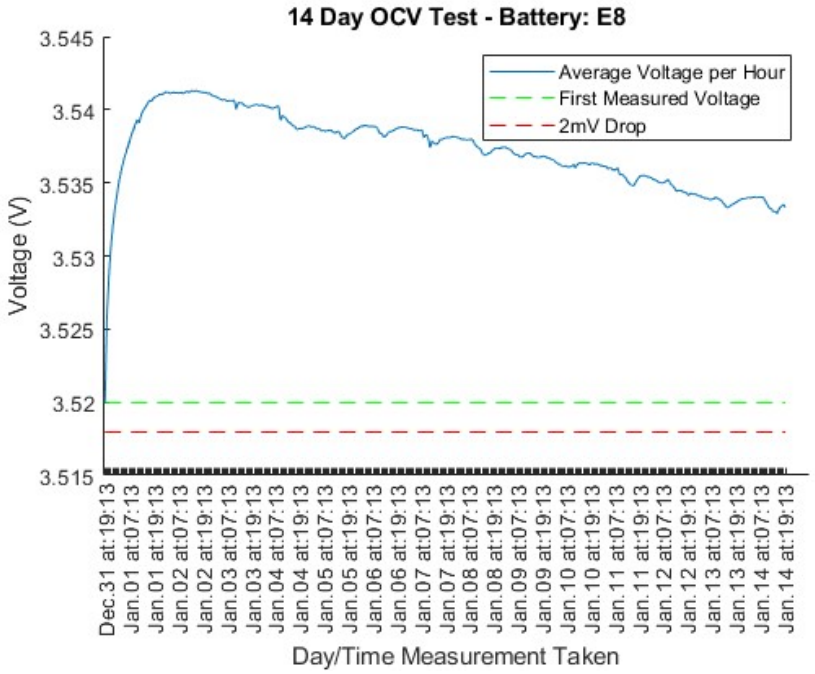

Fig. E.60: 14-day OCV E8 – Passed

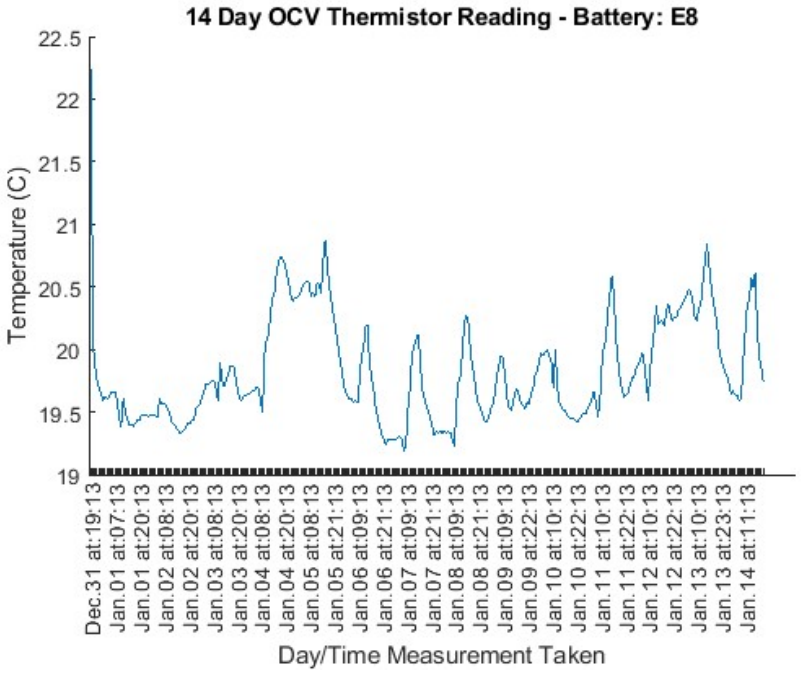

Fig. E.61:14-day OCV Temperature Readings – E8

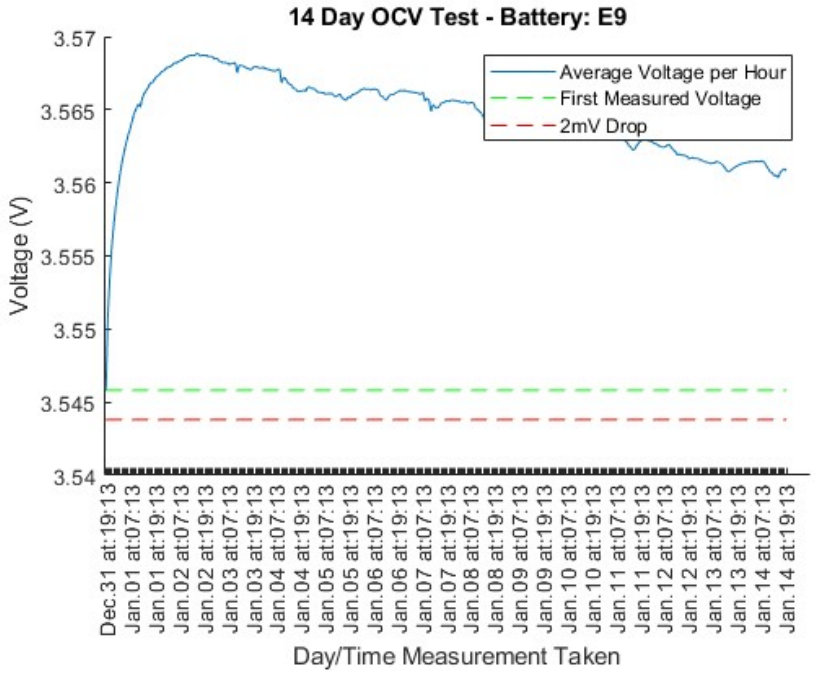

Fig. E.62: 14-day OCV E9 – Passed

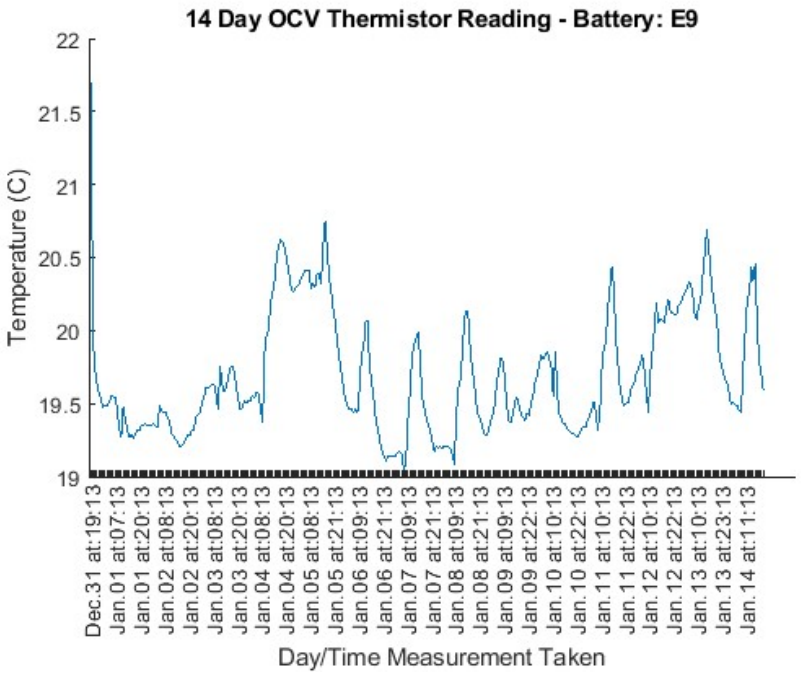

Fig. E.63:14-day OCV Temperature Readings – E9

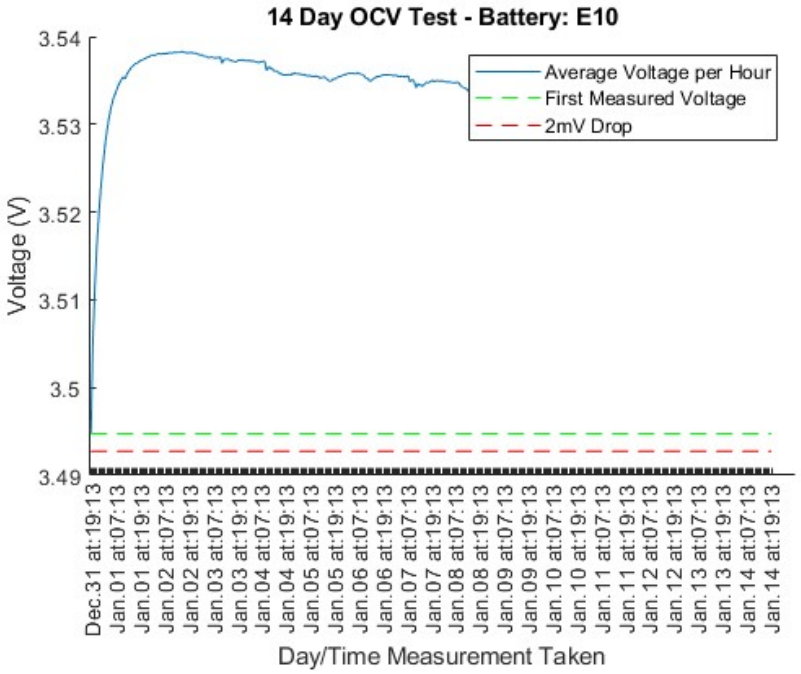

Fig. E.64: 14-day OCV E10 – Passed

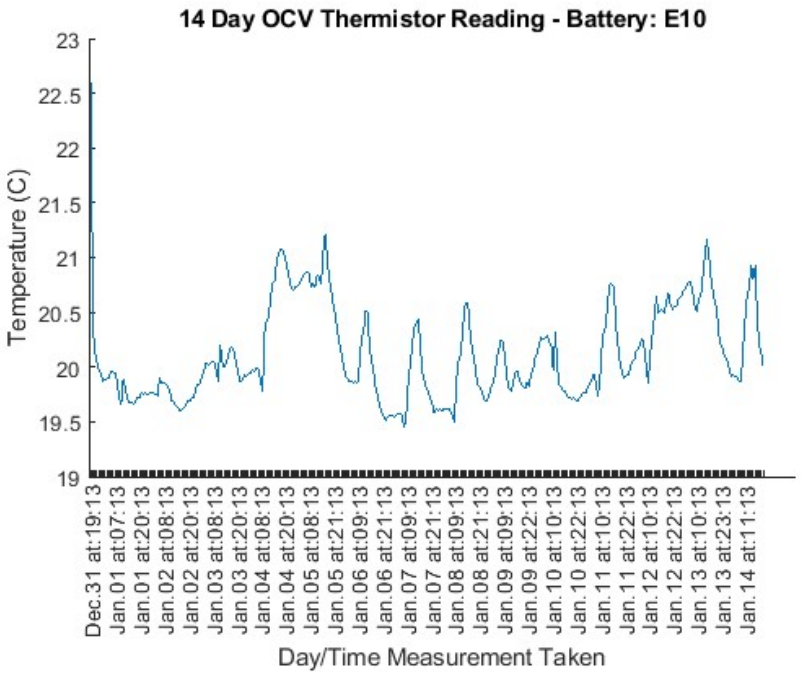

Fig. E.65:14-day OCV Temperature Readings – E10

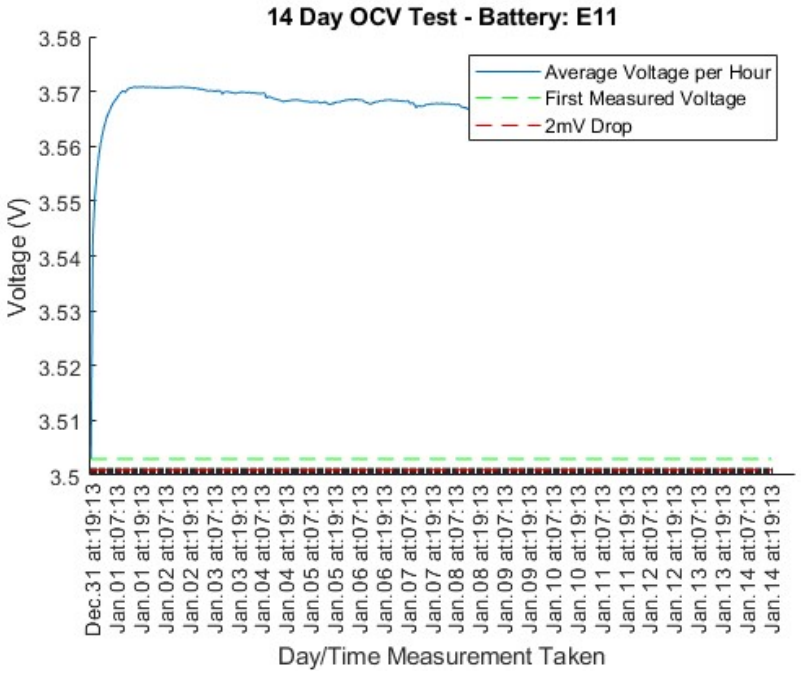

Fig. E.66: 14-day OCV E11 – Passed

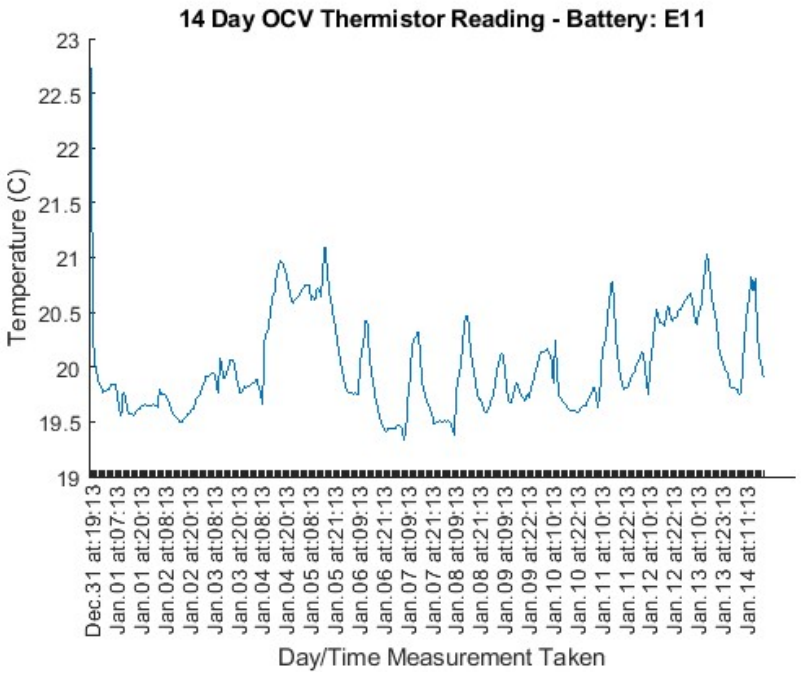

Fig. E.67:14-day OCV Temperature Readings - Battery E11

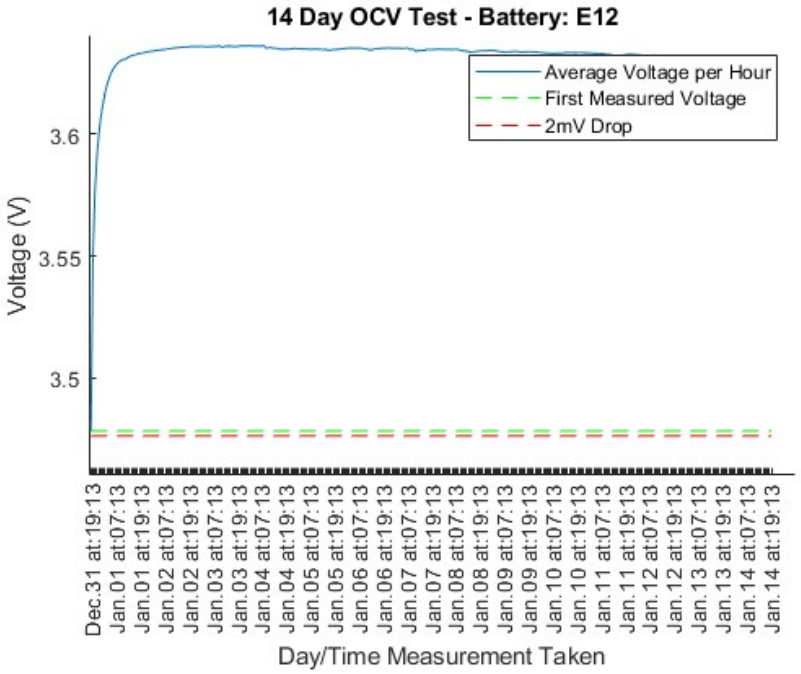

Fig. E.68: 14-day OCV E12 – Passed

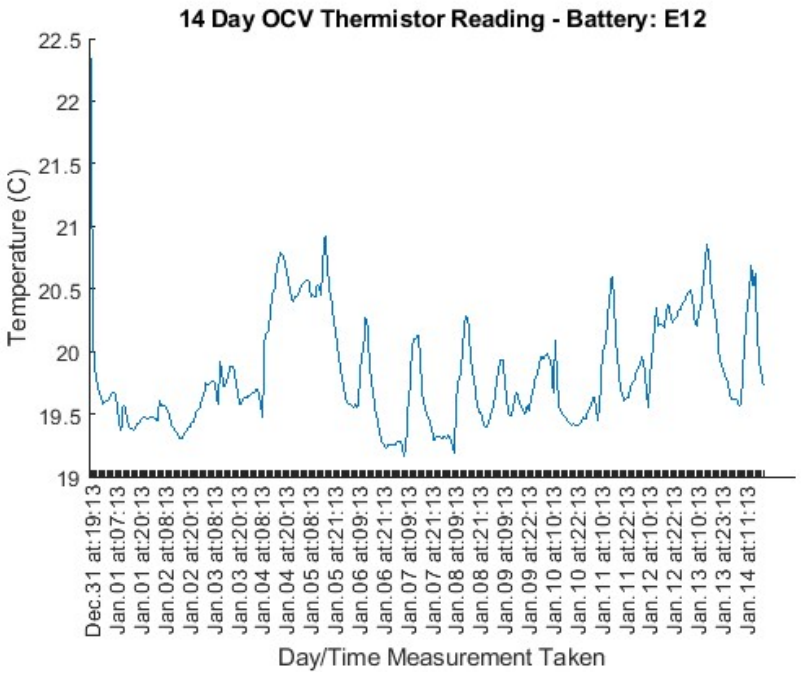

Fig. E.69:14-day OCV Temperature Readings – E12

F. Raw Data

Table F.1:Batch C battery physical measurements and initial voltage readings

Serial Number	L (mm)	W (mm)	H (mm)	OCV (V)+	CCV (V)*
C1	14.0	13.2	6.2	4.2	3.961
C2	14.1	12.8	6.1	4.2	4.063
C3	14.1	12.9	6.1	4.2	4.091
C4	14.1	12.8	6.0	4.2	3.971
C5	14.2	12.8	6.0	4.2	3.984
C6	14.0	13.0	5.9	4.2	4.043
C7	14.0	13.4	6.2	4.2	3.986
C8	14.3	13.1	6.0	4.2	3.785
C9	14.1	13.3	5.9	4.2	3.884
C10	14.2	12.9	6.1	4.2	4.045
C11	14.4	13.1	6.2	4.2	3.855

Table F.2:Batch C initial volume and mass measurements.

Serial Number	Initial Volume (cm^3)	Mass (g)
C1	1.1458	2.1
C2	1.1009	2.1
C3	1.1095	2.1
C4	1.0829	2.1
C5	1.0906	2.1
C6	1.0738	2.1
C7	1.1631	2.1
C8	1.1240	2.1
C9	1.1064	2.1
C10	1.1174	2.1
C11	1.1696	2.1
C12	1.1587	2.1

Table F.3:Batch D battery physical measurements and initial voltage readings

Serial Number	L (mm)	W (mm)	H (mm)	OCV (V)+	CCV (V)*
D1	14.1	13.6	6.0	4.2	4.157
D2	14.1	13.4	6.0	4.2	4.157
D3	14.1	13.6	6.0	4.2	4.161
D4	14.6	13.5	6.1	4.2	4.154
D5	14.2	13.6	6.1	4.2	4.156
D6	14.3	13.3	6.2	4.2	4.154
D7	14.4	13.3	6.0	4.2	4.146
D8	14.4	13.6	6.1	4.2	4.152
D9	14.5	13.4	6.0	4.2	4.143
D10	14.5	13.4	6.1	4.2	4.153
D11	14.5	13.4	5.9	4.2	4.153

Table F.4: Batch D battery volume and mass measurements

Serial Number	Initial Volume (cm^3)	Mass (g)
D1	1.1525	2.1
D2	1.1336	2.1
D3	1.1506	2.1
D4	1.2023	2.1
D5	1.1780	2.1
D6	1.1792	2.1
D7	1.1491	2.1
D8	1.1946	2.1
D9	1.1658	2.1
D10	1.1885	2.1
D11	1.1464	2.1
D12	1.1427	2.1

Table F.5: Batch E battery physical measurements and initial voltage readings

Serial Number	L (mm)	W (mm)	H (mm)	OCV (V)+	CCV (V)*
E1	14.6	12.9	6.3	4.2	4.156
E2	14.4	13.3	6.1	4.2	4.144
E3	14.4	12.9	6.1	4.2	4.152
E4	14.2	13.0	6.1	4.2	4.148
E5	14.2	12.9	6.0	4.2	4.144
E6	14.0	12.9	6.1	4.2	4.152
E7	14.1	12.9	6.1	4.2	4.155
E8	13.7	12.8	6.3	4.2	4.142
E9	13.9	12.8	6.1	4.2	4.159
E10	13.8	12.8	6.1	4.2	4.161
E11	14.0	13.0	6.0	4.2	4.139

Table F.6: Batch E battery volume and mass measurements

Serial Number	Initial Volume (cm^3)	Mass (g)
E1	1.1865	2.1
E2	1.1683	2.1
E3	1.1331	2.1
E4	1.1261	2.0
E5	1.0991	2.1
E6	1.1017	2.1
E7	1.1095	2.1
E8	1.1048	2.1
E9	1.0853	2.1
E10	1.0775	2.1
E11	1.0920	2.1
E12	1.1076	2.1

G. LTO Structure

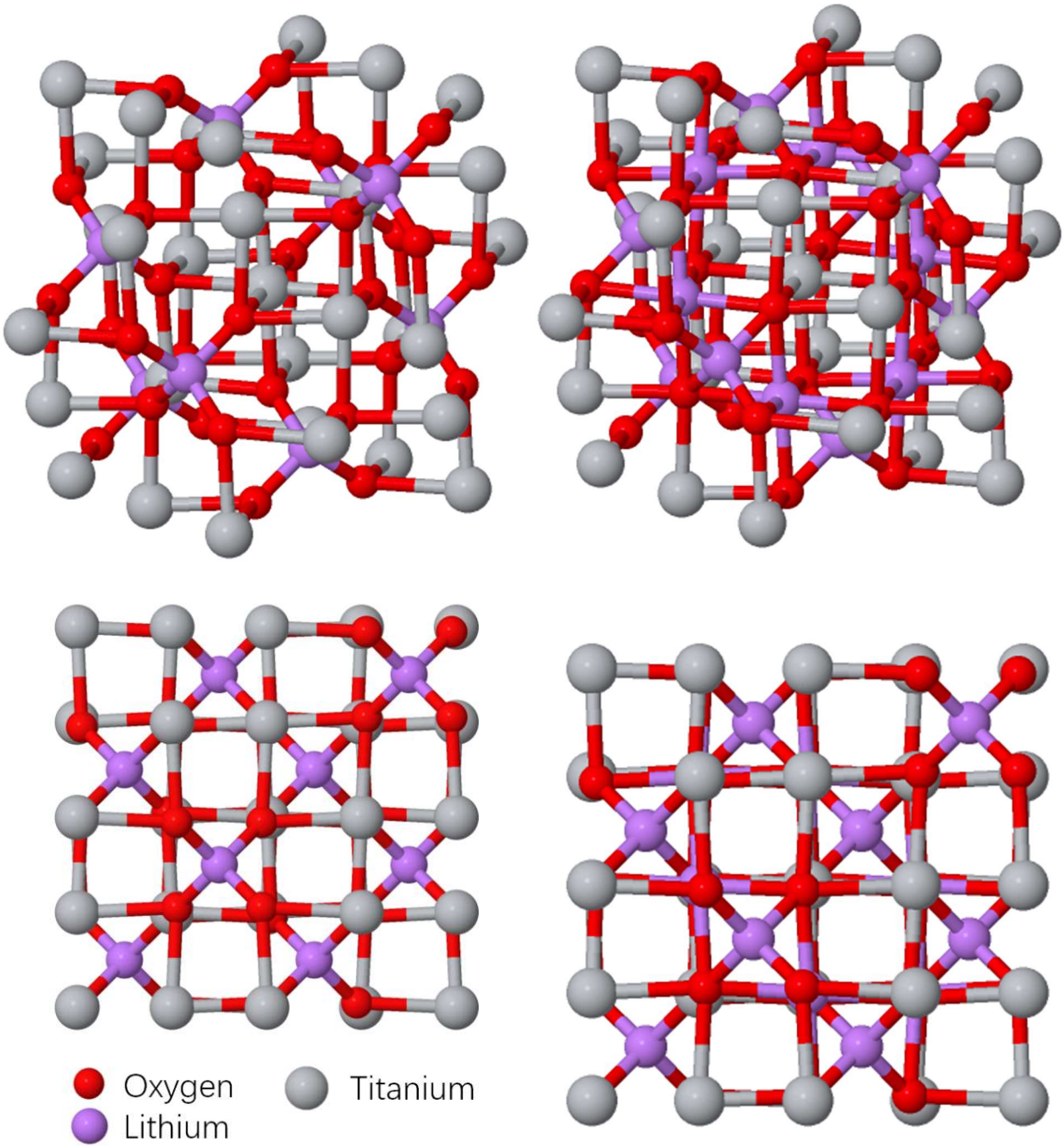

Figure G.1: Delithiated and lithiated LTO. **Top Left**: Isometric view of LiTi5O12. **Bottom Left**: Face view of LiTi5O12. **Top Right**: Isometric view of LiTi7O12. **Bottom Right**: Face view of LiTi7O12.

H. Sampling Rate Calculations

With National Instruments (NI) DAQs the sampling rates must be a division of the source clock, in this case the analog hardware clocks were used. If the requested sampling rate is not an allowable division of the source clock, then the DAQ will actually sample at an allowable division that is as close as possible to the requested amount. Per [113], the equation for allowable sampling rate divisions is shown here:

$$Allowable\ Sample\ Rate = \frac{Timebase}{2^n} \quad \text{(H.1)}$$

Where n is an integer between 1 and the maximum bits of the sample clock divisor, and Timebase is the frequency of the source clock.

The only concern is with AO channels, as the analog measurements are the only part that need to be recorded at a consistent rate. The relevant information is shown in Table H.1.

Table H.1: Relevant NI DAQ properties used to calculate allowable sample rates.

DAQ #	Model #	AO Sample Clock divisor (bits)	Timebase (MHz)
Dev1	PCI-6035E	24	20
Dev3	USB-6211	32	80
Dev5	PCIe-6259	32	80*

*Note: E series listed “up to 80 MHZ”. 80 was chosen just to be consistent.

Tables H.2 and H.3 were compiled using the data from Table H.1 with Eq. H.1. Note that for n less than 13 in Table H.2 the allowable sample rate is not shown because a sampling rates of ~2.4k and greater caused too large of files. This is the same reason that n less than 15 are shown on Table H.3.

Table H.2: The allowable sample rates for DAQs with a 20 MHz Timebase

n	Allowable Sample Rate (Hz)
1	10×10^6
2	5×10^6
…	
13	2441.406250
14	1220.7031250
15	610.35156250
16	305.175781250
17	152.5878906250
18	76.29394531250
19	38.146972656250
20	19.0734863281250
21	9.53674316406250
22	4.768371582031250
23	2.38418579115620
24	1.19209289557810

Table H.3: The allowable sample rates for DAQs with an 80 MHz Timebase

n	Allowable Sample Rate (Hz)
1	40×10^6
2	20×10^6
…	
15	2441.406250
16	1220.7031250
17	610.35156250
18	305.175781250
19	152.5878906250
20	76.29394531250
21	38.146972656250
22	19.0734863281250
23	9.53674316406250
24	4.768371582031250
…	
32	0.018626451

I. -Discharge Plots

I.1 Batch C Plots

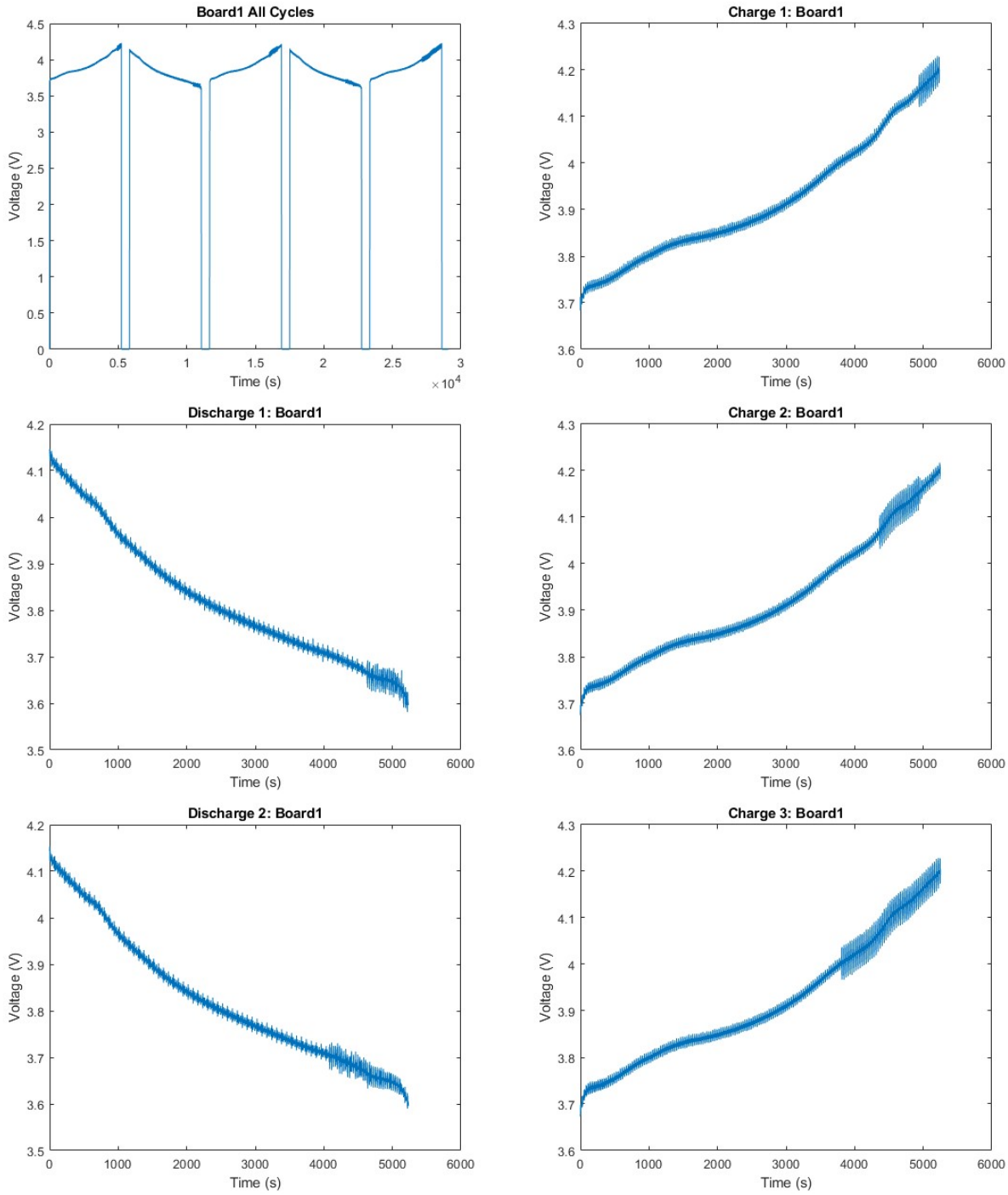

Fig. I.1:Charge-discharge curves for C2

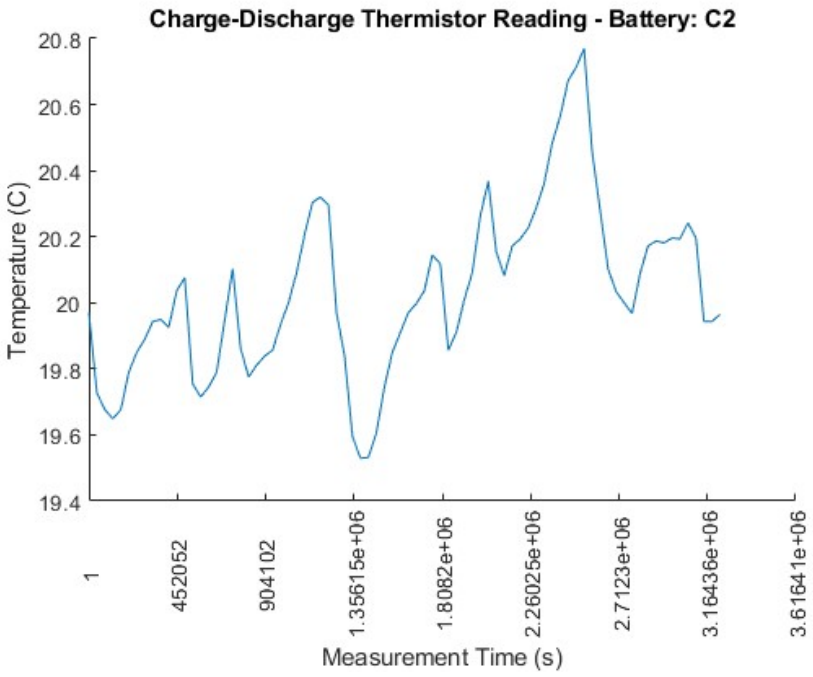

Fig. I.2: Temperature of C2 during Charge-Discharge Test

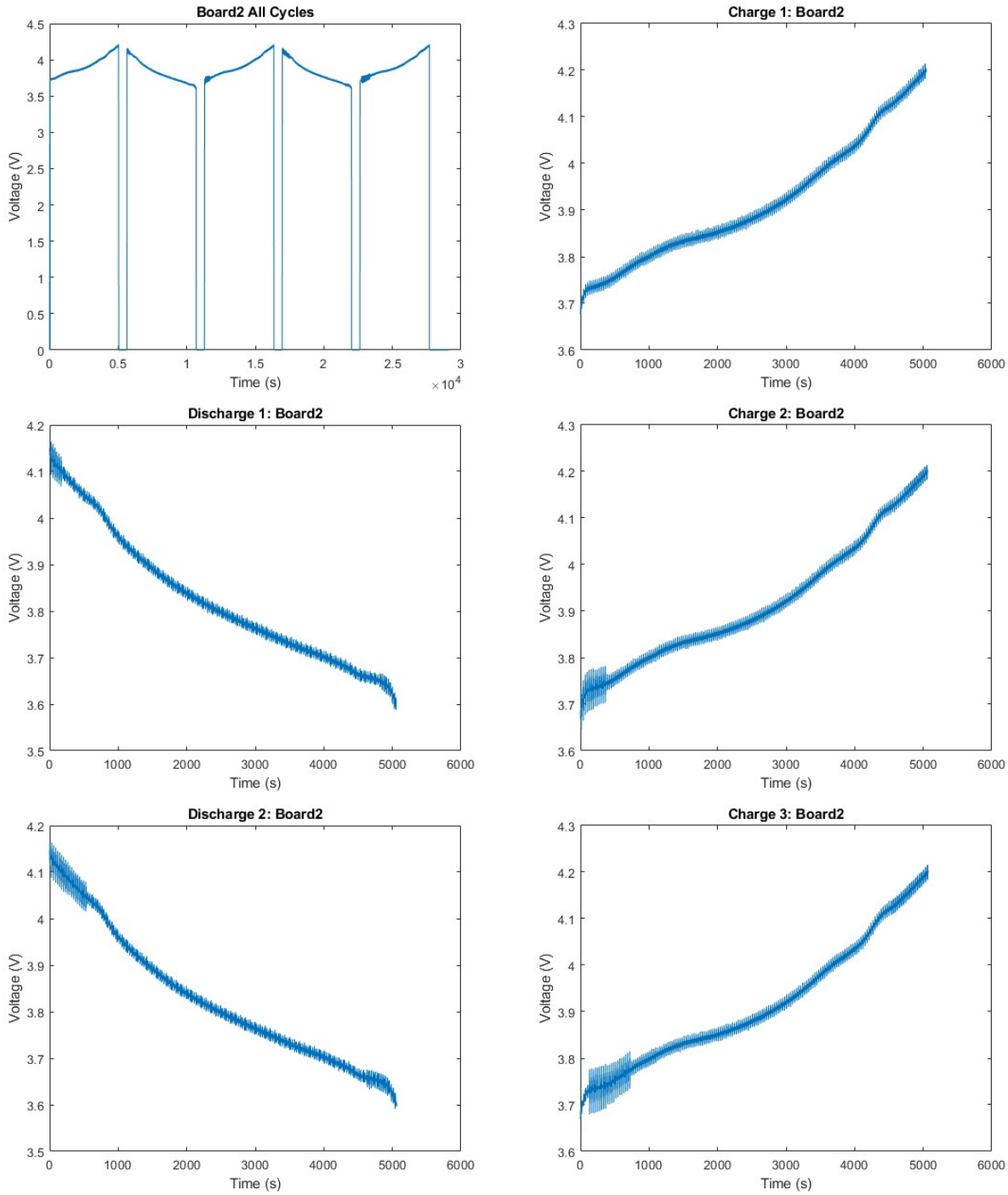

Fig. I.3: Charge-discharge curves for C3

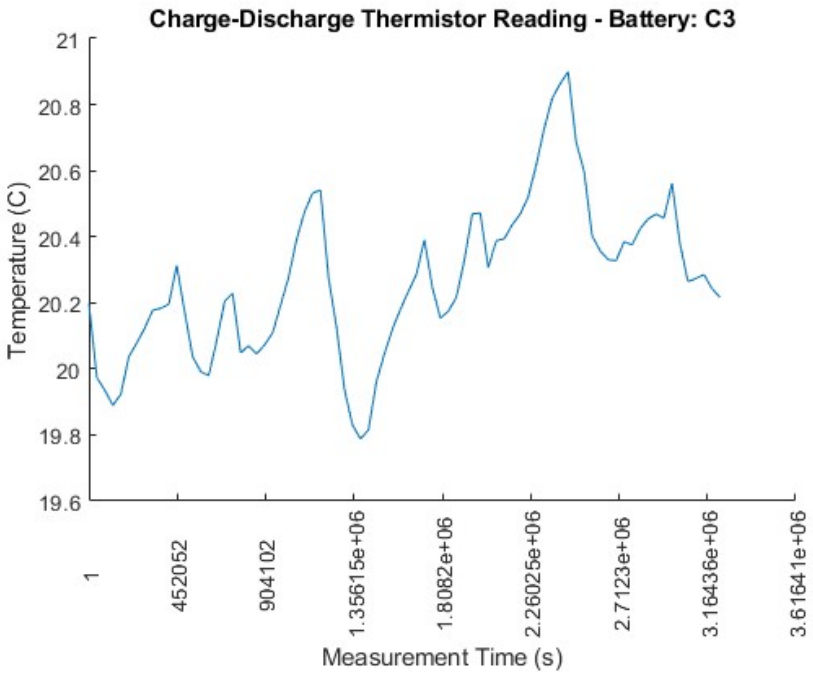

Fig. I.4: Temperature of C3 during Charge-Discharge Test

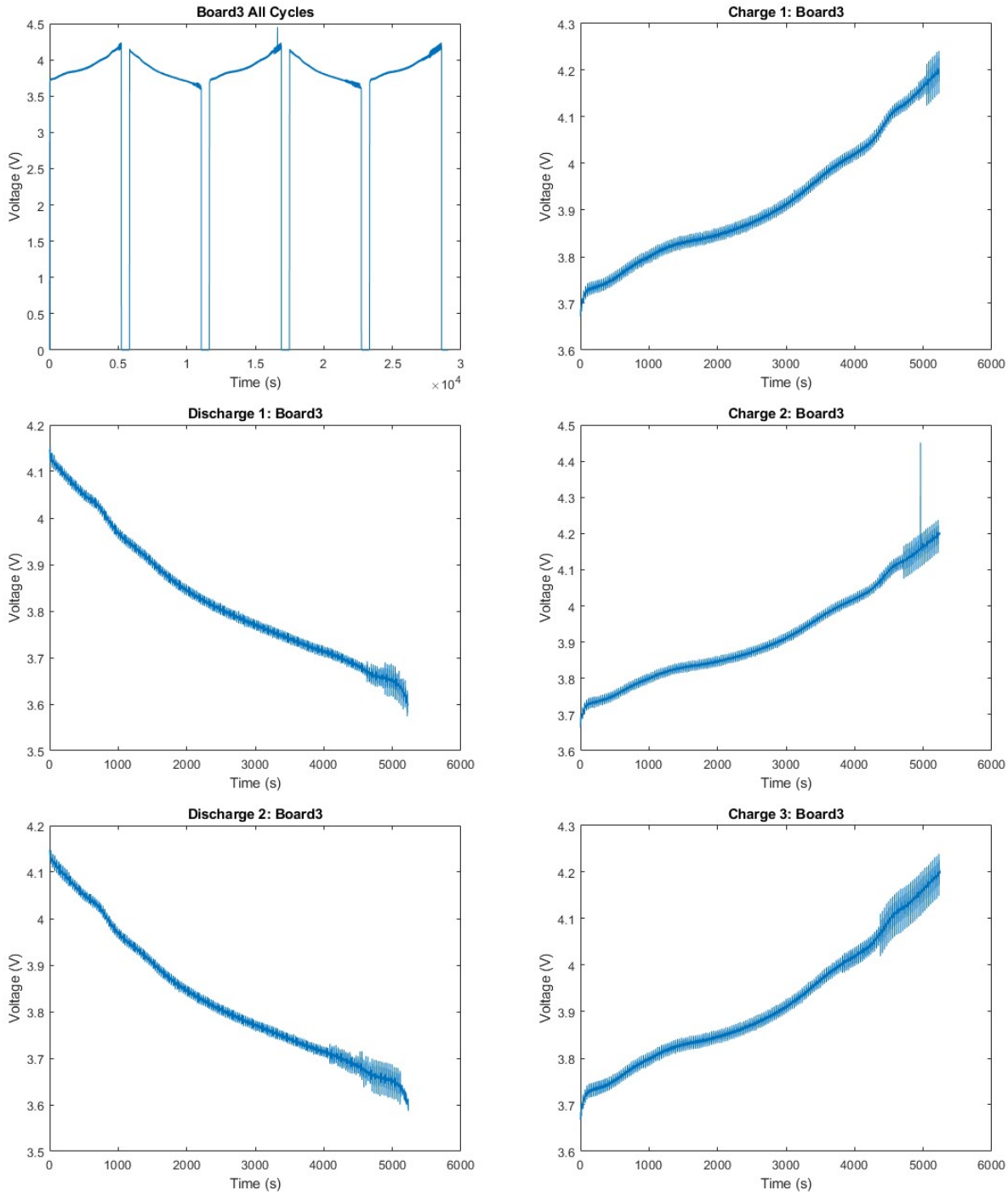

Fig. I.5: Charge-discharge curves for C4

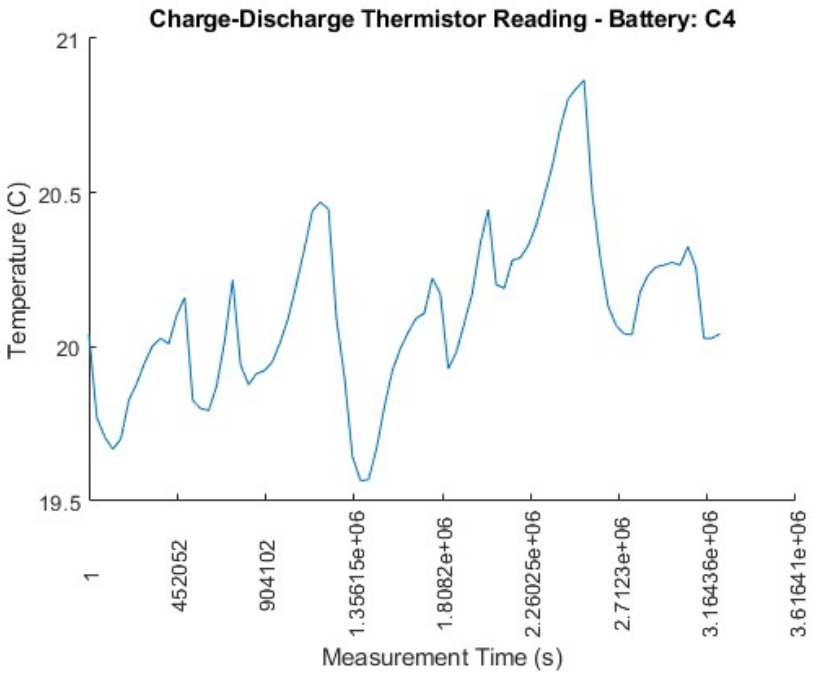

Fig. I.6:Temperature of C4 during Charge-Discharge Test

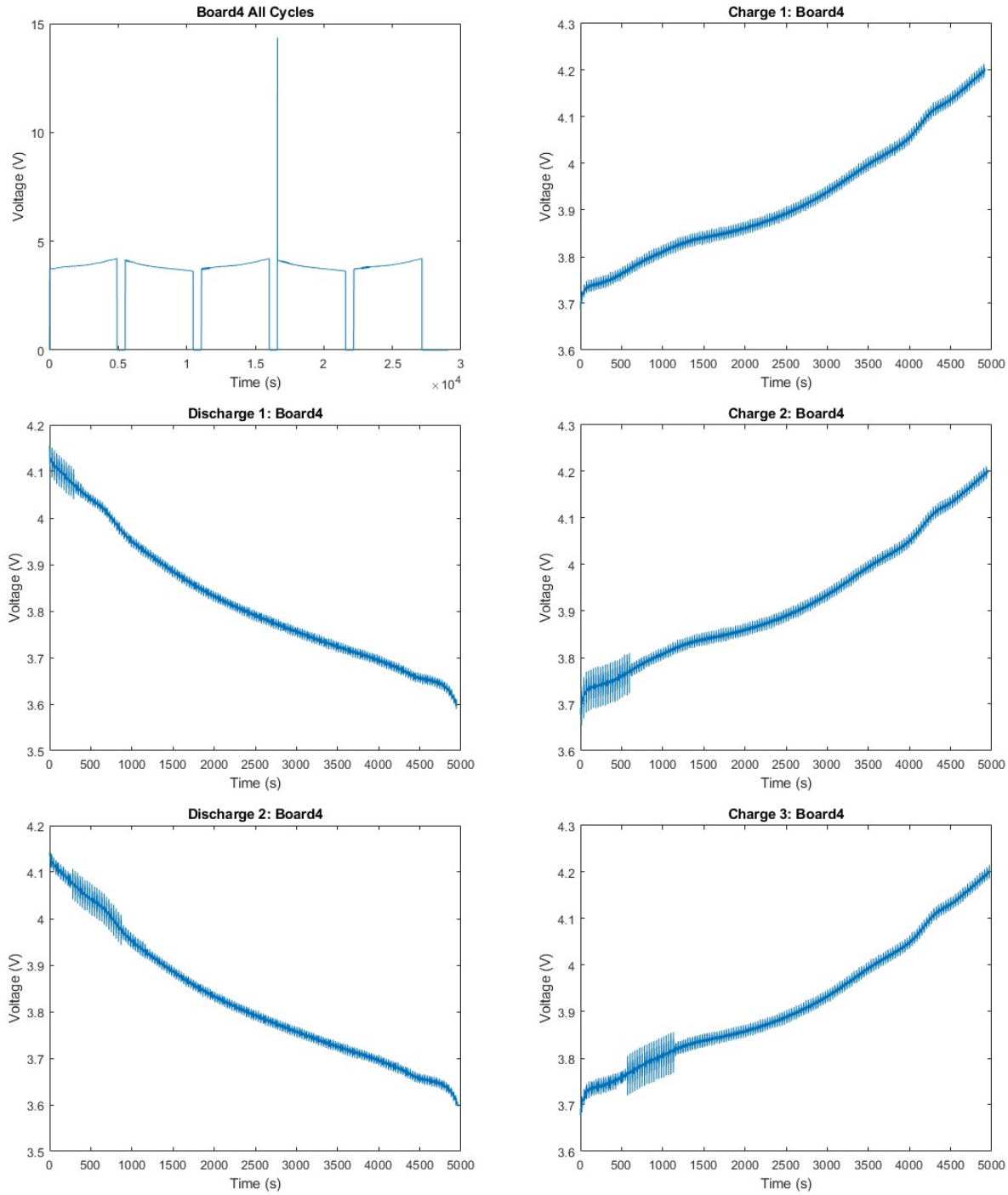

Fig. I.7: Charge-discharge curves for C5

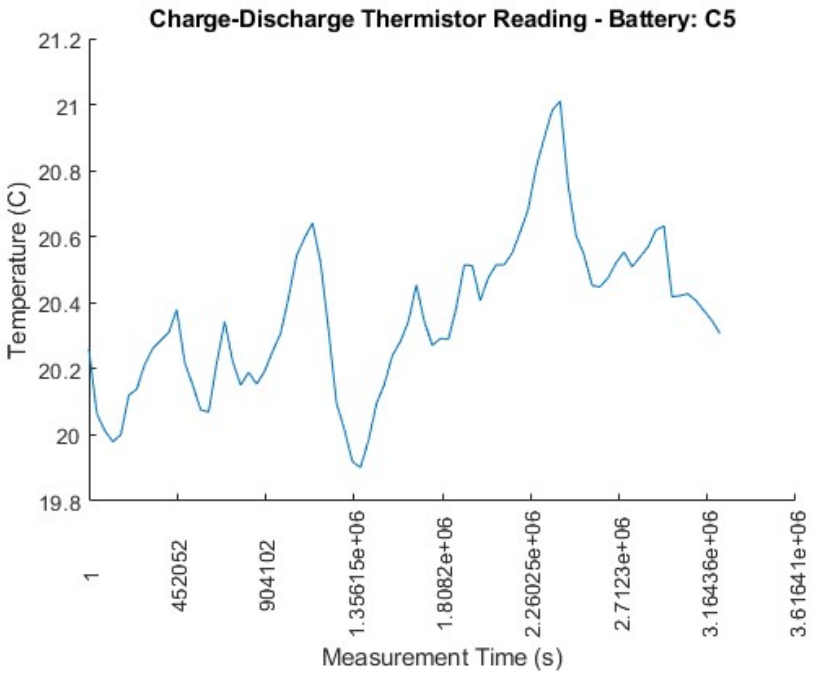

Fig. I.8:Temperature of C5 during Charge-Discharge Test

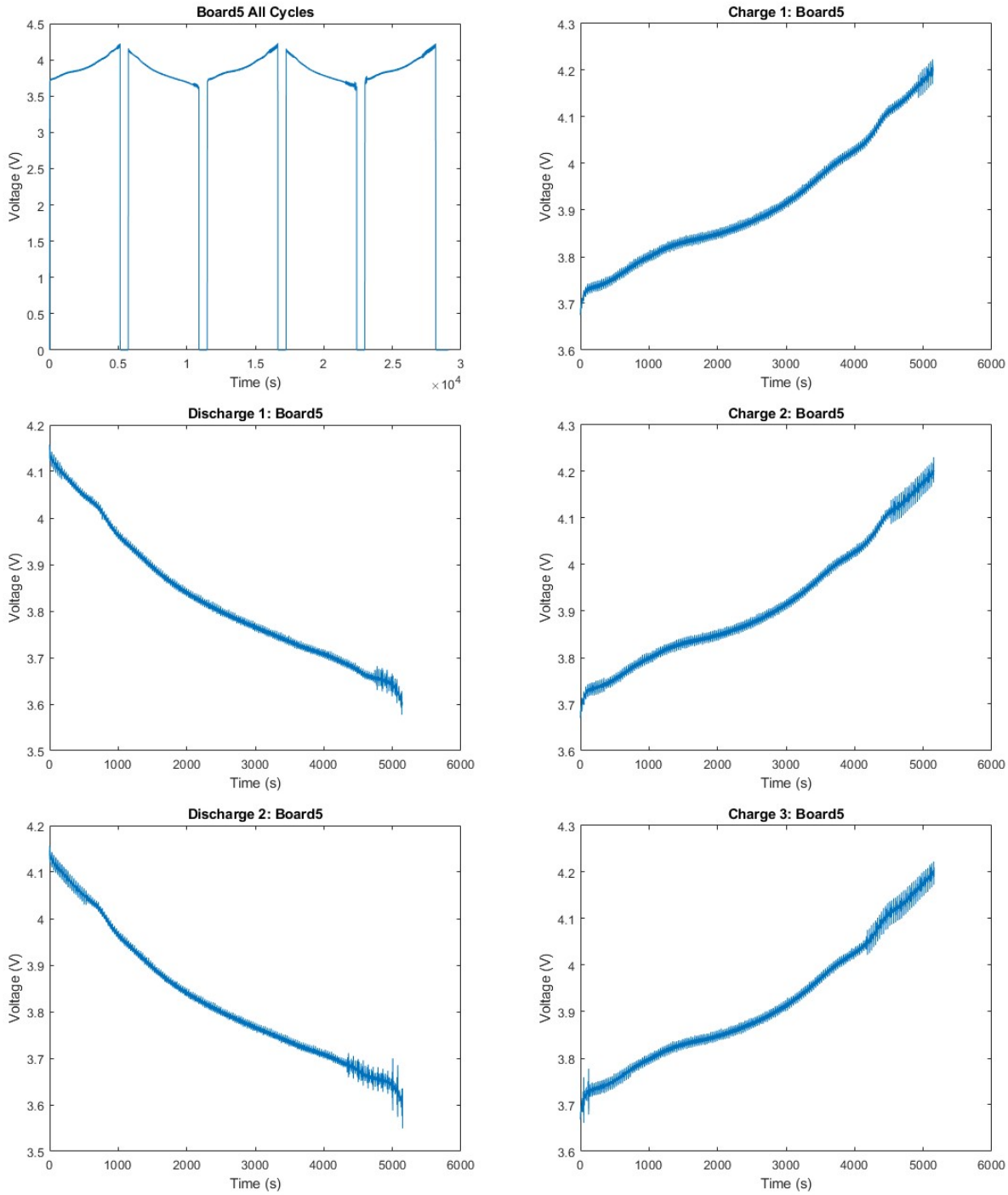

Fig. I.9: Charge-discharge curves for C6

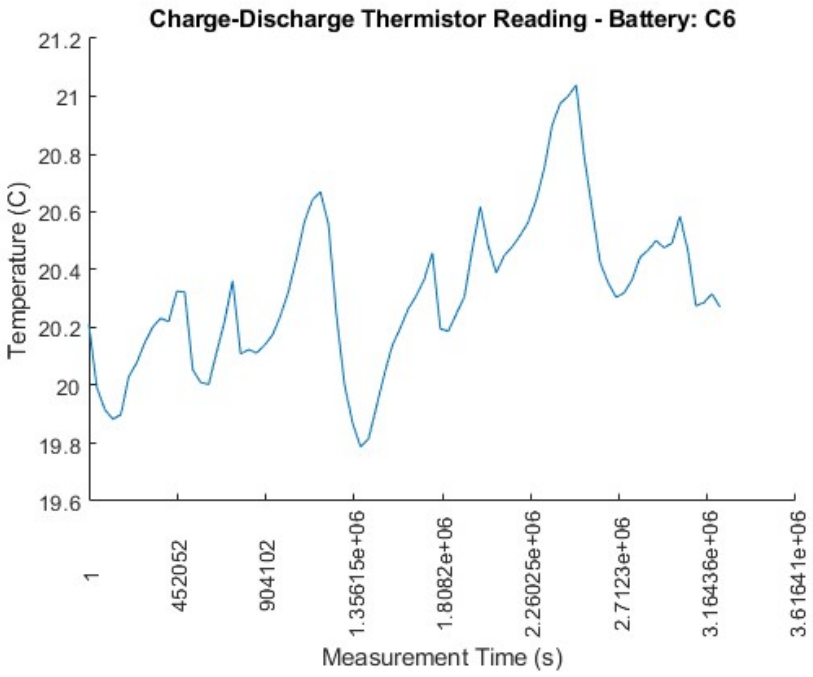

Fig. I.10:Temperature of C6 during Charge-Discharge Test

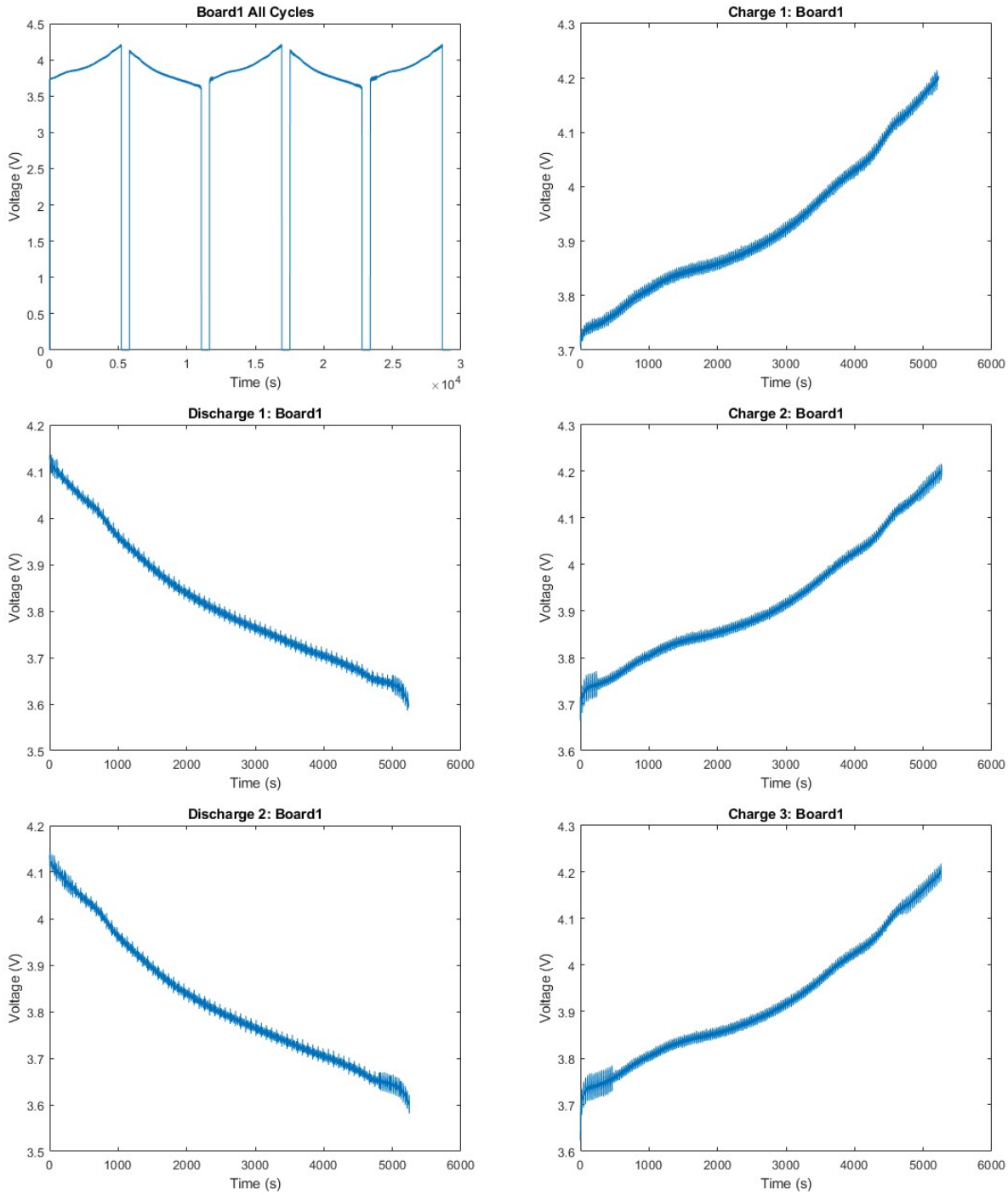

Fig. I.11: Charge-discharge curves for C7

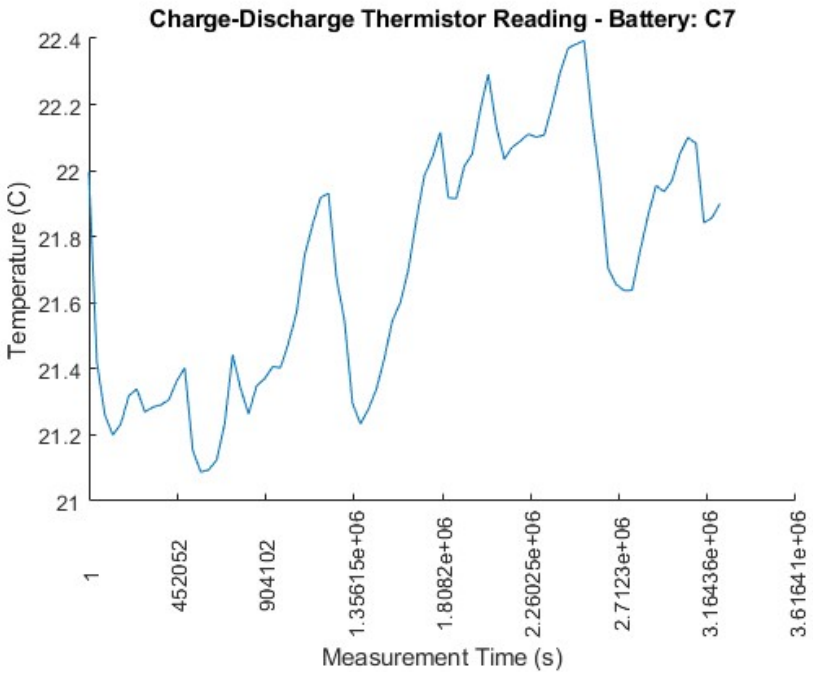

Fig I.12:Temperature of C7 during Charge-Discharge Test

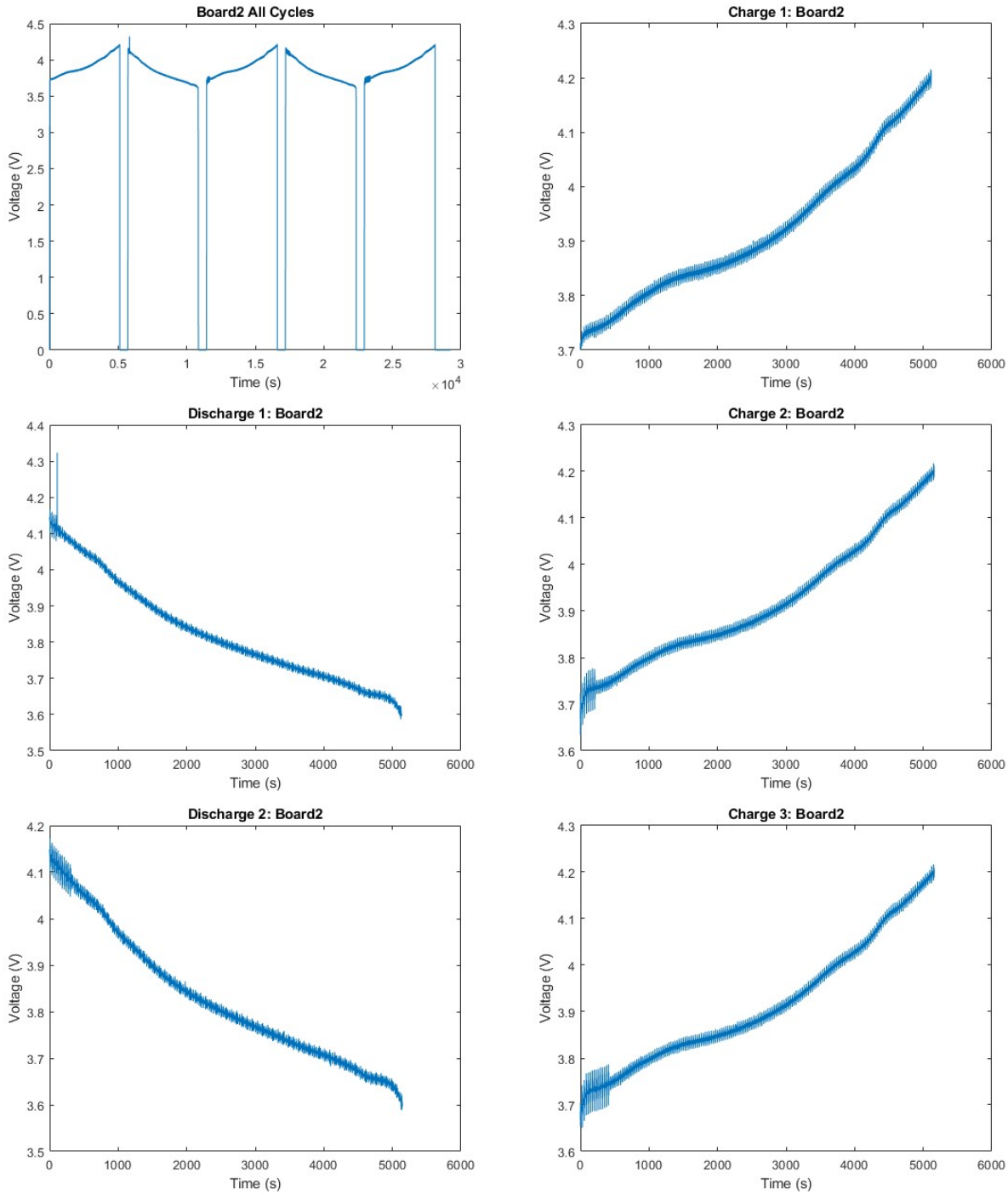

Fig. I.13: Charge-discharge curves for C8

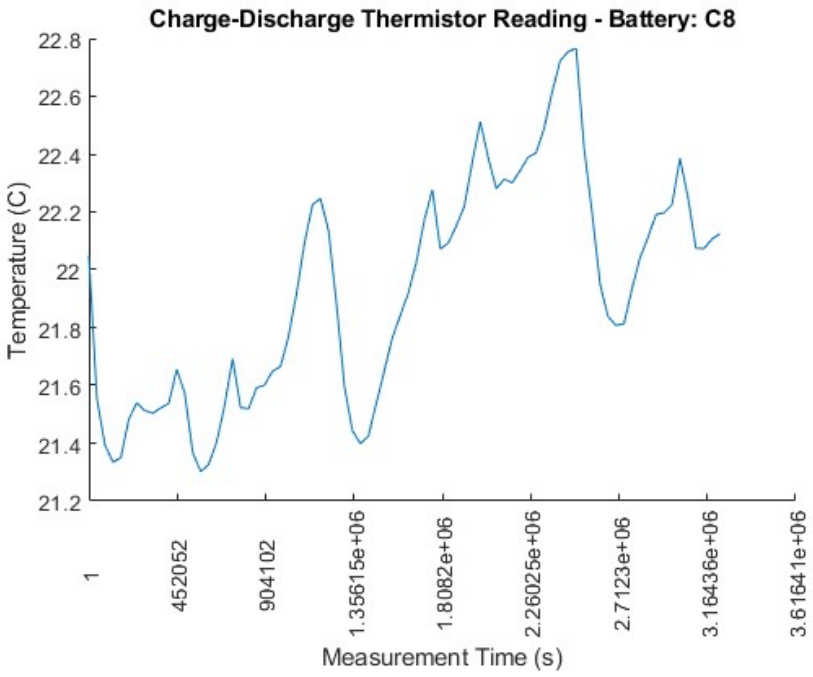

Fig. I.14:Temperature of C8 during Charge-Discharge Test

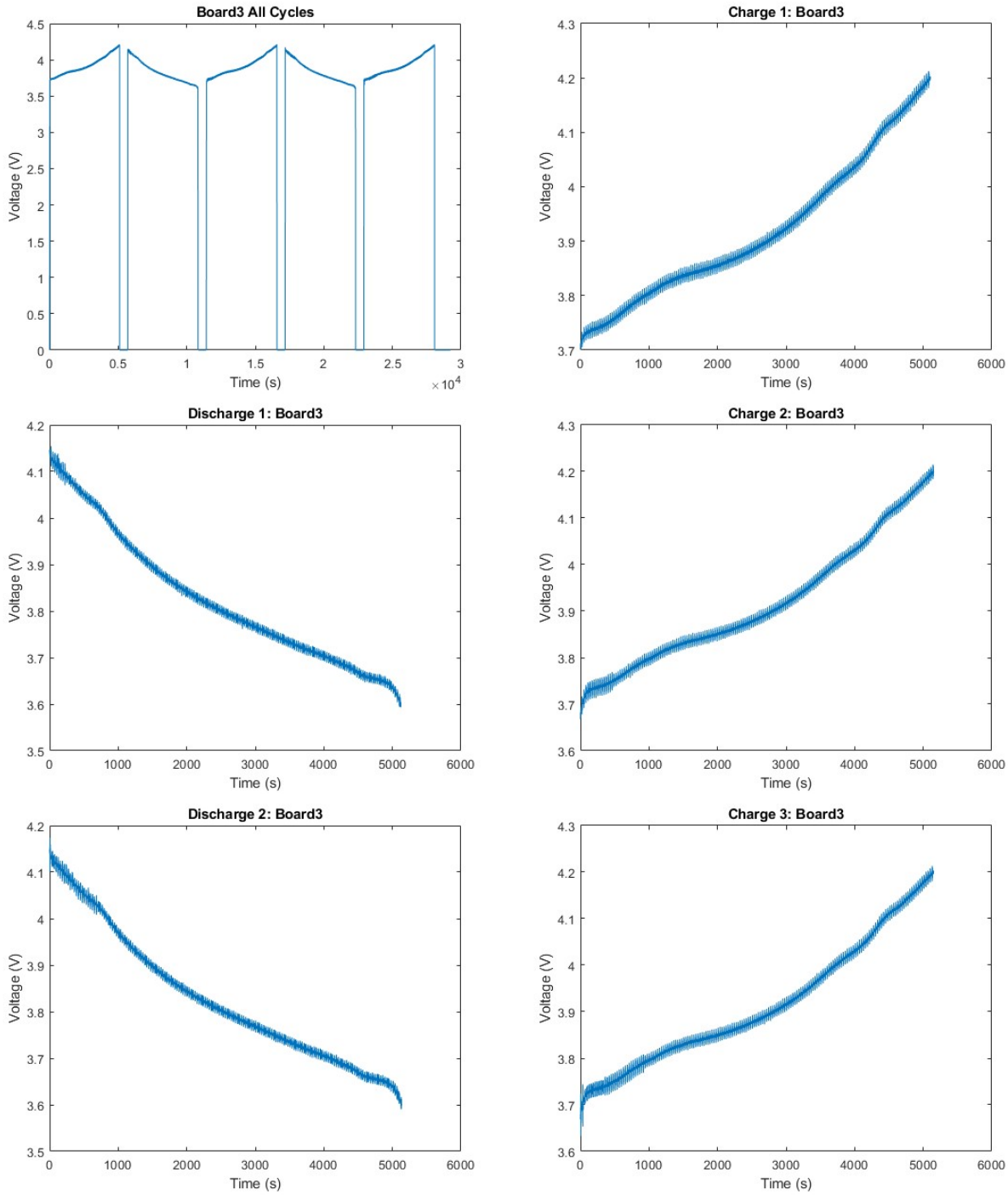

Fig. I.15: Charge-discharge curves for C9

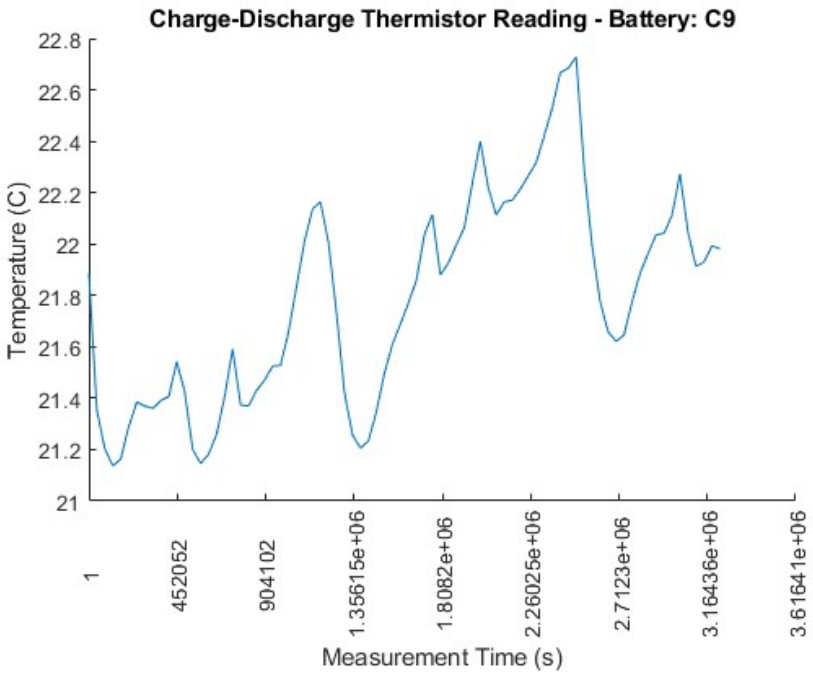

Fig. I.16:Temperature of C9 during Charge-Discharge Test

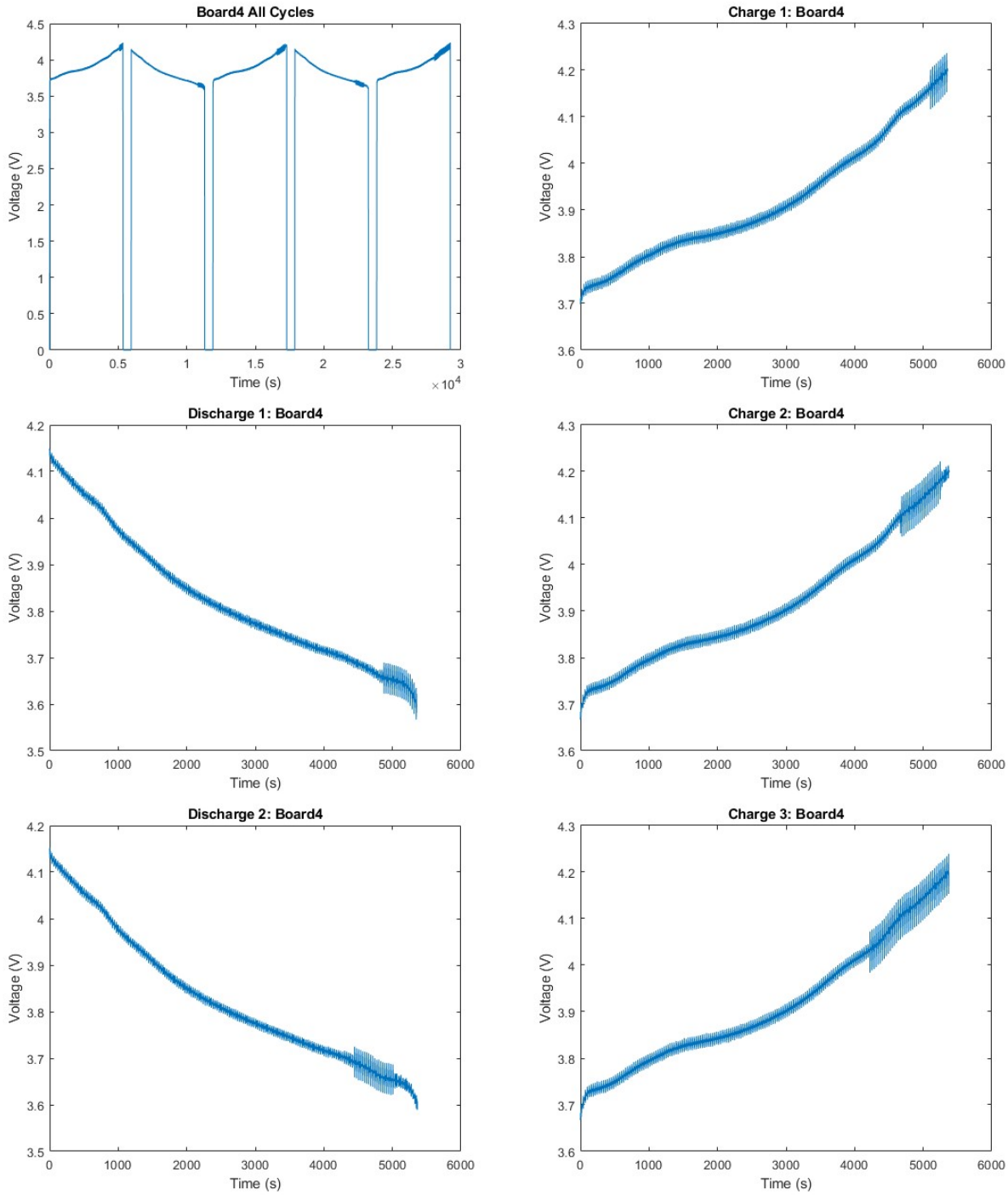

Fig. I.17: Charge-discharge curves for C11

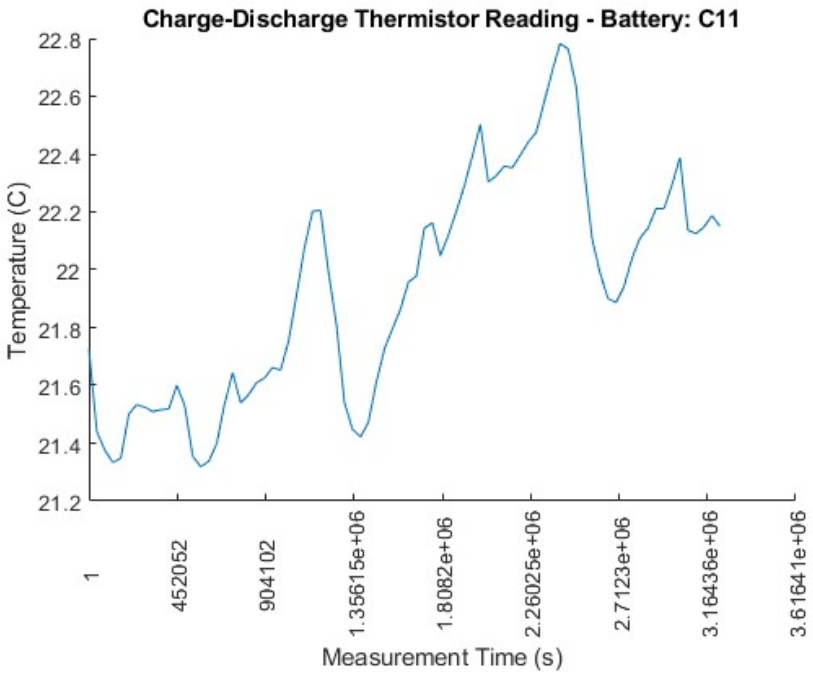

Fig. I.18:Temperature of C11 during Charge-Discharge Test

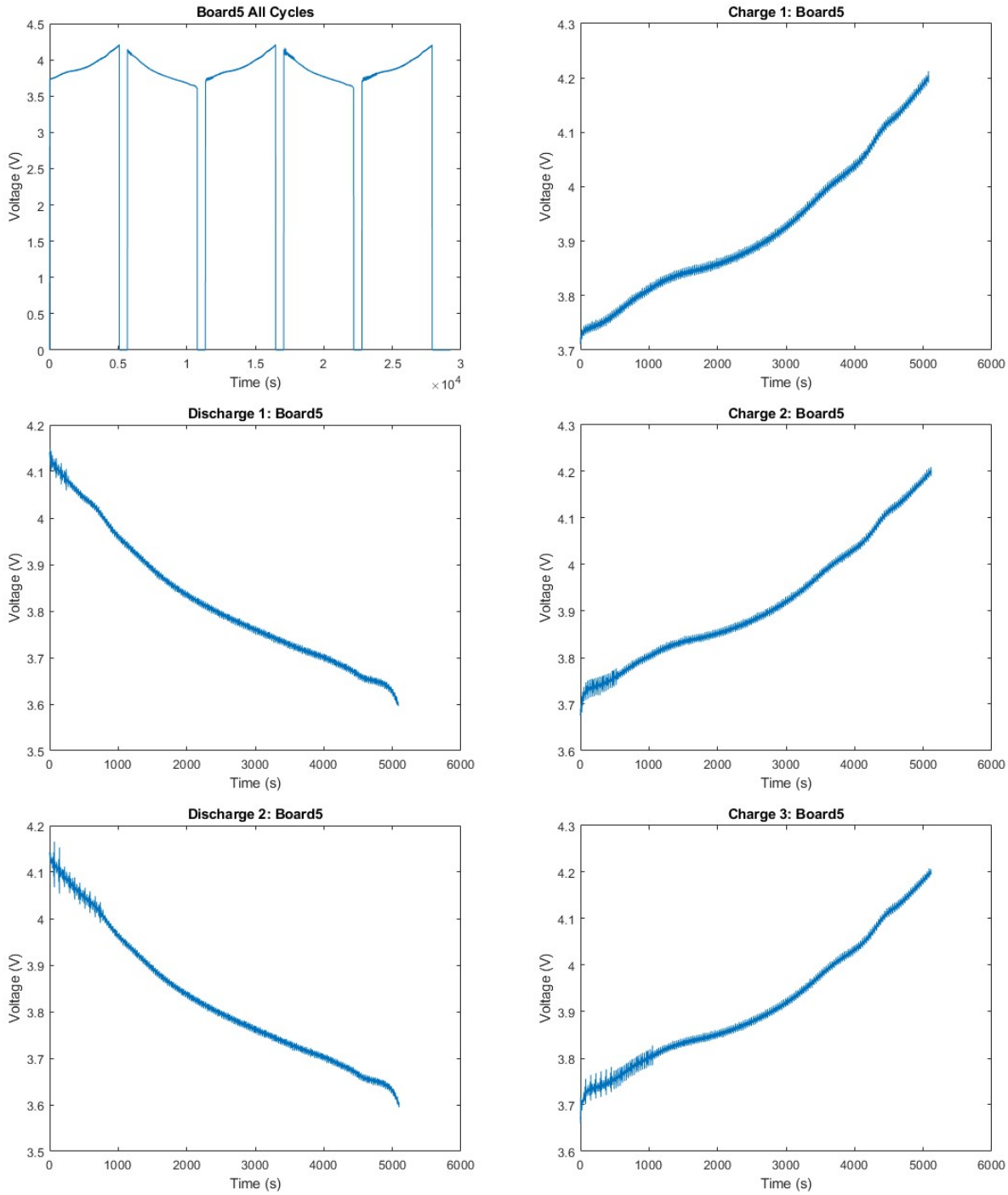

Fig. I.19: Charge-discharge curves for C12

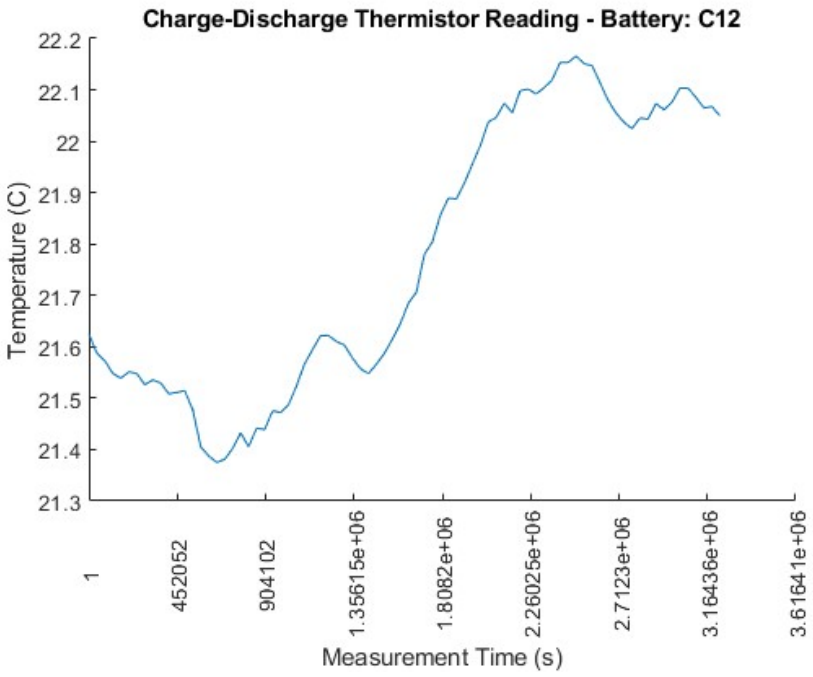

Fig. I.20:Temperature of C12 during Charge-Discharge Test

I.2 Batch D Plots

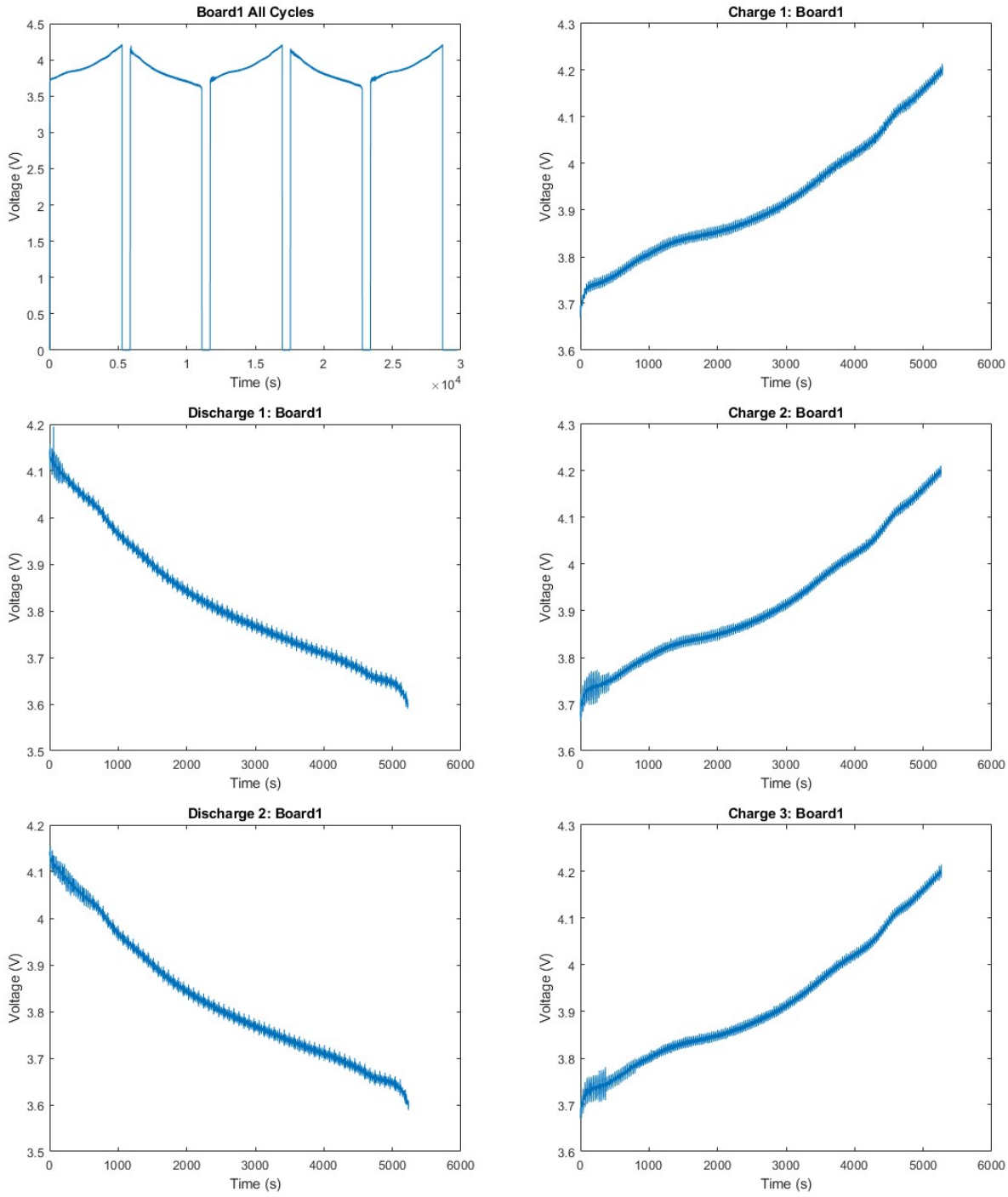

Fig. I.21: Charge-discharge curves for D1

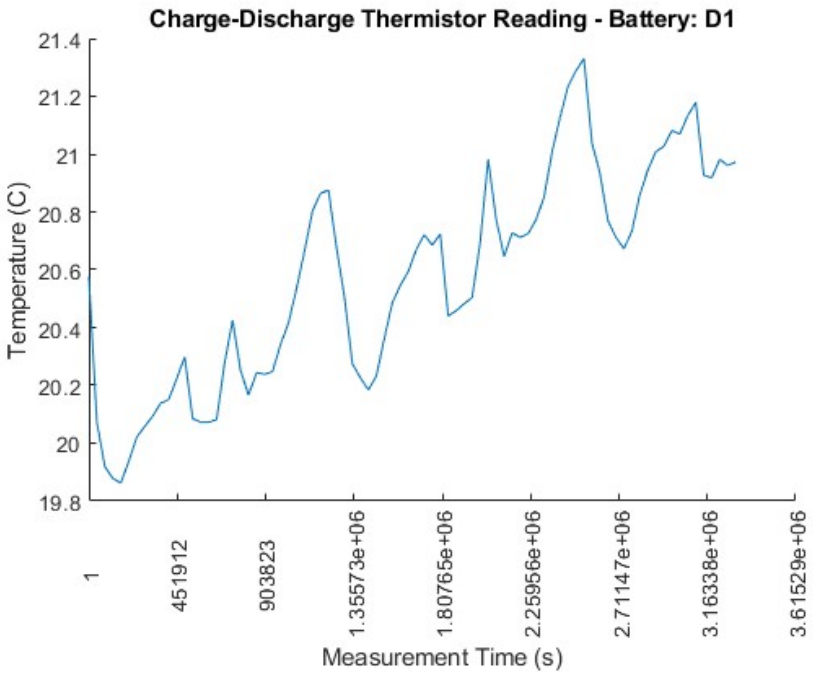

Fig. I.22:Temperature of D1 during Charge-Discharge Test

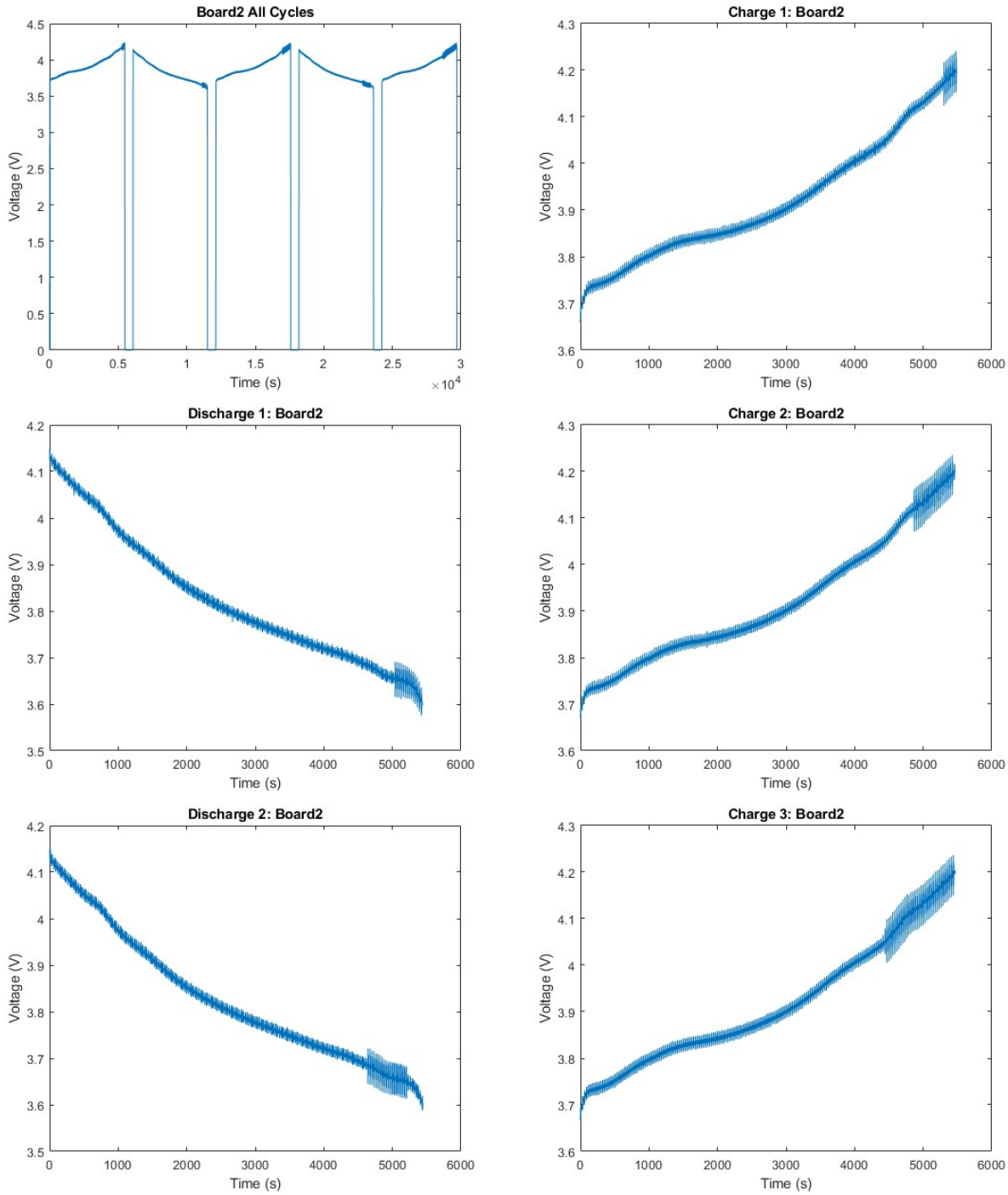

Fig. I.23: Charge-discharge curves for D2

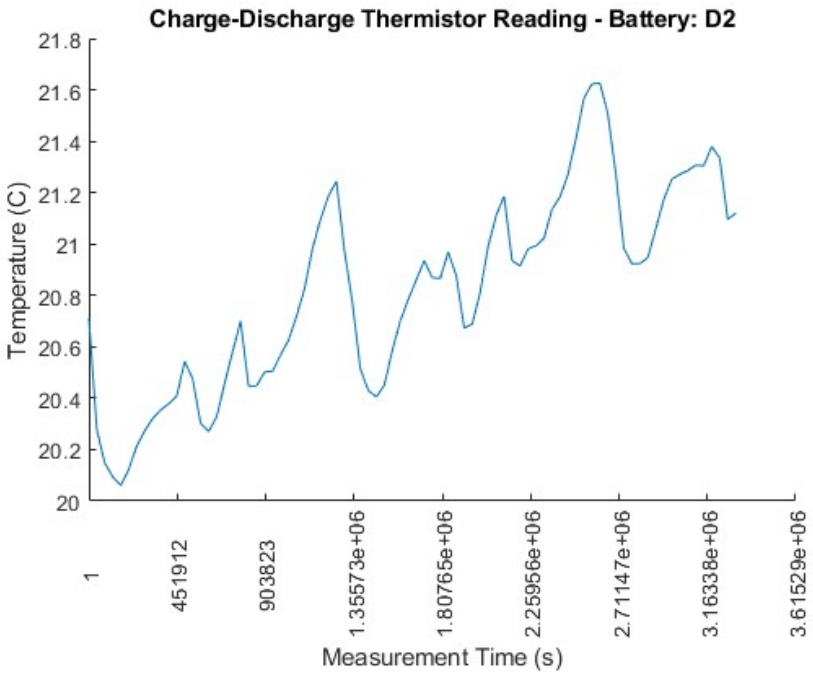

Fig. I.24:Temperature of D2 during Charge-Discharge Test

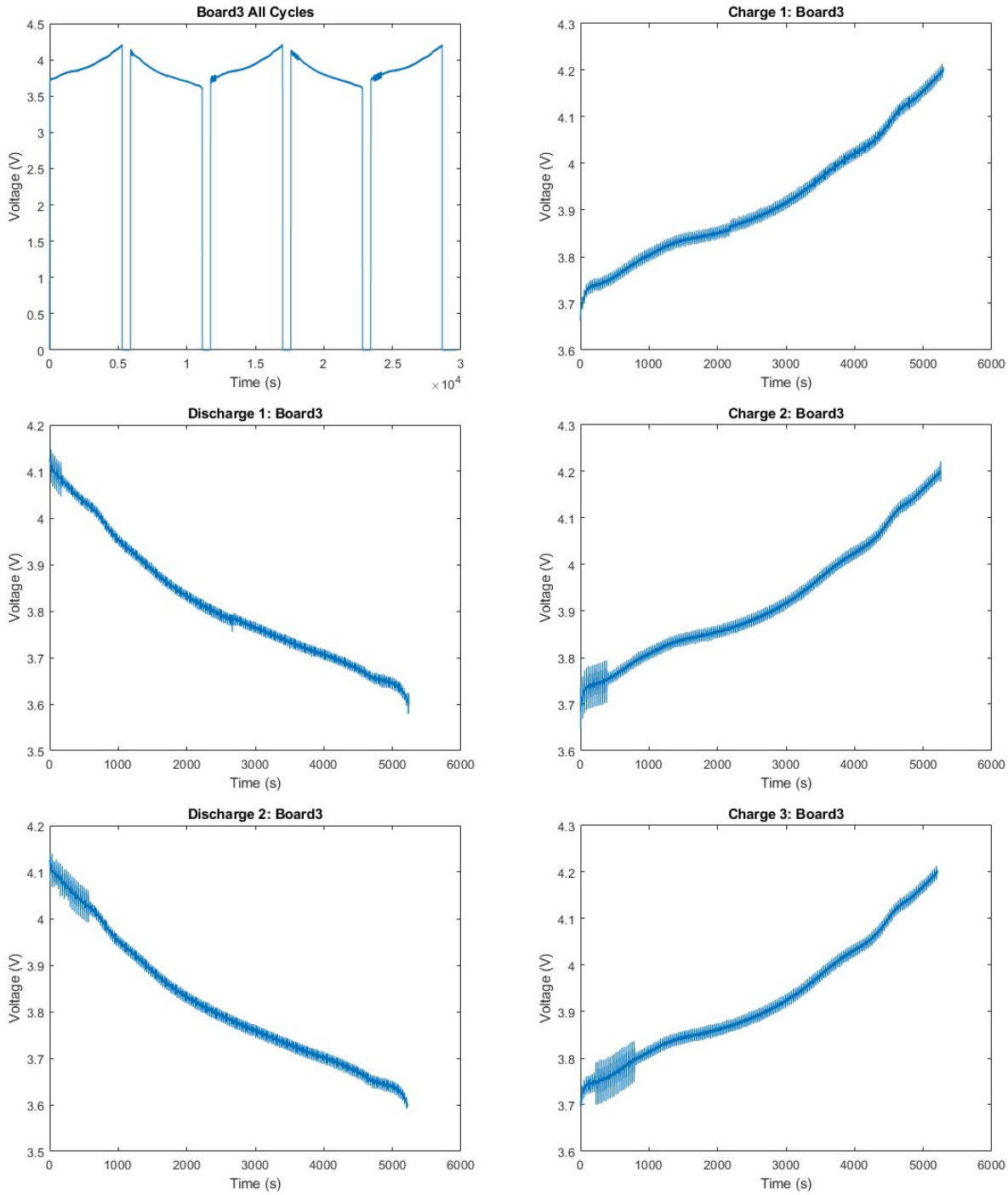

Fig. I.25: Charge-discharge curves for D3

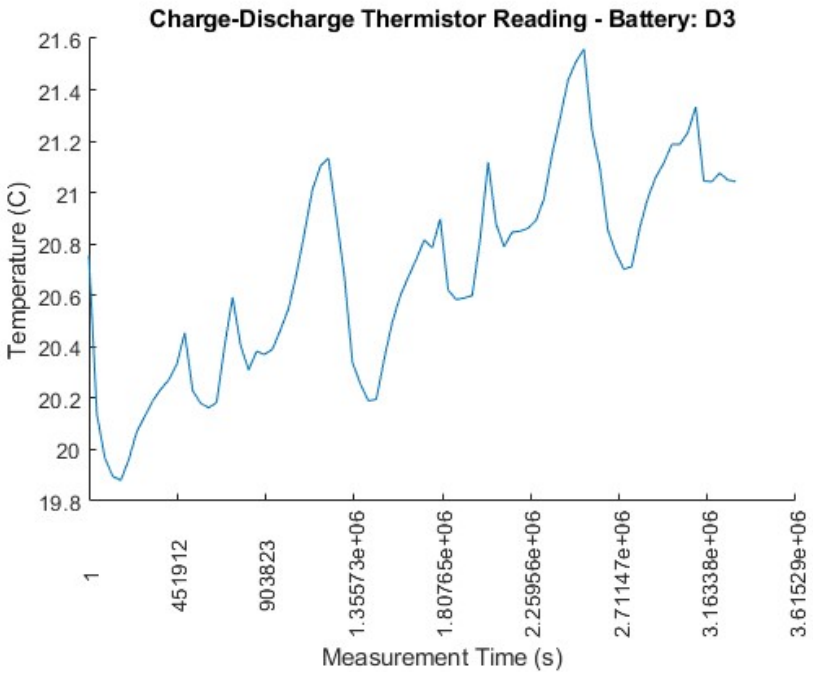

Fig. I.26:Temperature of D3 during Charge-Discharge Test

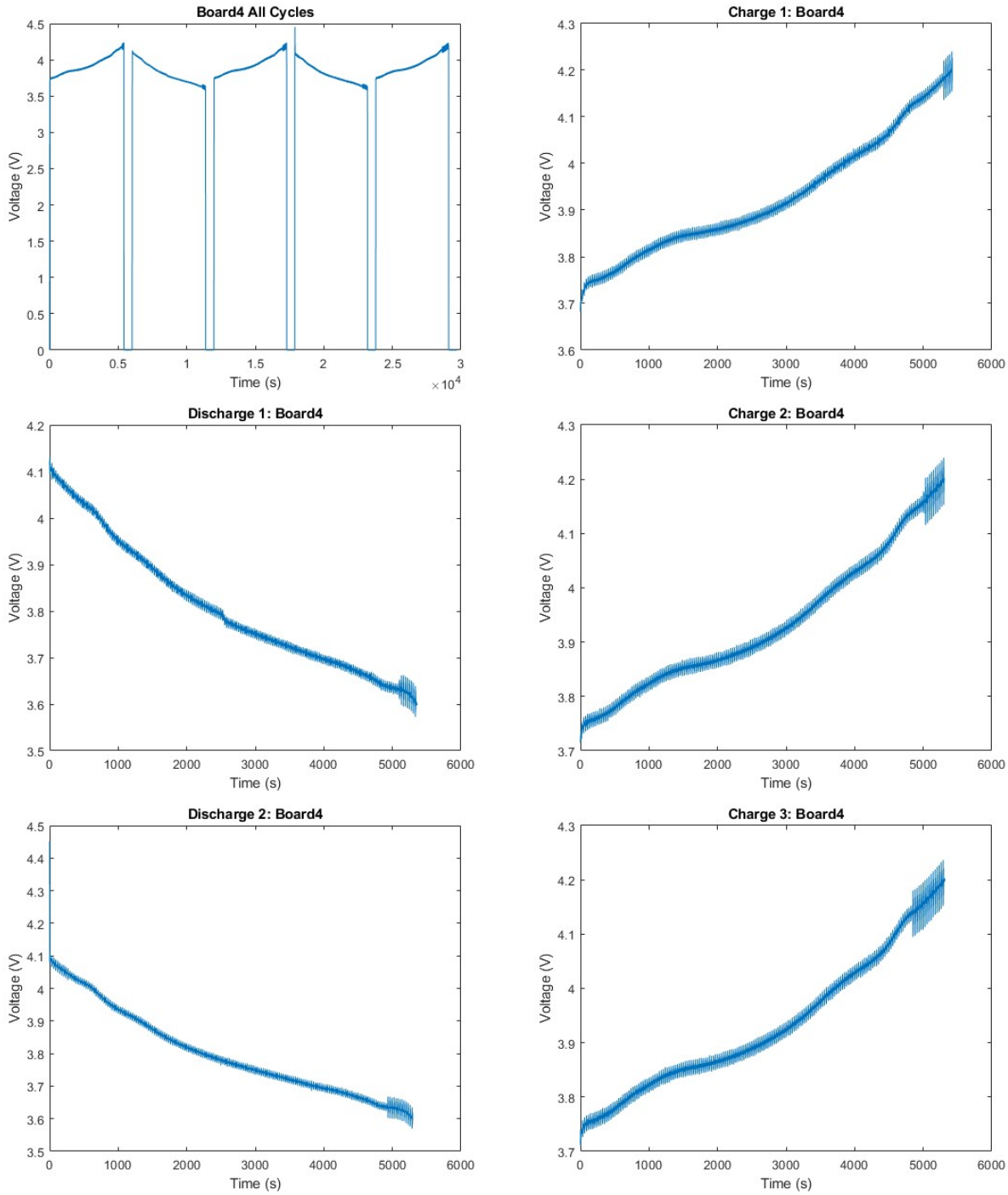

Fig. I.27: Charge-discharge curves for D4

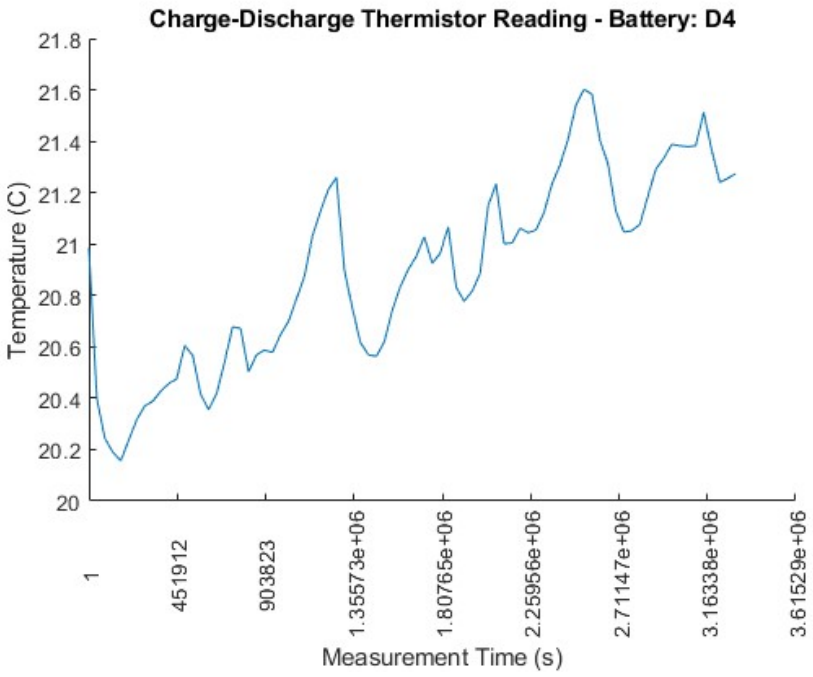

Fig. I.28:Temperature of D4 during Charge-Discharge Test

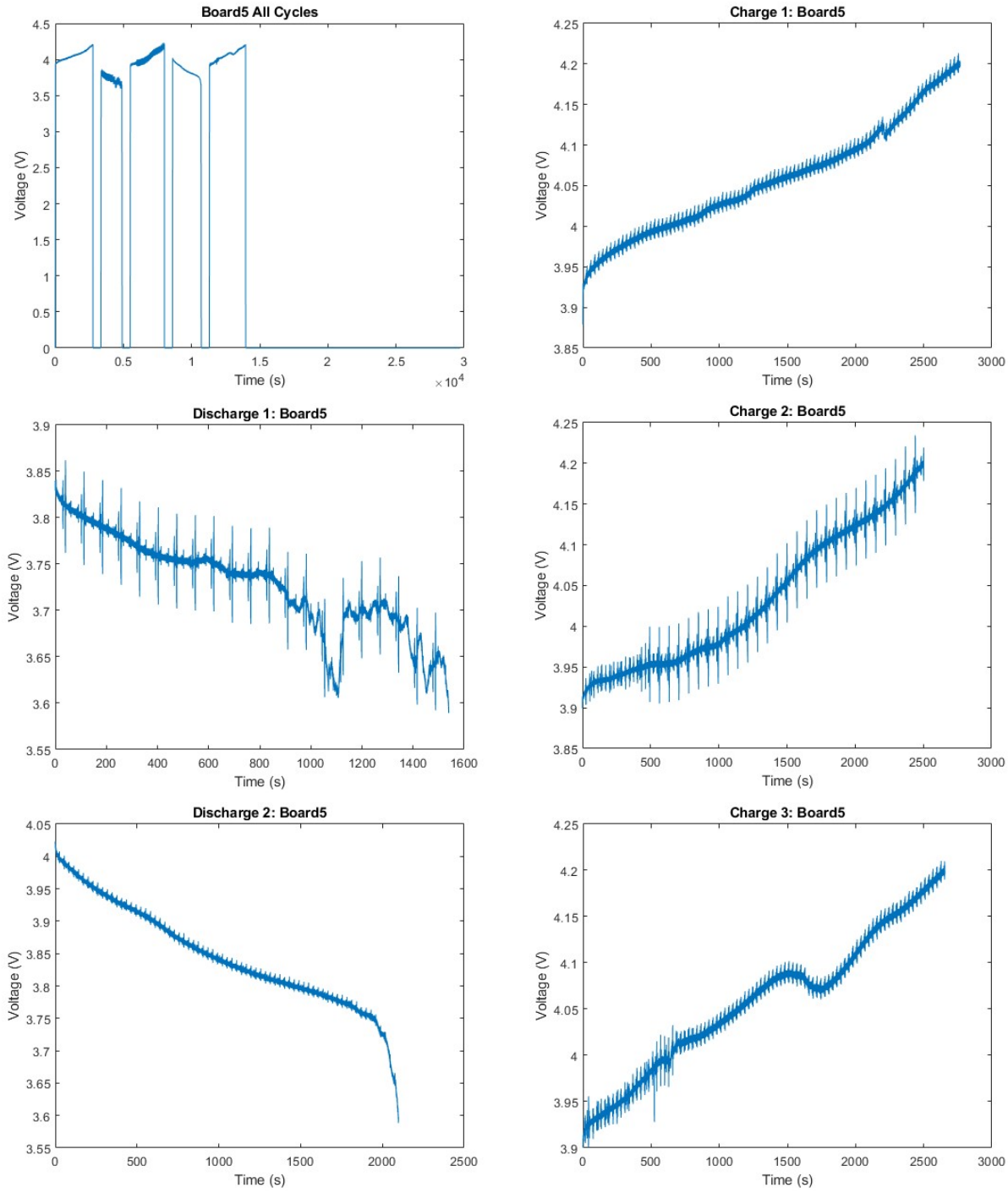

Fig. I.29: Charge-discharge curves for D5

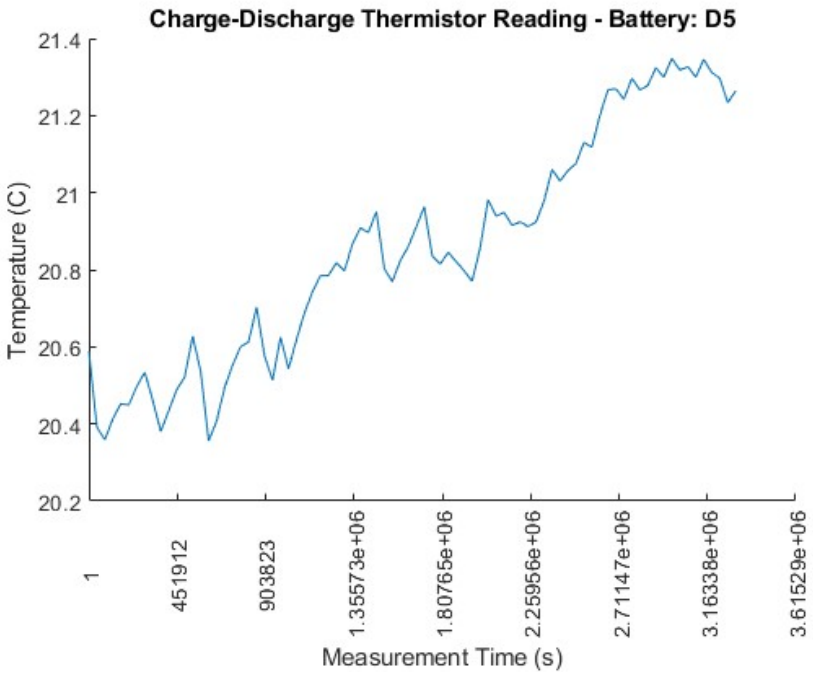

Fig. I.30:Temperature of D5 during Charge-Discharge Test

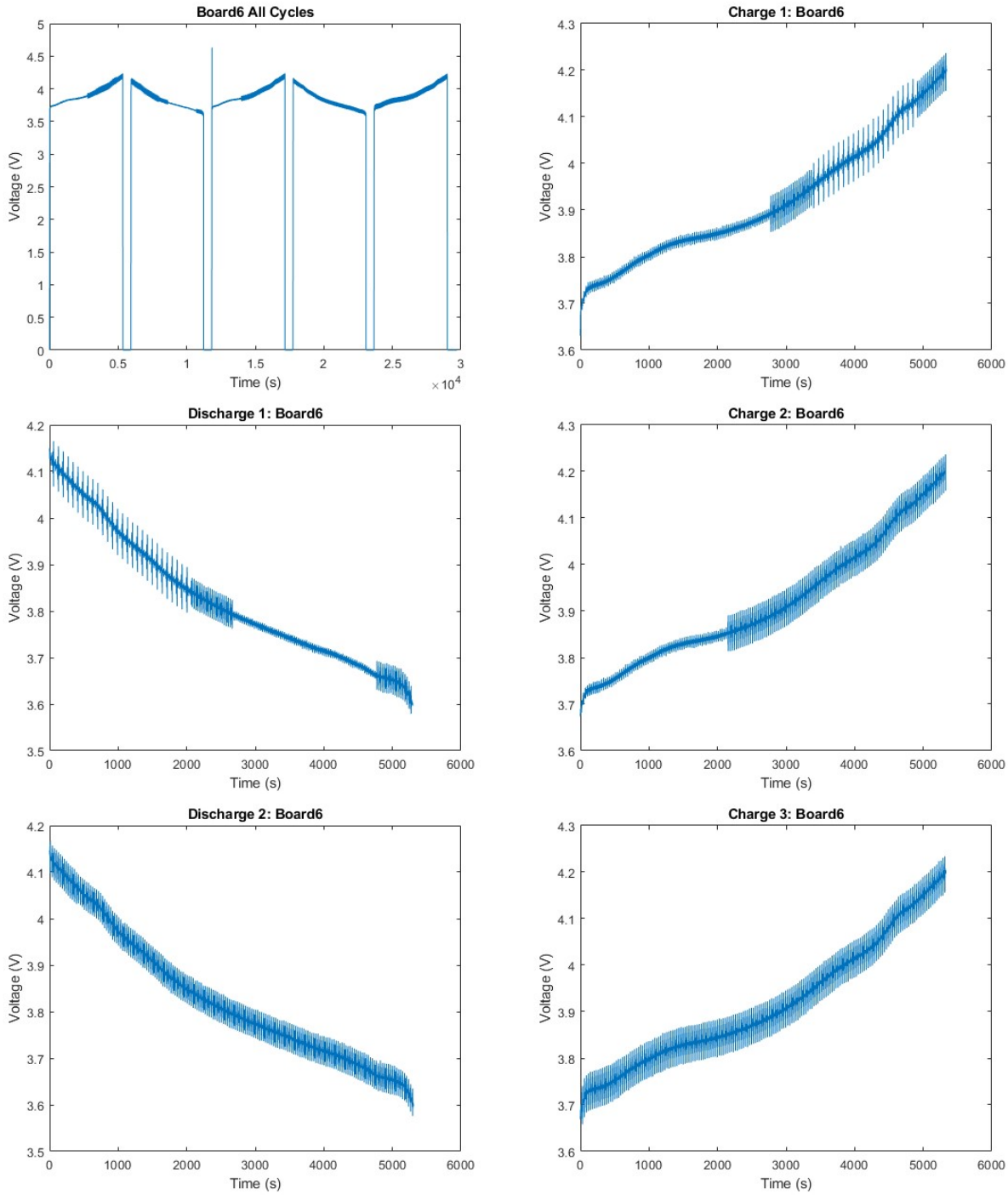

Fig. I.31: Charge-discharge curves for D6

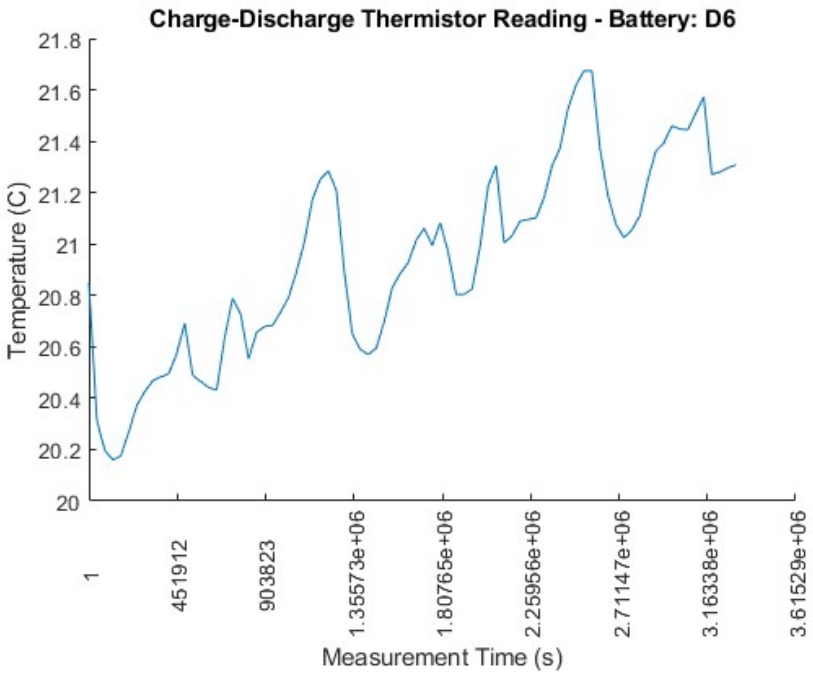

Fig. I.32:Temperature of D6 during Charge-Discharge Test

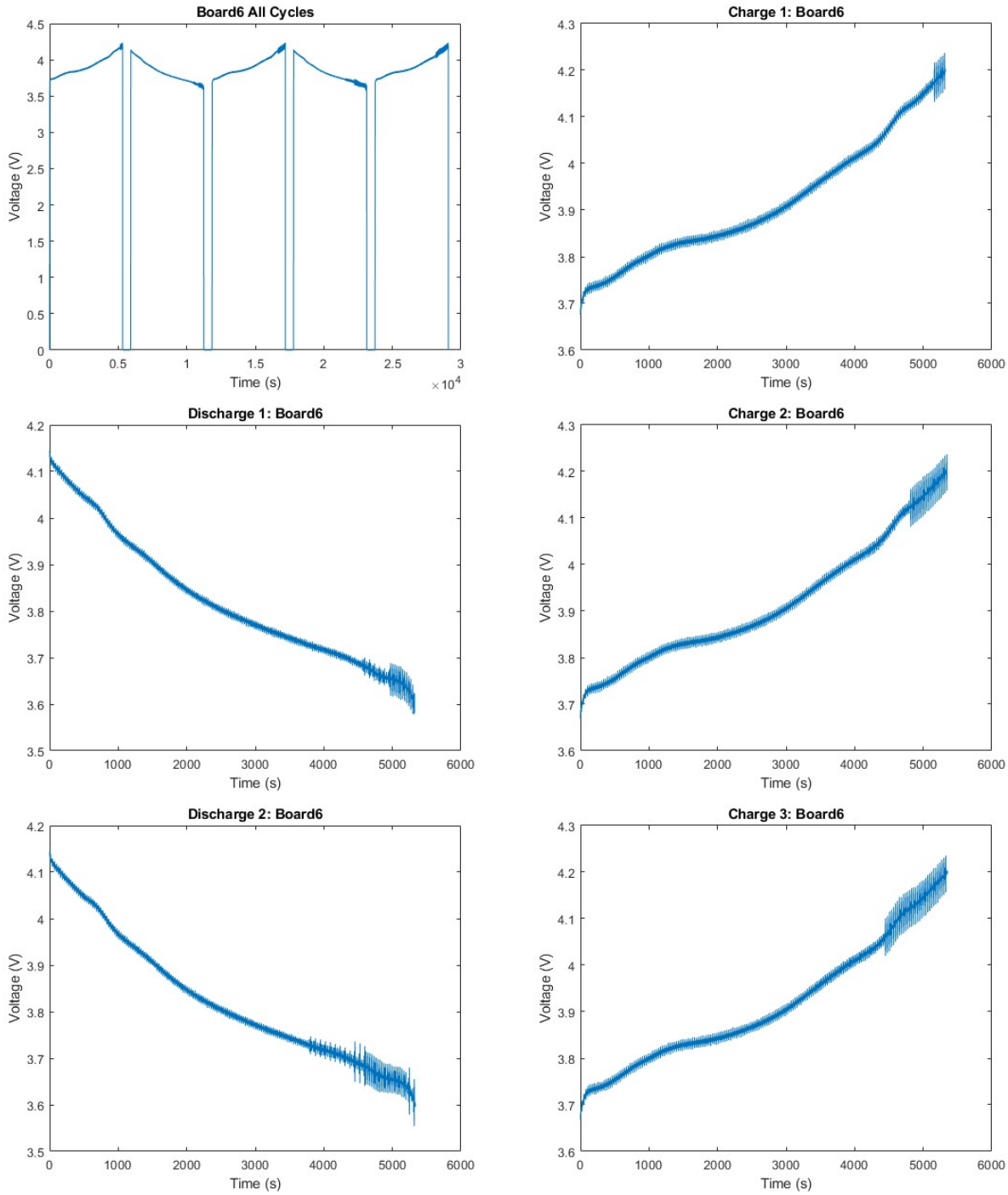

Fig. I.33: Charge-discharge curves for D7

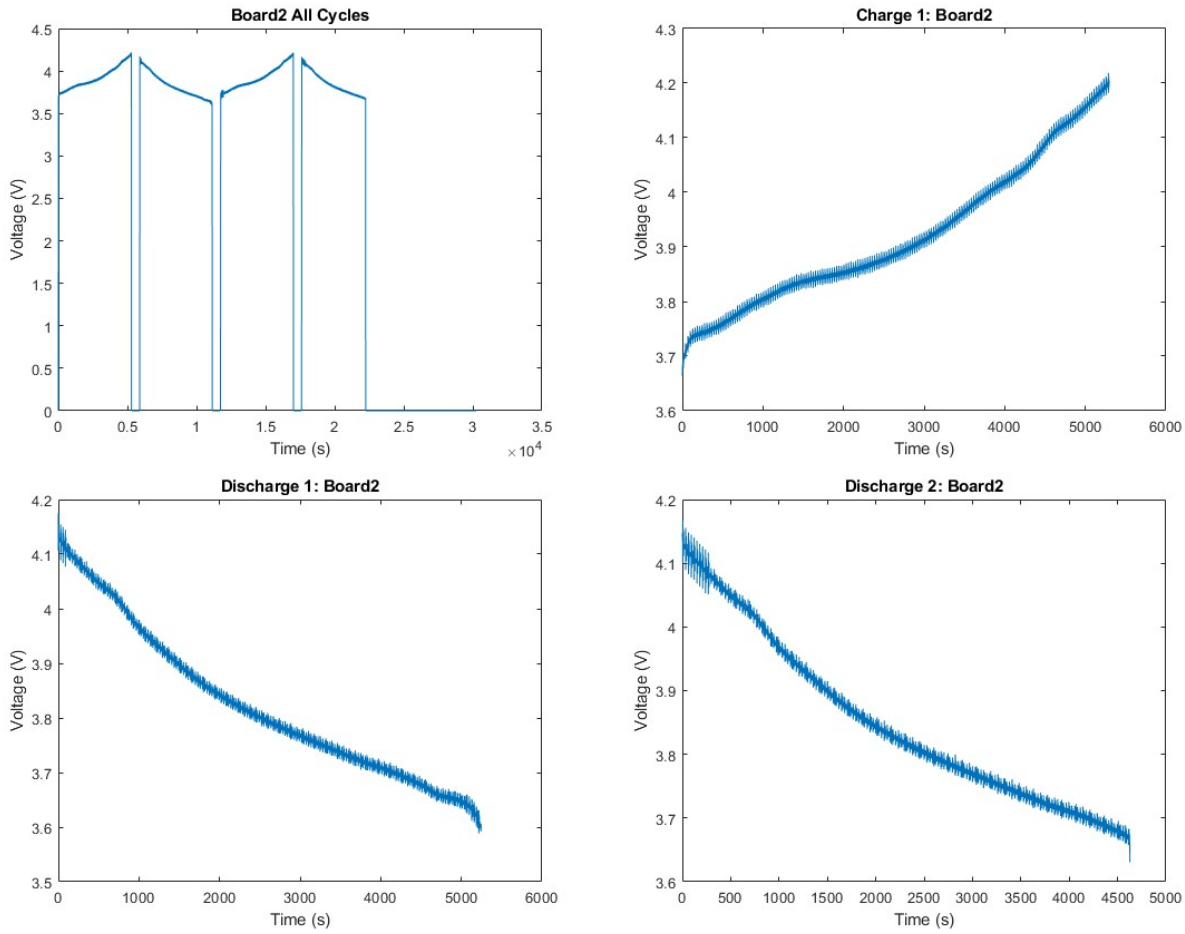

Fig. I.34: Charge-discharge curves for D8

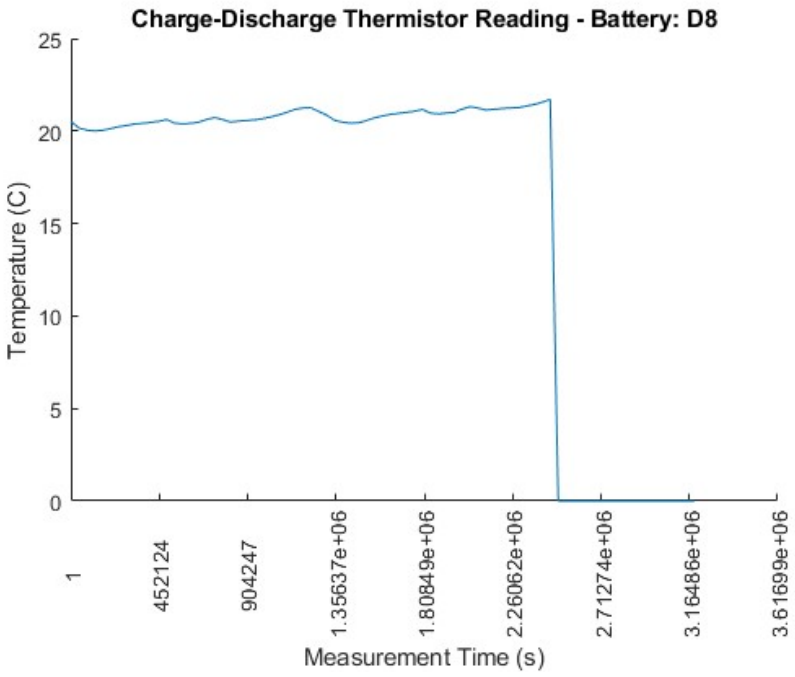

Fig. I.35:Temperature of D8 during Charge-Discharge Test

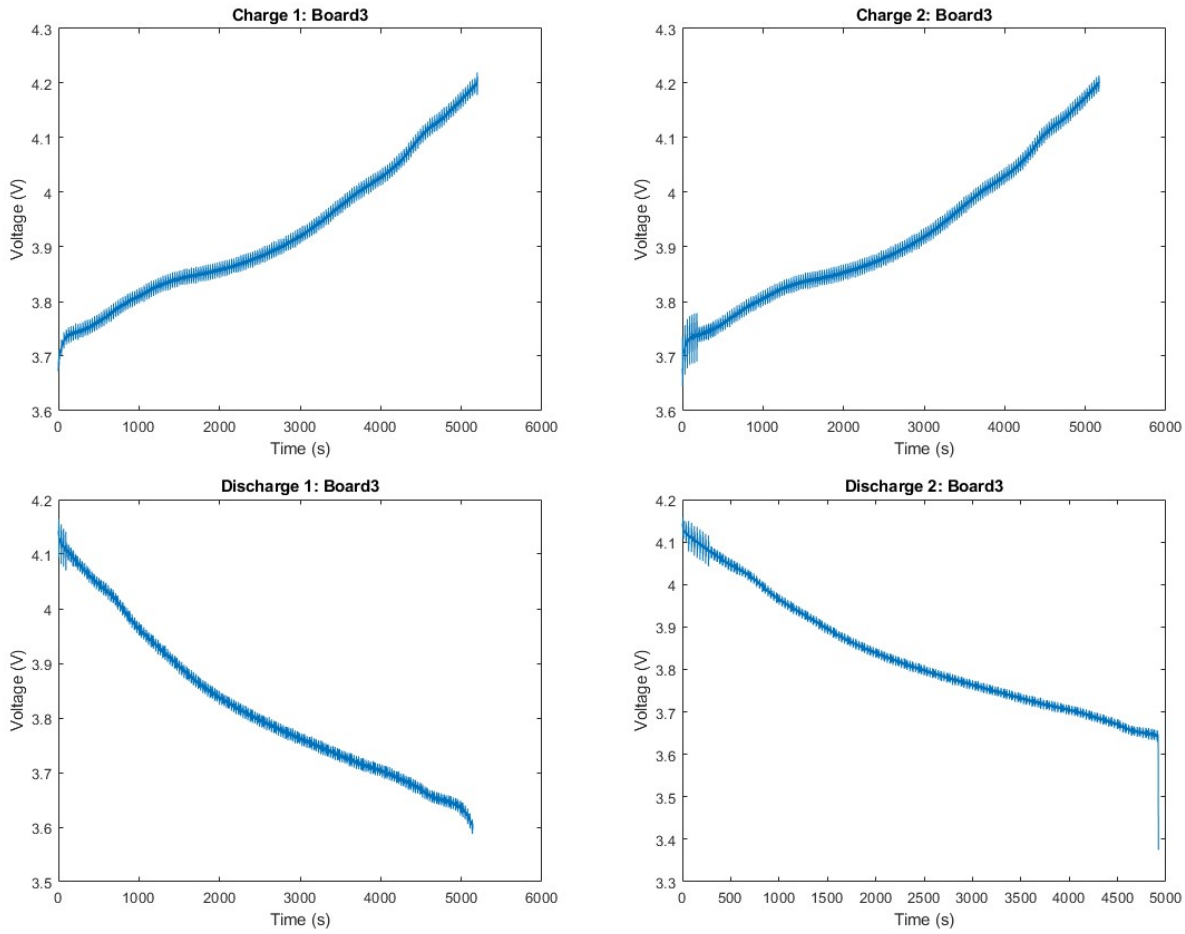

Fig I.36: Charge-discharge curves for D9

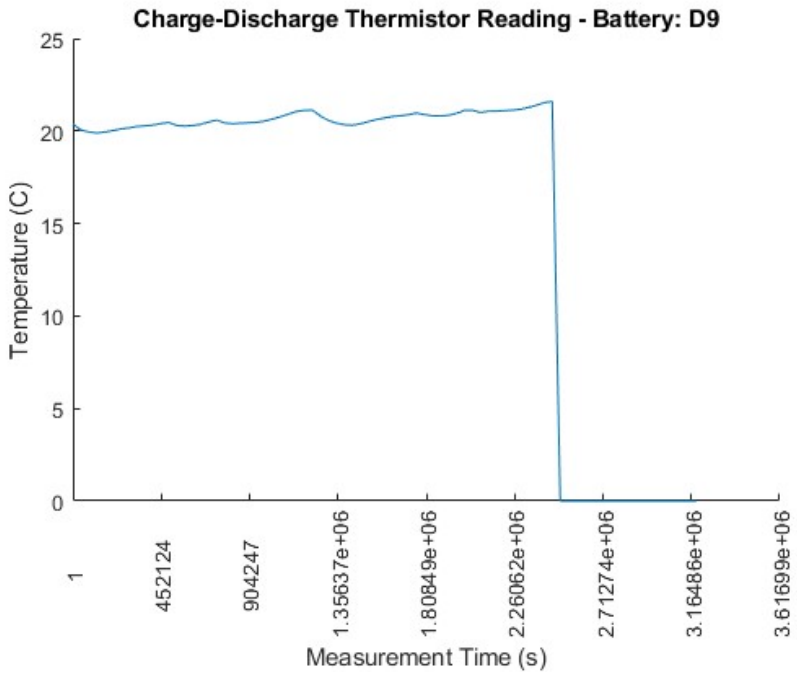

Fig. I.37:Temperature of D9 during Charge-Discharge Test

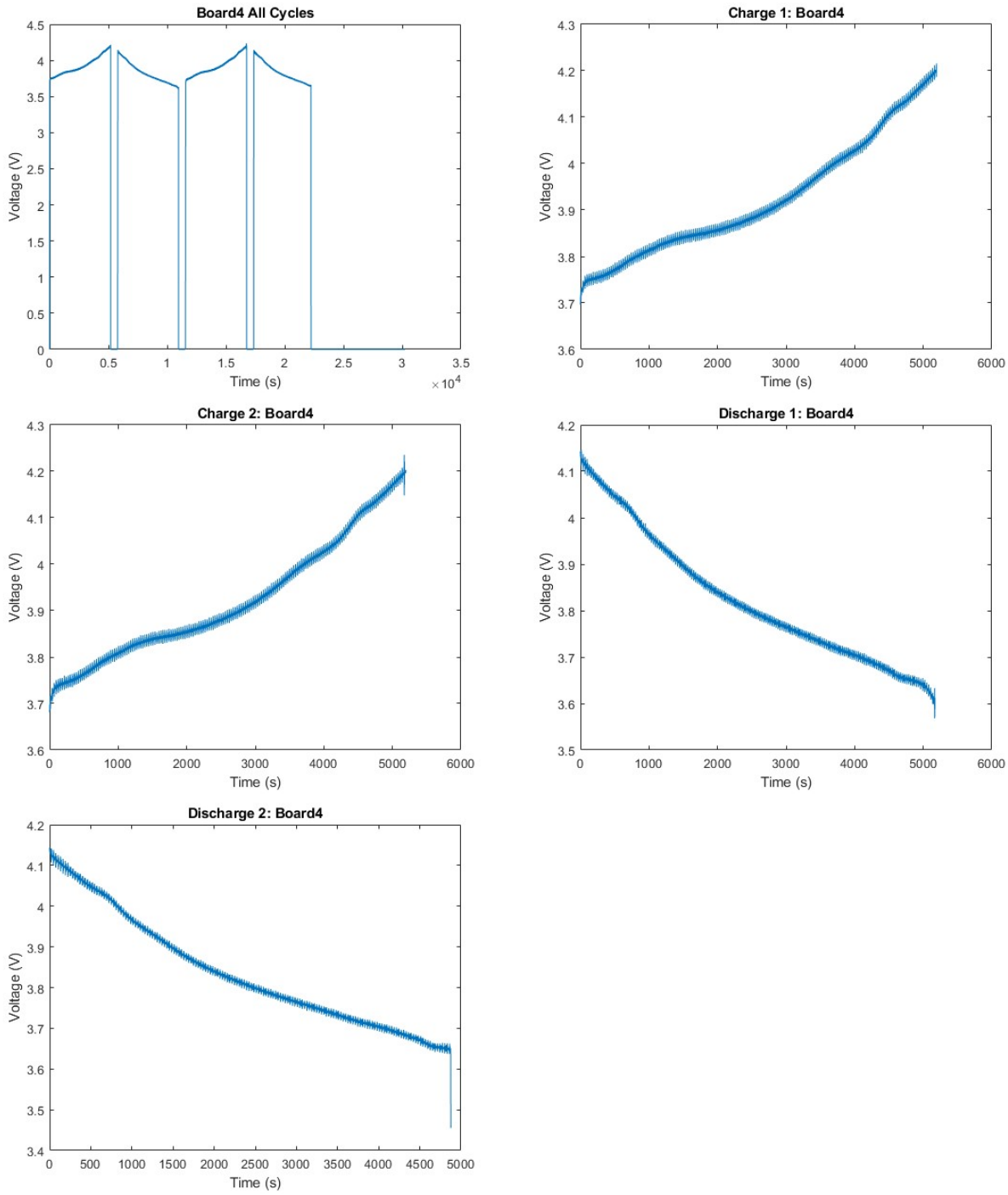

Fig. I.38: Charge-discharge curves for D10

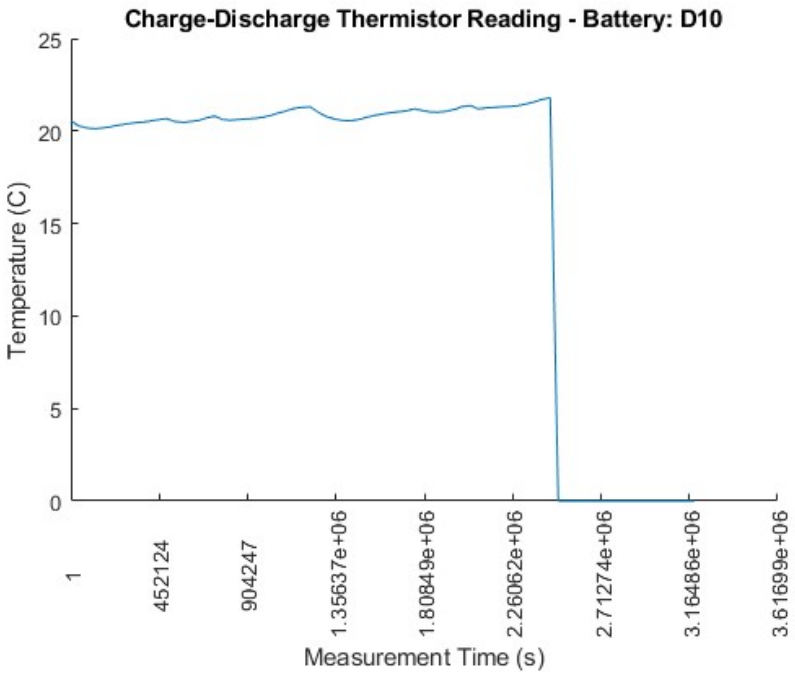

Fig. I.39:Temperature of D10 during Charge-Discharge Test

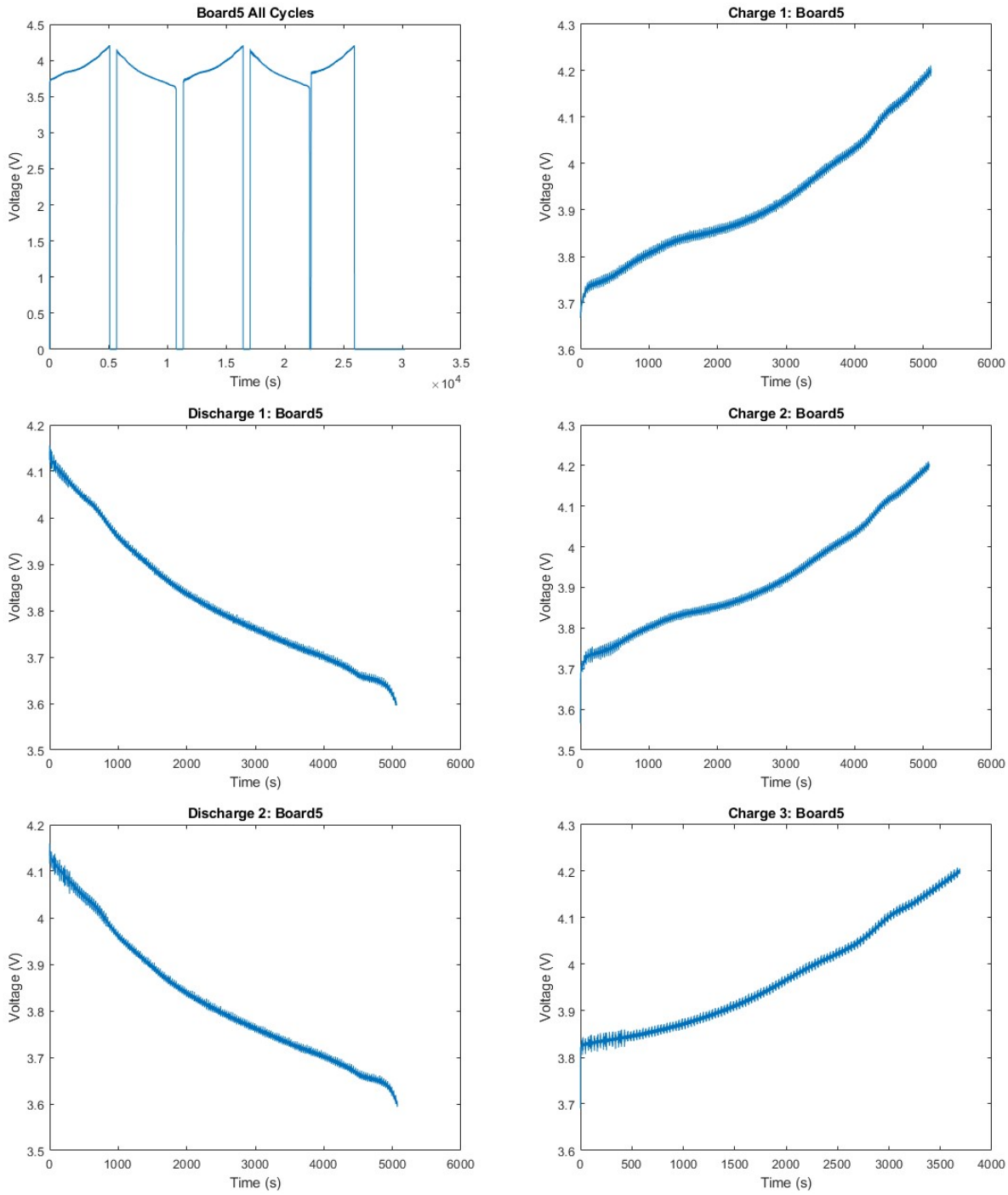

Fig. I.40: Charge-discharge curves for D11

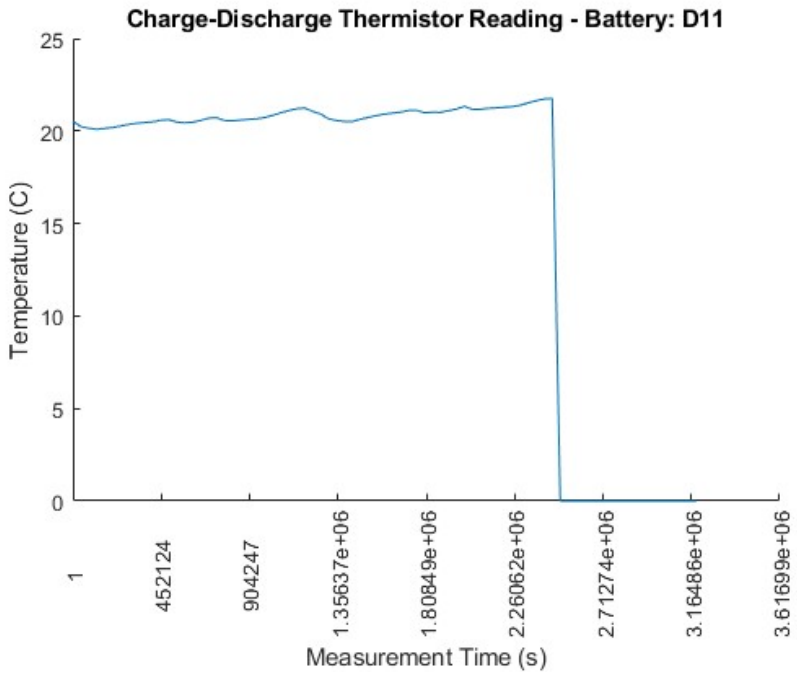

Fig I.41:Temperature of D11 during Charge-Discharge Test

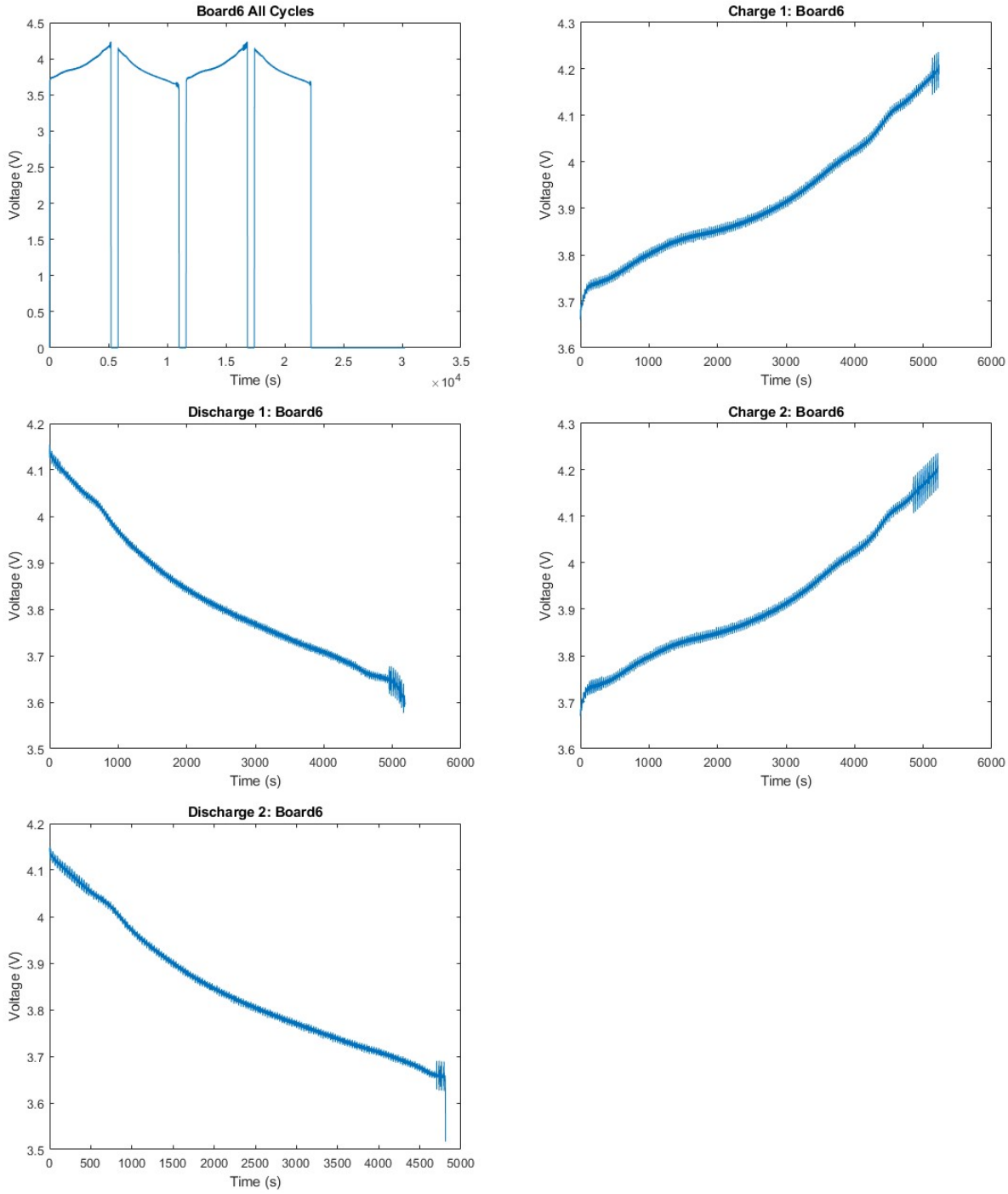

Fig. I.42: Charge-discharge curves for D12

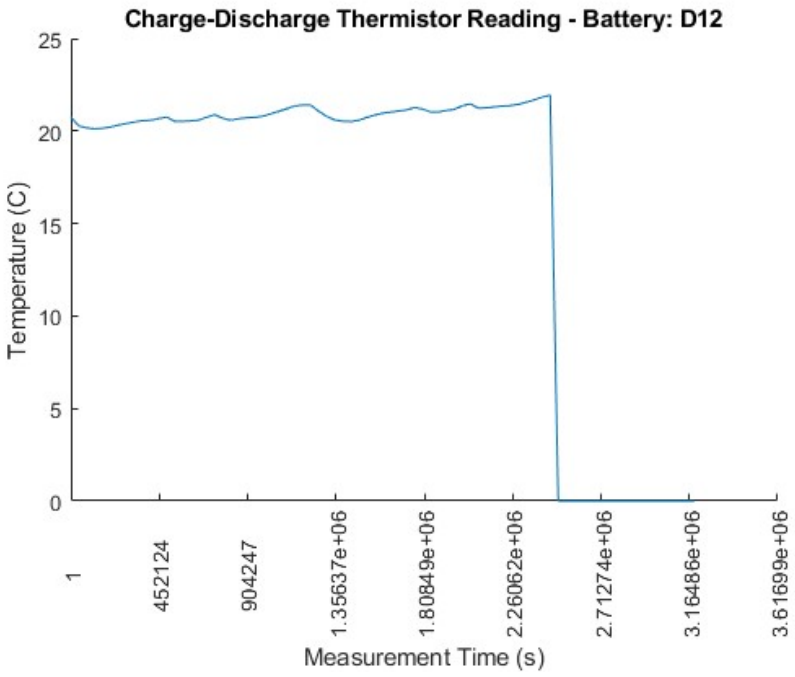

Fig. I.43:Temperature of D12 during Charge-Discharge Test

I.3 Plots for Batch E

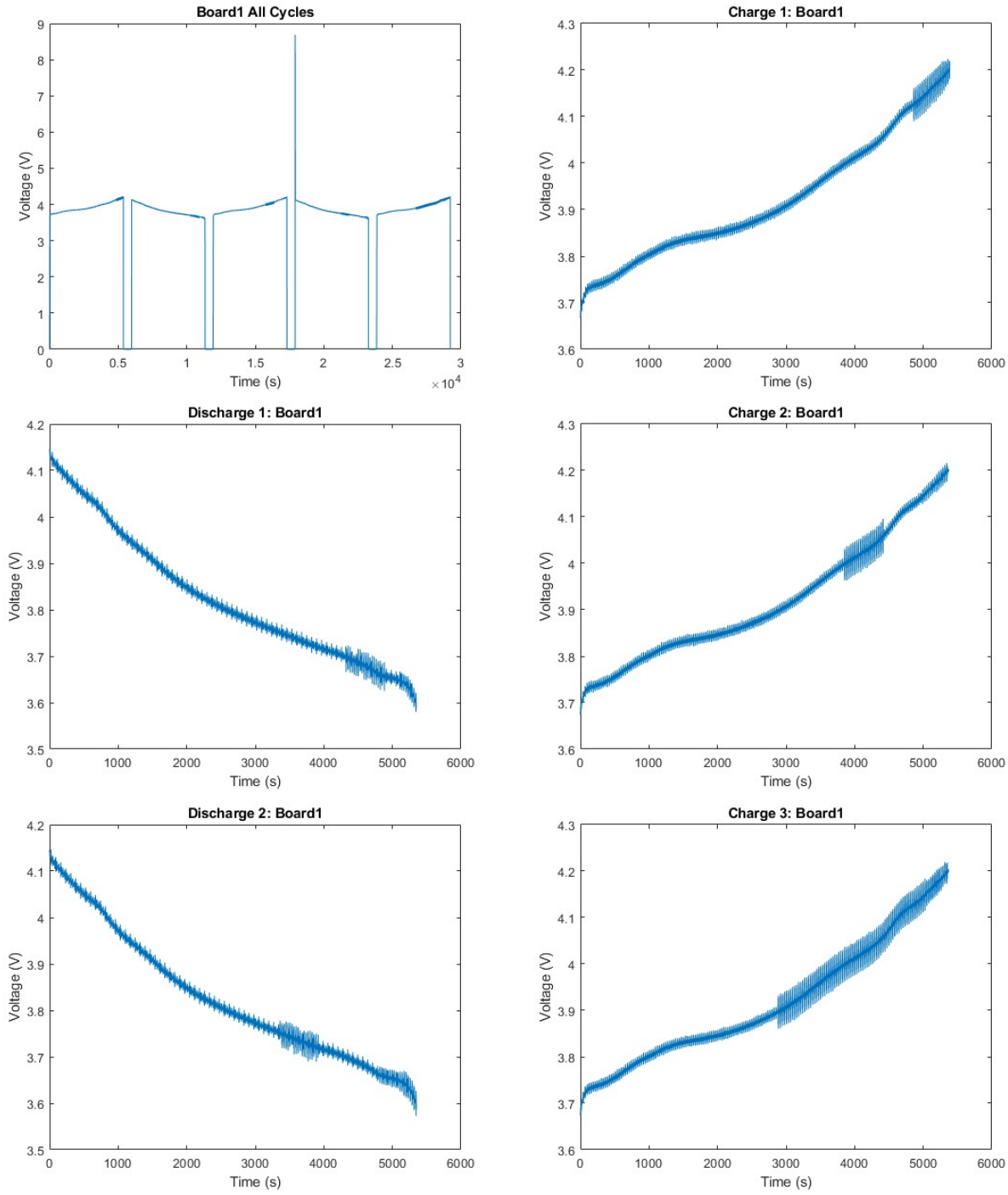

Fig. I.44: Charge-discharge curves for E1

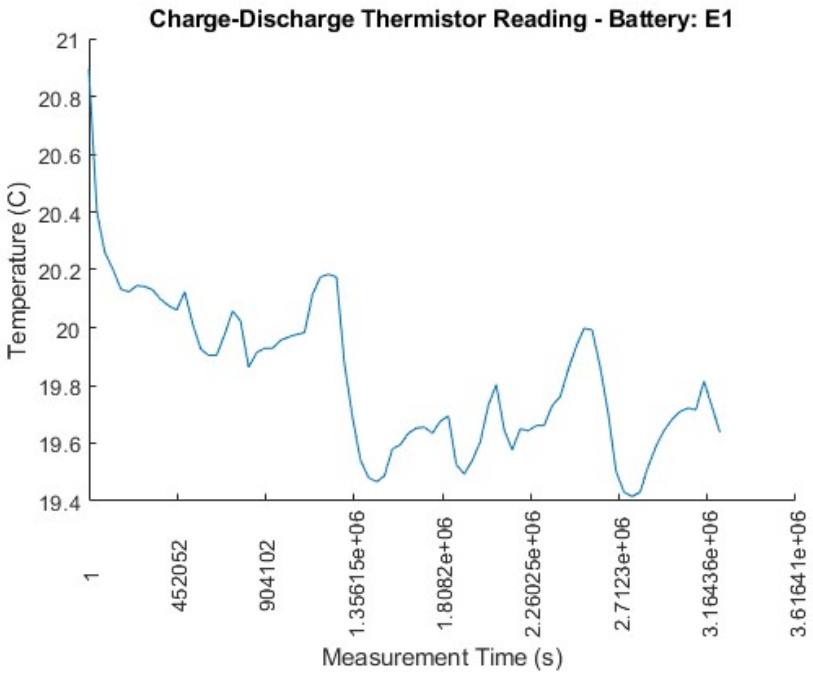

Fig. I.45:Temperature of E1 during Charge-Discharge Test

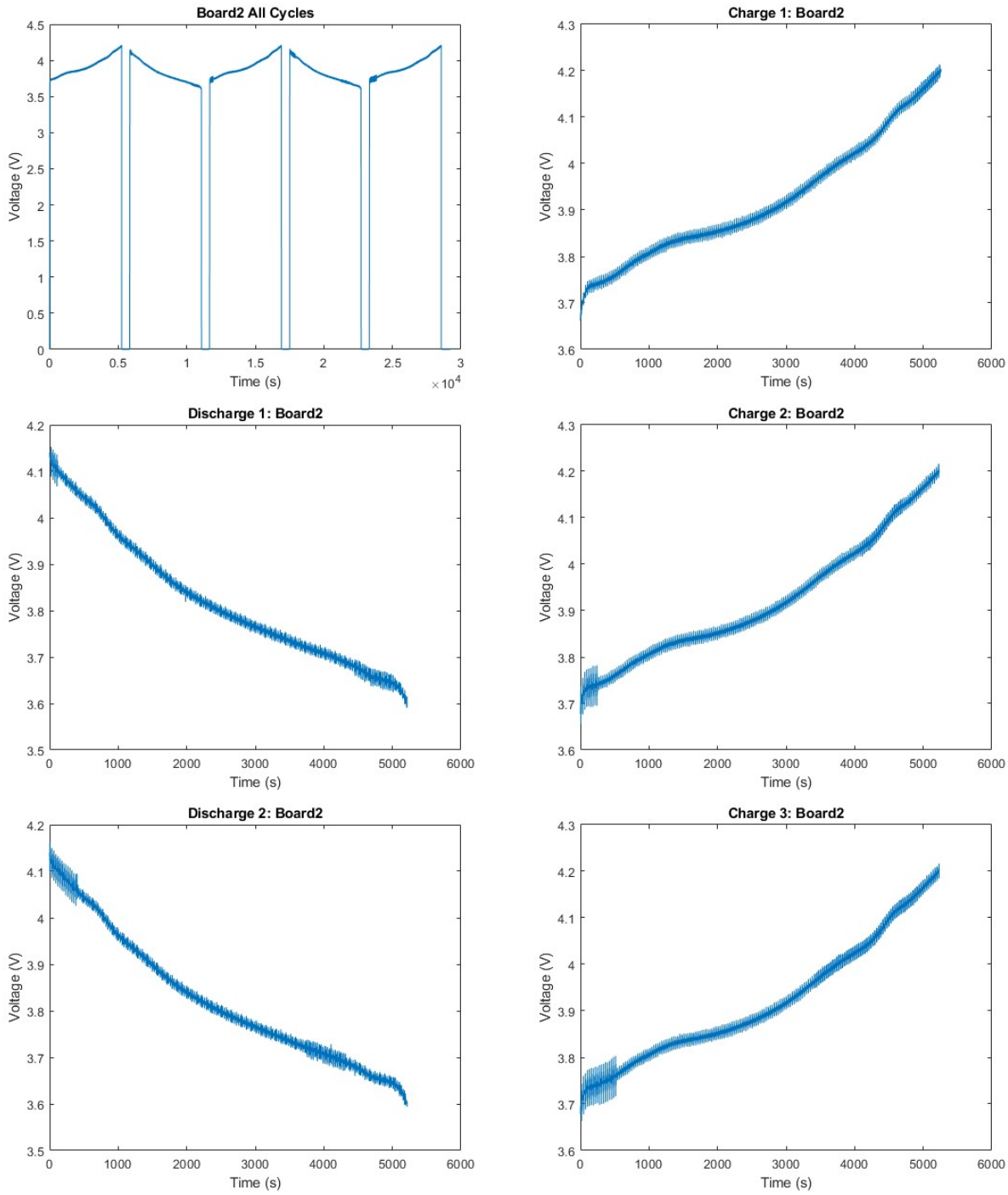

Fig. I.46: Charge-discharge curves for E2

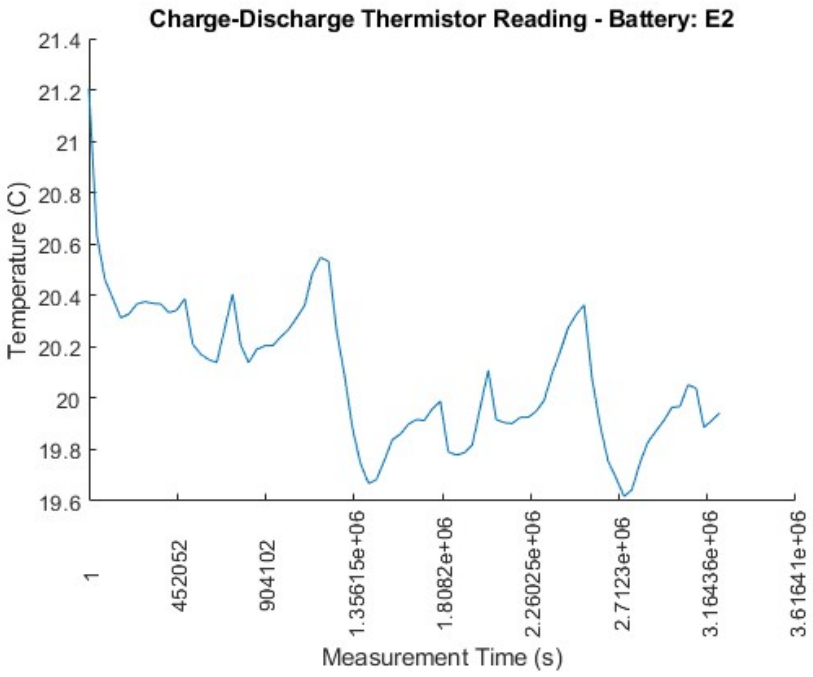

Fig. I.47:Temperature of E2 during Charge-Discharge Test

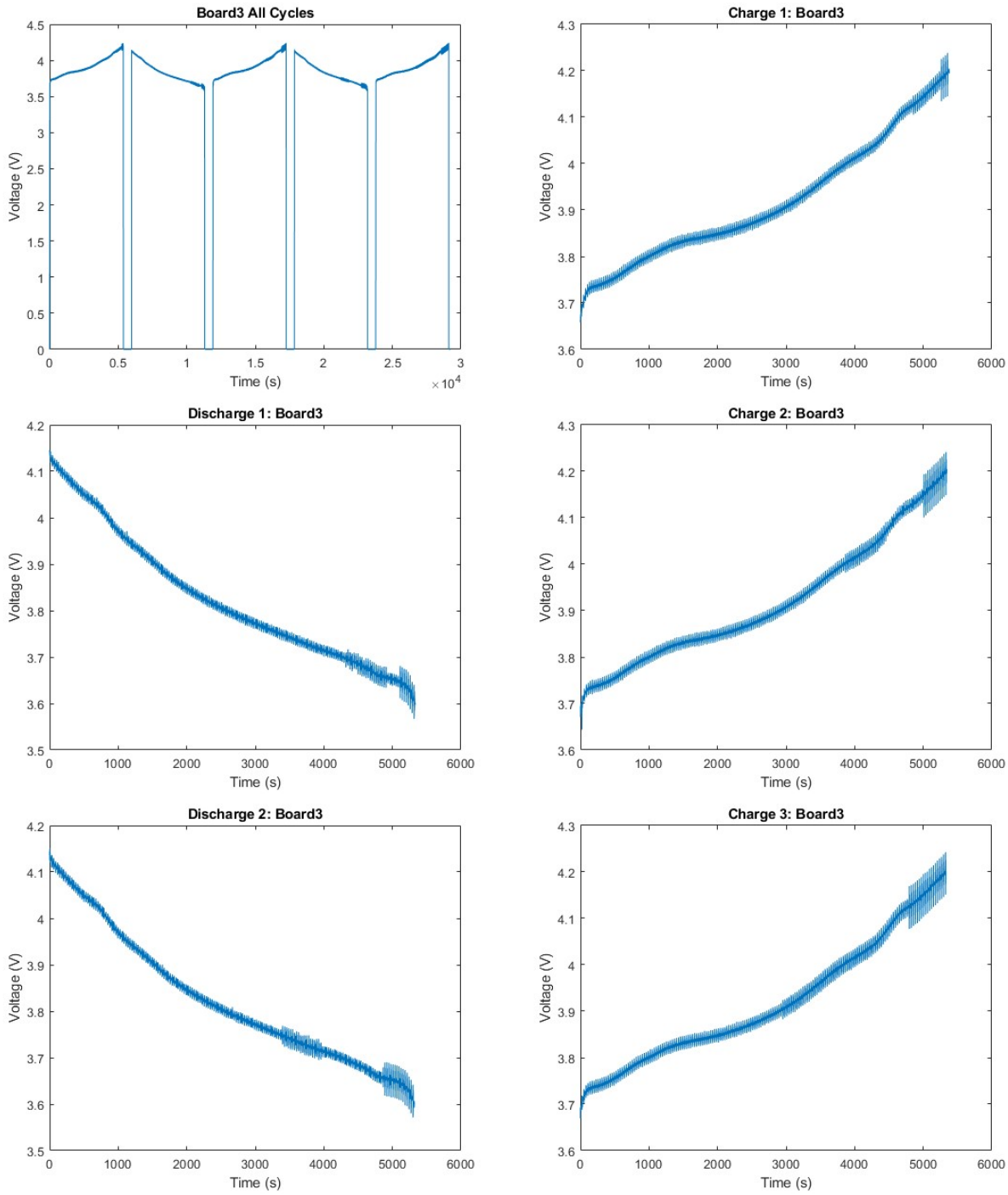

Fig. I.48: Charge-discharge curves for E3

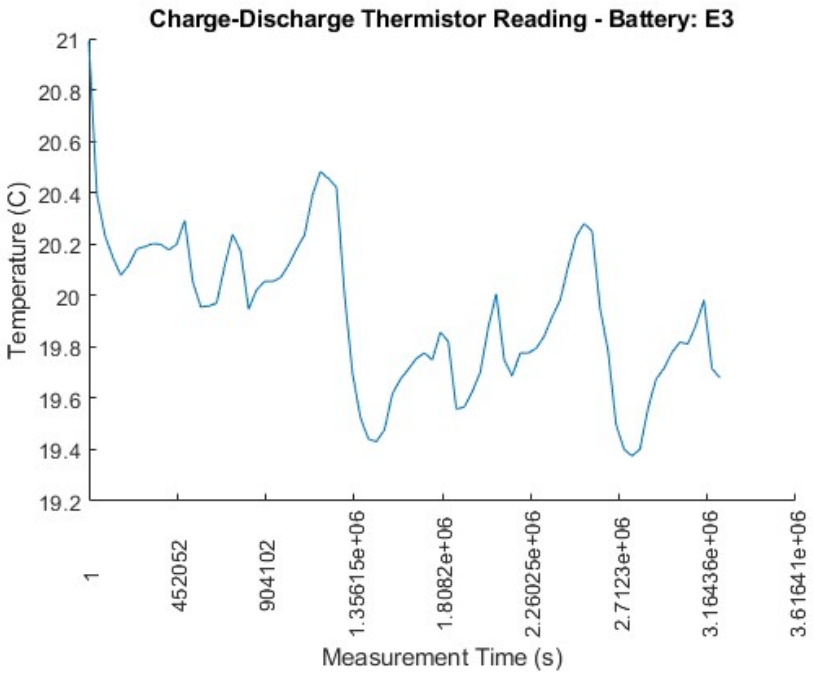

Fig I.49:Temperature of E3 during Charge-Discharge Test

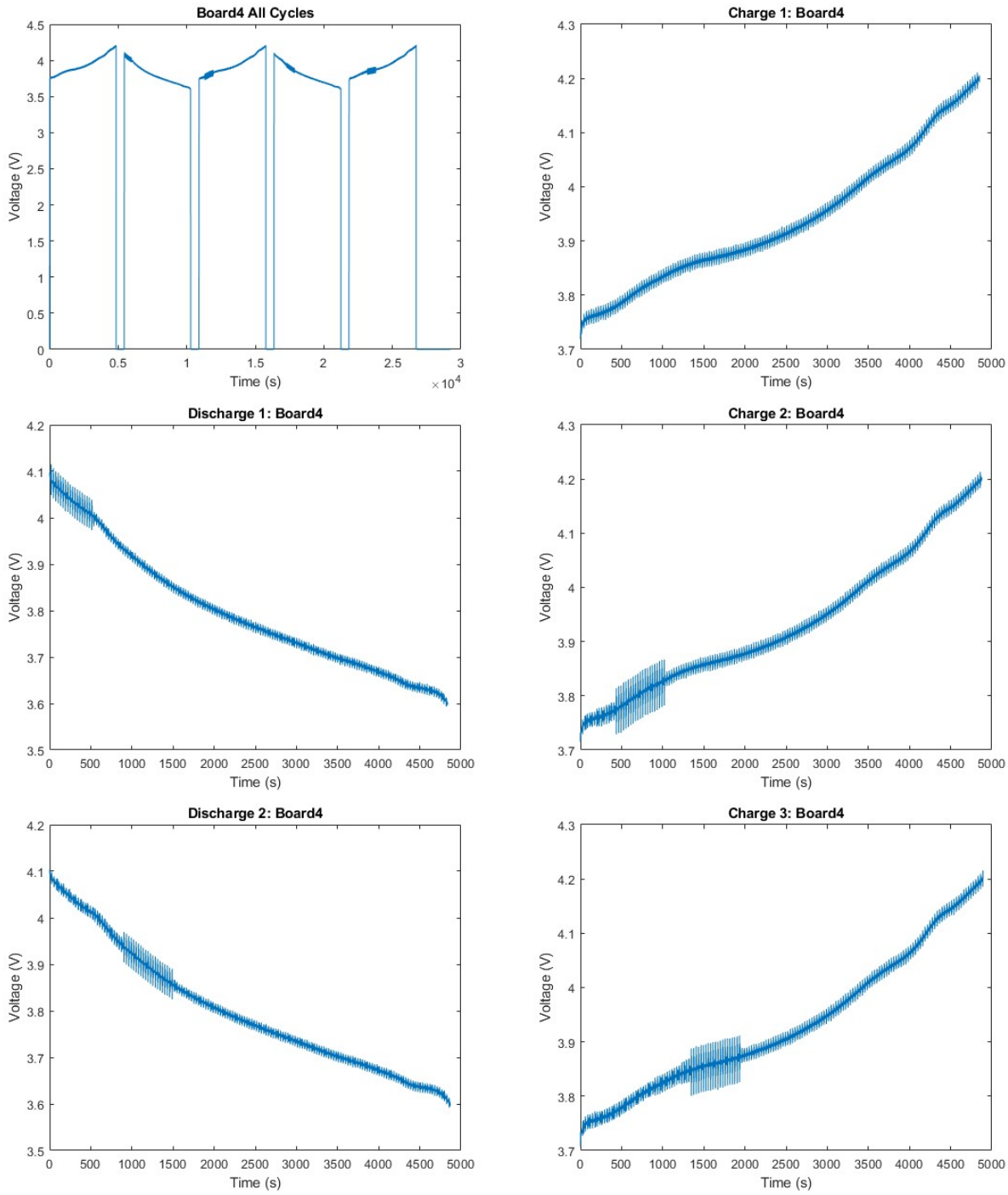

Fig. I.50: Charge-discharge curves for E4

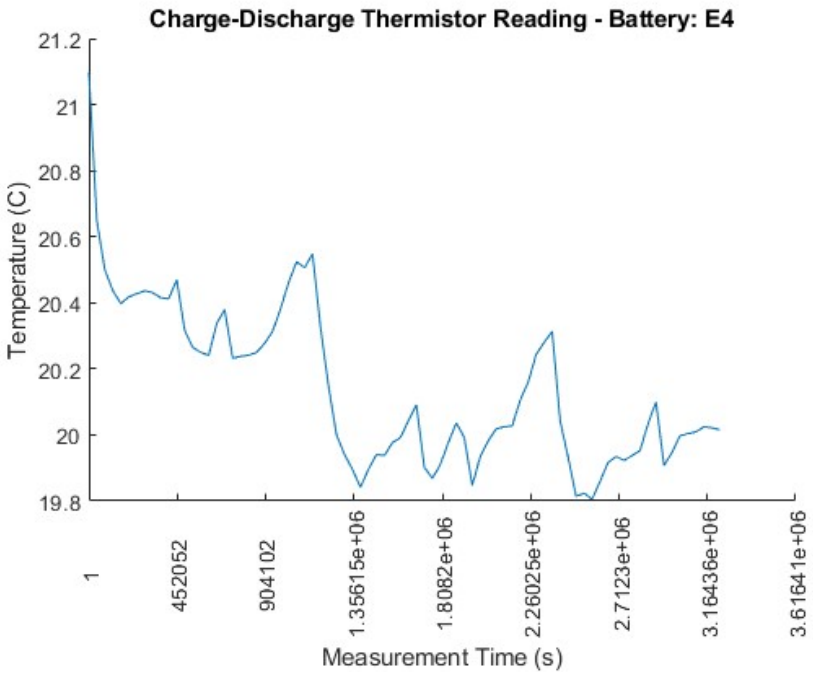

Fig. I.51:Temperature of E4 during Charge-Discharge Test

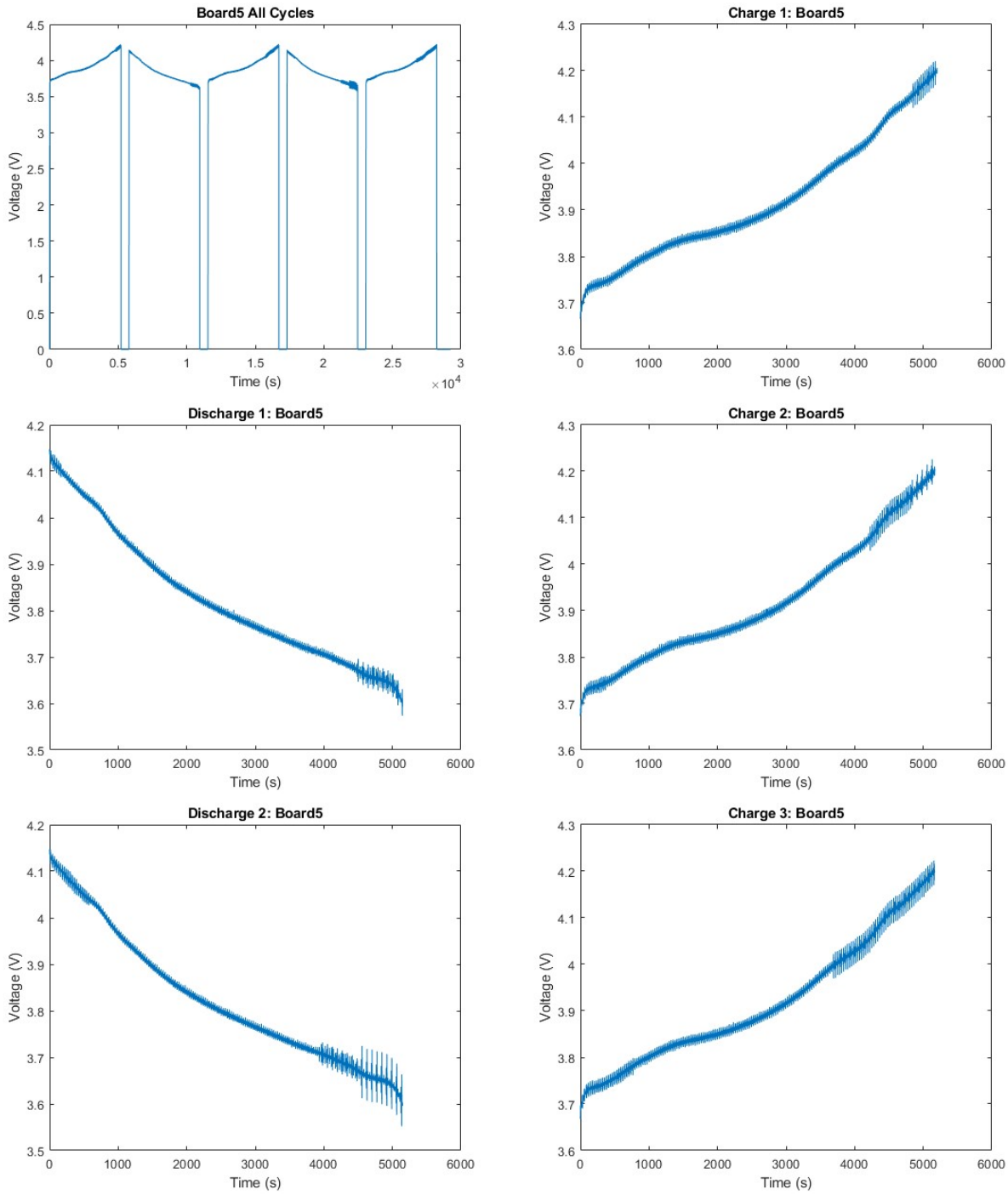

Fig. I.52: Charge-discharge curves for E5

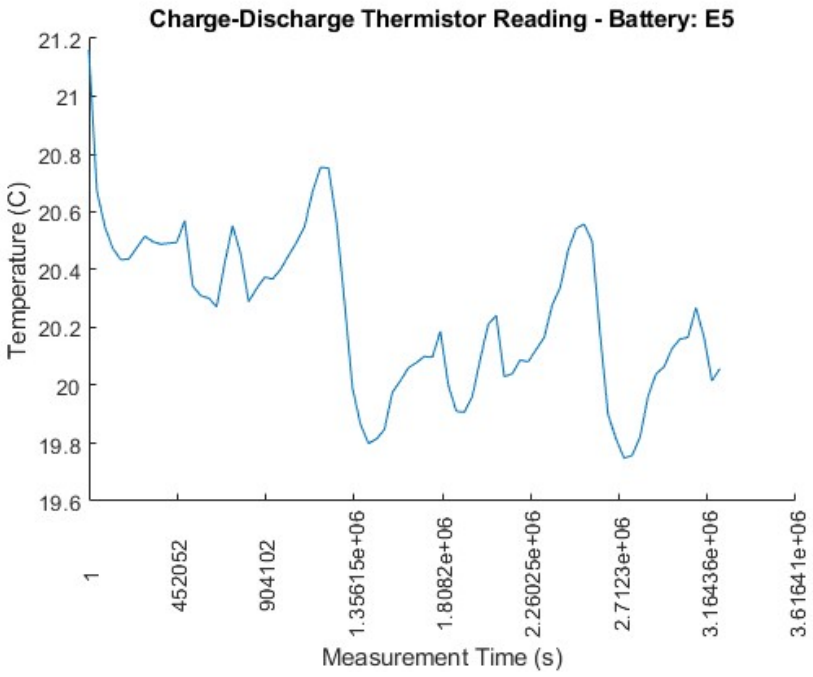

Fig. I.53:Temperature of E5 during Charge-Discharge Test

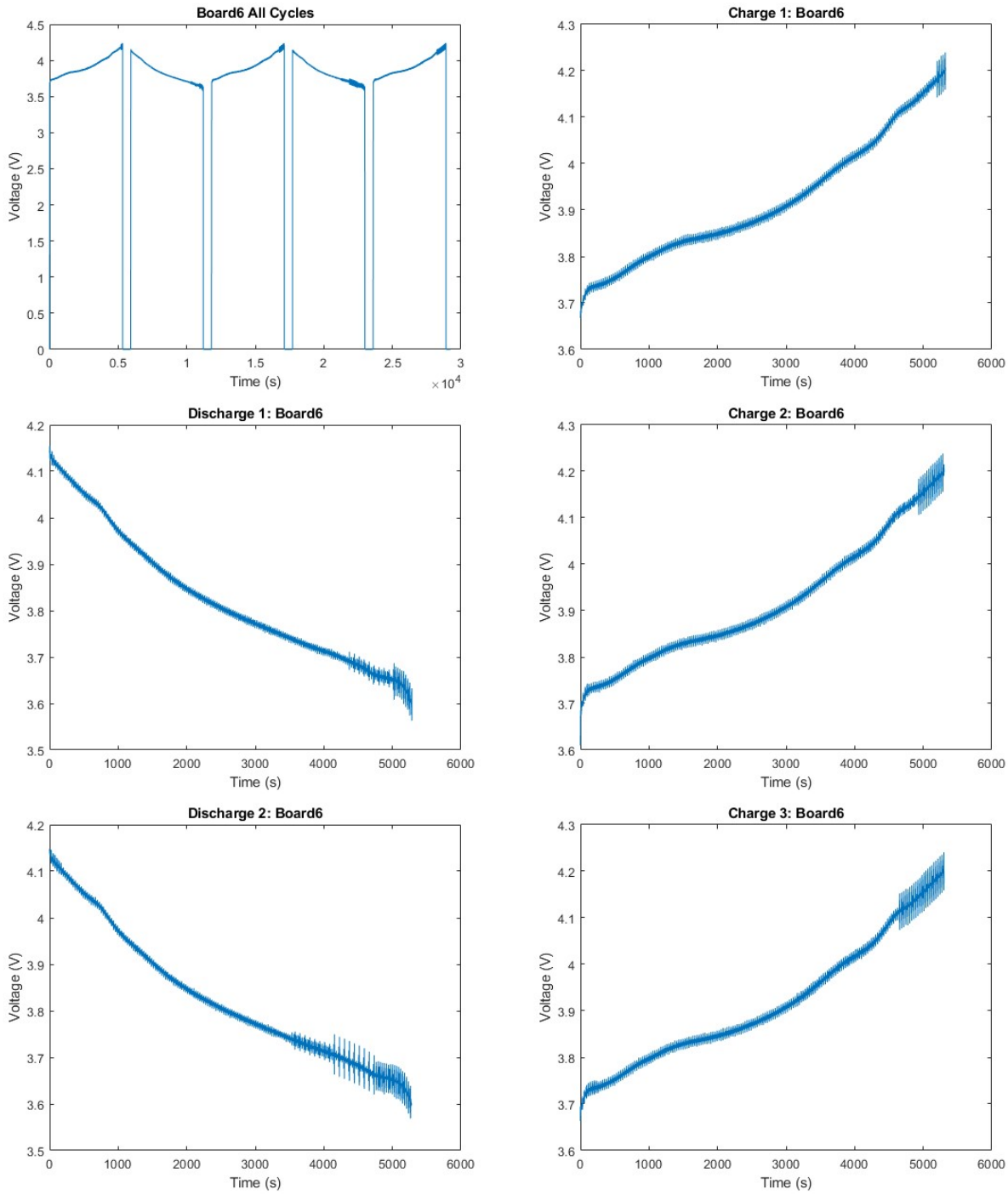

Fig. I.54: Charge-discharge curves for E6

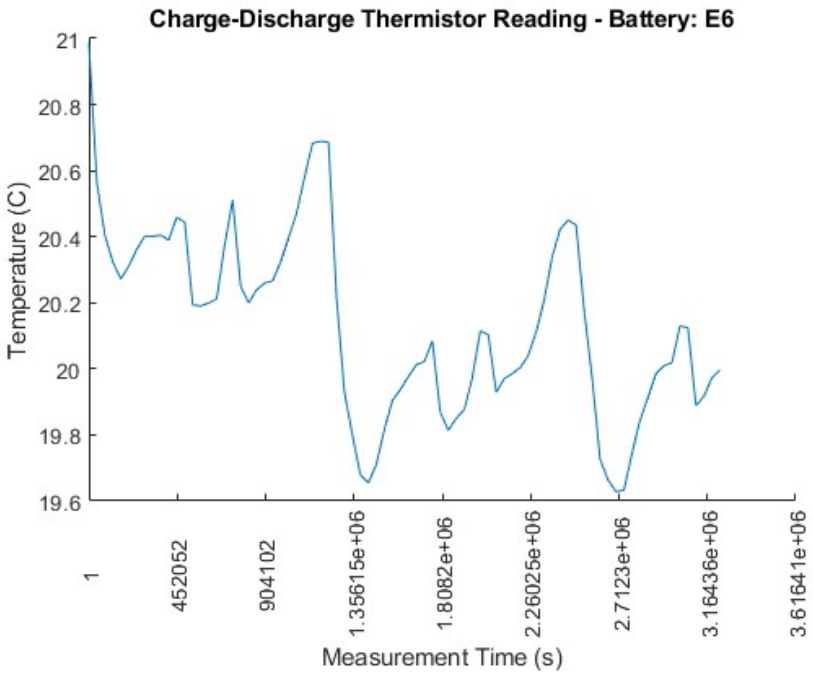

Fig. I.55:Temperature of E6 during Charge-Discharge Test

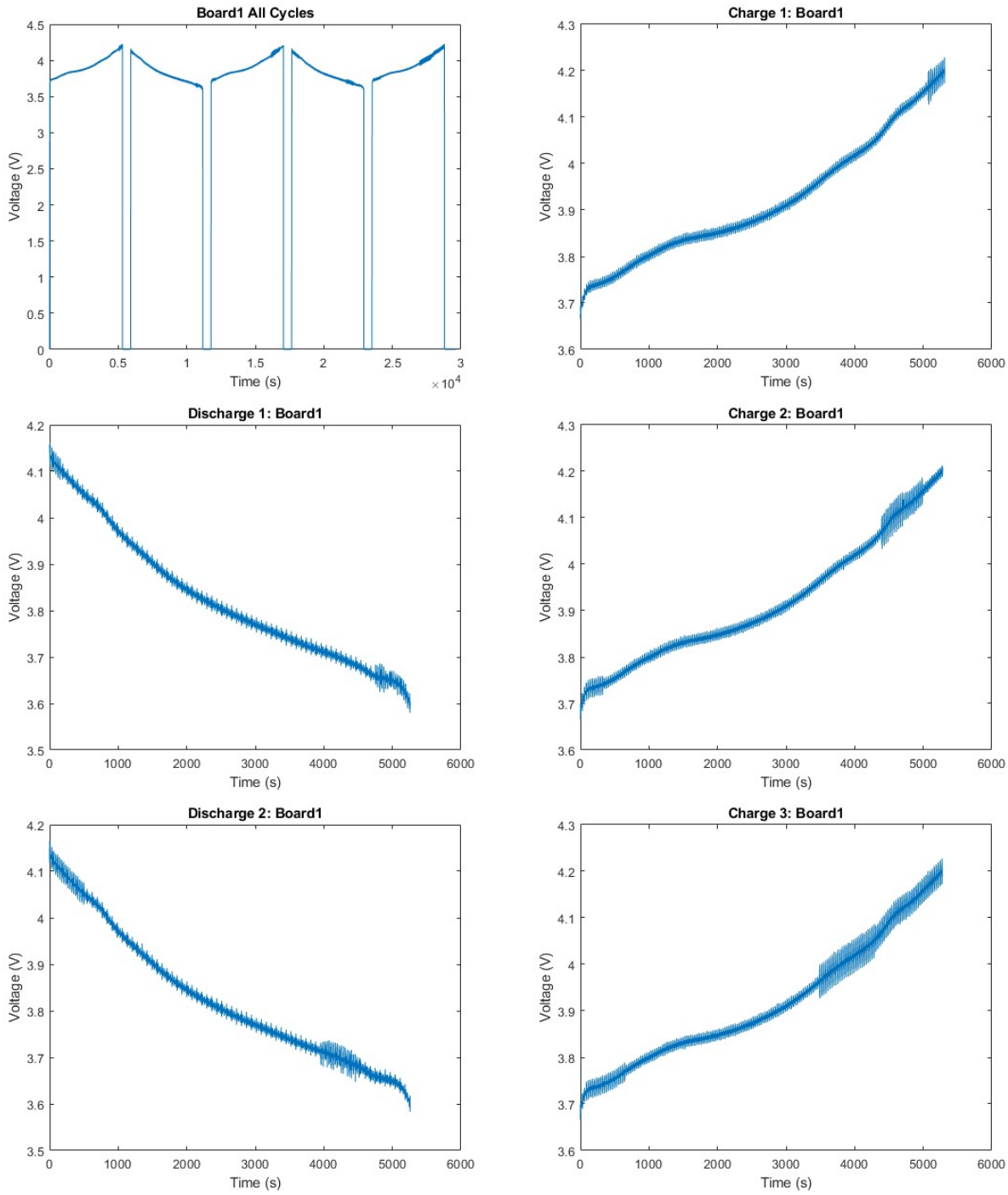

Fig. I.56: Charge-discharge curves for E7

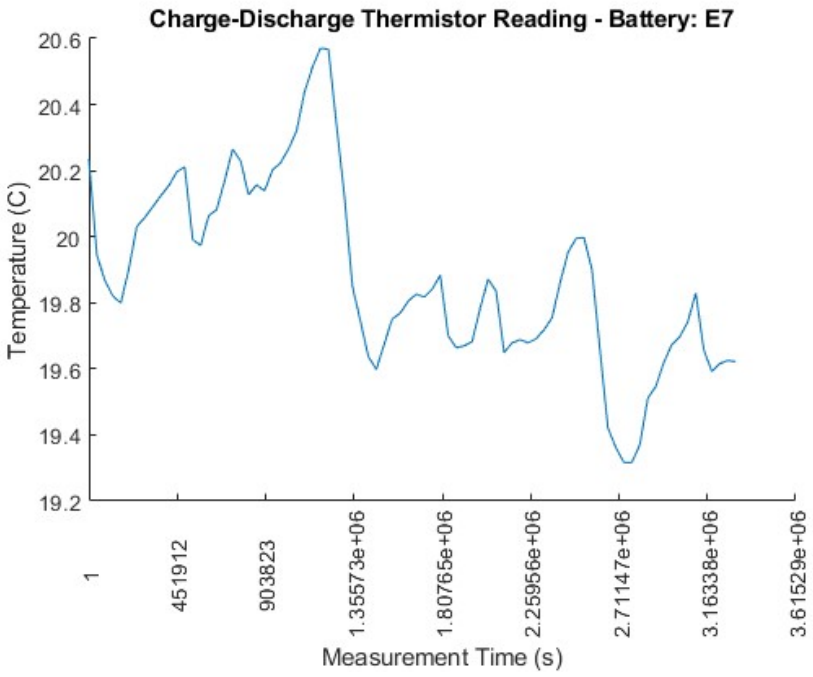

Fig. I.57:Temperature of E7during Charge-Discharge Test

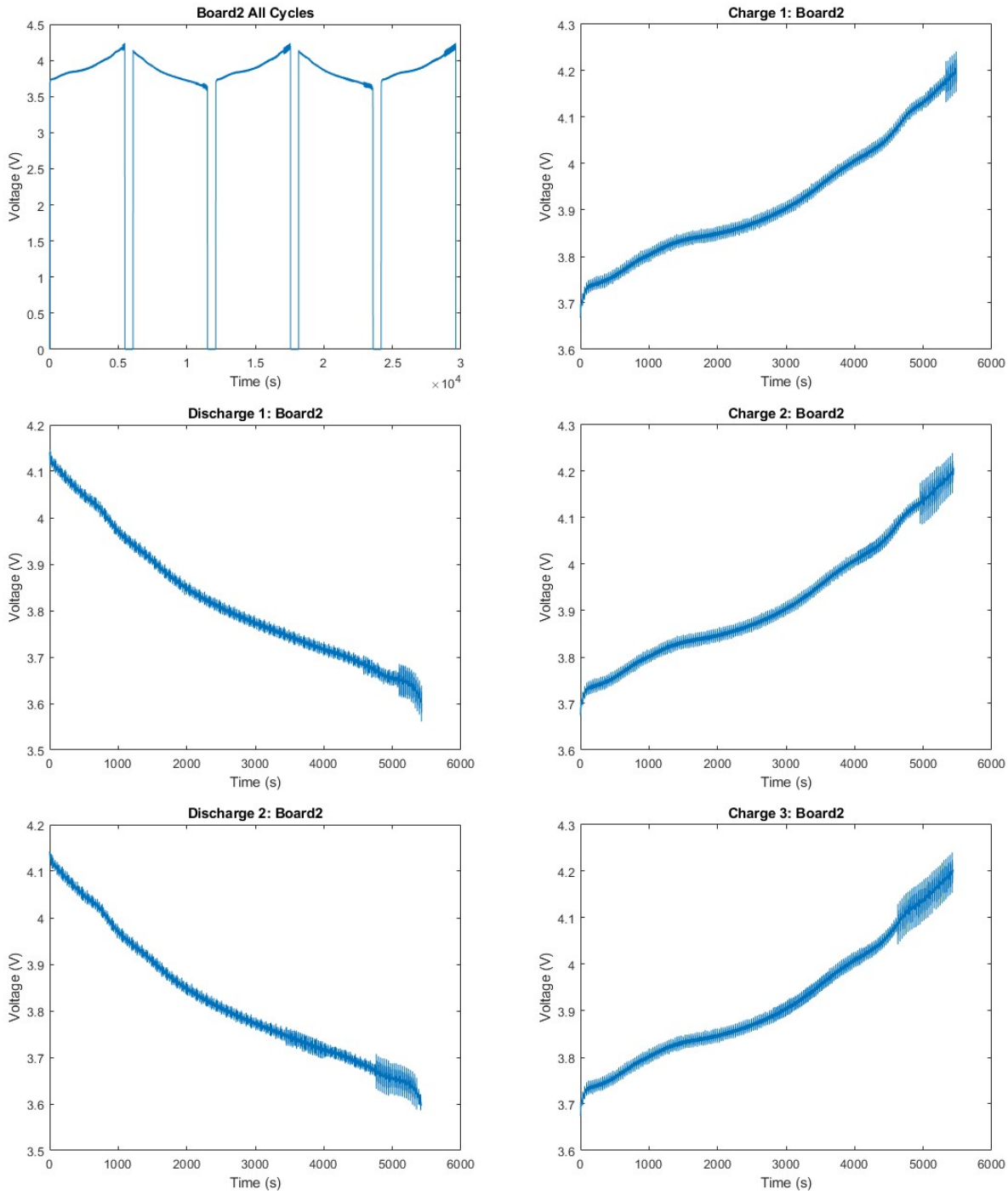

Fig. I.58: Charge-discharge curves for E8

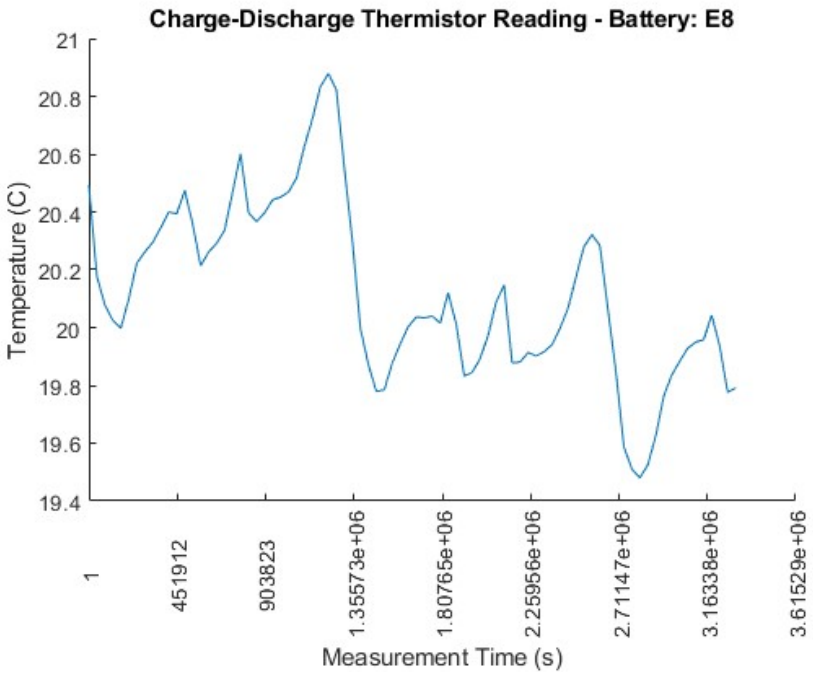

Fig. I.59:Temperature of E8 during Charge-Discharge Test

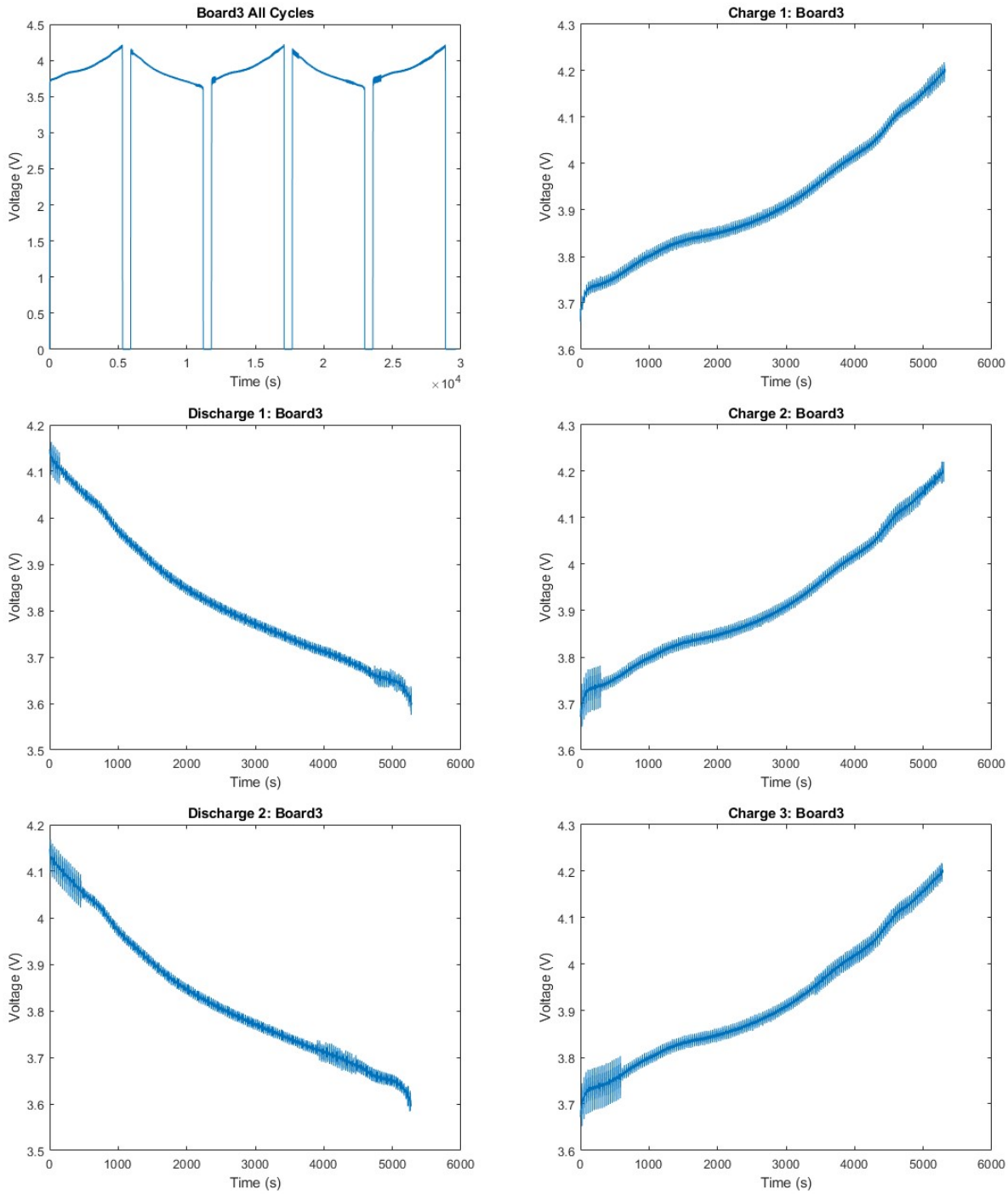

Fig. I.60: Charge-discharge curves for E9

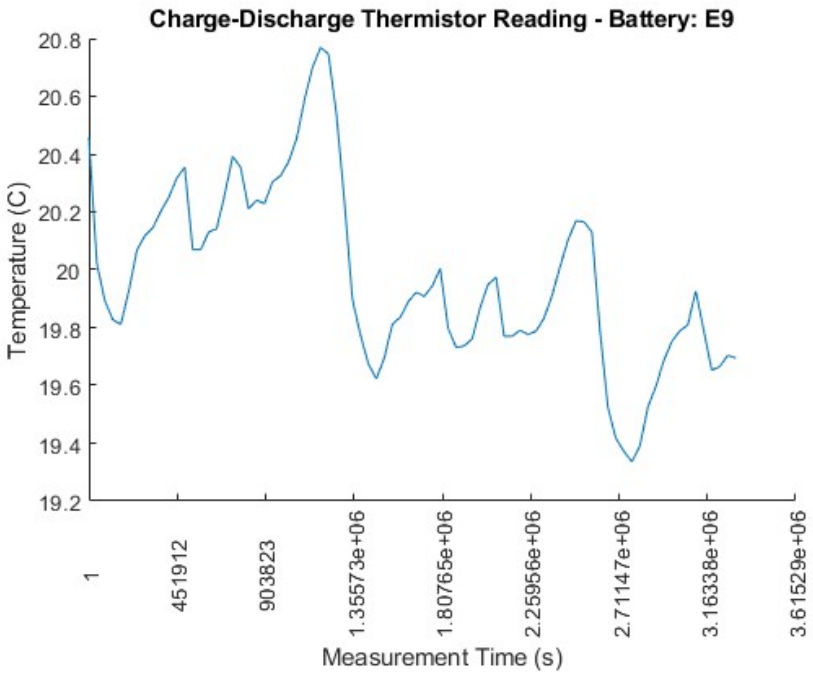

Fig. I.61:Temperature of E9 during Charge-Discharge Test

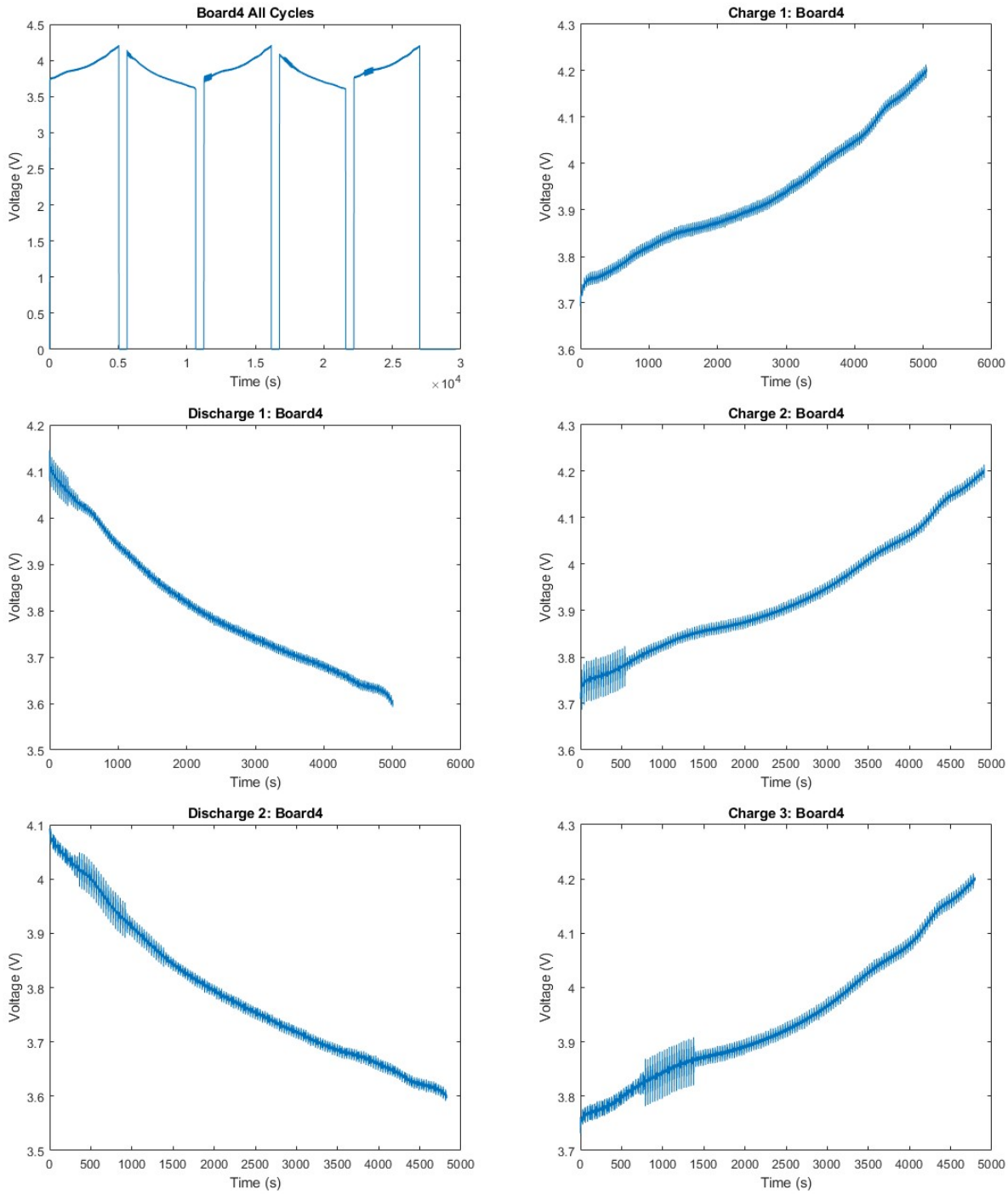

Fig. I.62: Charge-discharge curves for E10

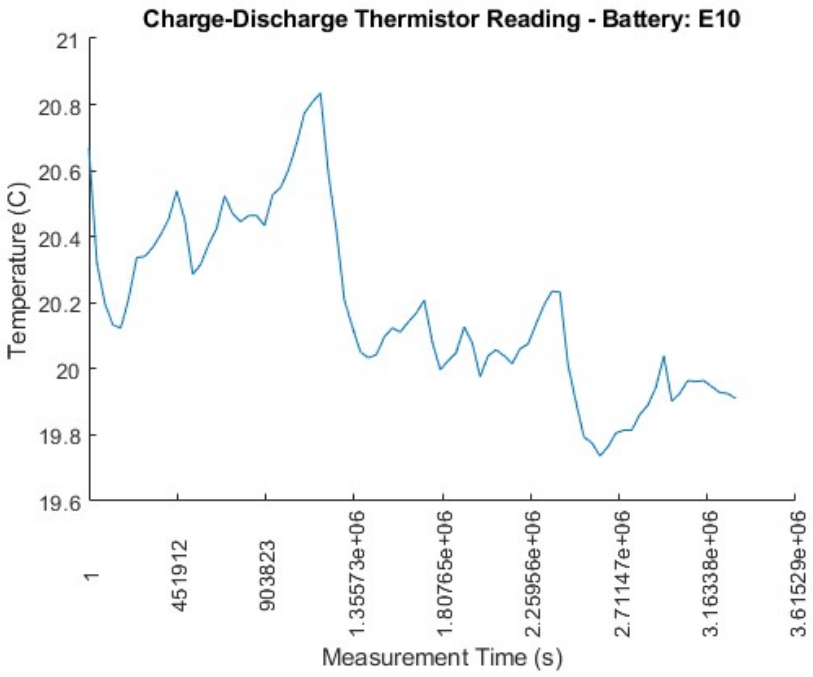

Fig. I.63:Temperature of E10 during Charge-Discharge Test

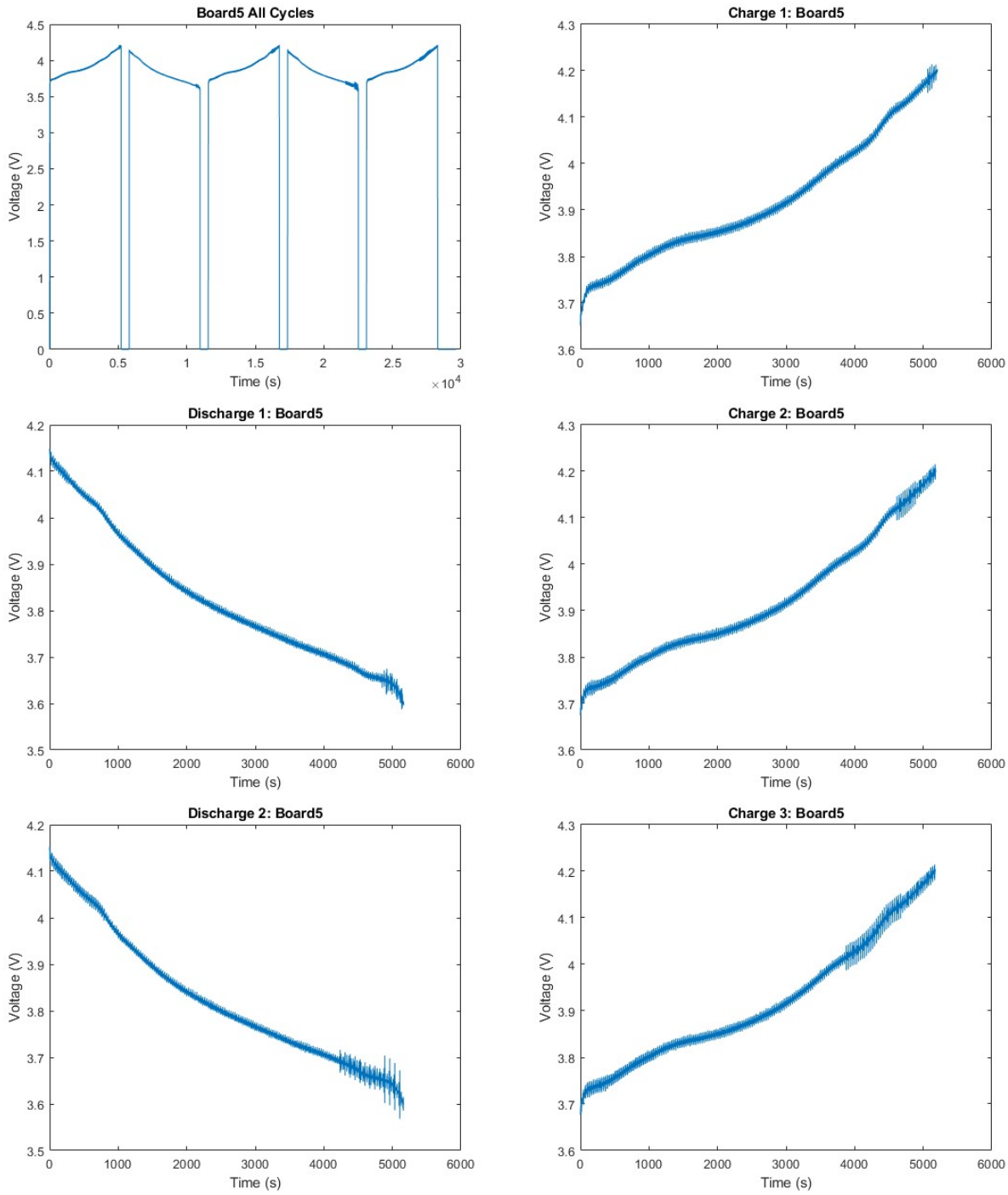

Fig. I.64: Charge-discharge curves for E11

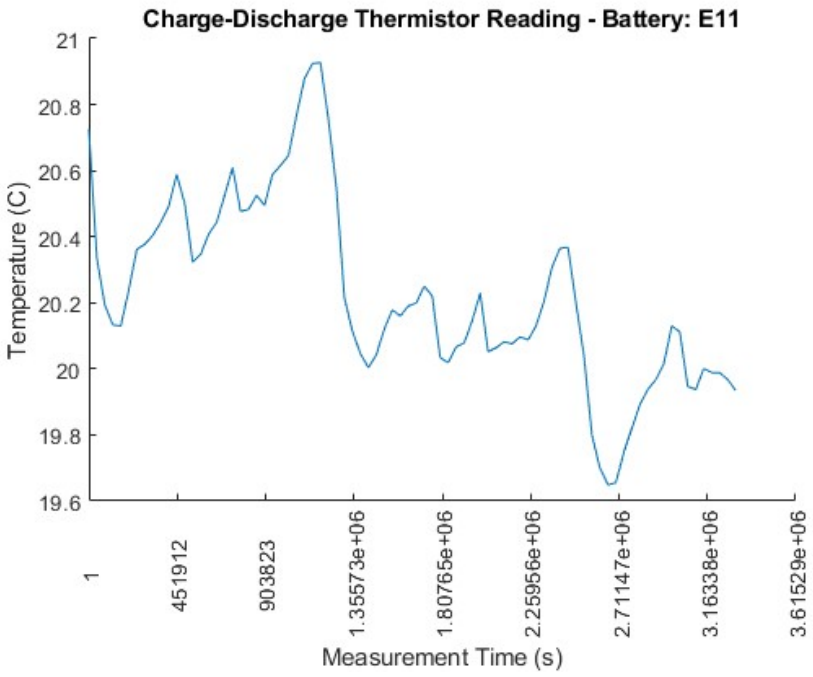

Fig. I.65:Temperature of E11 during Charge-Discharge Test

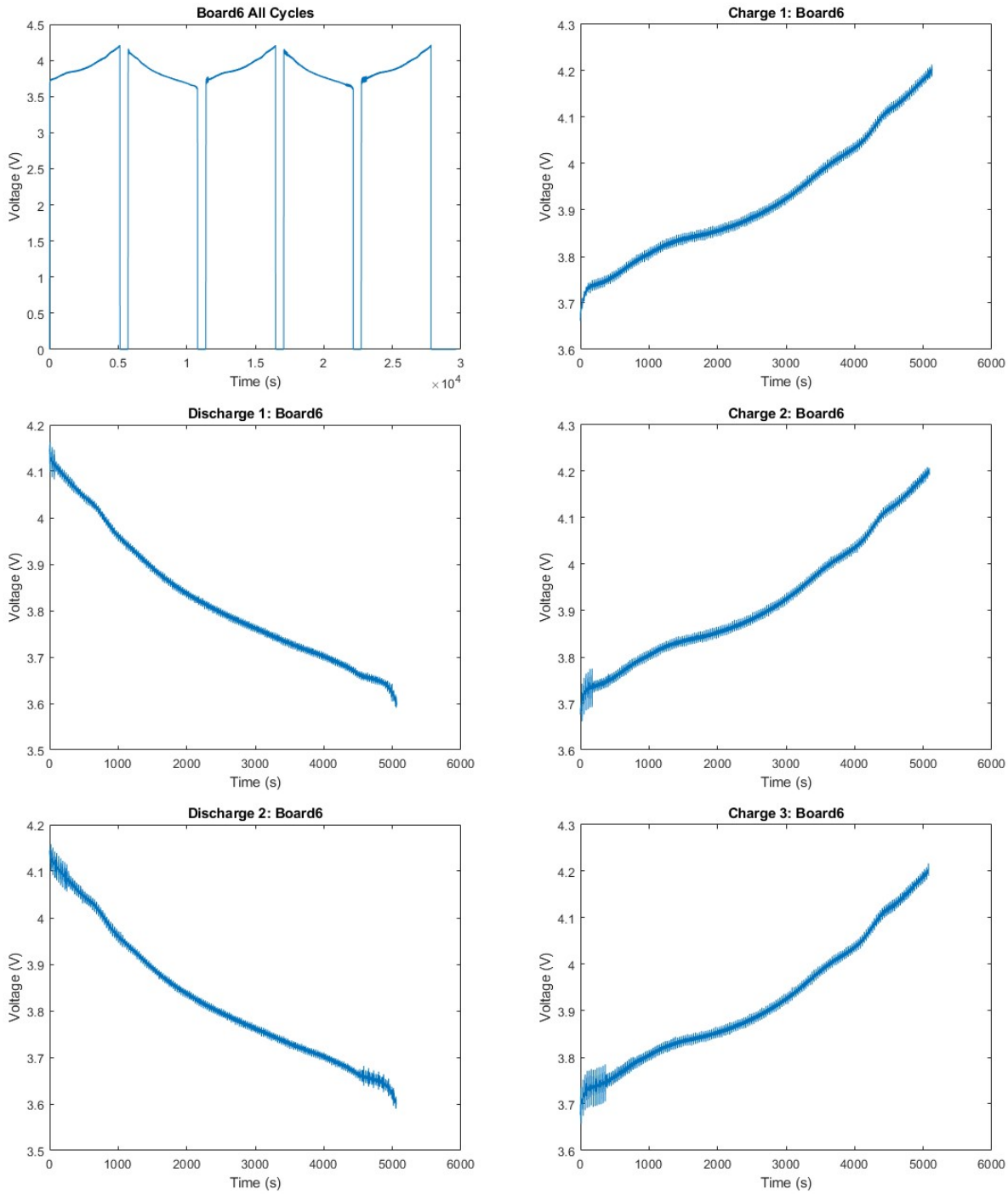

Fig. I.66: Charge-discharge curves for E12

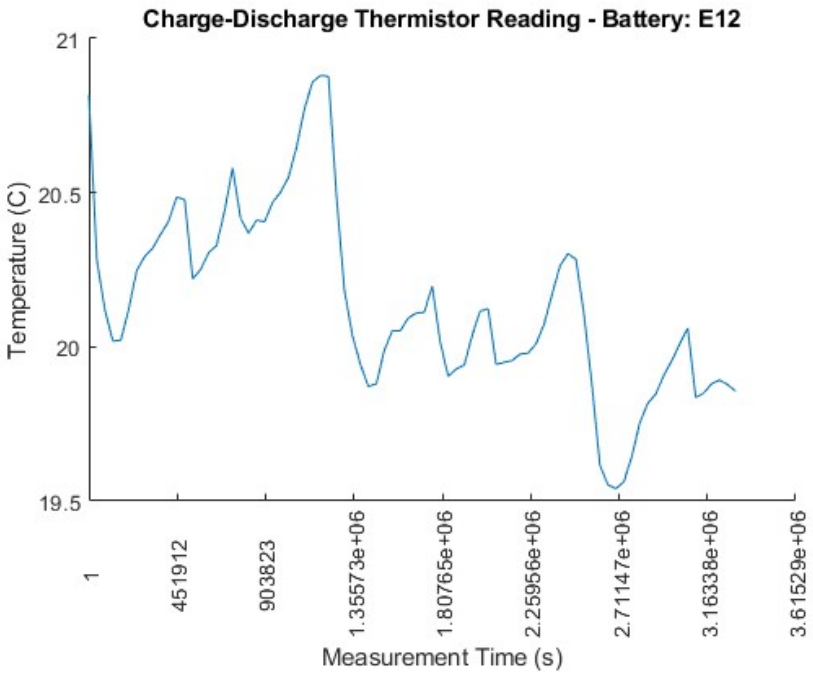

Fig I.67:Temperature of E12 during Charge-Discharge Test